The Dynamic Nature of the POMC Neuron Landscape, and the Impact of POMC Peptides and Body Composition States in Motivated Feeding

By

Graham Lewis Jones

A dissertation submitted in partial fulfillment
of the requirements for the degree of
Doctor of Philosophy
(Neuroscience)
in The University of Michigan
2019

Doctoral Committee:

Professor Malcolm J. Low, Chair
Assistant Professor Carrie R. Ferrario
Associate Professor Shelly B. Flagel
Professor Martin G. Myers
Professor Randy J. Seeley

Because something is happening here but you don't know what it is.

Do you, Mr. Jones?

Robert Allen Zimmerman

Graham Lewis Jones

gjonz@umich.edu

ORCID iD: 0000-0002-3851-3341

To everyone who has given me an opportunity,

And to those who didn’t

ACKNOWLEDGMENTS

First, I would like to express my appreciation and thanks to my mentor, Malcolm Low. You have always encouraged me to think critically and have allowed me to arrive at my own conclusions. The patience and trust that you have placed in me has given me the confidence to keep trying without fear of failure. Our experiences have taught me many lessons that I will take with me and continue to learn from. Thank you for always being understanding, for keeping your door open, and for being aware that life goes beyond the lab.

Thank you to the many people who I have had the pleasure to share the lab with: Jessica, Courtney, Jessica B., Kavaljit, Surbhi, Dan, Aaron, Lakshmi, Gary, Talisha, Nick, Zoe, Eva, and Hui. All of you helped make the lab a place that I wanted to be. I especially want to thank Kavaljit for always lending his ear, entertaining my questions no matter how small, and for encouraging me to think big and to pursue my ideas.

I would also like to thank my dissertation committee for all of the patience and support that they have shown me. For helping to keep me on track and for all of the insight and time that they have provided, I will always be grateful.

Thank you to Larry Zweifel, Ali Güler, and Sheri Mizumori. I could never had made it to grad school without the opportunities that you gave me or without your unwavering support.

To my family and my future family, thank you for always making me feel loved, having your support has made me comfortable with whatever the future holds, knowing that you're there no matter what.

Big thank yous to all of my Michigan support systems, without whom I never could have made it this point. To my neuroscience-associated family, Brittany, Jackie, Rob, Scott, Nicole, Nicholas, Hank, Chris, James, Jonte, Nadia, Willie, Veronica, and Alex for the many experiences that we have shared over the last 5 and a half years. To my cohort, few things unite people like commiserating, I wish the best for all of you. To Zoe, Jessica, Ian, and Allen, for all of the nights of trivia. To the Lansdowne crew, for keeping me somewhat active and for my dubious string of 2nd place finishes. To the softball team, you all go Second Deck. To Christian, for organizing, golfing, brewing, and teaching. To PIBS and Friends, for the frozen nights on the flag football field. To Lois, for entrusting us with Milo and Zoey, and for always being there with advice. To Lisa and Larry, thank you for truly making Caitlin, Penny, and I part of your family by opening your home to us and including us in your Thanksgivings, Passovers, and 4th of Julys.

Finally, most of all to my fiancé Caitlin. You truly are my favorite part of Michigan. There's no one else that I would rather do new things with or do nothing with. Thank you for always finding new adventures for us, and for always taking initiative to get things done. Thank you for leading us to Penny, I can't imagine life without either of you. I can't wait to see what CA has in store for us, and am excited for our next chapter and the big changes that await us.

TABLE OF CONTENTS

LIST OF FIGURES

FIGURE

LIST OF TABLES

TABLE

LIST OF APPENDICES

APPENDIX

LIST OF ABBREVIATIONS

ACTH – adrenocorticotropic hormone
AgRP – agouti-related peptide
AH – anterior hypothalamus
AP – area postrema
Arc – arcuate nucleus of the hypothalamus
Arc*Pomc*$^{-/-}$ – neuron-specific *Pomc*-deficient mice
β-End – beta endorphin
β-FNA – beta funaltrexamine
BLA – basolateral amygdala
CART – cocaine-amphetamine-regulated transcript
CeA – central nucleus of the amygdala
CNO – clozapine-N-oxide
D1R – dopamine receptor type 1
D2R – dopamine receptor type 2
DA – dopamine
DAMGO – [D-Ala2, N-MePhe4, Gly-ol]-enkephalin (MOR agonist)
db/db – leptin receptor knockout
DIO – diet-induced obese
DMH – dorsomedial hypothalamus
DOPAC – 3,4-Dihydroxyphenylacetic acid
DREADD – designer receptor exclusively activated by designer drugs
DsRed – discosoma red
EPSC – excitatory post-synaptic current
FNeo – floxed neomycin-resistance cassette
hM3 – G_q-coupled excitatory DREADD
HFD – high-fat diet
HFHSD – high-fat high-sucrose diet
HPA – hypothalamic-pituitary-adrenal axis
ICV – intracerebroventricular
IPSC – inhibitory post-synaptic current
ITI – inter-trial interval
Lepr – leptin receptor
LH – lateral hypothalamus
MCR – melanocortin receptor (e.g. MC3R or MC4R)
MOR – mu opioid receptor
MPO – medial preoptic nucleus
MSH – melanocyte stimulating hormone (i.e. α-MSH, β-MSH, and γ-MSH)
MTII – melanotan II (MC3/4R agonist)
NAc – nucleus accumbens (NAcC & NAcS, core and shell, respectively)

NDP-MSH – [Nle4,D-Phe7]-α-MSH (MC3/4R agonist; a.k.a. melanotan I)
nPE – neural Pomc enhancer (i.e. nPE1 or nPE2)
NPY – neuropeptide Y
NTS – nucleus of the solitary tract
ob/ob – leptin knockout
OVX – ovariectomized
PBN – parabrachial nucleus
PBS – phosphate buffered saline
PCSK – prohormone convertase (i.e. PCSK1/3 or PCSK2)
PD – Pomc-deficient, neuron-specific
POMC – proopiomelanocortin
PVH – paraventricular nucleus of the hypothalamus
PVT – paraventricular nucleus of the thalamus
PYY – peptide YY
SNA – sympathetic nerve activity
SON – supraoptic nucleus
T3 – triiodothyronine
T4 – thyroxine
TRH – thyrotropin releasing hormone
TSH – thyroid stimulating hormone
VMH – ventromedial nucleus of the hypothalamus
VTA – ventral tegmental ar

ABSTRACT

The importance of proopiomelanocortin (POMC) in maintaining normal metabolic homeostasis is well established. However, due to the phenotypes associated with human-patients and animal models with dysfunctional melanocortin systems, this propeptide and the neurons that produce it are dogmatically cast into an oversimplified role as merely being the satiety-signaling counterpart to the hunger-signaling agouti-related peptide (AgRP) neurons. In actuality POMC neurons represent an extremely diverse cell population, whose impact and function increase in complexity as our understanding grows. In my thesis I explore the anatomical and behavioral landscape of neuronal POMC in the mouse.

First, I discuss the heterogeneity of POMC neurons and the paradoxical relationships associated with POMC-derived peptides and their neurotransmitter identities. POMC neurons are known to be both glutamatergic and/or GABAergic, which are predominantly excitatory and inhibitory, respectively. Yet methodological differences used to measure these characteristics the relative proportions reported for each subpopulation are unresolved. Deciphering the relationship between these fast neurotransmitters in POMC neurons is critical to being able to place POMC neurons into the proper short-term contexts of homeostatic regulation. The POMC propeptide is processed into α-melanocyte stimulating hormone (α-MSH) and β-endorphin (β-End), which respectively suppress and stimulate feeding. Pharmacology and genetic models have taught us a lot about these signaling hormones, but their specific roles are still unclear.

Next, I investigated the histological overlap between POMC-peptide and a lineage trace for glutamate neurons, finding that there was an even split in glutamatergic and non-

glutamatergic- POMC neurons. Then I assessed the impact of restoring *Pomc* expression specifically to glutamatergic neurons, using a Cre recombinase reversible *Pomc*-deficient mouse and a glutamate-neuron specific Cre driver. This resulted in a nearly complete normalization of the POMC system, including the presence of GABAergic POMC neurons, contradicting the lineage trace data. Together these findings uncovered a previously unknown phenomenon, wherein POMC neurons can exhibit plasticity in their neurotransmitter identity. This work finished with triple-label in situ hybridization (ISH) for *Pomc*, *Vglut2* (a glutamate neuron-associated gene), and *Gad67* (a GABA neuron-associated gene). Overlap between all of the labels revealed a sizeable population of *Pomc* neurons that express both *Vglut2* and *Gad67*, and that there is a distinct rostral-caudal pattern in the localization of *Pomc* neurons that express one or both of the markers.

Finally, I studied the behavioral impact of *Pomc*-deficiency, obesity, weight loss, *Pomc*-restoration after weight loss, and agonism of melanocortin receptors (MCRs) in operant feeding. I utilized two mouse models of obesity, *Pomc*-deficient mice and diet-induced obese (DIO) mice, and assessed their feeding behavior while obese, following weight loss to normal body mass, and after restoring *Pomc* in animals that had lost weight. Between these groups I found that weight loss and *Pomc*-deficiency each uniquely impart an increased drive to earn and eat food, and that they act additively in *Pomc*-deficient mice who have lost weight. I then showed that a history of weight loss intensifies future mild hunger, without a lasting impact on basal drive. Next, I established that the increase in operant feeding performance is correlated with the degree of weight loss. Then, I showed that hyperleptinemia potentiates the drive to earn food, but not eat it, after leptin sensitivity has been restored. Lastly, I demonstrated that pharmacological agonism of

MCRs suppresses food intake, overcoming *Pomc*-deficiency and weight loss, with minimal impact on other motivated behavior.

CHAPTER I

POMC neurons & POMC peptides

POMC, ARC ANATOMY AND NEURONAL ACTIVITY

Most of the components that are involved in the central regulation of metabolism and feeding have been identified, yet we still have only a preliminary understanding of how these complex functions are orchestrated. At the center of this neural puzzle is the arcuate nucleus of the hypothalamus (Arc). Few nuclei in the brain manifest as profound of an impact on overall metabolic physiology and feeding behavior as this area located in the medial-basal hypothalamus. It is critical in the central regulation of energy balance, receives peripheral signals from the gut and adipose tissue and sends processes throughout the hypothalamus, hindbrain and many sub-cortical limbic nuclei. The association with limbic structures implicates signaling in the Arc as a pivotal portal between the neural control of metabolism (homeostatic) and motivated behavior (hedonic).

Proopiomelanocortin (POMC) neurons situated in the arcuate nucleus of the hypothalamus are an integral cog in the neural circuitry regulating metabolism and feeding behavior. Dogmatically, POMC neurons are portrayed as the satiety signaling counterpart to the hunger driving agouti-related peptide (AgRP) neurons. Perturbation of either system results in severe consequences. Human mutations in *POMC* [1-4] or *MCR*s [5-8] are known to lead to

massively obese individuals, as well as adrenal insufficiency and red hair pigmentation. In mice, ablating POMC neurons [9] or mice that lack neuronal POMC (Arc*Pomc*$^{-/-}$) become morbidly obese due to excess fat mass that is accrued through stereotypical consumption of large meals combined with reduced energy expenditure and motor activity. These mice will be discussed in greater detail later. In contrast, the ablation of AgRP neurons in adult, but not neonatal, mice leads to starvation without intervention [10, 11], and overexpression of *Agrp* leads to massive weight gain [12].

POMC is an evolutionarily conserved vertebrate propeptide [13-17] expressed principally by a subset of neurons in the Arc and also in the pituitary gland by anterior lobe corticotrophs and by intermediate lobe melanotrophs. POMC is initially cleaved by the prohormone convertase PCSK1/3, subsequently processed by PCSK2, with further refinement aided by carboxypeptidase E, N-acetyltransferase, and/or peptidyl α-amidating monooxygenase to produce POMC's biologically active compounds: α-, β-, and γ-melanocyte-stimulating hormone (α-MSH, β-MSH, and γ-MSH), β-endorphin (β-End), and adrenocorticotropic hormone (ACTH). POMC undergoes a variety of manipulations and transitions, with many variations of its intermediates that are described in detail elsewhere [18-20]. Prolylcarboxypeptidase is an extracellular protease that is partly responsible for inactivation of α-MSH [21]. AgRP is also highly conserved, but unlike POMC it is inherently bioactive without proteolytic processing. However, modification by PCSK1/3 increases its potency [19]. Neuronal transcription of *Pomc* is regulated by two neural *Pomc* enhancer elements (nPE1 and nPE2), while pituitary transcription is regulated independently through an additional enhancer (pPE) [22].

POMC-derived peptides act both centrally and peripherally to regulate a variety of functions. Immunohistochemistry (IHC) for POMC-peptides and AgRP has established

connections to the forebrain, midbrain, brainstem, and spinal cord. Distinct target sites receive input from different subsets of POMC and AgRP neurons [23, 24]. Additionally, areas of the cortex, dorsal striatum, and hippocampus contain MCRs, despite their absence of immunoreactive (IR) fibers, raising the possibility of melanocortin influence through volume transmission via the ventricular system [25]. It has also been suggested that many of the actions of β-End may be carried out via volume transmission in addition to synaptic signaling [26]. Centrally, the melanocortins act through melanocortin-3 and -4 receptors (MC3R and MC4R) and β-End signals via μ-opioid receptors (MOR). In the periphery, ACTH produced in the pituitary gland is a primary element in the hypothalamic-pituitary-adrenal (HPA) axis, regulating the stress response and the production and release of the glucocorticoid, corticosterone (cortisol in humans) from the adrenal gland. Neural activity mediated through MC3R and MC4R, whose primary endogenous agonist and antagonist are α-MSH and AgRP, respectively, is primarily associated with metabolic homeostasis and feeding behavior, whereas MOR signaling is most often associated with analgesia. Agonism of MCRs leads to cellular excitation through Gαs and mTOR signaling and G-protein independent closure of Kir7.1 channels, while AgRP leads to cellular inhibition by competing with α-MSH binding, preventing constitutive MC4R activity and the opening of Kir7.1 channels [27-29]. The function of MC4R is further modulated by its interaction with melanocortin receptor protein 2 (MRAP2) [30]. Agonism of MORs leads to cellular inhibition through G_i-coupled signaling, which inhibits adenylate cyclase, lowers cAMP levels and opens an inwardly rectifying K+ channel. Most MOR antagonists act via competitive binding with agonists to block their activity at the receptor.

In addition to producing their nominative peptides, POMC- and AgRP-neurons synaptically release rapidly acting amino acid neurotransmitters. AgRP neurons are GABAergic

and located in the ventral-medial Arc. POMC neurons are comprised of subpopulations of GABAergic and/or glutamatergic cells found in the ventral-medial and dorsal-lateral Arc, respectively. Not surprisingly, AgRP and POMC neurons exhibit opposite patterns of firing activity in vivo. AgRP neurons are active prior to feeding and display an increase in firing rate with mounting caloric deficit, but food or even the sensory detection of food rapidly reduces AgRP neuron activity and initiates the activation of POMC neurons. Palatability of the food and an animal's nutritional state also influence the magnitude and timing of these reversals of activation states [31-33]. It has also been suggested that AgRP neurons serve as orexin-activated pacemaker cells in the Arc [34].

Direct activation of AgRP neurons through pharmacogenetic [35] or optogenetic [36] approaches elicits voracious feeding in wildtype mice that are otherwise sated. Dogmatically, we would expect that activation of POMC neurons would lead to an immediate cessation of feeding. Yet, similar experiments activating POMC neurons have yielded less convincing results on feeding behavior [9, 36, 37]. Beyond feeding behavior, activation of AgRP neurons can assert a negative valence on other behaviors, whereas inhibition of AgRP neurons can convey a positive valence [32], and AgRP neurons can also drive stereotypic behaviors [38]. Studies have suggested that the effects of AgRP neurons are predominately carried out through fast GABAergic neurotransmission, rather than by AgRP itself [39]. Selective removal of the vesicular GABA transporter from AgRP neurons leads to weight loss and decreased ghrelin sensitivity [40], and administration of benzodiazepines ($GABA_A$ agonist) after AgRP neuron ablation prevented the anorexia that is normally observed [41]. Another striking finding was found following AgRP neuron ablation, whereby either stimulating mesolimbic and nigrostriatal dopamine neurons or providing highly palatable food can circumvent the need for AgRP

neurons, and allow normal overall food intake and body weight [42]. The homogenous nature of AgRP neurons has made them more amenable to the detection of behavioral changes elicited through modulating their activity. Historically, isolating specific metabolic roles attributable to POMC neurons has been elusive, and muddied by the use of imperfect genetic tools. Early studies using global POMC KOs were informative, but the results achieved and interpretation of the data cannot disentangle effects of neuronal- from pituitary-POMC deficiency. Expression of genetic tools through breeding crosses with constitutive POMC-Cre activity have been shown to be extremely pervasive and developmentally affect a myriad of cell types throughout the brain and in the hypothalamus, and that a sizeable population of AgRP neurons is derived from neurons that have expressed Pomc at some point in development [37, 43].

The following will focus on addressing two characteristics of POMC neurons of the mouse Arc, which are paradoxical in and of themselves. First, most POMC neurons exhibit either or both glutamatergic and GABAergic fast neurotransmitter identities. This is the framework that the experiments in Chapter 2 contribute to. Finally, distinct POMC-derived peptides suppress and induce feeding. Furthermore, genetic disruption of *Pomc* to prevent the translation of β-End, which induces feeding, unexpectedly leads to mild obesity. Both Chapter 2 and Chapter 3 utilize Arc*Pomc*$^{-/-}$ mice, and this section highlights signaling and genetic considerations that are implicated with POMC-peptides.

POMC NEURONS SYNAPTICALLY RELEASE GLUTAMATE AND/OR GABA

Expression of biosynthetic and vesicular markers for Glutamate and GABA in POMC neurons

In addition to peptidergic actions, POMC neurons elicit fast neurotransmission by synaptic release of GABA and/or glutamate. Identifying and characterizing the neurotransmitter identity of POMC neurons has been the focus of several histological and physiological studies (Table 1.1). However, depending on the labeling and detection methods and tissue preparation, the proportions of glutamatergic and GABAergic POMC neurons reported vary greatly from study to study such that the relative proportions and functions of these POMC neuron subclasses is unresolved. While the number of publications dedicated to deciphering these distinctions is relatively small compared with the number of pharmacological and genetic KO studies of melanocortin function, each subsequent report has added depth to our understanding of the complexity of the POMC landscape.

POMC neurons have documented GABA and glutamate release in physiological preparations. In 2004, Hentges et al. [44] prepared primary hypothalamic cultures from POMC-eGFP mice and measured electrophysiological properties from identified neurons whose axons made autaptic contacts onto their own dendrites or soma. Electrical stimulation of these cultured POMC neurons produced autaptic PSCs, which were blocked by the $GABA_A$ receptor antagonist bicuculline, but not glutamatergic antagonists, indicating that the recorded currents were due to GABA release. Then in 2009, Hentges et al. [45] generated primary hypothalamic cultures from a cross of POMC-DsRed and GAD67-GFP mice. GABAergic autaptic PSCs were recorded from POMC neurons expressing both DsRed and GFP as before [44]. However, they also measured autaptic PSCs from the smaller population of presumably non-GABAergic cells that expressed only DsRed. These PSCs were blocked by the AMPA receptor antagonist DNQX and not by antagonists of ionotropic $GABA_A$ receptors, indicating that the induced currents were due to synaptic glutamate release [45]. Dicken et al. [46] microinjected AAV vectors encoding Cre-

dependent channelrhodopsin (ChR2) into the Arc of *Pomc*-Cre animals and used sagittal *ex vivo* slices for path-clamp electrophysiology. Light-evoked stimulation of POMC neurons produced repeated IPSCs and EPSCs in neighboring cells in the Arc. Alternate applications of bicuculline and/or DNQX demonstrated that ~69% of the interrogated postsynaptic cells received inhibitory GABAergic inputs, ~23% received glutamatergic inputs and ~8% received both types of inputs from stimulated POMC neurons. This last study was particularly informative in demonstrating that some POMC neurons can synaptically release both GABA and glutamate. However, several questions are yet to be addressed. First, what are the identities of the neighboring postsynaptic cells that were the basis for the recordings? Do cells downstream of POMC neurons in more distal brain nuclei receive the same proportions of fast neurotransmitter input? Would the same proportions of post synaptic currents be measured if the viral vector was injected at different rostral-caudal positions in the Arc?

The histological picture is more mixed due to differences in methodologies among reports. In 2004, Hentges et al. [44] performed dual-label *in situ* hybridization (ISH) for *Pomc* (digoxigenin) and *Gad67* (^{33}P) in fixed tissue from 8 week old male mice and measured ~35% overlap between both markers in the Arc. Then in 2009, Hentges et al. [45] measured ~42% overlap between the genetically encoded fluorescent markers for *Pomc* and *Gad67* in the Arc of 6-10 week old male and female mice. In 2011, Vong et al. [47] crossed *Pomc*-hrGFP animals to *Vglut2*-ires-Cre and lox-tdTomato mice, or to *Vgat*-ires-Cre and lox-tdTomato mice of nondisclosed age or sex. IHC was used to detect the hrGFP and tdTomato reporters from each cross. The authors reported ~10% overlap between the detected *Vglut2* and *Pomc* reporters, and <1% overlap between the *Vgat* and *Pomc* reporters.

In 2012, Jarvie and Hentges [48] were able to further tease apart the neurotransmitter identity of POMC neurons even more by using several combinations of labeling methods for ISH and immunodetection of genetically encoded fluorescent reporters in fixed tissue from 8-12 week old male mice. ISH for *Pomc* (digoxigenin) in *Gad67*-GFP tissue showed ~10% overlap with IHC for GFP, whereas FISH for *Gad67* (fluorescein) in *Pomc*-eGFP tissue showed ~38% overlap with GFP IHC. Similarly, ISH for *Gad65* (digoxigenin) in POMC-eGFP tissue demonstrated ~45% overlap with GFP IHC. FISH for *Vglut2* (fluorescein) in POMC-eGFP tissue showed ~7% overlap with GFP IHC (the tissue for these counts underwent an additional digoxigenin hybridization step for *Gad65*). Additionally, they performed ISH for *Vgat* in *Pomc*-eGFP tissue or ISH for *Pomc* in *Vgat*-eGFP tissue and found very little overlap between signals from either genetic cross, consistent with earlier findings [47] indicating that although POMC neurons package GABA into synaptic vesicles, VGAT is not the responsible transporter. ISH (digoxigenin) for *Gad67* in V*gat*-eGFP tissue showed only partial overlap in the Arc. The authors stated that the ISH tissue preparation caused a massive reduction in the endogenous fluorescence of the reporters used, necessitating the use of immunodetection to visualize them.

Addressing the discrepancies that were emerging due to methodological differences, Wittmann et al. [49] compared the detection sensitivity between IHC for POMC combined with ISH (^{35}S) for *Vglut2* or *Gad67* in tissue fixed by paraformaldehyde perfusion of the mice versus dual label ISH for *Pomc* (digoxigenin) and *Vglut2* or *Gad67* (^{35}S) in fresh-frozen tissue from 19 to 21 gram male mice. Overall, dual label ISH with the fresh-frozen tissue yielded greater cell counts for all of the markers including twice as many total *Pomc* and *Gad67/Pomc* neurons and five times as many *Vglut2/Pomc* cells. This method resulted in ~43% overlap between *Pomc* and

Vglut2 and ~54% overlap between *Pomc* and *Gad67*, surpassing all of the previously reported measures.

Previous work documented that in many hypothalamic cell types there is widespread transient embryonic *Pomc* expression and consequently only around half of all adult cells that express *Pomc* developmentally do so in the adult CNS [43, 50, 51]. In 2015, Dennison et al. [52] first addressed the issue of postnatal plasticity within the POMC neuron population by measuring co-expression of *Pomc*-eGFP (IHC) and *Vglut2* or *Gad67* (ISH) in fixed tissue from male and female mice through early postnatal development. They uncovered a developmental shift in the *Vglut2* or *Gad67* identity of POMC neurons. During early postnatal time points there is a much higher proportion of *Vglut2*/POMC cells that then diminishes by 8 weeks of age (Postnatal day 1: ~40% overlap; 8 weeks: ~8% overlap). In contrast, an opposite temporal pattern was found for double-labeled *Gad67*/POMC neurons (Postnatal day 1: ~8% overlap; 8 weeks: ~46% overlap). Interestingly, they also found that the overall intensity of the *Vglut2* signal progressively decreased from postnatal day 1 through 8 weeks of age. Unfortunately, all of the overlap data was presented as the proportion of POMC neurons per section (170±6.61 SEM) that in turn was averaged over 4 sections per mouse, 49 mice and all time points. Without knowledge of POMC neuron count at each time point, it is impossible to determine the mechanism for the observed switch from *Vglut2* to *Gad67*. Could there be an increase in the number of POMC neurons through postnatal development and the majority of these new cells express *Gad67* but not *Vglut2*, leading to the measured increase in the proportion of *Gad67*POMC neurons?

In a recently published manuscript [53], our group crossed *Vglut2*-ires-Cre and lox-tdTomato mice to create our own lineage trace of all *Vglut*$^{+}$ cells. We then used IHC for POMC to identify overlap with the tdTomato reporter, and found that ~47% of all POMC neurons were

also tdTomato-positive. This result sits in stark contrast to the ~10% overlap reported by Vong et al. [47] using IHC for surrogates of both markers. We then crossed the Vglut2-ires-Cre animals to Cre-reversible *Pomc*-KO mice [54-57] to test whether glutamatergic POMC neurons serve a distinct role in maintaining energy homeostasis. However, we found that there was complete normalization of the obesity phenotype exhibited by neuron-specific *Pomc*-null animals, Arc *Pomc* mRNA expression and POMC immunoreactivity in 12 week old male and female animals. Dual label in situ was also performed as described [49] for *Pomc* and *Vglut2* or *Gad67* in a subset of these animals, and unexpectedly, a high proportion of *Gad67/Pomc* neurons was found in these mice that were expected to be *Pomc*-null in non-glutamatergic cells. Furthermore, in both the *Pomc*-restored mice and in control mice the cumulative total of glutamatergic- and GABAergic-*Pomc* cells exceeded 100%, indicating that there must be *Pomc* neurons that express both *Vglut2* and *Gad67* mRNA. Dennison et al. [52] also reported the presence of the dual neurotransmitter phenotype *Pomc* neurons at three postnatal time points, but there were few such cells (Postnatal day 1: ~10%, 3 weeks: ~8%, and 5 weeks: ~7%).

At this point we were faced with a conundrum. On the one hand, based on the lineage trace results, all POMC neurons cannot have expressed *Vglut2*. Yet on the other hand, restoring *Pomc* expression via constitutive *Vglut2*-ires-Cre almost completely normalized the *POMC* neuron architecture, including the GABAergic compartment, indicating that all of these *Pomc* neurons had to have expressed *Vglut2* at some point in their development. We were forced to conclude that the neurons expressing *Pomc* from the *Vglut2*-ires-Cre restoration must have undergone an atypical developmental program, wherein the POMC neurons transitioned from a glutamatergic to a GABAergic phenotype at a frequency greater than occurs in wildtype mice. The mechanism underlying the transdifferentiation is unknown, but it highlights the potential for

POMC neurons to exhibit flexibility in their fast neurotransmitter identity. To follow up on the inferred dual phenotype POMC neurons and assess their abundance and location, we performed triple label ISH for *Pomc*, *Vglut2* and *Gad67* throughout the rostral-caudal extent of the Arc in wildtype C57BL/6J male mice. We found that ~35% of *Pomc* neurons express *Gad67*, ~21% express *Vglut2*, ~38% express both *Gad67* and *Vglut2*, and ~7% express neither *Vglut2* nor *Gad67*. Additionally, there was a striking pattern in the rostral-caudal distributions of the four *Pomc* cell subtypes, with the greatest abundance of the *Vglut2/Pomc*, *Gad67/Pomc*, and *Pomc*-only cells located toward the rostral Arc, with very little expression in the caudal Arc. In contrast, dual phenotype *Vglut2/Gad67* POMC neurons predominated in the caudal Arc with very few located in the rostral Arc.

It is a common oversimplification to categorically label glutamate as an excitatory and GABA as an inhibitory neurotransmitter in the CNS. However, without knowing the intrinsic membrane properties of the postsynaptic cells and their receptor and ion transporter composition we cannot blindly label the presynaptic neurons as either excitatory or inhibitory based on their expression of markers characteristic for the biosynthesis and vesicular packaging of glutamate or GABA. GABA has been shown to be excitatory in the developing CNS [58], in the regulation of adult GNRH neuronal activity [59], and in adult vasopressin neurons in the hypothalamus [60]. Additionally, unlike ionotropic glutamate and NMDA receptors, Group 2 and 3 metabotropic glutamate receptors are primarily inhibitory in response to their engagement by glutamate. Furthermore, as pointed out earlier, there appears to be an almost complete lack of *Vgat* in POMC neurons [47, 48] raising the mechanistic question of which components mediate their vesicular storage and release of GABA?

Posttranslational processing of POMC produces α-MSH and β-End, which pharmacologically inhibit and initiate feeding, respectively.

Most of the actions attributed to POMC neurons or POMC peptides are rooted in MCR signaling, specifically to α-MSH, despite the fact that the amount of β-End present outweighs α-MSH almost 4:1 [61]. Melanocortin and opioid signaling have been studied in many functional and behavioral contexts. However, for the sake of this chapter I will only discuss findings concerning motivated-, consummatory-, and maintenance-behaviors, metabolism, and the regulation of body composition. Neither the use of genetic knockout models nor pharmacological studies alone are ideal ways to gain an understanding of the mechanistic underpinnings for any physiological process. The majority of genetic knockouts are constitutive and the resultant animals have undoubtedly gone through an atypical developmental program, which can drastically shape how any system normally functions in the adult state. Pharmacological studies rarely stay within the confines of physiological ranges of endogenous ligands, nor do they adhere to the same temporal kinetics (Tables 1.2 and 1.3).

PHARMACOLOGICAL ANALYSES OF THE CENTRAL MELANOCORTIN AND B-END SYSTEMS

MCR agonists and/or antagonists

Pharmacological experiments focused on MCR function have utilized full-length synthetic α-MSH or AgRP, or modified versions of those peptides, the synthetic agonists Melanotan II (MTII) and [Nle4,D-Phe7]-α-MSH (NDP-MSH), or the synthetic antagonists SHU9119, HS014 and HS131. Typically, agonism of central MCRs leads to suppression of

feeding, while inverse agonism or antagonism by AgRP leads to food-seeking and initiation of feeding. Furthermore, a larger dose of an antagonist preceding or co-administered with an agonist prevents or at least mitigates the agonistic effect. The studies referenced here utilize intracerebroventricular (ICV) administration of pharmacological agents or local microinfusion via cannulation into the paraventricular nucleus of the hypothalamus (PVH), dorsomedial hypothalamus (DMH), medial preoptic nucleus (MPO), central nucleus of the amygdala (CeA), ventral tegmental area (VTA), or anterior hypothalamus (AH).

The majority of findings that define our understanding MCR signaling have used synthetic peptides. However, α-MSH is considered dogmatically to be the principal POMC peptide delivering an anorectic signal even though there are only a handful of demonstrated examples of α-MSH itself reducing or preventing food intake. Among those studies it was demonstrated that ICV infusion of α-MSH suppressed refeeding and increased plasma corticosterone in fasted male rats, prevented κ-opioid receptor agonist induced feeding and reduced normal dark cycle feeding [62-66].

In fasted male mice, ICV administration of MTII potently suppresses immediate food intake for several hours before feeding behavior is normalized several hours later; an effect that is blocked by co-administration of SHU9119. Central administration of SHU9119 alone in mice fed *ad libitum* stimulates feeding for up to 24 hours [67]. Similar effects were reported for male rats, albeit using much lower drug doses [68, 69]. Likewise, ICV injection of MTII in male rats decreased overnight food consumption and infusion of SHU9119 increased overnight feeding, both in a dose-dependent manner. Co-administering equal doses of both drugs netted no effect, while a molar excess of MTII decreased overnight feeding and a molar excess of SHU9119 increased feeding. Additionally, moderate ICV doses of MTII were able to attenuate the effect of

NPY-induced feeding [70, 71]. ICV infusion of MTII decreases meal size and duration without affecting meal frequency, whereas infusion of SHU9119 increases meal size without impacting meal frequency or duration [72-74]. These data suggest that the melanocortin system preferentially alters satiation rather than appetite per se. ICV infusion of NDP-MSH suppressed fasting-induced refeeding for at least 8 hours. Although co-administration of β-End(1-31) blocked this effect for the first several hours, there was still a marked reduction in food intake over the last several hours. Chronic treatment with NDP-MSH decreased body weight, food intake, and circulating leptin levels. Treatment with NDP-MSH and β-End(1-31) also led to decreased food intake, body weight, fat pad mass, leptin and insulin levels, and Arc prolylcarboxypeptidase expression, while increasing *Agrp* expression [75]. Despite the potency of central MCR stimulation, entrainment to scheduled feeding or exposure to HFD attenuated the anorexigenic effects centrally administered MTII [76, 77].

Following MTII infusion, marked increases in cfos-like signal were observed in the PVH, SON, CeA, AP, and PBN [78]. A similar pattern of cfos-like immunoreactivity was also observed following ICV administration of α-MSH [65]. Like infusion of MTII, ICV treatment with NDP-MSH in male rats attenuated feeding behavior for 24 hours, and was also dose-dependently able to suppress NPY-induced feeding. Following ICV NDP-MSH infusion, strong cfos-like immunoreactivity was observed in the CeA, dorsal striatum, PVH, and lateral septum [79]. Interestingly, cfos-like immunoreactivity was also detected in the NAcS, lateral septum, PVH, CeA, BLA, Arc, and LH, 24 hours following ICV infusion of AgRP (83-132) [80, 81].

In fasted male rats, direct infusion of MTII into the PVH strongly suppressed feeding for several hours, and a slight reduction in food intake was still evident for 24 hours. Conversely, direct infusion of SHU9119 into the PVH intensely stimulated feeding in *ad libitum* fed rats for

24 hours [82]. Furthermore, site specific unilateral application of AgRP(83-132) in the PVH, DMH, MPO, CeA, and AH also initiated feeding in fed male rats [83]. Electrophysiological recordings from the PVH-containing slices showed that application of MTII or α-MSH potentiated the amplitude of evoked IPSCs, while application of SHU9119 did nothing to IPSC amplitude on its own, but blocked MTII-induced potentiation [68].

ICV administration of α-MSH in male rats led to massive increases in yawning, stretching, grooming, and penile erections, all of which were mitigated by co-treatment with HS014 [66]. These effects were also elicited following unilateral microinjections of α-MSH into the PVH, DMH, VMH, or AH, and were also blocked by pretreatment with HS014 [84]. Furthermore, α-MSH administration in the VTA leads to an increase in grooming, rearing, and locomotive behavior, as well as an increase in NAc DA release and DOPAC levels, effects that are blocked by co-administration of HS131 [85-87]. ICV infusion of NDP-MSH increased mean arterial pressure and induced grooming behavior [88]. ICV infusion of MTII robustly increased sympathetic nerve activity (SNA), whereas SHU9119 treatment did not affect basal SNA, but prevented the MTII-induced excitation [89]. The behavioral impacts of central MTII infusion have been reported for up to 48 hours, and when the MTII was administered following intraoral infusion of saccharin the animals developed a conditioned taste avoidance akin to pairing saccharin with lithium chloride. Yet, ICV infusion of MTII augmented the rewarding effect of amphetamine-induced LH self-stimulation, while infusion of SHU9119 had no effect [90]. Additionally, peripheral, ICV, LH, NAc, or VTA administered MCR agonist decreased ethanol consumption [91, 92].

Cfos-like expression following central MCR agonist administration suggests that MCRs alter behavior primarily through activation of the PVH, CeA, SON, PBN, AP, dorsal striatum,

and lateral septum. Yet local infusion into the DMH, VMH, AH, and VTA was sufficient to drive changes in behavior, despite no notable increases in fos-like expression after central infusion. This can reflect one of several scenarios: due to internuclear connectivity MCR-mediated activation of one area can inhibit other connected targets, superceding the effects of direct activation; MCR-agonism at these targets does not actually lead to neuronal activation at all of the sites; or there is activation at the target sites, just not sufficient to induce nuclear cfos-like signal or that there was signal but it was either not reported or not different from control conditions.

MOR agonists and/or antagonists

In addition to β-End, endogenous enkephalins and endomorphins activate MOR signaling. This overlap complicates the attribution of phenotypic data from manipulation of MOR activity solely to endogenous β-End. Pharmacological experiments studying MOR function have typically utilized the agonists morphine, DAMGO ([D-Ala2, N-MePhe4, Gly-ol]-enkephalin) and β-End, as well as the antagonists naloxone, naloxonazine, naltrexone and the irreversible MOR and DOR antagonist β-funaltrexamine (β-FNA). In general, agonism of MORs initiates feeding behavior while antagonism prevents feeding.

Similar to MCR agonism with α-MSH, the majority of MOR agonist studies have used exogenous compounds rather than β-End itself. In *ad libitum* fed male rats, ICV infusion of β-End initiated food intake; pretreatment with a lower molar dose of naltrexone augmented this effect, whereas higher doses of naltrexone mitigated food intake. Pretreatment with β-FNA or MTII also suppressed β-End-induced feeding [62, 93, 94].

In fasted male rats, peripheral injection of a high dose of morphine suppressed refeeding, while low doses in *ad libitum* fed animals induced feeding [95]. In *ad libitum* fed male rats, bilateral infusion of morphine or DAMGO into most striatal targets, the VTA or PVH initiated feeding, although the strongest striatal feeding responses were elicited by infusion into the NAc and ventromedial striatum (VMS) [96-99]. Bilateral DAMGO infusion into the NAcS and VTA initiated feeding, which was blocked by pretreatment with β-FNA, naltrexone, or naloxone [98, 100, 101]. NAcS-DAMGO-induced feeding can be potentiated by pretreatment with the $GABA_A$ antagonist bicuculline, while NAcS-bicuculline alone was not different than vehicle treatment, and NAcS-saclofen ($GABA_B$ antagonist) pretreatment prevented the DAMGO-induced feeding. NAcS infusion of either muscimol ($GABA_A$ agonist) or baclofen ($GABA_B$ agonist) on their own also induces feeding comparable to DAMGO infusion [102]. In fasted mice, microinfusion of naloxone into the NAc, VTA, or LH suppressed refeeding for a couple of hours [103].

Feeding was also induced in *ad libitum* fed male rats by microinfusion of DAMGO into the NAcC, but could be blocked by infusion of muscimol into the LH, VTA, or NTS. Paradoxically, muscimol infusion in the DMH with NAcC DAMGO reduced the feeding response, yet DMH muscimol without NAcC DAMGO initiated feeding [104]. NAcS- or VTA-DAMGO-induced feeding can also be blocked by bilateral microinfusion of naltrexone or SCH 23390 (dopamine receptor 1 antagonist) in the other target region, but not by raclopride (dopamine receptor 2 antagonist) [105, 106]. NAcS-DAMGO-induced feeding can also be blocked by ICV administration of MTII [107]. Furthermore, naloxonazine infusion in the VTA prevented the NAc DA release that is normally observed upon the presentation of food following a fast or the presentation of palatable food [108]. Bilateral DAMGO microinfusion into the CeA initiates feeding as well, which can be blocked by bilateral infusion of naltrexone into the NAcS

or PVH. The reversal of the drug pairings between the CeA and NAcS also yields the same results, while naltrexone infusion in the CeA can also prevent NAcS-DAMGO-induced feeding [109]. However, naltrexone infusion in the CeA had no effect on PVH-DAMGO-induced feeding, but was able to prevent PVH-NPY-induced feeding [99]. Additionally, bilateral infusion of DAMGO into the CeA of sign-tracker and goal-tracker rats potentiated each respective behavior, indicating that opioid action in the CeA can increase the salience of pre-existing motivators [110].

In *ad libitum* fed male rats, peripheral naloxone treatment reduced ICV AgRP- or orexin-induced feeding [111, 112]. Long-term treatment with naltrexone in male rats reduced α-MSH and β-End peptide levels without impacting *Pomc* mRNA expression [113]. In another study using *ad libitum* fed male rats, repeated morphine treatment over several days lowered Arc *Pomc* expression; while naloxone treatment increased Arc *Pomc* expression [114].

Anghel et al. treated 12-16 week old male mice with morphine for either 6 hours or 4 days and assessed gene expression in the hypothalamus and the pituitary (microarray & qRT-PCR). Mice treated with morphine for 4 days exhibited symptoms of opioid abstinence withdrawal. Following 6-hour morphine treatment, *Npy* and *Agrp* were upregulated. Following 4-day treatment *Npy*, *Npyr1*, *Agrp*, and *Lepr* were upregulated, and *Cpe*, *Adiponutrin (PNPLA3)* and *Pomc* were downregulated. The 4-day morphine treated animals exhibited substantially decreased food intake for the first 2 days with concomitant weight loss. The 4-day morphine treatment also led to an increase in NPY, AgRP, CART, and α-MSH peptide contents in the hypothalamus [115].

GENETIC ANALYSES OF THE CENTRAL MELANOCORTIN AND β-END SYSTEMS

Global POMC KO mice

The first reported *Pomc* knockout (*Pomc*$^{-/-}$) mice taught us a lot about the potential ramifications that POMC-derived peptides can impart on the overall physiological function of a mammal. However, there was a major caveat to interpreting the results using these mice because of the problem distinguishing between the effects of neuronal vs. pituitary *Pomc*-deficiency. These mice do have an obesity phenotype, but they are also compromised by adrenal insufficiency secondary to the lack of corticotroph ACTH production needed to elicit corticosterone release. These mice have elevated fat and lean mass, longer body length and eat more chow compared to littermate controls. They also display blunted responses to leptin, ghrelin and AgRP, but are hypersensitive to α-MSH and retain normal sensitivity to Peptide YY (PYY) [116-118]. Despite their obese phenotype, *Pomc*$^{-/-}$ animals display primary hyperthyroidism with elevated plasma thyroxine (T4) and triiodothyronine (T3) levels, but suppressed pituitary thyroid stimulating hormone (TSH) and hypothalamic thyrotropin releasing hormone (TRH) [119]. *Pomc*$^{-/-}$ mice also have elevated hypothalamic *Cartpt* but reduced *Agrp* mRNA expression compared to wildtype controls [118]. Table 1.3 contains a summary of all the mouse models discussed. Strangely, double knockouts generated from crossing *Pomc*$^{-/-}$ mice to *Agrp* knockout mice, were not any different phenotypically than single *Pomc*$^{-/-}$ mice [120].

Neuron-specific POMC KO mice

Significant strides were made in dissociating the role of neuronal- from pituitary-POMC function when the first neuron specific *Pomc* KO mice (Arc*Pomc*$^{-/-}$) were made. They were generated through the intercross of global *Pomc*$^{-/-}$ mice with mice that re-express a *Pomc* rescue

transgene selectively in the pituitary gland (*Pomc*$^{-/-}$; *Tg*$^{+}$) and other peripheral tissues including the placenta, thereby restoring normal ACTH and corticosterone production [118, 121, 122]. A few years later, further refinement and elegance in achieving Arc*Pomc*$^{-/-}$ mice emerged through the genetic deletion of neural *Pomc* enhancers nPE1 and nPE2 by homologous recombination in mouse ES cells, avoiding the use of the global *Pomc*$^{-/-}$ model. In the process of generating the different permutations of nPE1 and nPE2 knockout mice characterized by Lam et al. [16], three mouse lines were created that retained a floxed neomycin-resistance cassette (FNeo), which aided clonal ES cell selection. The three lines are comparably obese mice and essentially devoid of neuronal POMC production in the Arc. In the first two lines, the FNeo cassette was inserted upstream of the deleted nPE1 with or without the deletion of nPE2 to yield FNΔ1Δ2 and FNΔ1 mice, respectively. In the third line, the FNeo cassette was inserted immediately upstream of the deleted nPE2 with an intact nPE1 to yield FNΔ2 mice. Because of the paired loxP recombination sites in the FNeo cassette, exposure to Cre results in excision of FNeo from the genome, and converts FNΔ2 to Δ2 mice. The latter mice exhibit ~80% of wildtype *Pomc* expression directed by the intact nPE1. They also contain normal α-MSH and β-End levels in the hypothalamus [16]. For all intents and purposes, *Pomc*$^{-/-}$; *Tg*$^{+}$, FNΔ1Δ2, FNΔ1 and FNΔ2 mice develop essentially the same post-weaning massive obesity phenotype, with the exception that only FNΔ2 mice can undergo Cre-mediated restoration of eutopic POMC function.

The first obvious difference between Arc*Pomc*$^{-/-}$ and the global *Pomc*$^{-/-}$ mice was greater weight gain in the former with almost two-fold more fat mass than the *Pomc*$^{-/-}$ mice. In addition, food intake was substantially more in Arc*Pomc*$^{-/-}$ mice compared to *Pomc*$^{-/-}$ mice (~50% vs ~25% more food, respectively, than their control littermates) [54, 57, 121, 122]. Interestingly, a meal pattern analysis of the Arc*Pomc*$^{-/-}$ mice showed that they actually spend less time eating

with larger but fewer meals than littermate controls [122]. The Arc*Pomc*$^{-/-}$ mice were also hyperinsulinemic with more than twice as much circulating insulin than *Pomc*$^{-/-}$ mice and around four times more than the control groups [57, 121]. Arc*Pomc*$^{-/-}$ mice have a blunted feeding response to AgRP, but are still more sensitive to AgRP than the *Pomc*$^{-/-}$ mice [118]. They do not display reductions in food intake or body weight in response to acute leptin administration, even when weight matched to wildtype controls indicating the development of leptin resistance [57]. Counterintuitively, Arc*Pomc*$^{-/-}$ mice display improved glucose tolerance despite their obesity. This observation was associated with a large decrease in the renal threshold for glycosuria from ~400 to ~200 mg/dL resulting in excessive glycosuria, all caused by a ~50% reduction in renal sympathetic nerve activity [123]. In addition, Arc*Pomc*$^{-/-}$ mice have an impaired hypoglycemic counterregulatory response manifested by inadequate acute glucagon and norepinephrine release [124].

We used a ubiquitously expressed tamoxifen-inducible Cre mouse line crossed to FNΔ2 mice, to restore eutopic *Pomc* expression at different postnatal time points throughout progression of their obesity phenotype. Intervention right after weaning and before the onset of obesity, or in combination with chronic food restriction starting at age 4-weeks to prevent the development of obesity resulted in maintenance of a normal body weight trajectory and energy balance throughout life. Restoration early in the obesity progression led to an attenuation of food intake and adiposity, both of which were then maintained. However, tamoxifen treatment of severely obese FNΔ2 mice led to only a mild reduction in adiposity and the animals were never able to achieve normal body weight [54]. Further experiments demonstrated that the magnitude of circulating leptin levels at the time of *Pomc* restoration, regardless of a history of obesity, is the critical factor in establishing the complete reprogramming of the body weight trajectory to

wildtype levels [57]. While Arc*Pomc*$^{-/-}$ mice clearly distinguished between the roles of pituitary and hypothalamic POMC for whole body metabolism, it remains difficult to completely attribute any of their phenotypes to a selective disruption of either MCR- or MOR-specific signaling.

MC4R KO mice

Like the Arc*Pomc*$^{-/-}$ animals, there are multiple genetic models that have been used to study MC4R deficiency, including a constitutive *Mc4r* KO mouse and an inducible mouse with a floxed-stop cassette preventing *Mc4r* transcription, which can be deleted by tissue-specific expression of Cre recombinase. *Mc4r* KO mice invariably become obese when housed with ad libitum access to food, but their maximum weight falls below that of age-matched Arc*Pomc*$^{-/-}$ mice. Mc4r KO mice are hyperinsulinemic and hyperglycemic [125-129]. Meal pattern analysis of these mice showed that they eat the same number of meals with the same meal length, intermeal interval, and eating rate as their wildtype littermates. The only parameter that differs is ingestion of larger nocturnal meals [130, 131]. In contrast to Arc*Pomc*$^{-/-}$ mice, *Mc4r* KO mice do not appear to have any deficits in sympathetic nerve activity, consistent with their impaired glucose tolerance [132]. However, comparison of the GTT data is difficult due to methodological differences in the assays used. The Arc*Pomc*$^{-/-}$ mice were administered a fixed dose of glucose by oral gavage, regardless of body weight, whereas the *Mc4r* KO mice were given 1 gram of glucose per kg of bodyweight by intraperitoneal injection [123, 132]. Finally, in several behavioral assays used to measure the valence of stimuli, *Mc4r* KO mice typically showed either a preference or indifference for stimuli that elicited strong aversions in wildtype control mice, which could be reversed by treatment with dopamine receptor 1 agonists during training [133].

MC3R KO mice

Mc3r KO mice do not exhibit the overt phenotypes that are present in *Pomc*$^{-/-}$ or Arc*Pomc*$^{-/-}$ animals. However, they do exhibit late onset mild obesity despite less overall food consumption. They also have reduced energy expenditure and locomotor activity, but increased sensitivity to develop adiposity and adipocyte hypertrophy in response to a high-fat diet (HFD) [134-137]. Furthermore, when intercrossed to *Mc4r* KOs, the double receptor KO mice gain more weight than either of the individual mutants [135]. They display deficits in fasting-induced lipolysis and activation of the HPA axis [138]. Finally, adult female *Mc3r* KO mice have elevated midbrain dopamine and DOPAC levels [139, 140]. A recent report has conceptualized the functional role of the MCR3 as a rheostat that is required for metabolic responses to opposing homeostatic challenges, including either insufficient or excessive availability of calories. A potential mechanism for this function is the presynaptic inhibition of GABA release onto MC4R neurons located in the PVH [140].

β-End KO mice

The targeting vector to produce β-End KO mice was generated by editing a plasmid containing the entire *Pomc* gene and introducing a point mutation in exon 3 that introduces a premature stop codon and truncates the associated *Pomc* transcript at the β-End locus. Subsequently, this vector replaced the endogenous *Pomc* gene by homologous recombination in mouse ES cells [141, 142] (The Jackson Laboratory, B6.129S2-*Pomc*^{tm1Low}/J). Interestingly, the majority of phenotypic differences measured between β-End KO mice and their WT littermates are found only in male animals. They become mildly obese, reaching 15% greater body mass than their WT littermates, which is attributable to greater white adipose tissue mass. They also

have exacerbated weight gain when placed on a HFD. In the basal *ad libitum* state they are hyperinsulinemic, have decreased insulin sensitivity and impaired glucose tolerance and are hyperresponsive to orexigenic stimulation by NPY administration. They also show deficits in instrumental responding in a progressive ratio task that is normalized when the animals are challenged by chronic food restriction [143, 144]. β-End KO mice also display a severe aversion to approach and eat novel food following acute exposure to a stressor (3 min. forced swim) [145].

MOR KO mice

Similar to β-End KO animals, the majority of studies using MOR KOs have focused on analgesia or ethanol consumption. Unsurprisingly, these mice have impaired pain perception and are insensitive to the antinociceptive action of pharmacological agents targeting MORs [146-149]. Like *Mc3r* and β-End KOs, male MOR KO mice exhibit a late onset mild increase in body weight [150]. This is manifest through increased adiposity, which is greatest in males [151]. In contrast to β-End KO mice, MOR KOs are resistant to HFD-induced weight gain and they are not hyperinsulinemic [150]. There are differing reports on glucose tolerance in these mice. Tabarin et al. [152] reported that they have improved glucose tolerance while Han et al. [150] stated that there is no difference. Zuberi et al. [151] indicated that the male animals exhibit impaired glucose tolerance but found no difference for the females. Despite the sex differences, both results are counterintuitive to what would be expected from loss of a peptide that stimulates feeding. The fact that these animals are not leaner than wildtype animals suggests that β-End signaling through MORs aids in the initiation of feeding, but is not necessary for this behavior. In males, this signaling provides necessary feedback to keep orexigenic circuits in check.

MOR KO mice also have impaired operant performance, regardless of the trained response, reinforcer used or schedule of reinforcement. They voluntarily drink less and nosepoke less for ethanol [153, 154], they nosepoke less for chow and sucrose pellets and have a lower breakpoint for each reinforcer in progressive ratio tests [155] and they have diminished licking responses for sucrose or sucralose solutions even in a food deprived state [156]. MOR KO mice have decreased conditioned place preference for ethanol [154] or cocaine [157]. Yet, they display heightened amphetamine- [158] and cocaine-induced [157] locomotor activity. MOR KO mice also display atypical food anticipatory behavior, or at least a deficit in entrainment to a fixed 3-hour daily food access schedule, where they are hypo-locomotive prior to food access and hyper-locomotive during food access compared to wildtype animals [158]. MOR KO mice have deficits in Morris water maze performance including longer latencies to learn and remember the location of the escape platform [159]. Male MOR KO mice also exhibit substantial deficiencies in mating behavior with struggles to mount, intromit, and successfully impregnate females. When successful, their litters are smaller. They also have lower sperm counts and reduced sperm motility [160]. Finally, male MOR KO animals express more than two-fold times as much whole-brain *Npy* mRNA that is especially evident in the Arc [150].

An interesting point of comparison can be drawn between the studies conducted by Appleyard et al. [143] and that of Smart et al. [121] In the former study, the researchers included a panel of data based on a genetic intercross of β-End KO with MC4R KO mice and reported a massive increase in food intake in the double KOs compared to either of the individual KO lines or WT mice. Unfortunately, these were the only data reported from the double KO animals. Yet, perhaps it was foretelling of what would be found several years later from the first study to produce neuron-specific POMC KO mice, because these mice exhibited an almost identical

increase in food intake to that observed in all of the Arc*Pomc*$^{-/-}$ animals. Given the findings using the FNΔ2 animals [54, 57] to identify body weight set point reprogramming through restoration of *Pomc* expression and management of circulating leptin levels, the question remains whether the ability to achieve the reprogramming is mediated through both MCRs and/or MORs? The double KO cross used by Appleyard et al. [143] may be the closest data to start addressing that distinction. With a minor substitution, it would be straight-forward to substitute the MC4R-loxTB mice introduced by Balthasar et al. [127] for the constitutive MC4R KO mice. The MC4R-loxTB mice could then be crossed to a ubiquitous tamoxifen-inducible CreERT2 line and the constitutive β-End KO mice. The resulting mice should become massively obese with metabolic deficiencies similar or identical to those observed in the neuron-specific POMC KO animals. However, in this triple cross tamoxifen administration would restore eutopic Mc4R expression with an expected result of partial restoration of body weight trajectory set-point. Granted this is still an imperfect model, because AgRP function might be affected secondarily and any measured effects following restoration of MC4R expression could not be attributed solely to POMC-derived melanocortin peptide signaling via MC4Rs.

Ultimately, in order to fully understand and piece together the complexities of the efferent POMC neuron signals with the location and signaling of their cognate receptors will necessitate undertaking a continuing effort to query both the ligand release sites and their pre- and postsynaptic targets.

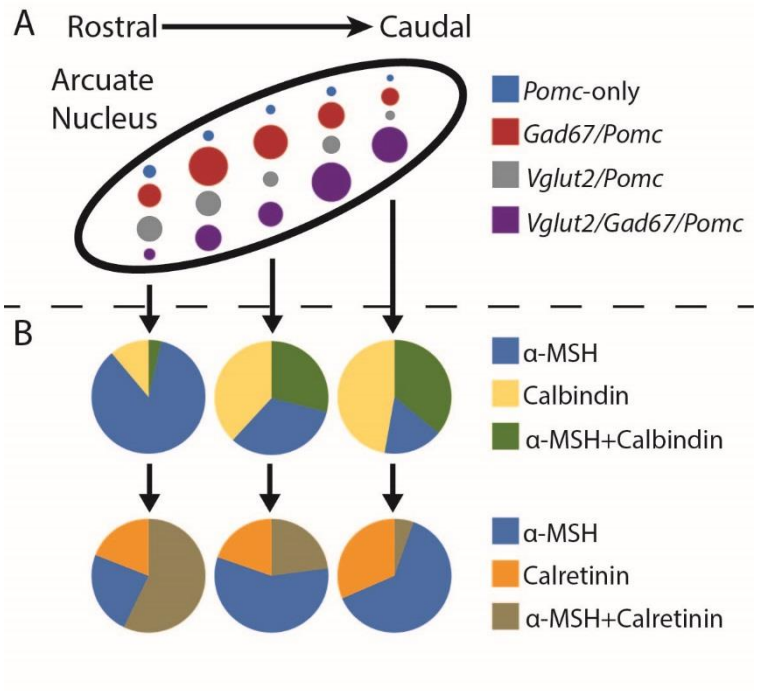
A
Rostral
Caudal
Arcuate
Nucleus
Pomc-only
Gad67/Pomc
Vglut2/Pomc
Vglut2/Gad67/Pomc
B
α-MSH
Calbindin
α-MSH+Calbindin
α-MSH
Calretinin
α-MSH+Calretinin

Fig 1.1: Schematic of POMC neuron heterogeneity along the rostral-caudal Arc axis. (adapted from Jones et al. [53] and Foo, Hellysaz, & Broberger [161]). **A.** Triple-label ISH for *Pomc*, *Vglut2*, and *Gad67* showed distinct differences in the representation and overlap of the markers at five positions along the rostral-caudal Arc axis in the mouse hypothalamus. *Gad67/Pomc* and *Vglut2/Pomc* neurons were most abundant in the rostral Arc, whereas *Vglut2/Gad67/Pomc* neurons predominated in the caudal Arc. The size of the circles represents the relative abundance of each in the total measured *Pomc*-population. **B.** In another example of POMC neuron identity varying throughout the Arc, double-label IHC for α-MSH and calbindin or calretinin in rat neural tissue also showed distinct changes in the abundance and colocalization of the signals across the rostral-, mid- and caudal-Arc.

Table 1.1: Reported GABA and/or glutamate identities attributed to POMC neurons

Method	GABA	Glutamate	GABA + Glutamate	Reference
Electrophysiology	69%	23%	8%	[46]
Dual-label ISH	35%			[44]
	54%	43%		[49]
	65%	56%		[53]
Dual reporter expression	42%			[45]
IHC for reporter expression	< 1%	10%		[47]
ISH + IHC for reporter expression	10%			[48]
	38%			[48]
	45%			[48]
		7%		[48]
IHC + reporter expression		47%		[53]
Triple-label ISH	35%	21%	38%	[53]

Table 1.2: Pharmacological agents used in discussed studies

Drugs	
DAMGO	[D-Ala2, N-MePhe4, Gly-ol]-enkephalin; MOR agonist
HS014	MC4R antagonist
HS131	MC4R antagonist
Morphine	MOR agonist
MTII	melanotan II; MC3/4R agonist
Naloxonazine	MOR antagonist
Naloxone	MOR antagonist
Naltrexone	MOR antagonist
NDP-MSH	[Nle4,D-Phe7]-α-MSH; MC3/4R agonist
Raclopride	dopamine receptor 2 antagonist
SCH23390	dopamine receptor 1 antagonist
SHU9119	MC3/4R antagonist
β-FNA	beta funaltrexamine; MOR antagonist

Table 1.3: Behavioral findings from pharmacology studies

Primary Action	Location	Effect	Reduced by	Location	Reference
MC3/4R Agonism	ICV	Decreased feeding	MC3/4R antagonist	ICV	[62-69, 79]
			MOR agonist	ICV	[75]
		Yawning, stretching, grooming, and penile erections	MC4R antagonist	ICV	[66, 88]
	PVH	Decreased feeding			[82]
	PVH	Yawning, stretching, and grooming	MC4R antagonist	PVH	[66]
	DMH	Yawning, stretching, and grooming		DMH	[66]
	VMH	Yawning, stretching, and grooming		VMH	[66]
	AH	Yawning, stretching, and grooming		AH	[66]
	VTA	Grooming, rearing, and locomotion		VTA	[85-87]
MC3/4R Antagonism	ICV	Increased feeding	MC3/4R agonist	ICV	[67, 70, 71]
			MOR antagonist	IP	[80]
	PVH	Increased feeding			[82, 83]
	DMH	Increased feeding			[83]
	MPO	Increased feeding			[83]
	CeA	Increased feeding			[83]
	AH	Increased feeding			[83]
MOR Agonism	ICV	Increased feeding	MOR antagonist	ICV	[62, 93]
			MC3/4R agonist	ICV	[94]
	PVH	Increased feeding			[99]
	VTA	Increased feeding	MOR antagonist	VTA	[101]
				NAc	[105]
			D1R antagonist	NAc	[106]
	NAc	Increased feeding	MOR antagonist	NAc	[96, 97, 100]
				VTA	[105]
				CeA	[109]
			MC3/4R agonist	ICV	[107]
			$GABA_B$ agonist	NAc	[102]
			$GABA_A$ agonist	LH	[104]
				VTA	[104]
				DMH	[104]
				NTS	[104]
			D1R antagonist	VTA	[106]
	VMS	Increased feeding			[96, 97]
	CeA	Increased feeding	MOR antagonist	PVH	[99, 109]
				NAc	[109]
MOR Antagonism	NAc	Decreased feeding			[103]

	VTA	Decreased feeding			[103]
	LH	Decreased feeding			[103]

The table is organized by the primary action of the pharmacological agent, where it was administered and the behavioral impact, other drugs that attenuated the primary effect and where they were administered.

Table 1.4: Observed phenotypes from the different mouse lines discussed

Mice	Phenotypes	Reference
Pomc$^{-/-}$	obesity, adrenal insufficiency, increased body length, hyperthyroidism, blunted response to leptin, ghrelin, and AgRP	[116-119]
Arc*Pomc*$^{-/-}$	extreme obesity, larger meal size, hyper-insulinemic, -leptinemic, improved glucose tolerance, impaired hypoglycemic counterregulatory response, reduced renal SNA	[16, 54, 57, 118, 121-124]
Mc4r KO	extreme obesity, larger meal size, hyper-insulinemic, -leptinemic, and -glycemic, maybe impaired glucose tolerance, abnormal valence attribution reversed by D1R agonism	[125-133]
Mc3r KO	mild obesity, decreased food consumption, reduced energy expenditure, increased sensitivity to HFD-induced adipocyte hypertrophy, deficits in fasting-induced lipolysis and HPA axis activation, elevated midbrain DA and DOPAC levels	[134-140]
β-End KO	mild obesity, increased sensitivity to HFD-induced weight gain, hyperinsulinemic, decreased insulin sensitivity, impaired glucose clearance, decreased motivation to earn food, abnormal stress and feeding interaction	[141-145]
MOR KO	impaired pain perception, mild obesity, impaired operant performance for ethanol or sucrose, decreased conditioned place preference for ethanol or cocaine, increased amphetamine- or cocaine-induced locomotor activity, impaired food anticipatory behavior, spatial memory deficits, deficiencies in mating behavior, most phenotypes are stronger in males than females	[146-160]

CHAPTER II

Selective restoration of Pomc expression in glutamatergic POMC neurons: Evidence for a dynamic hypothalamic neurotransmitter network[1]

Abstract

Hypothalamic proopiomelanocortin (POMC) deficiency leads to obesity and metabolic deficiencies, largely due to the loss of melanocortin peptides. However, POMC neurons in the arcuate nucleus (ARC) are comprised of glutamatergic and GABAergic subpopulations. The developmental program, relative proportion and function of these two subpopulations are unresolved. To test whether glutamatergic POMC neurons serve a distinct role in maintaining energy homeostasis, we activated *Pomc* expression Cre-dependently in *Vglut2*-expressing neurons of mice with conditionally silenced *Pomc* alleles. The *Vglut2-Pomc* Restored mice had normal ARC *Pomc* mRNA levels, POMC immunoreactivity, as well as body weight and body composition at age 12 weeks. Unexpectedly, the cumulative total of glutamatergic- and GABAergic-*Pomc* neurons exceeded 100% in both *Vglut2- Pomc* Restored and Control mice, indicating that a subpopulation of *Pomc* neurons must express both neuronal markers.

[1] This work is published and performed in collaboration with the Lechan Lab at Tufts University. Gábor Wittmann performed the ISH, Eva Yokosawa measured weekly body weights and conducted genomic DNA PCR. DOI: https://doi.org/10.1523/ENEURO.0400-18.2019

Consistent with this hypothesis, triple in situ hybridization of C57BL/6J hypothalami revealed that 35% of ARC *Pomc* neurons were selectively *Gad67*$^{+}$, 21% were selectively *Vglut2*$^{+}$, and 38% expressed both *Gad67* and *Vglut2*. The single *Gad67*$^{+}$ and *Vglut2*$^{+}$ *Pomc* neurons were most prevalent in the rostral ARC, while the *Vglut2/Gad67*$^{+}$ dual-phenotype cells predominated in the caudal ARC. A lineage trace using Ai9-tdTomato reporter mice to label fluorescently all *Vglut2*-expressing neurons showed equal numbers of tdTomato^{+} and tdTomato^{-} POMC immunoreactive neurons. Together, these data suggest that POMC neurons exhibit developmental plasticity in their expression of glutamatergic and GABAergic markers, enabling re-establishment of normal energy homeostasis in the *Vglut2-Pomc* Restored mice.

Introduction

POMC-derived peptides are critical in maintaining energy balance and body composition, as well as in regulating feeding behavior. Neuronal *Pomc* dysfunction leads to morbid obesity, hyperphagia, hypolocomotion, and metabolic abnormalities [16, 54, 57, 162]. Evidence indicates that POMC neurons are comprised of both GABAergic and glutamatergic cells. However, little is known about the functional impact or genetic programs of these neuronal subclasses. Furthermore, there is not a consensus on the relative proportions of each POMC neuron subtype, due to differences in methodologies used to classify the cells [45-47, 49, 52].

Many studies have revealed plasticity in neurotransmitter identity or in neurotransmitter co-release. These phenomena are evident during development or in response to environmental stimuli, and span diverse cell groups and neurotransmitter types [163-177]. Work by Dennison et al. [52] uncovered a postnatal shift in the proportions of *Vglut2*$^{+}$ and *Gad67*$^{+}$ POMC neurons,

where the *Vglut2-Pomc* overlap was the highest (~40%) immediately after birth, but was reduced by 4-fold (~10%) when the animals had matured to 8 weeks old. The opposite temporal pattern was observed with *Gad67-Pomc* overlap. However, the mechanism of this shift in proportionality is unclear. One possibility is that POMC neurons are glutamatergic early in hypothalamic development and then transdifferentiate to a GABAergic phenotype in postnatal life. Alternatively, there may be a selective increase in the absolute number of de novo GABAergic POMC neurons that arise postnatally. There are also reports of some POMC neurons expressing both *Vglut2*$^{+}$ and *Gad67*$^{+}$, indicating the possibility of a shift between neurotransmitter phenotypes or the potential that a subset of POMC neurons can synaptically release both glutamate and GABA. Recent work from Stincic et al. [178] also indicates that POMC neurons can locally regulate the function of neuropeptide Y/agouti-related peptide neurons in the ARC via glutamatergic and β-endorphin input, expanding our functional understanding of melanocortin circuitry. Additionally, there are data indicating a partial dissociation between peptidergic and fast neurotransmitter synaptic terminals from POMC neuron projections at sites throughout the brain [179], further complicating the interpretation of the specific functions of these neurons.

This study was conceived initially to test the hypothesis that glutamatergic and GABAergic POMC neurons serve distinct and dissociable roles in overall POMC neuron function related to the maintenance of energy homeostasis. We chose to investigate the impact of selectively restoring *Pomc* function in the developing hypothalamus from a conditionally silent allele (FneoΔ2 mice) using a *Vglut2*-IRES-Cre knockin mouse model and then determine how restoration of *Pomc* expression only in the glutamatergic subpopulation of POMC neurons shapes hypothalamic POMC neural circuitry and impacts energy balance in the obesity-destined

mice. Additionally, we sought to capture the overlap between glutamate-associated neurons and hypothalamic POMC expression. We also used *Vglut2*-Cre driven reporter expression to create a lineage trace of all cells that have expressed *Vglut2* at some point in their existence to compare with POMC immunoreactivity. Finally, triple-label ISH was performed on wild-type tissue to establish the degree of overlap between *Pomc*, *Vglut2*, and *Gad67* gene expression in adult mice.

Materials and Methods

Animal Care

All animal procedures were performed in accordance with the University of Michigan IACUC regulations. Mice were housed under a 12-hour light/12-hour dark photoperiod at constant temperature of 22° C in ventilated cages with *ad libitum* access to water and chow (5L0D; LabDiet containing 28.5 kcal% protein, 13.5 kcal% fat, and 58.0 kcal% carbohydrates.

Mouse strains and breeding strategy

Ai9 tdTomato reporter mice (Allen Institute – The Jackson Labs; *Gt(ROSA)26Sor*$^{tm9(CAG\text{-}tdTomato)Hze}$) were crossed to *Vglut2*-ires-Cre/+ mice (The Jackson Labs; *Slc17a6*$^{tm2(cre)Lowl}$/J; [47]) to generate *Vglut2*-tdTomato compound mice for a developmental lineage trace of all neurons that have expressed the gene encoding the vesicular glutamate transporter Vglut2 at some point in their existence. Male (M) and female (F) mice were used in all experiments.

Arc*Pomc*$^{+/-}$ (ARC specific Cre-reversible *Pomc* KO or FneoΔ2) mice [54, 55, 57, 162] were crossed to *Vglut2*-ires-Cre$^{+/-}$ mice to obtain compound heterozygous Arc*Pomc* $^{+/-}$; *Vglut2*-ires-Cre$^{+/-}$ mice. Those mice were mated to Arc*Pomc* $^{+/-}$ mice to yield all control and

experimental groups for POMC restoration and ISH studies. These three groups were: *Vglut2*-ires-Cre$^{+/-}$; *Pomc*$^{+/+}$ (Control), +/+; Arc*Pomc*$^{-/-}$ (FNΔ2) and *Vglut2*-ires-Cre$^{+/-}$; Arc*Pomc* -/- (Restored). FNΔ2 animals have a floxed-neomycin cassette inserted between neural *Pomc* enhancer 1 (nPE1) and the deleted neural *Pomc* enhancer 2 (ΔnPE2) locus, which prevents the transcription of *Pomc* in neurons, while leaving pituitary transcription intact. After Cre-mediated excision of the floxed-neomycin cassette, neuronal *Pomc* transcription is restored.

Growth curves, body composition, and tissue collection

Mice were weighed weekly from ages 3-12 weeks. Body composition was assessed using nuclear magnetic resonance (NMR) at age 12 weeks. Following NMR, a cohort of animals was killed by decapitation; gonadal and inguinal fat pads were collected and weighed, and bilateral 2mm^3 tissue blocks were collected from the medial-basal hypothalamus (Coordinates from bregma; A-P: -1 to -3 mm, M-L: + or - 0 to 1 mm, and D-V: 0 to 1 mm from ventral surface) and the dorsal striatum (Coordinates from bregma; A-P: +1 to -1 mm, M-L: + or - 1 to 2 mm, and D-V: -2.5 to -3.5 mm from dorsal surface) for use in genomic DNA PCR and qRT-PCR. The brains used in the in situ hybridization (ISH) studies were collected at age 9-13 weeks, and fresh tissue was flash frozen using isopentane (2-methyl butane) cooled on dry-ice. Tissue used for immunohistochemistry (IHC) was collected from 12-13 week old mice, anesthetized with an overdose of 2% tribromoethanol (Avertin; 400mg/kg; intraperitoneal) and perfused transcardially with phosphate buffered saline (PBS; pH 7.4), followed by 4% paraformaldehyde (PFA; Sigma-Aldrich; CAT# 158127) dissolved in PBS (pH 7.4). Brains were post-fixed overnight in 4% PFA at 4° C, and then cryoprotected with 30% sucrose (ThermoFisher Scientific; CAT# BP220) in PBS (pH 7.4).

PCR verification of Cre-mediated genomic DNA recombination in Restored mice

Genomic DNA samples were extracted from one of the bilateral 2mm^3 blocks of fresh brain tissue described above. The samples were then analyzed by PCR using primers designed to detect the presence of the floxed neomycin cassette and the recombined DNA sequence following Cre-mediated excision of the neo cassette (Forward1: TACTTGGGCCTCAGGGTACTGAAA – 0.67mM; Forward2: TGGGGCTCGACTAGAGGAT – 0.67mM; Reverse: CCCATCCAGCTACAGCTGT – 0.67mM). 25 µL PCR reactions were set up using 5X Green GoTaq® Reaction Buffer (Promega; CAT# M7123), the aforementioned primers, the extracted DNA, BioReady rTaq DNA Polymerase (Bulldog Bio, CAT# BSA12L050), and nuclease-free water. The reactions were run using a touchdown protocol on a Peltier Thermal Cycler (MJ Research; PTC-100). The reaction conditions started with a 4 min. denaturing step at 94°C, followed by a 16 cycle touchdown, where each cycle starts with a 1 min. denaturing step at 94°C, followed by a 1 min. annealing step starting at 67°C and decreasing by 1°C each cycle, and a 1 min. extension at 72°C. Following the 16 touchdown cycles were 16 additional cycles structured in the same way, except that the annealing temperature was constant at 52°C. Thermal cycling terminated with a 10 min. extension step at 72°C, followed by holding at 4°C. PCR products were then run on a 2% agarose gel in TBE buffer. Gel images were processed in ImageJ to measure relative band intensity of the two PCR products. Recombined band intensities were quantified from neural tissue collected from the Restored mice as follows: (Recombined (287 bp) Product – Gel Background)/(Non-Recombined (180 bp) Product – Background). Quantified band intensities were compared between the medial-basal hypothalamus and the dorsal striatum of Restored mice, using a paired t-test.

RNA extraction, cDNA synthesis, and qRT-PCR

RNA was extracted from one of the bilateral 2mm^3 blocks of the medial-basal hypothalamus and analyzed for *Pomc* transcript expression using qRT-PCR. RNA was extracted from hypothalamic samples homogenized by trituration in 50 µL of TRIzol Reagent® (ThermoFisher Scientific – Ambion – Life Technologies; CAT# 15596). Following extraction, the RNA samples were treated with a TURBO DNA-*free*™ kit (ThermoFisher Scientific – Ambion – Life Technologies; CAT# AM1907) to remove residual genomic DNA. Then 500 ng of each RNA sample was converted to a 20 µL cDNA library using the GoScript™ Reverse Transcription System (Promega; CAT# A5000), after which the libraries were diluted 1:4 in nuclease-free water.

20 µL qPCR reactions were set up using 2x SYBR® Green PCR Master Mix (ThermoFisher Scientific – Applied Biosystems; CAT# 4309155), and *Pomc*- or *Ppia*-transcript primers, with 2 µL of diluted cDNA, and nuclease-free water. The *Pomc* primers were designed to span exons 2 and 3 of splice variant 1 (Forward: GAGCTGGTGCCTGGAGAG – 3nM; Reverse: TTTTCAGTCAGGGGCTGTTC – 3nM). The *Ppia* primers were designed to span exons 1 and 3 of all splice variants (Forward: CACCGTGTTCTTCGACATCA – 3nM; Reverse: CAGTGCTCAGAGCTCGAAAGT – 3nM). The reactions were performed in duplicate and loaded onto a MicroAmp® Fast Optical 96-Well Reaction Plate (ThermoFisher Scientific – Applied Biosystems; CAT# 4346906) and run on a StepOnePlus™ Real-Time PCR System (ThermoFisher Scientific – Applied Biosystems; CAT# 4376600). The reaction conditions started with a 10 min. denaturing step at 95°C, followed by 40 cycles of a two-step PCR protocol with a 15 sec. 95°C denaturing step and a 1 min. 60°C annealing step.

C_T values were determined by manually setting the threshold at 1, which was in the middle of the exponential phase of amplification for each sample. Baseline readings were automatically assessed by the StepOne™ Software (ThermoFisher Scientific – Applied Biosystems). Standard curves for each transcript were established by pooling equal amounts of cDNA from all control samples and making serial dilutions (1:1, 1:4, 1:16, 1:64, 1:256, and 1:1024). The percent dilution was Log_{10} transformed (e.g. 1:4 = 25% and $Log_{10}(25) = 1.398\%$) and plotted against its respective C_T value. The slope and y-intercept of the line formed between all of the dilutions were used to evaluate the relative Log_{10} copy number for each sample (i.e. Log_{10} copy number = [Sample C_T - Y Intercept]/Slope), which was then linearized. For each sample, the *Pomc* and *Ppia* linear copy numbers were averaged across duplicates and the *Pomc* average was divided by the *Ppia* average, to yield a normalized *Pomc* expression value. The *Pomc* expression value for each sample was then further standardized to the group average of the Control animals to generate a relative quantification of *Pomc* transcript expression. Due to the number of samples, male and female samples were run independently on separate plates with the same standard dilutions, and then normalized within sex.

IHC

Sucrose-saturated brains, preparation described above, were cryosectioned at 30 µm and collected in triplicate with a freezing stage sliding microtome (Leica Biosystems; SM 2010R) into PBS. The sections were then incubated with antisera to POMC [1:1,000 (Control and Restored mice) or 1:10,000 (*Vglut2*-tdTomato animals); Phoenix; rabbit; H-029-30]. Following triplicate washes, one set of the sections from Control and Restored mice was incubated with a biotinylated goat anti-rabbit secondary antisera (1:500, Vector Labs; CAT# BA-1000 ROS23)

followed by treatment with a Vectastain ABC HRP Kit (Vector Labs; CAT# PK-4000) and development of a colorimetric stain with diaminobenzidine (250 μg/mL in TBS with 0.1% H_2O_2). A second set of sections from Control and Restored mice was incubated with Alexa Fluor® 568 (A568) goat anti-rabbit secondary antibody (1:500; ThermoFisher Scientific; CAT# A-11036). *Vglut2*-tdTomato brain sections were incubated with Alexa Fluor® 488 (A488) goat anti-rabbit secondary antibody (1:500; ThermoFisher Scientific; CAT# A-11034).

IHC image analysis

Images from the DAB-treated IHC tissue sections were acquired with a 6.3x/0.20 160 NPL Fluotar objective on a Leitz Dialux 22 microscope with a Leica DFC280 camera (Leitz/Leica; Wetzlar, Germany). Fluorescent images used for the *Pomc*-restoration and tdTomato-POMC overlap counts were taken with a 10x objective on a Nikon Eclipse 90i digital upright microscope with a Photometrics CoolSNAP HQ2 CCD Camera. The images were acquired using a 1 s exposure for the POMC signal and a 50 ms exposure time for the tdTomato signal. Resulting tdTomato pictures were then double-processed with ImageJ (http://imagej.nih.gov/ij/), by adjusting the brightness and contrast, to account for different background fluorescence levels in the GABA-rich basomedial ARC and in the glutamate-rich lateral ARC. The representative image was acquired using a Nikon A1 Confocal Microscope.

Hybridization probes

Riboprobes for in situ hybridization (ISH) were generated from cDNA sequences as follows (NCBI GenBank Accession Numbers in parenthesis): *Pomc*, bases 502-1008 (short probe) or bases 1-1008 (long probe) (NM_001278584.1); *Vglut2*, bases 1,762-2,390

(NM_080853.3); and *Gad67*, bases 317-892 (NM_008077.4). The *Vglut2* and *Gad67* plasmid templates are a gift from Dr. Erik Hrabovszky (Institute of Experimental Medicine, Budapest), the long *Pomc* template was synthesized by Genscript (Piscataway, NJ). For dual-label ISH, the short *Pomc* probe was labeled with digoxigenin-11-UTP (Roche Applied Sciences, Basel, Switzerland), the *Vglut2* and *Gad67* probes with [35S]-uridine 5'-(alpha-thio) triphosphate (PerkinElmer, Waltham, MA). For triple-label ISH, the long *Pomc* probe was labeled with fluorescein-12-UTP (Roche), the *Gad67* probe with digoxigenin-11-UTP, and the *Vglut2* probe [35S]-uridine 5'-(alpha-thio) triphosphate.

Dual-label ISH

16 µm coronal sections were cut through the rostrocaudal extent of the hypothalamic arcuate nucleus using a Leica CM3050 S cryostat, thaw-mounted on Fisherbrand™ Superfrost™ Plus Microscope Slides (ThermoFisher Scientific; CAT# 12-550-15), air-dried and stored at -80°. The mounted sections were fixed with 4% paraformaldehyde in 0.1 M phosphate buffer (pH 7.4) for 20 min., rinsed in PBS for 5 min., acetylated with 0.25% acetic anhydride in 0.1 M triethanolamine for 10 min., treated with ascending ethanol series and chloroform (10 min.), partially rehydrated in 95% ethanol, and then processed for hybridization. Two adjacent series of sections, each containing every 7'th section, were hybridized with the mixture of the digoxigenin-labeled short *Pomc* riboprobe and the [^{35}S]-labeled riboprobe for either *Vglut2* or *Gad67* (diluted to 50,000 cpm/µl) overnight at 56° in a humidified chamber. The *Pomc* probe was detected with peroxidase-conjugated anti-digoxigenin antibody (diluted 1:100 in 1% blocking reagent, Roche), amplified using the TSA Biotin Tyramide system (PerkinElmer) for 30 min., and labeled with Alexa Fluor 488-conjugated Streptavidin (diluted 1:500 in 1% blocking

reagent, Life Technologies) for 2 hours. To detect the radiolabeled *Vglut2* or *Gad67* probe, sections were then rinsed in PBS, dehydrated, air-dried and coated with Kodak NTB autoradiography emulsion (Carestream Health Inc., Rochester, NY). The autoradiograms were developed using Kodak D19 developer after 7 days (*Gad67*) or 12 days (*Vglut2*) exposure.

Triple-label ISH

Triple-label ISH was performed on serial hypothalamic sections of 3 male and 3 female wild type C57BL/6J mice, euthanized on postnatal day 65 by decapitation under deep ketamine/xylazine anesthesia. Tissue collection and processing was identical to the dual-label ISH procedure. Sections were hybridized with the mix of the fluorescein-labeled long *Pomc*, digoxigenin-labeled *Gad67*, and [^{35}S]-labeled *Vglut2* riboprobes. Following hybridization, sections were first incubated in the peroxidase-conjugated sheep anti-digoxigenin antibody, and the signal was amplified with the TSA Plus DIG Kit (Cat# NEL748E001KT, Perkin Elmer) for 30 min, using the DIG amplification reagent at 1:500 dilution in 0.05M Tris (pH 7.6) containing 0.01% H_2O_2. Sections were then incubated in a rabbit monoclonal anti-digoxigenin antibody (Thermo Fisher, Cat# 700772; at 1 μg/ml concentration) for 3h, in the presence of 2% sodium azide to inactivate peroxidase activity. Sections were thoroughly washed in PBS, and incubated overnight in peroxidase-conjugated sheep anti-fluorescein antibody (Roche, Cat# 11426346910; diluted 1:100 in 1% blocking reagent). Signal amplification was applied for 30 min, using the TSA Plus Biotin Kit (Perkin Elmer) with the TSA Plus biotin reagent diluted 1:300 in 0.05M Tris and 0.01% H_2O_2. The biotin deposits and the anti-digoxigenin-antibody were detected with Alexa Fluor 488-conjugated Streptavidin and Alexa 594-conjugated anti-rabbit IgG (Jackson

Immunoresearch; 1:200), respectively. The sections were then dehydrated, dipped in Kodak NTB autoradiography emulsion, and developed after 10 days as described above.

ISH image analysis

Fluorescent signals and darkfield emulsion autoradiography images of the same field were captured with the 10x objective of a Zeiss Axioplan 2 microscope (Carl Zeiss, Göttingen, Germany) equipped with a RT SPOT digital camera (Diagnostic Instruments, Sterling Heights, MI). Every 14th section (5 sections per mouse), covering the rostro-caudal extent of the Arc was used to count the number of *Pomc*, dual-labeled *Pomc*-*Vglut2* and *Pomc*-*Gad67*, and triple-labeled *Pomc*-*Vglut2*-*Gad67* neurons. To be considered specifically labeled with the radioactive *Vglut2* or *Gad67* probes, *Pomc* neurons had to exhibit at least a 5-fold higher silver grain density than over background regions. This was confirmed by ImageJ for each *Pomc* neuron with lighter silver grain label. For publication images, the green fluorescence of Alexa 488 (*Pomc*) was pseudocolored to red (Figure 2.4) or blue (Figure 2.6) to better visualize colocalization with the silver grain autoradiography signal.

Data analysis

All statistical testing was performed using GraphPad Prism 7.04 for Windows (GraphPad Software, La Jolla California USA, www.graphpad.com). Data sets with an $n \geq 8$ were tested for normality using the D'Agostino & Pearson normality assessment, while groups with $n < 8$, were assessed with the Shapiro-Wilk normality test. All sample sizes, means ± SEM, and measured units are located in Table 2.1 (Descriptive Statistics Table). The data structures, specific statistical tests used and numerical results are located in Table 2.2 (Statistical Tests Table). Both

Table 2.1 and Table 2.2 are organized and labeled according to the respective figure panels representing the data, or when appropriate, annotated as not shown.

Results

A lineage trace of *Vglut2*-tdTomato neurons revealed that approximately half of all immunoreactive POMC neurons were colabeled with tdTomato

Because of differing reports for the percentage overlap of *Vglut2* expression in POMC neurons [45-47, 49, 52], we initially performed a lineage trace by crossing *Vglut2*-IRES-Cre mice with floxed tdTomato mice. In contrast to data obtained by the laboratory that originally generated the *Vglut*2-IRES-Cre strain, which showed only a 10% overlap of their lineage trace with POMC neurons [47], we found that there was a nearly even split in the number of POMC neurons that were co-labeled or unlabeled with the *Vglut2*-tdTomato reporter (Figure 2.1A-H). There was no effect of the rostral-caudal position in the arcuate nucleus on the overlap counts (Figure 2.1I). The reason for this large discrepancy in the fraction of glutamatergic POMC neurons is unclear, but there were technical differences in the identification method for POMC neurons. The previous group performed their lineage trace using a second transgenic reporter strain, POMC-hrGFP, and then quantified the coexpression of tdTomato and the surrogate marker hrGFP. We chose to quantify the overlap of tdTomato with POMC neurons using the immunohistochemical detection of POMC itself.

Vglut2-Cre mediated activation of *Pomc* expression in the hypothalamus of Restored mice normalized body weight and composition, and POMC immunoreactivity.

The specificity of *Vglut2*-ires-Cre mediated DNA recombination was assessed using PCR analysis of genomic DNA extracted from the relatively glutamatergic neuron-rich medial-basal hypothalamus and the relatively GABAergic neuron-rich dorsal striatum from Restored mice. The three primer PCR design amplifies a 180 bp band from the intact FNΔ2 allele and a 287 bp band from the same allele after Cre-mediated recombination (Figure 2.2A and B). No PCR product is generated from control DNA because the reverse primer cannot hybridize to the intact nPE2 enhancer. The degree of recombination was significantly higher in hypothalamic samples compared to striatal samples and there was no evidence of recombination in the brains of FNΔ2 mice lacking the *Vglut2*-IRES-Cre allele (Figure 2.2C).

Weekly body weights showed identical growth curves between Restored and Control mice. Both groups diverged significantly from FNΔ2 mice by age 5 (female) or 6 (male) weeks (Figure 2.3A and B; Only pairwise comparisons from one week prior to divergence to one week following are included in Table 2.2). Body composition measurements by NMR confirmed that these differences in body weight were due to excess fat mass in FNΔ2 mice compared to Control and Restored mice, with no differences in lean mass across all groups (Figure 2.3C and D). Furthermore, weights of the gonadal and inguinal fat pads showed that there were no depot-specific differences between Restored and Control animals, while both fat pads in each group were substantially smaller than those from obese FNΔ2 mice (Figure 2.3E and F).

IHC for POMC was performed on neural tissue from Control and Restored mice. Three sections from each mouse taken between A-P coordinates from -1.5 to -1.9 mm posterior to bregma were included for analysis. There was no difference in either fluorescent (Figure 2.4A-B) or DAB treated (Figure 2.4C-D) cell counts between Restored and Control mice. However, there

was an overall difference between labeling methods. DAB-treated sections displayed significantly higher cell counts than fluorescently labeled sections (Figure 2.4E).

Dual-label ISH for *Pomc* and *Gad67* in Restored mice identified a substantial population of *Gad67*$^+$ *Pomc* neurons.

While we didn't measure any difference between Control and Restored mice with POMC IHC, we found significantly fewer total *Pomc*$^+$ cells in Restored animals compared to Controls using ISH (data not shown; Table 2.1 and 2.2 – Figure 2.5). Dual-label ISH showed that Restored mice had a greater degree of *Pomc*-*Vglut2* and less *Pomc*-*Gad67* overlap than was observed in Control animals (Figure 2.5A-E). However, as noted earlier, the total number of *Pomc* labeled neurons was less in the Restored animals, thus it follows that Restored mice had less total *Pomc*-*Vglut2* and *Pomc*-*Gad67* labeled neurons than Control animals (Figure 2.5F). There was no difference in the cumulative sum of the percentage of *Pomc*-*Vglut2* and *Pomc*-*Gad67* cells between Restored and Control animals, indicating that each group possesses a proportionately comparable population of dual *Vglut2*$^+$/*Gad67*$^+$ phenotype *Pomc* neurons. qRT-PCR for relative *Pomc* expression was performed on cDNA derived from RNA extracted from the medial-basal hypothalamus. Despite detecting fewer *Pomc* neurons with ISH, there was no difference in total steady-state *Pomc* mRNA levels between Restored and Control animals, and levels in both groups were ~25-fold greater than FNΔ2 mice (Figure 2.5G).

Triple-label ISH in WT mice showed distinct *Pomc*-only, *Gad67*$^+$/*Pomc*, *Vglut2*$^+$/*Pomc*, and *Gad67*$^+$/*Vglut2*$^+$/*Pomc* neuron subpopulations with varying anatomic distribution along the rostral-caudal ARC axis.

The individual hybridization signals for *Pomc*, *Gad67* and *Vglut2* from a representative hemi-section of the medial basal hypothalamus including the ARC and VMH are shown in Figure 2.6 A-C. The merged image is shown in Figure 2.6 D. Both *Pomc* and Gad67 expression are primarily located in the ARC while *Vglut2* mRNA is most densely located in the VMH. Neurons of interest were identified as shown in representative higher magnification sections from the rostral Arc (Figure 2.6 E-H) and the caudal ARC (Figure 2.6 I-L). There was a main effect on *Pomc* neuron counts along the rostral-caudal axis of the ARC. However, none of the Levels differed significantly from one another after *post hoc* multiple comparisons (Figure 2.6 M). Of the possible phenotypic combinations of *Pomc* expression overlapping with the two neurotransmitter markers throughout the entirety of the ARC, the *Pomc*-only cells constituted the smallest group, followed by double *Pomc/Vglut2*$^{+}$ and double *Pomc/Gad67*$^{+}$ neurons. Triple *Pomc/ Vglut2*$^{+}$*/Gad67*$^{+}$ cells comprised the largest group. Except for the *Pomc/Gad67*$^{+}$ count compared to the *Pomc/Vglut2/Gad67*$^{+}$ population, the size of every group was significantly different from every other group (Figure 2.6N). Analysis of linear regression revealed several patterns that emerged along the rostral-caudal axis of the ARC. The *Pomc*-only and *Vglut2*$^{+}$ populations exhibited a similar trend of having the highest presence at the rostral end of the ARC and the lowest at the caudal end, while the *Vglut2/Gad67*$^{+}$ cells showed the opposite pattern. The *Gad67*$^{+}$ population didn't exhibit a linear trend like the other groups, due to a sharp increase in expression between the two most rostral ARC positions. However, analyzing levels 2 through 5 showed that their numbers also diminished toward the caudal ARC (Figure 2.6O-P).

We also observed a small number of dual *Vglut2/Gad67*$^{+}$ cells in the ARC that were not positive for *Pomc* mRNA. The phenotypic identity of these cells is not known. Furthermore, the density of non-*Pomc* dual *Vglut2/Gad67*$^{+}$ cells was higher in the DMN (data not shown).

Together, these data indicate that neuron populations in the hypothalamus, other than POMC neurons, may also exhibit both glutamatergic and GABAergic characteristics.

Discussion

The global impact of POMC-peptides on metabolic homeostasis, body composition, and feeding behavior is widely recognized. However, studies investigating the fast synaptic transmission roles that POMC neurons serve are in their early stages. The initial rationale for conducting the current study was to decipher the physiological significance of glutamate-producing POMC neurons, using an experimental paradigm previously used to study leptin receptor POMC neurons [55] and 5HT-2cR POMC neurons [56], by selective induction of *Pomc* transcription in these cell populations during hypothalamic development. We sought to characterize the function of a specific neuronal subset, but what we uncovered instead is a broader phenomenon of neural adaptation or plasticity.

The complete prevention of the obesity phenotype of FNΔ2 mice by *Vglut2*-ires-Cre induction of *Pomc* expression in hypothalamic neurons did not support our initial hypothesis that a subpopulation of glutamatergic POMC neurons would have selective effects on energy homeostasis. It is possible that more extensive metabolic phenotyping of the Restored mice, including environmental challenges such as a high fat diet, might have unveiled subtle alterations from Control mice. However, the existing data for body weight growth over 12 weeks, normal body composition and normalized steady state *Pomc* mRNA levels at age 12 weeks, combined with the observed developmental alterations in neurotransmitter markers, suggested that additional metabolic phenotyping was unlikely to be informative or fully interpretable. Previous

work indicated that *Pomc* mRNA levels above a threshold of 30% of control levels and evenly distributed spatially across the rostral-caudal axis of the ARC produced only a mild obesity phenotype in low fat chow fed mice. Furthermore, *Pomc* mRNA levels above 50% of control levels protected mice from obesity, even when challenged with a high fat diet [16].

A first line of evidence for fast neurotransmitter plasticity within the POMC neuronal network arises from a discrepancy that we found between *Pomc* restoration in FNΔ2 mice and the *Vglut2* lineage trace experiments, even though each study was dependent on the same Cre-driver mouse strain. On one hand, we found a nearly complete restoration in the number of POMC-expressing neurons, indicating that all of those neurons either contemporaneously expressed or were derived from cells that had expressed *Vglut2* at some time-point. On the other hand, we found that only half of POMC immunoreactive cells were also positive for the lineage trace, suggesting that all POMC neurons could not have expressed or be derived from cells that were *Vglut2*$^{+}$ at some point. We can only speculate about the exact mechanism underlying these differences, but there may be a combination of multiple processes including sensitivity issues in the methods of detection between the two studies. Furthermore, distinct floxed alleles may have different thresholds for recombination by the same Cre-driver strain [180].

It is possible that the Restored mice had differences in developmental timing en route to normalization of the POMC system, which were not evident in measurements of body mass and composition. In the *Vglut2* lineage trace, normal POMC function should be intact and allow POMC neurons to follow a normal developmental program, resulting in an even split between tdTomato^{+} and tdTomato^{-} POMC neurons. In contrast, the *Pomc*-restoration experiment used FNΔ2 mice that are incapable of transcribing *Pomc* in neurons, and arguably undergo an altered developmental program that differentially impacts the hypothalamic landscape and ultimately

global metabolic function. This fact is evident in the phenotypic traits of the latter mice: morbid obesity, hyperphagia, hypolocomotion, insulin resistance and alterations in glucose tolerance and glycosuria [54, 57, 162]. However, when *Pomc* expression was induced in these mice by the *Vglut2*-IRES-Cre driver, the animals were phenotypically normal and had the same proportion of dual-labeled *Pomc*-*Gad67*$^{+}$ cells and POMC immunoreactive cells as control animals. Both of these results were unanticipated, we expected to restore function to only a subset of POMC neurons and that relatively few of them would be *Gad67*$^{+}$. We used GAD67 instead of VGAT as a marker of GABAergic phenotype because the latter transporter is not expressed in POMC neurons [178]. Despite this, there is substantial electrophysiological evidence of synaptic GABA release from POMC neurons. Together, these data suggest one or both of the following: *Gad67*-expressing POMC neurons also express *Vglut2*, and/or there is turnover and overlap from a glutamatergic- to a GABAergic-identity in POMC neurons. Whether these phenomena represent the normal pattern of activity for this cell population, or if they arose from a compensatory mechanism initiated from an atypical developmental program remains to be determined.

The differences that we found in cell counts between ISH and IHC experiments, as well as the difference observed between the ISH studies and the qRT-PCR measures, may be due to differences in the sensitivities in the assays used. The ISH experiments on the Restored mice were conducted on tissue that was collected from animals that were between 9 and 13 weeks old, whereas the IHC studies and qRT-PCR were conducted on tissue that was collected from mice that were between 12 and 13 weeks old. While this age gap is not typically regarded as a critical developmental period, there may be changes occurring in the neurotransmitter landscape which could account for the different cell counts that we measured. The means of ISH tissue preparation and probing method used to label cells can profoundly impact the sensitivity and

interpretation of the assay, which may account for the varying proportions of glutamatergic POMC neurons that have been reported via ISH, let alone IHC. However, our results fit with the numbers reported previously using the same preparation and detection methods [45-47, 49, 52]. For IHC, we used three different secondary antibodies and colorimetric or fluorescent techniques to label POMC neurons. The inconsistencies in our data were not between experimental groups, but between the detection methods that were used. We found the greatest number of POMC neurons using colorimetric DAB as the labeling method, followed by the fluorescent markers Alexa Fluor 488 and Alexa Fluor 568, respectively. Albeit, we also utilized two different dilutions of the POMC primary antibody, 1:1000 for the DAB and Alexa Fluor 568 sections and 1:10,000 for the Alexa Fluor 488 sections. However, given that we measured a greater number of POMC neurons with Alexa Fluor 488 than with Alexa Fluor 568, we conclude that differences that we see are more a reflection of detection subjectivity of the secondary antibodies than of the efficiency of the primary antibody used.

Overlap between GABAergic and glutamatergic cellular phenotypes and machineries is not a novel concept. Several studies have identified instances of these intersections in multiple systems, which can be influenced by cellular excitability, developmental timing, or environmental factors. For example, Kao et al. [163] found that there is a subset of retinal bipolar cells in cats that use both glutamate and GABA, and express vesicular transporters for each molecule. Using subcellular fractionation and synaptosomal isolation, Zander et al. [164] identified sizeable vesicle pools containing both VGLUT2 and VGAT. Furthermore, they also showed that VGAT immunoisolates transport glutamate, and that VGLUT activity enhances the uptake of GABA and monoamines. Several studies have demonstrated that following stimulation-induced hyperexcitability of granule cells in the rat dentate gyrus, their mossy fibers

can transition from a glutamatergic to a GABAergic neurotransmission and that these cells possess a GABAergic phenotype during early postnatal periods, which is suppressed in mature cells [165-168]. In 2005, Gómez-Lira et al. [169] further showed that the presence of TrkB-mediated BDNF signaling can also lead to a similar glutamatergic-to-GABAergic transition in mature cultured rat granule cells, showing that this phenomenon is not limited to a critical developmental period or supraphysiological stimulation. Ottem et al. [170] also demonstrated that nearly all neurons in the female rat anteroventral periventricular nucleus are both GABAergic and glutamatergic and that both their excitability and VGLUT2 and VGAT vesicular pools are regulated by estradiol and photoperiodic signals, highlighting another case of external regulation of phenotypic identity. In the rat medial nucleus of the trapezoid body Gillespie et al. [171] found GABA and glutamate co-release in the developing auditory system, which may aid in synaptic refinement and formation of the tonotopic map. More recently, Root et al. [172] demonstrated in rats and mice that neurons from the ventral tegmental area innervating the lateral habenula (LHb), possess markers for both GABAergic and glutamatergic transmission. Furthermore, optogenetic stimulation of these cells exerts both excitatory and inhibitory influences on LHb neurons. Finally, a review by Mestikawy et al. [173] outlines the overlap of VGLUT1, 2 and 3 with other transmitter systems throughout the central nervous system, highlighting the versatility and pervasiveness of this transporter family, both in function and anatomy. Beyond sharing neurotransmitter phenotypes, work from the Spitzer lab has highlighted complete switches from one neurotransmitter identity to another [174, 175]. In 2013, Dulcis et al. [176] found a switch between dopamine and somatostatin neurons in response to exposure to different photoperiod lengths in adult mice, which was independent of neurogenesis or cell death. Meng et al. [177] went on to show that in the rat paraventricular nucleus of the

hypothalamus this switch occurs exclusively in dopaminergic neurons that co-express VGLUT2 and that the switch is contingent on elevated activity in those cells.

Coexpression of *Vglut2* and *Gad67* in *Pomc* neurons has been reported from single-cell RNA sequencing [181], where they observed a 24% overlap between the markers. They also reported 87% of Pomc neurons express *Gad67* and 50% express *Vglut2*. The overall *Vglut2* and *Gad67* counts, and the triple counts seem to mostly be in agreement with the numbers that we measured in our dual- and triple-label ISH experiments, where we report more dual-labeled cells (38%) and total *Vglut2*$^+$ cells (dual-label: 56%, triple-label: 58%), but 15-22% less total *Gad67*$^+$ cells (dual-label: 65%, triple-label: 72%). The directionality of the *Vglut2* and *Gad67* counts between the studies are in agreement; where, *Gad67* represents a larger proportion of the *Pomc* population than *Vglut2*. Additionally, we can infer from their reported proportions that 13% of the sequenced *Pomc* neurons were *Pomc*-only, 50% were *Gad67*$^+$, 13% were *Vglut2*$^+$, and 24% were *Gad67*$^+$/*Vglut2*$^+$; these counts are different than our respective measures of 7.1%, 34.7%, 20.6%, and 37.6%. These differing counts could arise from a few factors: they used younger mice in their study, and their dataset arises from 163 cells, which might not fully cover the entire *Pomc*-neuron population.

An important question that can be asked regarding the Restored mice arises from the lack of temporal control in the *Vglut2*-Cre induced, cell specific *Pomc* transcription. Given the widespread expression and subsequent decrease in *Vglut2* expression from early postnatal development to maturation [52, 182], VGLUT2 alone may not be the best indication of mature glutamatergic neurons. It is also possible that other differentiated neurons in the ARC may transiently express VGLUT2 during development. For the current experiments with the Restored mice, we were limited to the available genetic mouse lines, and the best option was a

constitutively active Vglut2-Cre driver line. Using an inducible-Cre model could potentially provide more specific insight for the role of glutamatergic POMC neurons in adult animals. However, those experiments would come with their own caveats and considerations. One such consideration is that without sufficiently early intervention the FNΔ2 animals exhibit juvenile-onset obesity. An early history of excess adiposity could by itself permanently shape the hypothalamic landscape and its plasticity.

In conclusion, our triple ISH data highlight a previously overlooked phenomenon that could not be measured with previous reports using dual ISH alone. There is spatial heterogeneity between phenotypically different POMC neurons based on their markers of fast synaptic neurotransmitters along the rostral-caudal axis of the ARC. Previous work [183] has demonstrated that there is an anatomical difference in in leptin- and insulin-induced responses in POMC neurons. Where most leptin-induced hyperpolarization of POMC neurons occurred in the rostral ARC, whereas most insulin-induced depolarization of POMC neurons occurred in the caudal portion of the ARC. Furthermore, Betley et al. [23] demonstrated in AgRP neurons that the rostral-caudal location of the cell bodies was associated with their projection targets, where the most rostral neurons tended to project to forebrain areas, while the caudally located cells projected to hindbrain areas. These findings raise questions of how overall ARC function changes developmentally and whether other ARC neuron subtypes, such as kisspeptin and dopamine neurons, also exhibit phenotypic shifts in their fast synaptic neurotransmitters.

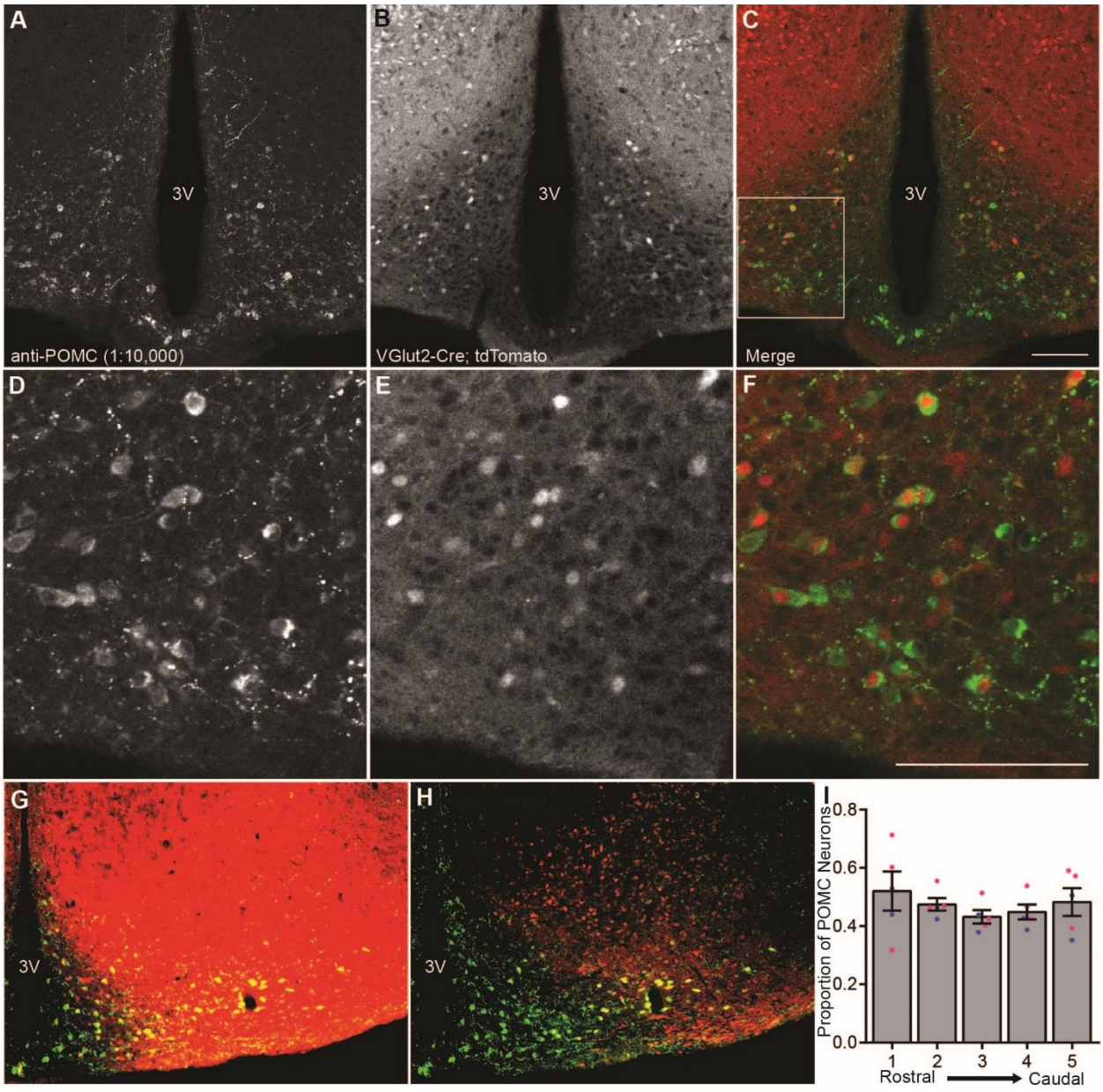
A
3V
anti-POMC (1:10,000)
B
3V
VGlut2-Cre; tdTomato
C
3V
Merge
D
E
F
G
3V
H
3V
I
Proportion of POMC Neurons
0.0
0.2
0.4
0.6
0.8
1
2
3
4
5
Rostral
Caudal

Figure 2.1: Genetic lineage trace of *Vglut2* expression and overlap with POMC IHC. **A-C**, Confocal images of POMC immunoreactivity from a male mouse (A); *Vglut2*-Cre-mediated tdTomato expression (B); and overlap between the two signals (C). **D-F**, 40x zoom of the inset outlined in Panel C with the same signals as in A-C. **G-H**, 20x epifluorescent image from a female mouse with post-hoc processing to identify tdTomato^{+}-POMC overlap in the medial (G) and lateral (H) ARC. **I**, Quantification of the proportion of tdTomato^{+}-POMC overlap throughout the rostral-caudal ARC axis. Male data for each group represented by filled blue circles and female data shown by filled pink circles. The scale bars represent 100µm.

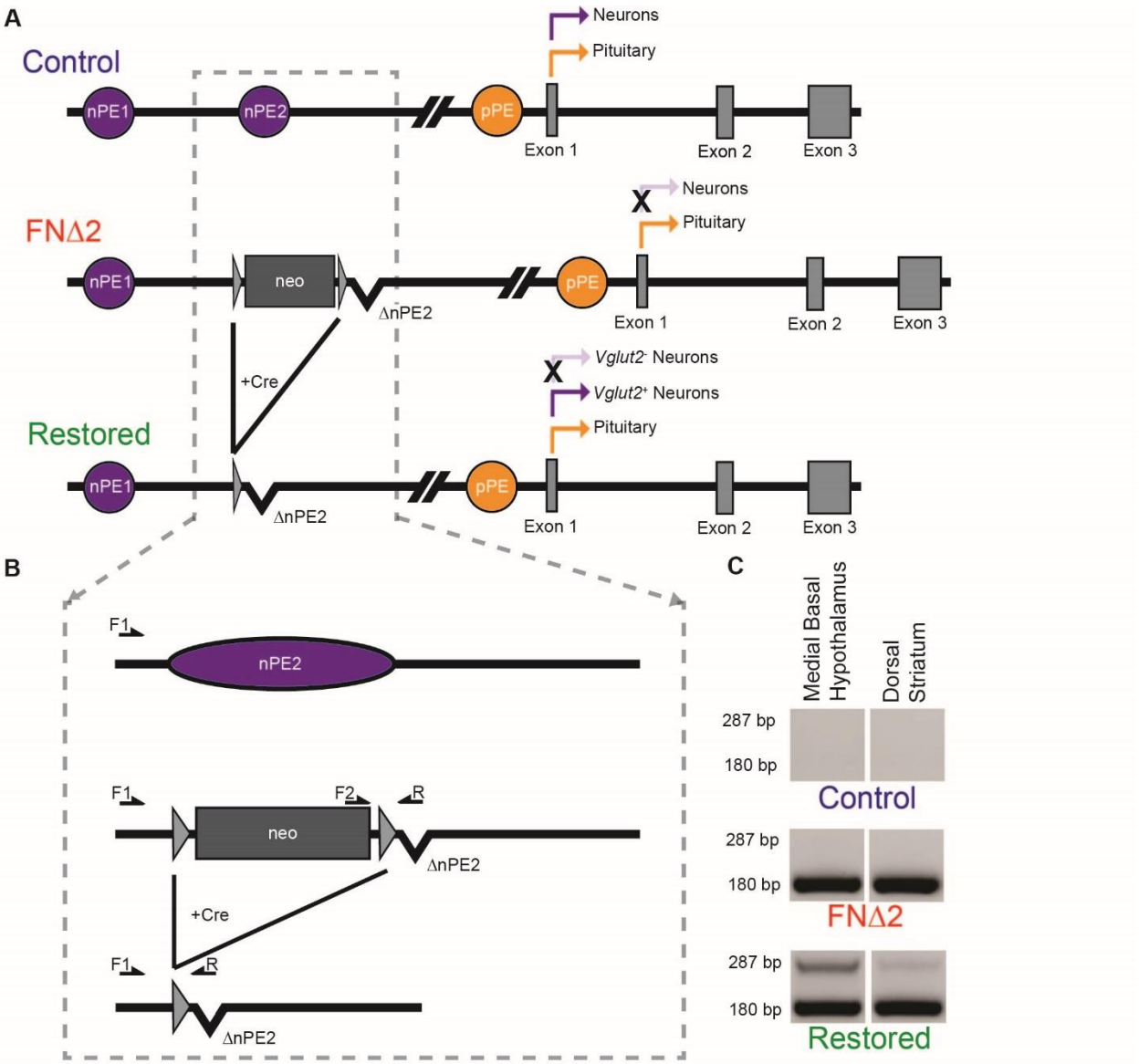
A
Control
nPE1
nPE2
pPE
Neurons
Pituitary
Exon 1
Exon 2
Exon 3
FNΔ2
neo
ΔnPE2
X
+Cre
Restored
Vglut2- Neurons
Vglut2+ Neurons
B
F1
F2
R
C
Medial Basal Hypothalamus
Dorsal Striatum
287 bp
180 bp

Figure 2.2: Vglut2-ires-Cre-specific recombination of the *Pomc* FNΔ2 allele. **A**, Schematic representing the WT *Pomc* locus (Control), the presence of the Cre-excisable floxed neomycin cassette along with the knockout of nPE2 (FNΔ2), and the FNΔ2 allele after Cre-mediated excision leaving only the knockout of nPE2 (Restored). **B,** Hybridization location of the three oligonucleotide primer set used to assess the integrity of the Cre-mediated recombination. The Forward 1 (F1) primer hybridizes upstream of nPE2, the Forward 2 (F2) primer hybridizes to the intact neomycin cassette, and the Reverse (R) primer is specific to the knocked out nPE2 locus. **C,** Verification of Cre-mediated genetic excision of the floxed-neomycin cassette from the *Pomc* neural enhancer locus in Restored mice. The intensity of the recombined band (PCR product of F1 and R; 287 bp) versus the non-recombined band (PCR product of F2 and R; 180 bp) was much stronger in the medial basal hypothalamus than in the dorsal striatum.

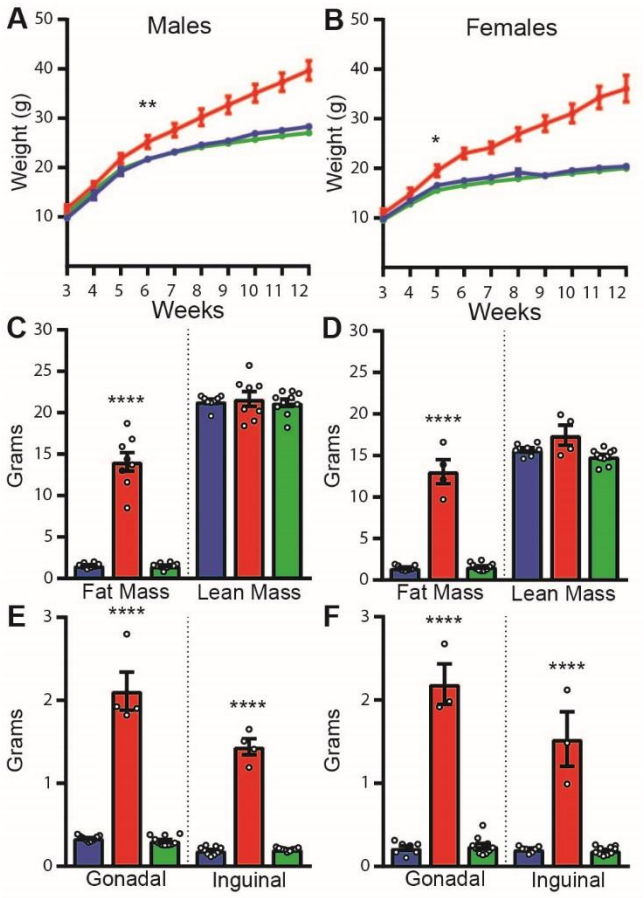
A
Males
Weight (g)
**
Weeks
B
Females
Weight (g)
*
Weeks
C
Grams
****
Fat Mass
Lean Mass
D
Grams
****
Fat Mass
Lean Mass
E
Grams
****
****
Gonadal
Inguinal
F
Grams
****
****
Gonadal
Inguinal

Figure 2.3: Vglut2-ires-Cre-mediated recombination of *Pomc* normalizes body composition. **A,** Growth curves from male mice. FNΔ2 (red line) mice significantly diverged from both Control (blue line) and Restored (green line) mice by 6 weeks of age. **B**, Growth curves from female mice. FNΔ2 mice significantly diverged from both Control and Restored mice by 5 weeks of age. **C-D**, NMR assessment of body composition. Male (C) and female (D) FNΔ2 mice (red bars) had substantially more body fat than Control (blue bars) or Restored (green bars) mice, while there were no differences in lean mass. **E-F**, Weight of gonadal and inguinal fat depots. Male (E) and female (F) FNΔ2 mice (red bars) had substantially larger fat depots (both gonadal and inguinal) than Control (blue bars) or Restored (green bars) mice.

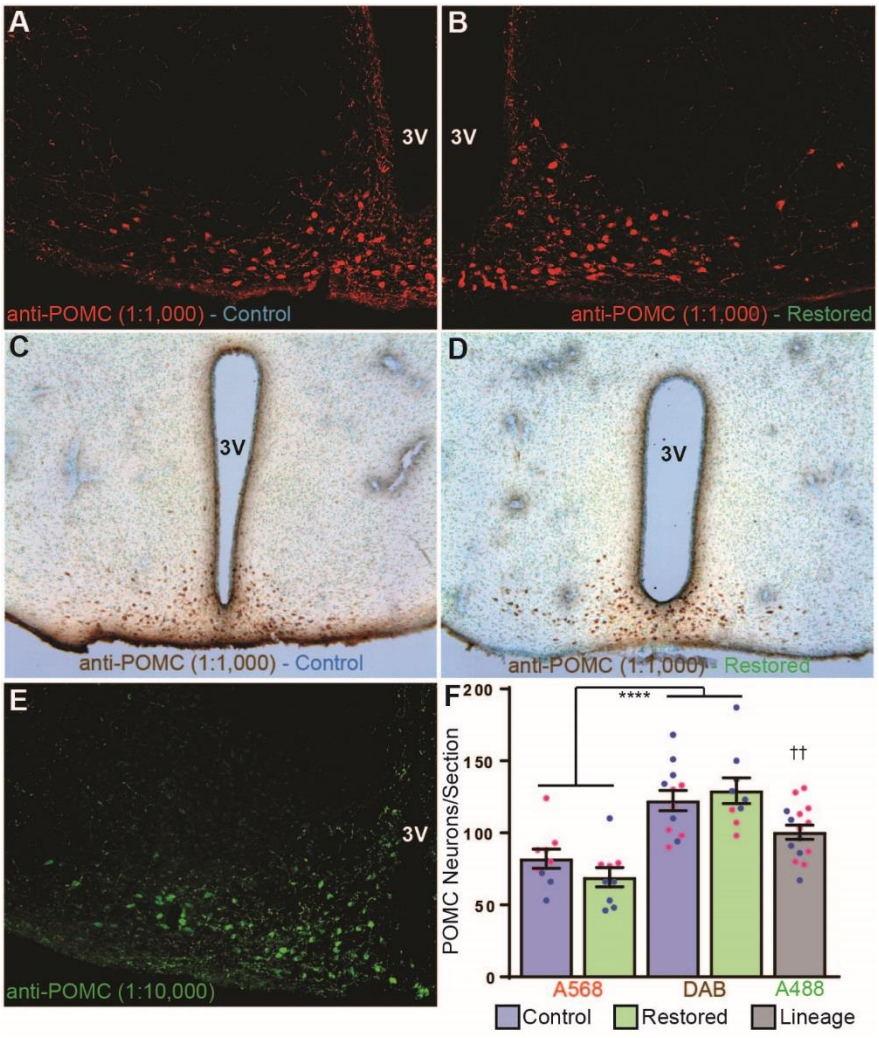
A
3V
anti-POMC (1:1,000) - Control
B
3V
anti-POMC (1:1,000) - Restored
C
3V
anti-POMC (1:1,000) - Control
D
3V
anti-POMC (1:1,000) - Restored
E
3V
anti-POMC (1:10,000)
F
POMC Neurons/Section
200
150
100
50
0
****
††
A568
DAB
A488
Control
Restored
Lineage

Figure 2.4: IHC for POMC cell counts in Control and Restored mice, and from VGlut2-Cre; tdTomato animals. **A**, POMC-IR in a male Control mouse detected with an AlexaFluor-568 secondary antibody (1:500). **B**, POMC-IR in a male Restored mouse detected with an AlexaFluor-568 secondary antibody (1:500). **C**, POMC-IR in a female Control mouse detected with biotinylated secondary antibody (1:500) and visualized with a DAB reaction. **D**, POMC-IR in a female Restored mouse detected with biotinylated secondary antibody (1:500) and visualized with a DAB reaction. **E**, POMC-IR in a female Vglut2-Cre; tdTomato mouse detected with an AlexaFluor-488 secondary antibody (1:500) (mirrored section from Figure 1G-H). **F,** POMC neuron cell counts from sections (3 per mouse). There was no difference between Control (blue bars) or Restored (green bars) mice, but only in the method of secondary labeling used. Male data for each group represented by filled blue circles and Female data shown by filled pink circles. **** denotes the difference between all A568 counts compared to all DAB counts, †† denotes the difference between all A488 counts compared to all A568 and DAB cell counts.

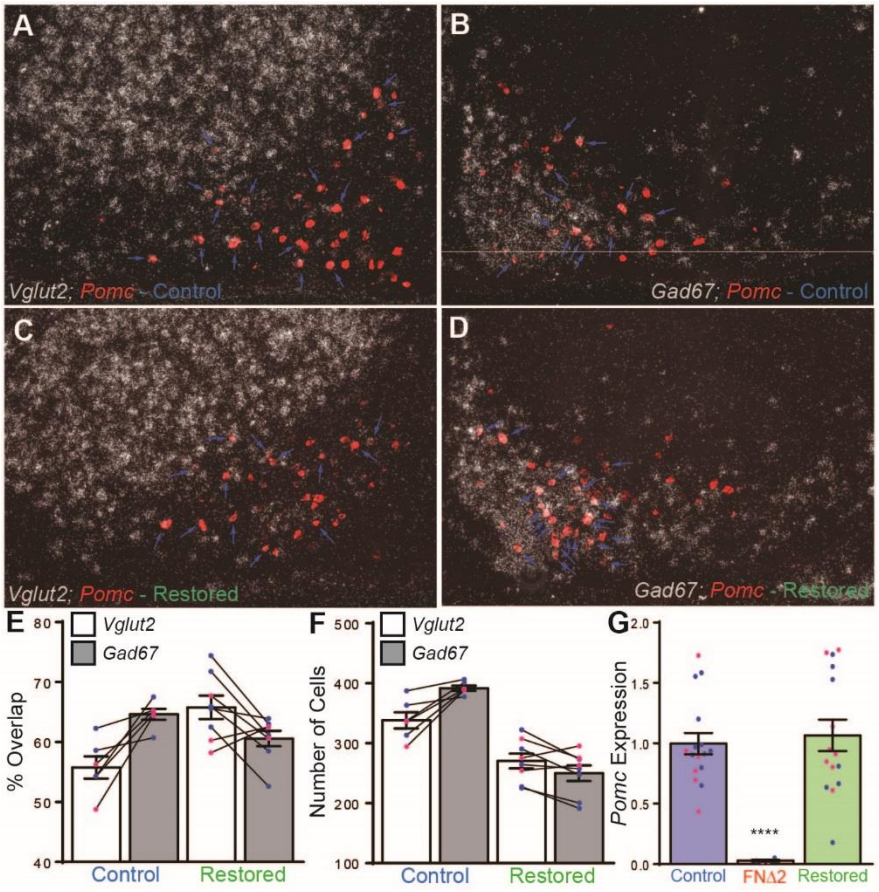
A
Vglut2; Pomc - Control
B
Gad67; Pomc - Control
C
Vglut2; Pomc - Restored
D
Gad67; Pomc - Restored
E
Vglut2
Gad67
% Overlap
80
70
60
50
40
Control
Restored
F
Vglut2
Gad67
Number of Cells
500
400
300
200
100
Control
Restored
G
Pomc Expression
2.0
1.5
1.0
0.5
0.0
****
Control
FNΔ2
Restored

Figure 2.5: Dual-label ISH for *Pomc* and *Vglut2* or *Gad67*, and relative *Pomc* expression in the medial basal hypothalamus of Control and Restored mice. **A**, ISH for *Vglut2* (silver grains) and *Pomc* (red) in a female Control mouse. **B**, ISH for *Gad67* (silver grains) and *Pomc* (red) in a female Control mouse. **C**, ISH for *Vglut2* (silver grains) and *Pomc* (red) in a female Restored mouse. **D**, ISH for *Gad67* (silver grains) and *Pomc* (red) in a female Restored mouse. In panels A-D, blue arrows indicate overlap between *Pomc* and the silver grain (*Vglut2* or *Gad67*) signal. **E**, Degree of overlap between *Pomc* and *Vglut2* (white bars) or *Gad67* (grey bars) in Control and Restored mice, each animal's *Vlgut2/Pomc* and *Gad67/Pomc* overlap percentage is connected by the solid black lines. **F**, Cell count of overlap between *Pomc* and *Vglut2* (white bars) or *Gad67* (grey bars) in Control and Restored mice, each animal's *Vlgut2/Pomc* and *Gad67/Pomc* overlap count is connected by the solid black lines. **G**, Relative qRT-PCR of *Pomc* expression in the medial-basal hypothalamus of Control (blue bar, left), FNΔ2 (red bar, middle), and Restored (green bar, right) mice. Male data are represented by filled blue circles and female data by filled pink circles.

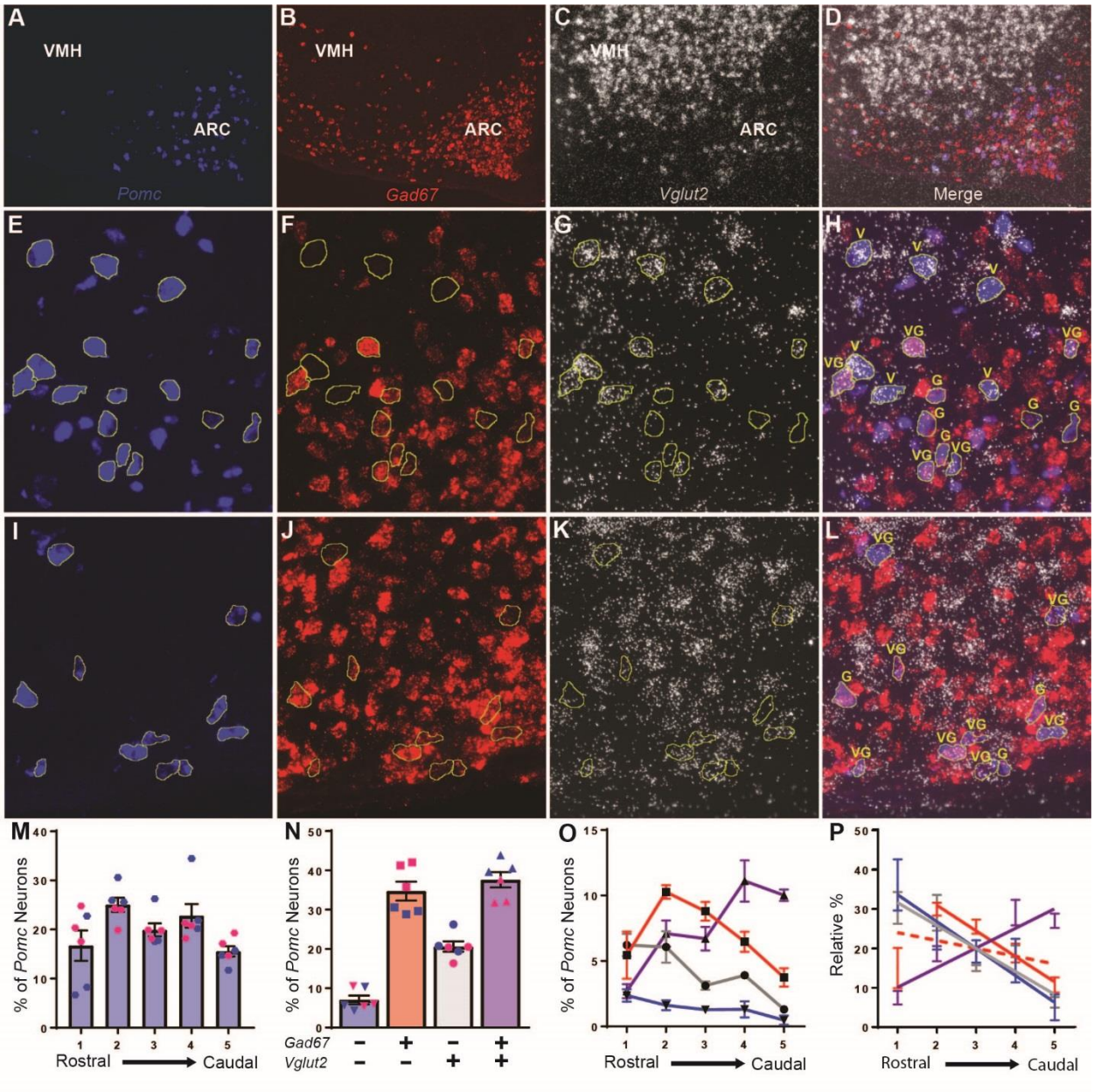
A
VMH
ARC
Pomc
B
VMH
ARC
Gad67
C
VMH
ARC
Vglut2
D
Merge
E
F
G
H
V
VG
G
I
J
K
L
M
% of Pomc Neurons
Rostral
Caudal
N
% of Pomc Neurons
Gad67
Vglut2
O
% of Pomc Neurons
Rostral
Caudal
P
Relative %
Rostral
Caudal

Figure 2.6: Triple-label ISH for *Pomc*, *Gad67*, and *Vglut2* in WT mice throughout the rostral-caudal ARC axis. *Pomc* (A,E,I), *Gad67* (B,F,J), *Vglut2* (C,G,K), and overlaid signals (D,H,L). **A-D**, Low magnification image of ISH signal for *Pomc*, *Gad67*, *Vglut2*, and the overlay of all signals from a male mouse. **E-H**, 40x images from the rostral ARC from a male mouse with *Pomc* neuron profiles outlined in yellow. **I-L**, 40x images from the caudal ARC from a female mouse with *Pomc* neuron profiles outlined in yellow. V indicates *Vglut2*$^+$ *Pomc* neurons, G indicates *Gad67*$^+$ *Pomc* neurons, and VG indicates *Vglut2/Gad67*$^+$ *Pomc* neurons. **M**, the dispersion of *Pomc* neurons along the rostral-caudal ARC axis. **N**, the overall distribution of *Pomc*-only (blue bar with filled inverted triangles), *Gad67*$^+$ (red bar with filled squares), *Vglut2*$^+$ (grey bar with filled circles), and *Vglut2/Gad67*$^+$ (purple bar with filled triangles) *Pomc* neurons. Male data are represented by filled blue symbols and female data by filled pink symbols. **O**, the dispersion of *Pomc*-only (blue line with filled inverted triangles), *Gad67*$^+$ (red line with filled squares), *Vglut2*$^+$ (grey line with filled circles), and *Vglut2/Gad67*$^+$ (purple line with filled triangles) *Pomc* neurons along the rostral-caudal ARC axis. **P**, Linear regression of the relative expression of each phenotypic *Pomc* neuron throughout the rostral-caudal ARC axis (*Pomc*-only solid blue line, *Gad67*$^+$ dotted red line, *Gad67*$^+$ (Levels 2-5) solid red line, *Vglut2*$^+$ solid grey line, *Vglut2/Gad67*$^+$ solid purple line).

Table 2.1: Descriptive statistics table for Chapter II

Figure	Sample size	Mean±SEM	Units
2.1i	n = 5 (2M,3F)	Level 1: 0.52±0.07 Level 2: 0.48±0.02 Level 3: 0.43±0.02 Level 4: 0.45±0.03 Level 5: 0.48±0.05	Proportion of POMC neurons
Figure	Sample size	Mean±SEM	Units
2.2c Restored Group	n = 9	Hypothalamus: 0.51±0.03 Striatum: 0.12±0.01	Arbitrary intensity units
Figure	Sample size	Mean±SEM	Units
2.3a Males	Control: n = 14 FNΔ2: n = 8 Restored: n = 22	Data order: Control, FNΔ2, Restored Week 3: 9.8±0.6, 11.7±0.7, 10.7±0.4 Week 4: 14.4±0.9, 16.4±0.8, 15.4±0.5 Week 5: 19.2±0.8, 21.8±1.0, 19.7±0.4 Week 6: 21.7±0.6, 25.2±1.3, 21.7±0.3 Week 7: 23.2±0.5, 27.6±1.3, 23.1±0.4 Week 8: 24.6±0.5, 30.2±1.7, 24.2±0.4 Week 9: 25.4±0.5, 32.7±1.7, 24.9±0.4 Week 10: 26.9±0.5, 35.1±1.8, 25.7±0.5 Week 11: 27.5±0.5, 37.3±1.8, 26.4±0.5 Week 12: 28.3±0.5, 39.7±2.0, 27.0±0.4	Grams
2.3b Females	Control: n = 12 FNΔ2: n = 6 Restored: n = 17	Data order: Control, FNΔ2, Restored Week 3: 9.8±0.4, 10.9±0.9, 9.6±0.3 Week 4: 13.4±0.6, 14.8±1.2, 12.8±0.4 Week 5: 16.6±0.5, 19.5±1.2, 15.6±0.3 Week 6: 17.5±0.5, 23.0±1.1, 16.6±0.3 Week 7: 18.2±0.6, 24.2±1.1, 17.3±0.2 Week 8: 19.2±0.7, 26.9±1.3, 17.9±0.3 Week 9: 18.6±0.4, 29.0±1.6, 18.5±0.3 Week 10: 19.6±0.5, 31.1±1.9, 19.0±0.3 Week 11: 20.1±0.5, 34.3±2.2, 19.5±0.3 Week 12: 20.4±0.5, 36.1±2.7, 20.0±0.3	Grams
2.3c Fat Mass - Males	Control: n = 8 FNΔ2: n = 8 Restored: n = 10	1.55±0.11 14.08±1.12 1.52±0.11	Grams
2.3c Lean Mass - Males	Control: n = 8 FNΔ2: n = 8 Restored: n = 10	21.36±0.27 21.66±0.90 21.20±0.44	Grams
2.3d Fat Mass - Females	Control: n = 7 FNΔ2: n = 4 Restored: n = 10	1.46±0.13 13.08±1.46 1.60±0.15	Grams
2.3d Lean Mass - Females	Control: n = 7 FNΔ2: n = 4 Restored: n = 10	15.67±0.28 17.45±1.21 14.88±0.28	Grams
2.3e Gonadal Fat - Males	Control: n = 9 FNΔ2: n = 4 Restored: n = 10	339±11 2,111±230 308±18	Milligrams
2.3e	Control: n = 9	189±17	Milligrams

Inguinal Fat - Males	FNΔ2: n = 4 Restored: n = 9	1,441±97 206±7	
2.3f Gonadal Fat - Females	Control: n = 7 FNΔ2: n = 3 Restored: n = 11	221±28 2,191±243 257±33	Milligrams
2.3f Inguinal Fat - Females	Control: n = 7 FNΔ2: n = 3 Restored: n = 10	206±14 1,532±327 192±15	Milligrams
Figure	Sample size	Mean±SEM	Units
2.4f	3 Sections/animal Control - animals A568: n = 3 (1M,2F) DAB: n = 4 (2M,2F) Restored - animals A568: n = 3 (2M,1F) DAB: n = 3 (2M,1F)	 82.11±6.67 122.40±7.04 69.22±6.64 129.30±8.87	POMC neurons/section
2.4f	3 Sections/animal A568: n = 6 (3M,3F) DAB: n = 7 (4M,3F) A488: n = 5 (2M,3F)	 75.67±4.83 125.4±5.45 100.5±4.88	POMC neurons/section
Figure	Sample size	Mean±SEM	Units
2.5 (not shown) # of Pomc neurons	Control: n = 6 (4M,2F) Restored: n = 9 (6M,3F)	606.30±7.28 407.10±14.19	Number of *Pomc* neurons
2.5e	Control: n = 6 (4M,2F) Restored: n = 8 (5M,3F)	*Vglut2*$^+$: 55.77±1.86 *Gad67*$^+$: 64.63±0.90 *Vglut2*$^+$: 65.80±1.95 *Gad67*$^+$: 60.59±1.29	% of *Pomc* neurons
2.5e (not shown) Difference	Control: n = 6 (4M,2F) Restored: n = 8 (5M,3F)	-8.87±2.21 5.21±2.14	%*Vglut2*$^+$ - %*Gad67*$^+$
2.5f	Control: n = 6 (4M,2F) Restored: n = 8 (5M,3F)	*Vglut2*$^+$: 338.30±13.65 *Gad67*$^+$: 391.80±4.21 *Vglut2*$^+$: 270.50±12.44 *Gad67*$^+$: 250.10±12.95	Number of *Pomc* neurons
2.5f (not shown) Difference	Control: n = 6 (4M,2F) Restored: n = 8 (5M,3F)	-53.5±12.92 20.38±8.87	#*Vglut2*$^+$ - #*Gad67*$^+$
2.5g	Control: n = 16 (10M,6F) FNΔ2: n = 4 (1M,3F) Restored: n = 15 (7M,8F)	1.00±0.10 0.03±0.00 1.07±0.10	Relative *Pomc* expression
Figure	Sample size	Mean±SEM	Units
2.6m	n = 6 (3M,3F)	Level 1: 16.73±3.10 Level 2: 25.04±1.41 Level 3: 19.90±1.33 Level 4: 22.78±2.39 Level 5: 15.55±1.04	% of *Pomc* neurons
2.6n	n = 6 (3M,3F)	*Pomc*-only: 7.05±1.10 *Gad67*$^+$: 34.71±2.42 *Vglut2*$^+$: 20.62±1.31 *Vglut2/Gad67*$^+$: 37.61±1.97	% of *Pomc* neurons
2.6o	n = 6 (3M,3F)	*Pomc*-only:	% of *Pomc* neurons

		Level 1: 2.37±0.47 Level 2: 1.62±0.37 Level 3: 1.28±0.18 Level 4: 1.30±0.62 Level 5: 0.48±0.35 *Gad67*$^{+}$: Level 1: 5.44±1.80 Level 2: 10.26±0.52 Level 3: 8.80±0.71 Level 4: 6.47±0.76 Level 5: 3.75±0.70 *Vglut2*$^{+}$: Level 1: 6.22±0.86 Level 2: 6.07±1.20 Level 3: 3.12±0.31 Level 4: 3.90±0.22 Level 5: 1.31±0.29 *Vglut2/Gad67*$^{+}$: Level 1: 2.69±0.54 Level 2: 7.09±1.00 Level 3: 6.71±0.91 Level 4: 11.12±1.58 Level 5: 10.02±0.44	
2.6p	n = 6 (3M,3F)	*Pomc*-only: y = -6.795x±1.15 + 40.39±3.81 *Gad67*$^{+}$: y = -1.977x±1.21 + 25.93±4.02 *Gad67*$^{+}$ (2-5): y = -6.449x±0.58 + 43.82±2.13 *Vglut2*$^{+}$: y = -5.784x±1.50 + 37.35±4.97 *Vglut2/Gad67*$^{+}$: y = 4.955x±1.30 + 5.14±4.31	y = mx + b

Table 2.2: Statistical tests table for Chapter II

Figure	Data structure	Type of test	Statistical data
2.1i	Normal Distribution	One-way RM ANOVA	Level: F(1.65,6.60) = 1.225, p = 0.34 Animal: F(4,16) = 5.038, p = 8.04e-3 Tukey's multiple comparisons test Level 1 vs Level 2, q = 1.04, p = 0.94 Level 1 vs Level 3, q = 2.11, p = 0.62 Level 1 vs Level 4, q = 1.80, p = 0.72 Level 1 vs Level 5, q = 1.07, p = 0.93 Level 2 vs Level 3, q = 10.01, p = 9.83e-3 Level 2 vs Level 4, q = 5.23, p = 8.90e-2 Level 2 vs Level 5, q = 0.25, p = 0.99 Level 3 vs Level 4, q = 2.68, p = 0.44 Level 3 vs Level 5, q = 1.57, p = 0.80 Level 4 vs Level 5, q = 1.21, p = 0.90
Figure	Data structure	Type of test	Statistical data
2.2c Restored Group	Normal Distribution	Paired t test	t = 11.98, df = 8, p = 2.17e-6
Figure	Data structure	Type of test	Statistical data
2.3a Males	Growth Curve	Two-way ANOVA	Interaction: F(18,384) = 8.76, p < 1.00e-15 Time: F(9,384) = 244, p < 1.00e-15 Genotype: F(2,384) = 198.2, p < 1.00e-15 Tukey's multiple comparisons test 5 Weeks: Control vs FNΔ2, q = 3.23, p = 5.97e-2 Control vs Restored, q = 0.80, p = 0.84 FNΔ2 vs Restored, q = 2.80, p = 0.12 6 Weeks: Control vs FNΔ2, q = 4.34, p = 6.46e-3 Control vs Restored, q = 0.00, p > 0.99 FNΔ2 vs Restored, q = 4.66, p = 3.07e-3 7 Weeks: Control vs FNΔ2, q = 5.46, p = 3.90e-4 Control vs Restored, q = 0.16, p = 0.99 FNΔ2 vs Restored, q = 5.99, p = 8.38e-5
2.3b Females	Growth Curve	Two-way ANOVA	Interaction: F(18,294) = 19.75, p < 1.00e-15 Time: F(9,294) = 158.4, p < 1.00e-15 Genotype: F(2,294) = 473.2, p < 1.00e-15 Tukey's multiple comparisons test 4 Weeks: Control vs FNΔ2, q = 1.98, p = 0.34 Control vs Restored, q = 1.13, p = 0.71 FNΔ2 vs Restored, q = 2.99, p = 8.94e-2 5 Weeks: Control vs FNΔ2, q = 4.11, p = 1.10e-2 Control vs Restored, q = 1.88, p = 0.38 FNΔ2 vs Restored, q = 5.82, p = 1.48e-4 6 Weeks: Control vs FNΔ2, q = 7.80, p = 2.32e-7 Control vs Restored, q = 1.69, p = 0.46 FNΔ2 vs Restored, q = 9.55, p = 2.31e-10
2.3c	Normal	One-way ANOVA	F(2,23) = 138.4, p < 15.1e-14

Fat Mass - Males	Distribution		Tukey's multiple comparisons test Control vs FNΔ2, q = 19.97, p = 2.39e-12 Control vs Restored, q = 0.05, p > 0.99 FNΔ2 vs Restored, q = 21.10, p = 7.78e-13
2.3c Lean Mass - Males	Normal Distribution	One-way ANOVA	F(2,23) = 0.167, p = 0.85 Tukey's multiple comparisons test Control vs FNΔ2, q = 0.50, p = 0.93 Control vs Restored, q = 0.29, p = 0.98 FNΔ2 vs Restored, q = 0.81, p = 0.84
2.3d Fat Mass - Females	Normal Distribution	One-way ANOVA	F(2,18) = 138.4, p = 1.18e-11 Tukey's multiple comparisons test Control vs FNΔ2, q = 21.01, p = 4.51e-11 Control vs Restored, q = 0.33, p = 0.97 FNΔ2 vs Restored, q = 21.98, p = 2.09e-12
2.3d Lean Mass - Females	Normal Distribution	One-way ANOVA	F(2,18) = 6.16, p = 9.17e-3 Tukey's multiple comparisons test Control vs FNΔ2, q = 3.24, p = 0.08 Control vs Restored, q = 1.83, p = 0.42 FNΔ2 vs Restored, q = 4.96, p = 6.74e-3
2.3e Gonadal Fat - Males	Normal Distribution	One-way ANOVA	F(2,20) = 157.4, p = 5.80e-14 Tukey's multiple comparisons test Control vs FNΔ2, q = 22.76, p = 2.00e-12 Control vs Restored, q = 0.51, p = 0.93 FNΔ2 vs Restored, q = 23.51, p = 1.09e-12
2.3e Inguinal Fat - Males	Normal Distribution	One-way ANOVA	F(2,19) = 354.5, p < 1.00e-15 Tukey's multiple comparisons test Control vs FNΔ2, q = 34.87, p < 1.00e-15 Control vs Restored, q = 0.60, p = 0.91 FNΔ2 vs Restored, q = 34.40, p < 1.00e-15
2.3f Gonadal Fat - Females	Normal Distribution	One-way ANOVA	F(2,18) = 173.8, p = 1.70e-12 Tukey's multiple comparisons test Control vs FNΔ2, q = 24.08, p = 4.26e-12 Control vs Restored, q = 0.62, p = 0.90 FNΔ2 vs Restored, q = 25.06, p = 2.12e-12
2.3f Inguinal Fat - Females	Normal Distribution	One-way ANOVA	F(2,17) = 57.55, p = 2.70e-8 Tukey's multiple comparisons test Control vs FNΔ2, q = 13.68, p = 7.26e-8 Control vs Restored, q = 0.20, p = 0.99 FNΔ2 vs Restored, q = 14.49, p = 3.12e-8
Figure	Data structure	Type of test	Statistical data
2.4f	Normal Distribution	Two-way ANOVA	Interaction: F(1,36) = 3.207, p = 0.11 Genotype: F(1,36) = 3.61e-5, p = 0.99 Detection: F(1,36) = 45.97, p = 6.39e-8 Tukey's multiple comparisons test Control-A568 vs Restored-A568, q = 1.57, p = 0.69 Control-A568 vs Control-DAB, q = 5.24, p = 3.76e-3 Control-A568 vs Restored-DAB, q = 6.65, p = 2.10e-4 Restored-A568 vs Control-DAB, q = 6.92, p = 1.19e-4 Restored-A568 vs Restored-DAB, q = 8.26, p = 6.60e-6 Control-DAB vs Restored-DAB, q = 1.74, p = 0.61
2.4f	Normal Distribution	One-way ANOVA	F(2,51) = 24.9, p = 2.85e-8 Tukey's multiple comparisons test A568 vs DAB, q = 9.97, p = 1.35e-8 A548 vs A488, q = 4.58, p = 5.87e-3

			DAB vs A488, q = 4.74, p = 4.31e-3
Figure	Data structure	Type of test	Statistical data
2.5 (not shown) # *Pomc* neurons	Normal Distribution	Student's t test	t = 10.75, df = 13, p = 7.76e-8
2.5e	Normal Distribution	Two-way ANOVA	Interaction: F(1,12) = 20.23, p = 7.30e-4 Genotype: F(1,12) = 3.181, p = 9.98e-2 Marker: F(1,12) = 1.363, p = 0.27 Sidak's multiple comparisons test Control-*Vglut2*$^+$ vs Restored-*Vglut2*$^+$, t = 4.37, p = 4.10e-4 Control-*Gad67*$^+$ vs Restored-*Gad67*$^+$, t = 1.76, p = 0.17 Control-*Vglut2*$^+$ vs Control-*Gad67*$^+$, t = 3.75, p = 5.56e-3 Restored-*Vglut2*$^+$ vs Restored-*Gad67*$^+$, t = 2.54, p = 5.09e-2
2.5e (not shown) Difference	Normal Distribution	Student's t test	t = 4.498, df = 12, p = 7.30e-4
2.5f	Normal Distribution	Two-way RM ANOVA	Interaction: F(1,12) = 23.86, p = 3.76e-4 Genotype: F(1,12) = 46.4, p = 1.87e-5 Marker: F(1,12) = 4.797, p = 4.90e-2 Sidak's multiple comparisons test Control-*Vglut2*$^+$ vs Restored-*Vglut2*$^+$, t = 3.96, p = 1.17e-3 Control-*Gad67*$^+$ vs Restored-*Gad67*$^+$, t = 8.27, p = 3.50e-8 Control-*Vglut2*$^+$ vs Control-*Gad67*$^+$, t = 4.68, p = 1.07e-3 Restored-*Vglut2*$^+$ vs Restored-*Gad67*$^+$, t = 2.06, p = 0.12
2.5f (not shown) Difference	Normal Distribution	Student's t test	t = 4.884, df = 12, p = 3.76e-4
2.5g	Normal Distribution	One-way ANOVA	F(2,32) = 10.63, p = 2.88e-4 Tukey's multiple comparisons test Control vs FNΔ2, q = 5.96, p = 5.43e-4 Control vs Restored, q = 0.65, p = 0.89 FNΔ2 vs Restored, q = 6.34, p = 2.54e-4
Figure	Data structure	Type of test	Statistical data
2.6m	Normal Distribution	Two-Way RM ANOVA	Interaction F(12,60) = 13.10, p = 1.19e-12 Neurotransmitter: F(3,15) = 47.14, p = 7.16e-8 Level: F(4,20) = 3.16, p = 3.63e-2 Tukey's multiple comparisons test Level 1 vs Level 2, q = 3.71, p = 0.10 Level 1 vs Level 3, q = 1.42, p = 0.85 Level 1 vs Level 4, q = 2.70, p = 0.35 Level 1 vs Level 5, q = 0.52, p > 0.99 Level 2 vs Level 3, q = 2.29, p = 0.50 Level 2 vs Level 4, q = 1.01, p = 0.95 Level 2 vs Level 5, q = 4.23, p = 5.02e-2 Level 3 vs Level 4, q = 1.28, p = 0.89 Level 3 vs Level 5, q = 1.94, p = 0.65 Level 4 vs Level 5, q = 3.22, p = 0.19
2.6n	Normal Distribution	Two-Way RM ANOVA	Interaction F(12,60) = 13.10, p = 1.19e-12 Neurotransmitter: F(3,15) = 47.14, p = 7.16e-8 Level: F(4,20) = 3.16, p = 3.63e-2 Tukey's multiple comparisons test *Vglut2*$^+$ vs *Gad67*$^+$, q = 6.87, p = 1.07e-3 *Vglut2*$^+$ vs *Vglut2/Gad67*$^+$, q = 8.29, p = 1.66e-4 *Vglut2*$^+$ vs *Pomc*-only, q = 6.62, p = 1.51e-3

			Gad67^{+} vs *Vglut2/Gad67*$^{+}$, q = 1.42, p = 0.75 *Gad67*$^{+}$ vs *Pomc*-only, q = 13.49, p = 5.09e-7 *Vglut2/Gad67*$^{+}$ vs *Pomc*-only, q = 14.90, p = 1.37e-7
2.6o	Normal Distribution	Two-Way RM ANOVA	Interaction F(12,60) = 13.10, p = 1.19e-12 Neurotransmitter: F(3,15) = 47.14, p = 7.16e-8 Level: F(4,20) = 3.16, p = 3.63e-2 Tukey's multiple comparisons test *Vglut2*$^{+}$: Level 1 vs Level 2, q = 0.23, p = 0.99 Level 1 vs Level 3, q = 4.54, p = 1.75e-2 Level 1 vs Level 4, q = 3.39, p = 0.13 Level 1 vs Level 5, q = 7.18, p = 3.80e-5 Level 2 vs Level 3, q = 4.31, p = 2.71e-2 Level 2 vs Level 4, q = 3.16, p = 0.18 Level 2 vs Level 5, q = 6.96, p = 6.80e-5 Level 3 vs Level 4, q = 1.15, p = 0.93 Level 3 vs Level 5, q = 2.64, p = 0.35 Level 4 vs Level 5, q = 3.79, p = 6.85e-2 *Gad67*$^{+}$: Level 1 vs Level 2, q = 7.05, p = 5.33e-5 Level 1 vs Level 3, q = 4.90, p = 8.36e-3 Level 1 vs Level 4, q = 1.50, p = 0.83 Level 1 vs Level 5, q = 7.18, p = 0.41 Level 2 vs Level 3, q = 2.15, p = 0.55 Level 2 vs Level 4, q = 5.55, p = 2.03e-3 Level 2 vs Level 5, q = 9.53, p = 6.85e-8 Level 3 vs Level 4, q = 3.40, p = 0.13 Level 3 vs Level 5, q = 7.38, p = 2.26e-5 Level 4 vs Level 5, q = 3.98, p = 4.98e-2 *Pomc*-only: Level 1 vs Level 2, q = 1.10, p = 0.94 Level 1 vs Level 3, q = 1.59, p = 0.79 Level 1 vs Level 4, q = 1.56, p = 0.80 Level 1 vs Level 5, q = 2.77, p = 0.30 Level 2 vs Level 3, q = 0.49, p = 0.99 Level 2 vs Level 4, q = 0.46, p = 0.99 Level 2 vs Level 5, q = 1.67, p = 0.76 Level 3 vs Level 4, q = 0.03, p = 0.99 Level 3 vs Level 5, q = 1.18, p = 0.92 Level 4 vs Level 5, q = 1.21, p = 0.91 *Vglut2/Gad67*$^{+}$: Level 1 vs Level 2, q = 6.44, p = 2.51e-4 Level 1 vs Level 3, q = 5.88, p = 9.63e-4 Level 1 vs Level 4, q = 12.31, p = 5.13e-11 Level 1 vs Level 5, q = 10.71, p = 2.63e-9 Level 2 vs Level 3, q = 0.56, p = 0.99 Level 2 vs Level 4, q = 5.87, p = 9.77e-4 Level 2 vs Level 5, q = 4.27, p = 2.92e-2 Level 3 vs Level 4, q = 6.43, p = 5.54e-4 Level 3 vs Level 5, q = 4.83, p = 9.68e-3 Level 4 vs Level 5, q = 1.60, p = 0.79 Level 1:

			Vglut2$^+$ vs *Gad67*$^+$, q = 1.14, p = 0.85 *Vglut2*$^+$ vs *Vglut2/Gad67*$^+$, q = 5.16, p = 3.00e-3 *Vglut2*$^+$ vs *Pomc*-only, q = 5.63, p = 1.05e-3 *Gad67*$^+$ vs *Vglut2/Gad67*$^+$, q = 4.02, p = 3.02e-2 *Gad67*$^+$ vs *Pomc*-only, q = 4.49, p = 1.23e-2 *Vglut2/Gad67*$^+$ vs *Pomc*-only, q = 0.47, p = 0.99 Level 2: *Vglut2*$^+$ vs *Gad67*$^+$, q = 6.14, p = 3.18e-4 *Vglut2*$^+$ vs *Vglut2/Gad67*$^+$, q = 1.50, p = 0.72 *Vglut2*$^+$ vs *Pomc*-only, q = 6.51, p = 1.29e-4 *Gad67*$^+$ vs *Vglut2/Gad67*$^+$, q = 4.64, p = 9.16e-3 *Gad67*$^+$ vs *Pomc*-only, q = 12.64, p = 2.74e-11 *Vglut2/Gad67*$^+$ vs *Pomc*-only, q = 8.00, p = 2.67e-6 Level 3: *Vglut2*$^+$ vs *Gad67*$^+$, q = 8.30, p = 1.20e-6 *Vglut2*$^+$ vs *Vglut2/Gad67*$^+$, q = 5.25, p = 2.48e-3 *Vglut2*$^+$ vs *Pomc*-only, q = 2.68, p = 0.24 *Gad67*$^+$ vs *Vglut2/Gad67*$^+$, q = 3.05, p = 0.15 *Gad67*$^+$ vs *Pomc*-only, q = 10.99, p = 7.50e-10 *Vglut2/Gad67*$^+$ vs *Pomc*-only, q = 7.94, p = 3.19e-6 Level 4: *Vglut2*$^+$ vs *Gad67*$^+$, q = 3.75, p = 4.92e-2 *Vglut2*$^+$ vs *Vglut2/Gad67*$^+$, q = 10.53, p = 2.60e-9 *Vglut2*$^+$ vs *Pomc*-only, q = 3.80, p = 4.45e-2 *Gad67*$^+$ vs *Vglut2/Gad67*$^+$, q = 6.78, p = 6.41e-5 *Gad67*$^+$ vs *Pomc*-only, q = 7.55, p = 8.88e-6 *Vglut2/Gad67*$^+$ vs *Pomc*-only, q = 14.33, p = 2.00e-11 Level 5: *Vglut2*$^+$ vs *Gad67*$^+$, q = 3.56, p = 6.73e-2 *Vglut2*$^+$ vs *Vglut2/Gad67*$^+$, q = 12.73, p = 2.58e-11 *Vglut2*$^+$ vs *Pomc*-only, q = 1.22, p = 0.83 *Gad67*$^+$ vs *Vglut2/Gad67*$^+$, q = 9.17, p = 1.13e-7 *Gad67*$^+$ vs *Pomc*-only, q = 4.78, p = 6.89e-3 *Vglut2/Gad67*$^+$ vs *Pomc*-only, q = 13.94, p = 2.01e-11
2.6p	Normal Distribution	Two-Way RM ANOVA	Interaction F(12,60) = 11.47, p = 1.69e-11 Neurotransmitter: F(3,15) = 2.105, p = 0.14 Level: F(4,20) = 3.205, p = 3.46e-2 Tukey's multiple comparisons test *Vglut2*$^+$: Level 1 vs Level 2, q = 0.45, p = 0.99 Level 1 vs Level 3, q = 5.48, p = 2.42e-3 Level 1 vs Level 4, q = 3.95, p = 5.22e-2 Level 1 vs Level 5, q = 8.61, p = 8.65e-7 Level 2 vs Level 3, q = 5.02, p = 6.49e-3 Level 2 vs Level 4, q = 3.50, p = 0.11 Level 2 vs Level 5, q = 8.16, p = 2.92e-6 Level 3 vs Level 4, q = 1.52, p = 0.82 Level 3 vs Level 5, q = 3.13, p = 0.19

			Level 4 vs Level 5, q = 4.65, p = 1.39e-2 *Gad67*$^+$: Level 1 vs Level 2, q = 5.36, p = 3.13e-3 Level 1 vs Level 3, q = 3.76, p = 7.27e-2 Level 1 vs Level 4, q = 1.37, p = 0.87 Level 1 vs Level 5, q = 1.54, p = 0.81 Level 2 vs Level 3, q = 1.60, p = 0.79 Level 2 vs Level 4, q = 4.00, p = 4.85e-2 Level 2 vs Level 5, q = 6.90, p = 7.79e-5 Level 3 vs Level 4, q = 2.39, p = 0.45 Level 3 vs Level 5, q = 5.30, p = 3.56e-3 Level 4 vs Level 5, q = 2.91, p = 0.25 *Pomc*-only: Level 1 vs Level 2, q = 4.81, p = 1.02e-2 Level 1 vs Level 3, q = 6.05, p = 6.39e-4 Level 1 vs Level 4, q = 6.88, p = 8.36e-5 Level 1 vs Level 5, q = 11.14, p = 8.14e-9 Level 2 vs Level 3, q = 1.24, p = 0.90 Level 2 vs Level 4, q = 2.07, p = 0.59 Level 2 vs Level 5, q = 6.33, p = 3.27e-4 Level 3 vs Level 4, q = 0.83, p = 0.98 Level 3 vs Level 5, q = 5.09, p = 5.66e-3 Level 4 vs Level 5, q = 4.26, p = 2.98e-2 *Vglut2/Gad67*$^+$: Level 1 vs Level 2, q = 4.02, p = 4.68e-2 Level 1 vs Level 3, q = 3.69, p = 8.14e-2 Level 1 vs Level 4, q = 7.75, p = 8.64e-6 Level 1 vs Level 5, q = 7.01, p = 6.00e-5 Level 2 vs Level 3, q = 0.32, p = 0.99 Level 2 vs Level 4, q = 3.74, p = 7.55e-2 Level 2 vs Level 5, q = 2.99, p = 0.23 Level 3 vs Level 4, q = 4.06, p = 4.31e-2 Level 3 vs Level 5, q = 3.32, p = 0.15 Level 4 vs Level 5, q = 0.75, p = 0.98 Level 1: *Vglut2*$^+$ vs *Gad67*$^+$, q = 5.49, p = 1.47e-3 *Vglut2*$^+$ vs *Vglut2/Gad67*$^+$, q = 8.19, p = 1.62e-6 *Vglut2*$^+$ vs *Pomc*-only, q = 2.08, p = 0.46 *Gad67*$^+$ vs *Vglut2/Gad67*$^+$, q = 2.70, p = 0.23 *Gad67*$^+$ vs *Pomc*-only, q = 7.56, p = 8.58e-6 *Vglut2/Gad67*$^+$ vs *Pomc*-only, q = 10.27, p = 5.40e-8 Level 2: *Vglut2*$^+$ vs *Gad67*$^+$, q = 0.33, p = 0.99 *Vglut2*$^+$ vs *Vglut2/Gad67*$^+$, q = 3.72, p = 5.11e-2 *Vglut2*$^+$ vs *Pomc*-only, q = 2.28, p = 0.38 *Gad67*$^+$ vs *Vglut2/Gad67*$^+$, q = 4.05, p = 2.87e-2 *Gad67*$^+$ vs *Pomc*-only, q = 2.61, p = 0.26 *Vglut2/Gad67*$^+$ vs *Pomc*-only, q = 1.44, p = 0.74 Level 3: *Vglut2*$^+$ vs *Gad67*$^+$, q = 3.75, p = 4.90e-2 *Vglut2*$^+$ vs *Vglut2/Gad67*$^+$, q = 0.98, p = 0.90

			Vglut2$^+$ vs *Pomc*-only, q = 1.50, p = 0.71 *Gad67*$^+$ vs *Vglut2/Gad67*$^+$, q = 2.77, p = 0.21 *Gad67*$^+$ vs *Pomc*-only, q = 2.25, p = 0.39 *Vglut2/Gad67*$^+$ vs *Pomc*-only, q = 0.53, p = 0.98 Level 4: *Vglut2*$^+$ vs *Gad67*$^+$, q = 0.17, p = 0.99 *Vglut2*$^+$ vs *Vglut2/Gad67*$^+$, q = 3.51, p = 7.26e-2 *Vglut2*$^+$ vs *Pomc*-only, q = 0.85, p = 0.98 *Gad67*$^+$ vs *Vglut2/Gad67*$^+$, q = 3.68, p = 5.50e-2 *Gad67*$^+$ vs *Pomc*-only, q = 0.68, p = 0.96 *Vglut2/Gad67*$^+$ vs *Pomc*-only, q = 4.36, p = 1.60e-2 Level 5: *Vglut2*$^+$ vs *Gad67*$^+$, q = 1.58, p = 0.68 *Vglut2*$^+$ vs *Vglut2/Gad67*$^+$, q = 7.42, p = 1.24e-5 *Vglut2*$^+$ vs *Pomc*-only, q = 0.45, p = 0.99 *Gad67*$^+$ vs *Vglut2/Gad67*$^+$, q = 5.85, p = 6.39e-4 *Gad67*$^+$ vs *Pomc*-only, q = 2.03, p = 0.48 *Vglut2/Gad67*$^+$ vs *Pomc*-only, q = 7.88, p = 3.74e-6
2.6p	Normal Distribution	Linear Regression	Slopes: F(3,11) = 20.84, p = 7.66e-5 *Vglut2*$^+$: F(1,28) = 33.87, p = 2.97e-6, R square = 0.83 *Gad67*$^+$: F(1,28) = 2.67, p = 0.11, R square = 8.69e-2 *Gad67*$^+$ (Levels 2-5): F(1,22) = 57.49, p = 1.42e-7, R square = 0.98 *Pomc*-only: F(1,28) = 23.72, p = 3.95e-5, R square = 0.92 *Vglut2/Gad67*$^+$: F(1,28) = 39.83, p = 7.95e-7, R square = 0.83

CHAPTER III

POMC-deficiency and weight loss each uniquely and additively intensify the motivation to eat

Abstract

The frequency of obesity is increasing worldwide at an alarming rate, predisposing to other disorders including diabetes, heart disease and cancer. Exacerbating the problem, people who have lost weight exhibit a high prevalence of relapse to weight gain. An understanding of the underlying neural modifications that accompany body composition changes is needed to curb this global epidemic. Proopiomelanocortin (POMC) and the adipose hormone leptin are essential for homeostatic energy balance. POMC- or leptin-deficiency cause obesity, while melanocortin receptor (MCR) agonism decreases feeding and dictates body weight trajectory in a leptin-dependent manner. MCR- and leptin-signaling converge in several hypothalamic nuclei and in mesolimbic centers that impact dopaminergic signaling, indicating a potential role for POMC neurons and adipose tissue in shaping motivation-based computations and behavior. Because neural POMC-deficiency and relapse to obesity after weight loss occur independent of each other, we hypothesized that POMC-deficiency and weight loss will increase appetitive drive by different mechanisms. To test this we utilized two mouse models of obesity, neuron specific *Pomc*-deficient mice (PD) and diet-induced obese (DIO) mice, and assessed their feeding behavior while obese (PDO and DIO), following weight loss to normal body mass (PDWL and

DIOWL), and after restoring *Pomc* expression in animals that had lost weight (Restore). Between these groups we found that DIOWL and PDO animals each exhibit an increased drive to earn and eat food compared to Control mice, and that PDWL eat more even faster, indicating an additive role of PD and weight loss. Surprisingly, the behavior of the Restore mice did not drop to the level of Control mice that we expected, but only a return to the performance level of PDO and DIOWL mice. We then showed that DIOWL mice only outperform Control mice under acute mild food restriction, but not when housed with *ad libitum* food. Next we established that PD mice increase their operant feeding behavior in a manner correlated with their degree of weight loss. Then using osmotic minipumps, we demonstrated that the reversal of hyperleptinemia potentiates the drive to earn food, but not eat it, after leptin sensitivity has been restored. Lastly, we showed that pharmacological agonism of central MCRs suppresses food intake, overcoming the enhanced drive to eat in PDWL mice, with minimal impact on avoidance of mild foot shocks.

Introduction

The frequency of obesity is increasing worldwide at an alarming rate, and predisposes to other disorders including diabetes, heart disease and cancer [184-186]. Exacerbating the problem, people who have lost weight exhibit a high prevalence of relapse to weight gain [187-191], yet the neural and behavioral underpinnings driving this effect are unresolved. Understanding these interactions could provide critical insight to prevent the onset of obesity and relapse after weight loss, aiding to curb this global epidemic. ARC neurons send processes to several areas that are also innervated by, or contain, dopaminergic neurons and leptin receptors

(LepR), including several hypothalamic nuclei, the paraventricular nucleus of the thalamus (PVT), the nucleus accumbens (NAc), the amygdala, and the ventral tegmental area (VTA) [192, 193]. Anatomical and functional evidence of the connectivity between ARC neurons and mesolimbic circuitry is an area of active research which continues to be refined [194]. The association of these signaling pathways with limbic structures implicates them as possibly being pivotal portals between the neural control of metabolism and motivated behavior. This notion is especially intriguing with regards to obesity, because dysfunction within limbic circuitry is commonly associated with other behavioral disorders, such as addiction, and affective disorders like anxiety, and could be key in identifying behavioral maladaptations that lead to obesity.

Compensatory growth is a phenomenon that has been documented for over 100 years [195-201], which can be briefly described as the rapid accrual of body mass following periods of nutritional challenge or deficit, and it is generally accounted for or speculated in early homeostatic and motivational theories [202, 203]. However, mechanistic nuances of this behavior are largely unidentified. What is known is derived from food restriction and deprivation studies, where there have been a myriad of gene expression, homeostatic, and behavioral changes reported that could collectively drive this behavior. Also lacking, are findings that address associated motivational changes measureable on a short-term timescale. The majority of studies that tackle this issue report weight changes and food intake on the scale of days or weeks.

The studies presented here address the primary question: does body weight influence appetitive consummatory behavior? As well as tests the following hypotheses regarding obesity, weight loss, Pomc expression, and MCR signaling. 1) Obese PD mice will exhibit deficits in operant feeding. 2) Weight loss will lead to a chronic increase appetitive consummatory behaviors. 3) *Pomc* restoration in PD mice will normalize behavior, as it does body weight

trajectory. 4) Pharmacological agonism of MCRs will suppress motivated feeding. To address these we utilized two mouse models of obesity, neuron specific *Pomc*-deficient (PD) mice and diet-induced obese (DIO) mice. Groups of mice were assayed while obese, following weight loss to normal body weight, through the progression of weight loss, and in different nutritional states. We also assessed the efficacy of genetically restoring *Pomc* expression and pharmacological targeting of central melanocortin receptors (MCR) in mitigating weight loss induced feeding behavior. Finally, we investigated the impact of hyperleptinemia and its reversal without the accrual of adipose tissue and subsequent weight loss.

Materials and Methods

Animal Care

All animal procedures were performed in accordance with the University of Michigan Institutional Animal Care and Use Committee regulations. All mice were group housed under a 12-hour light/12-hour dark photoperiod at constant temperature of 22° C in ventilated cages with *ad libitum* access to water. 12-35 week old male and female mice were used all experiments, except for the data in Figures 3.1 and 3.6, where only male animals were used. Data presented in each figure were obtained from separate cohorts of animals, except for Figures 3.4 and 3.5, which were from the same mice. Access to chow and type of chow were contingent on the experimental group and experimental stage. All Control and PD animals received standard lab chow (5L0D; LabDiet containing 28.7 kcal% protein, 13.4 kcal% fat, and 57.9 kcal% carbohydrates). The DIO and DIOWL groups were weaned onto high-fat high-sucrose (HFHS) diet utilized by Ishimoto et al.[204] (Custom Order from Bio-Serv; containing 20.8 kcal%

protein, 36 kcal% fat, and 43.2 kcal% carbohydrates), and maintained the HFHS chow for 6 months, at which point the DIOWL groups were switched to normal chow and the DIO groups stayed on the HFHS chow. Weight loss was induced in PD mice through calorie restriction of a fixed daily amount of standard chow over a two month period. Weight loss in DIO animals was carried out over 2 months through a switch from HFHS- to standard-chow, and further weight reduction through subsequent calorie restriction. During behavioral testing, all animals received the same caloric supplement of normal chow, male animals received 9.8 kcal and female animals received 7.4 kcal. The DIO groups were the exception to this rule, where they received the same caloric supplement of the HFHS chow.

Mouse Strains

In the process of generating the different combinations of neural *Pomc* enhancer knockout mice (Lam et al. 2015), two mouse lines were generated that retained a floxed neomycin-resistance cassette (FNeo) in the enhancer region, which had first helped in ES cell clonal selection. These mouse lines are essentially devoid of neuronal *Pomc* (Arc*Pomc*$^{-/-}$) and are phenotypically the same, the only difference is in the placement of the FNeo, which is Cre-excisable. One line has the ability to restore ~80% of *Pomc* expression when exposed to Cre (FNΔ2), whereas Cre-exposure in the other restores only ~10% of *Pomc* expression (FNΔ1Δ2), without any phenotypic improvement. Both lines were utilized in the experiments contained here and both are referred to as PD (*Pomc*-deficient, neuron specific), however only FNΔ2 mice were used to restore *Pomc* expression (Restore). All Control mice are the genetically wildtype littermates of these mice, and all of the DIO groups originated from similar WT mice that arose from the Arc*Pomc*$^{-/-}$ breeding scheme.

Breeding Strategies

PD and Restored mice used for the FR1 study: Reversible Arc*Pomc*$^{+/-}$ mice (Bumaschny et al., 2012; Lam et al., 2015a, Chhabra et al., 2016ab) were crossed to *Pomc*-CreERT2$^{+/-}$ mice to obtain compound heterozygous Arc*Pomc*$^{+/-}$; *Pomc*-CreERT2$^{+/-}$ mice. Those mice were mated to Arc*Pomc*$^{+/-}$ mice to yield all control and experimental groups for the *Pomc* restoration study. These three groups were: *Pomc*-CreERT2$^{+/-}$; Arc*Pomc*$^{+/+}$ (Control), +/+; Arc*Pomc*$^{-/-}$ (PD) and *Pomc*-CreERT2$^{+/-}$; Arc*Pomc* -/- (Restored). Restored animals have a floxed-neomycin cassette inserted between neural *Pomc* enhancer 1 (nPE1) and the deleted neural *Pomc* enhancer 2 (ΔnPE2) locus, which prevents the transcription of *Pomc* in neurons, while leaving pituitary transcription intact. After Cre-mediated excision of the floxed-neomycin cassette, neuronal *Pomc* transcription is restored. PD mice used for progressive weight loss, and interleaved appetitive and aversive studies originated from Arc*Pomc*$^{+/-}$ mice crossed to Arc*Pomc*$^{+/-}$ mice, to yield Arc*Pomc*$^{+/+}$ (Control) and Arc*Pomc*$^{-/-}$ (PD) animals.

Operant Behavior

All operant procedures were conducted in a sound attenuating cubicle (ENV-022V) with a mouse modular chamber (ENV-307[A/W]) outfitted with a grid floor (ENV-307[A/W]-GFW), a house light (ENV-315[M/W]), retractable levers (ENV-310[M/W]), and food pellet dispensers (ENV-203-20). For studies utilizing footshock, the chambers were also equipped with Standalone Aversive Stimulator/Scramblers (ENV-414S), to deliver electrical current through the grid floor. Escape pedestals were constructed from two steel plates (1.5 in. x 0.75 in.) epoxied to an acrylic plastic square (2 in. x 2 in.) and wired to a contact lickometer controller

(ENV-250), where the animals' presence was detected by simultaneous contact between both plates closing the open circuit. (Med Associates Inc., St. Albans, VT). The notation of "[x/x]" indicates the different product numbers associated with the standard versus the extra wide mouse modular chambers and their components. Our studies utilized four of each. To minimize spatial differences between the setups, all training and operant feeding paradigms were performed with a divider in place to limit the animals' available area from 6" x 5.25" (32.8 $in.^2$) to 3" x 5.25" (15.8 $in.^2$) for the standard chambers and from 8.5" x 7.1" (60.4 $in.^2$) to 3" x 7.1" (21.3 $in.^2$) for the extra wide chambers. The operant feeding procedures presented here utilize 20 mg Dustless Precision Pellets® (F0071; Rodent, Purified; Bio-Serv, Flemington, NJ; containing 20.8 kcal% protein, 13.9 kcal% fat, and 65.6 kcal% carbohydrates) as the food reinforcers.

Appetitive Training Procedure

All animals first underwent the following progression. For all operant feeding procedures the mice were immediately removed from the operant chambers, to discourage food hoarding behavior. One day prior to the start of training the mice were habituated in the operant chambers for 1 hour without any stimulus presentation. The following day was a Pavlovian training session. The mice were placed in the chamber, with the food hopper primed with 5 pellets. At commencement the houselight was illuminated and the response lever was extended. When the animal performed a head entry into the food hopper, the houselight was turned off, the lever was retracted, and a pellet was delivered. Three seconds after the head entry, the houselight was re-illuminated and the lever extended, awaiting the next head entry. This cycle continued until the animals received 50 pellets or until an hour had elapsed. This was repeated for each animal until they obtained at least 25 pellets. Once each animal displayed a Pavlovian response to the food

hopper, subsequent sessions required a lever press for pellet delivery. In the first stage of operant training, the response levers were primed with a paste made from the pellets mashed together with water. The mice were placed in the chamber and the houselight was illuminated and lever extended as before, both were presented for 30 seconds, and every 10 seconds the lever would retract and re-extend in an attempt to draw the animals' attention to the lever. If a lever press was performed, the houselight was extinguished, the lever retracted, and a pellet was delivered. Three seconds following pellet retrieval, assessed as a head entry into the food hopper, the next trial started. If the mouse failed to press the lever, the houselight was extinguished and the lever was retracted for 30 seconds. Each session consisted of 50 opportunities to earn a pellet. The mice underwent this procedure until they earned 25 pellets or until they displayed consistent earning for three days.

Fixed Ratio 1 (FR1) Paradigm

The FR1 program is identical to the last stage of the appetitive training, except that in these sessions the animals' had 10 seconds to press the lever instead of 30 seconds, and there were no lever extension and retractions or priming the lever with pellet paste. With a successful press, the next trial was initiated three seconds after pellet retrieval. Failure to press resulted in a 30 second timeout period to allow the mice to eat residual pellets. Animals were trained in this task until they exhibited stable performance for three days. To capture the two-dimensional nature of FR1 performance (Pellets and Session Time), we devised a Performance Score, which was calculated as: (Number of Pellet Opportunities / Session Time) * Pellets Earned. This score was then Log_2 transformed in order to better capture the performance of mice who earned less than half of the available pellets. Earning half of the pellets represents a benchmark of earning

and eating 1 pellet every ~50 seconds, a pace which any mouse is capable of maintaining given the time of the session and the amount of food available, and leads to a Log_2(Performance Score) of roughly zero.

Progressive Ratio (PR3) Paradigm

The PR3 paradigm was introduced after the animals had shown consistent performance in the FR1 task. The PR3 program starts with a trial that needs 1 lever press to receive a food pellet, then the required number of presses increments by 3 for each subsequent step, until 149 presses are needed to receive the last pellet. Similar to the FR1 program, each step starts with the concurrent houselight illumination and lever extension, and when a pellet is earned the light is turned off and the lever retracted. In contrast to other progressive ratio paradigms, this program proceeded until one of three scenarios occurred: 1) The mouse received 49 food pellets, 2) 15 minutes elapsed without earning a food pellet, or 3) 3 hours of total session time. The animals were so well trained to lever press at this point, we implemented those criteria instead of the traditional break point used in other progressive ratio programs. A Performance Score was also utilized to gauge behavior in this task, which was calculated as: (Cumulative Lever Presses / Session Time) * Pellets Earned.

Binge Paradigm

The Binge paradigm consisted of 200 rapidly presented opportunities for the animals to earn pellets. It utilized the same houselight illumination and lever extension as the FR1 paradigm. However, in this task the mice only had five seconds to respond, and the next trial would start after 5 seconds regardless of a successful press or failure. This task was designed to

prevent the possibility of a performance ceiling that was observed in the FR1 task, while allowing the animals to proceed at their own pace. At the end each session the residual pellet waste was collected and weighed to measure the amount of food that was actually eaten (Pellets earned * 20 mg minus Pellets wasted).

Interleaved Appetitive and Aversive Trials

PDWL and Control mice were trained in two stages. First, they were trained to lever press for food pellets in the FR1 task (Appetitive Trials) described previously until they exhibited stable performance for at least three days. Next, they were trained to avoid auditory-cued footshocks (Aversive Trials) until they displayed consistent performance. The trials started with the onset of the auditory tone. If the mouse stepped onto a platform in the corner of the operant chamber at any point during the tone presentation, the tone was extinguished and a 30 second inter-trial interval (ITI) started. If the mouse failed to step onto the platform within 10 seconds of tone onset, a 0.3mA 0.5 second footshock was delivered, followed by a 30 second ITI. After learning both tasks the mice were assayed in sessions that presented both types of trials (20 of each), randomized in their presentation order on 5 consecutive days. These combined sessions were preceded by an IP injection an hour before the session of either PBS or the MC3/4R agonist NDP-MSH (150ug; M8764; Sigma-Aldrich, St. Louis, MO). The dose of NDP-MSH was based on the findings of Fan et al. [67]. The mice received PBS on days 1, 2, 4, and 5, and NDP-MSH on day 3. The animals' performance did not differ on PBS days, and the values of PBS performance represent the average of all the days.

Acute Leptin Treatment

Group leptin sensitivity was assessed over a 72 hour period, where the mice underwent two 24 hour treatment periods separated by 24 hours. In the first treatment period, the mice were injected IP with PBS every 8 hours for a total of 3 doses. In the second treatment period, the mice were injected IP with recombinant mouse leptin (5mg/kg; National Hormone and Peptide Program) every 8 hours for a total of 3 doses. Food intake and body weight were measured at each point and compared between treatments. Groups were deemed to be leptin-sensitive if there was a significant reduction in body weight and food intake during leptin treatment compared to PBS treatment. Leptin sensitivity was measured 3 times; 2 weeks prior to minipump implantation, 2 weeks after minipump implantation, and 2 weeks after the manufacturer specified date of minipump depletion.

Osmotic Minipumps

Immediately following the cessation of the last behavioral session of the first experiment stage, mice were surgically implanted with subcutaneous osmotic minipumps (2004; Alzet, Cupertino CA). The mice received a minipump containing either PBS or leptin. The pumps delivered ~45µg/day of the same mouse recombinant leptin used in the acute treatments for 28 days.

Body Composition Measurements

Body composition was measured in the DIO, DIOWL, and their respective Controls by nuclear magnetic resonance (Minispec LF 90II, Bruker, Billerica, MA) conducted by the Michigan Mouse Metabolic Phenotyping Center. The measurements were conducted after the

mice had finished all behavioral testing and had been housed with *ad libitum* food access for at least one month.

Body Length Measurements

Measurements occurred immediately prior to euthanizing. The mice were deeply anesthetized with isoflurane via a drop jar, and pinned to a dissection mat. The snout-to-anus length was then measured with calipers.

Leptin ELISA Assay

Plasma was isolated from 50-70µL tail blood samples and leptin levels were measured by the Mouse/Rat Leptin Quantikine ELISA Kit as per the manufacturer's instructions (MOB00; R&D Systems, Minneapolis, MN).

Data Handling and Analysis

All behavioral data were collected with Med-PC IV (Med Associates Inc., St. Albans, VT), imported into and formatted with Matlab R2013a (MathWorks, Inc., Natick Massachusetts USA, www.mathworks.com). Statistical analysis was performed using Graphpad Prism 7.04 or 8.0.2 for Windows (GraphPad Software, La Jolla California USA, www.graphpad.com). All sample sizes, means ± SEM, and units measured are contained in the Descriptive Statistics Table (Table 3.1), and all statistical tests and results are contained in the Statistical Tests Table (Table 3.2). Significance was defined as p-values of less than 0.05.

Results

Obese Pomc-deficient mice display heightened operant feeding compared to control animals, which is potentiated by calorie restriction induced weight loss.

Male wild type Control, PD, and Restore mice were trained in a FR1 operant task, where they had to rapidly lever press and eat in order to achieve a maximum number of reward pellets (Figure 3.1B). The animals were assayed at three points: 1) while the PD and Restore mice were obese, 2) after they had lost weight through calorie restriction, and 3) after tamoxifen treatment to enable *Pomc* expression in the Restore mice (Figure 3.1A). Both the obese PD and Restore animals earned more pellets at a faster rate than the Controls (Figure 3.1C, Figure 3.1F-H Obese). Following weight loss, both the PD and Restore animals ate even more pellets in a shorter time (Figure 3.1D, Figure 3.1F-H Weight Loss).

***Pomc* restoration following obesity and weight loss is sufficient to normalize body weight trajectory, but only partially normalizes appetitive consummatory behavior.**

After the mice were assayed in the Weight Loss stage they were treated with tamoxifen, which allows *Pomc* expression in the Restore mice without impacting the Control or PD animals [54, 57]. We expected that the behavior of the Restore mice would drop to the level of the Controls. However, they only showed a partial normalization, similar to their performance while obese (Figure 3.1E, Figure 3.1F-H Tamoxifen). It is interesting to note that they did not display consistent behavior throughout the FR1 session. Their performance appears to mirror the Controls for the first ~10 and last ~15 trials, and the PD mice for the ~25 trials between, suggesting that there are mixed signals dictating their behavior throughout the session despite an ultimate performance landing between the other two groups.

The magnitude of the increased operant feeding performance is correlated with the amount of weight lost in both male and female PD animals.

A cohort of PD and WT littermates underwent biweekly behavioral testing, interleaved with a dieting period (Figure 3.2A) leading to progressive weight loss in PD animals until they reached (males) or approached (females) the same body weight of the Control animals, which followed a normal growth trajectory. Female PD mice never reached the body weight of the Control animals on this dieting schedule, and remained significantly heavier throughout all testing periods (Figure 3.2C-D). They were assayed in the more sensitive Binge lever-pressing task (Figure 3.2B), excess food leftover was collected and weighed to determine the amount of food eaten in each session. Measurement of food eaten in the task showed that PD mice exhibited an increase in food consumed with each subsequent drop in body weight, whereas Control mice did not change their consumption over the 10 week span (Figure 3.2E-F). Normalizing food consumed for each animal compared to their behavior during the first testing period, showed that PD mice first showed potentiated feeding during the second (females) or third (males) testing period (Figure 3.4G-H). Furthermore, there is a sex difference in the strategies utilized in the Binge task in PD animals throughout progressive weight loss. Male PD mice consistently earn a lot of pellets and waste less of what they earn as they lose more weight (Figure 3.2G and 3.2I), whereas female mice tend to eat most of the food they earn and increase their earning with subsequent weight loss (Figure 3.2H and 3.2J).

Pharmacological activation of MCRs attenuates appetitive consummatory behavior, with minimal impact on aversive avoidance.

Control and weight matched PDWL mice were separately trained to lever press for light-cued reward pellets (Figure 3.3A) and to actively avoid auditory-cued foot shocks (Figure 3.3B). After displaying consistent performance, both tasks were combined into a single-session assay with randomized presentation of each situation. Each session was preceded an hour before by an IP injection of PBS or NDP-MSH (150µg). Both groups were successful in nearly every appetitive trial with PBS pretreatment and NDP-MSH attenuated performance in both Controls and PDWL animals. However, PDWL mice were impacted substantially more (Figure 3.3C), similar to the observations of Tolle and Low [118] that PD mice are hypersensitive to MCR agonism. While there was a main effect of NDP-MSH treatment on the successful avoidance in the aversive trials, Control mice did not significantly differ between conditions, whereas the PDWL mice had impaired performance with NDP-MSH. Yet they still avoided more than 50% of the footshocks (Figure 3.3D). Female mice mirrored these performances (Figure B.2A-B). When the mice successfully lever pressed during the NDP-MSH treatment it took them longer to do so than in the PBS sessions (Figure 3.3E). This was also found in the female animals, and the PDWL females were even slower to lever press than the Controls (Figure B.2C). In the aversive trials, when successful, the PDWL mice actually avoided the footshock faster than they did during the PBS sessions, whereas the Control mice showed no change (Figure 3.3F). The female mice showed no differences in the latency to avoid footshocks in either treatment (Figure B.2D).

In contrast to obese Pomc-deficient mice, DIO mice display attenuated operant feeding compared to Control animals. However, weight loss still increases this behavior in DIO animals, but only to the performance level observed in obese Pomc-deficient and Pomc-Restored mice.

Male wild type Control, DIO, and DIOWL mice were trained in the FR1 operant task mentioned previously, where they had to rapidly lever press and eat in order to maximize the number of reward pellets earned. Opposite to the relationship of the obese PD mice, the DIO mice earned less pellets than the Control animals. Yet, the DIOWL group still earned more pellets in a shorter time (Figure 3.4B), although not to the level of the weight loss PD mice. Using the Log_2 transformed Performance Score to account for both the pellets earned and the total session time, WT animals consistently scored around 0, DIO mice around -0.75, and DIOWL around 1 (Figure 3.4C), similar to the obese PD and Restore mice presented in Figure 3.1. The same relationships were observed after analyzing the number of pellets earned (Figure 3.4D) and the total session time (Figure 3.4E). Female Control, DIO, and DIOWL mice displayed the same relative group differences as the male DIO animals (Figure B.3).

A history of weight loss intensifies the motivation to earn food under future mild acute calorie restriction.

Control and DIOWL mice were assayed in the PR3 task described, for 5 sessions in both an *ad libitum* and mild calorie restricted state. The session traces presented represent the performances from the 2 sessions for each animal in which they had the most lever presses in the shortest time in *ad libitum* (Figure 3.5C) and a calorie restricted states (Figure 3.5D), respectively. Comparison of the average performance scores for each mouse calculated from the 2 sessions depicted in Figure 3.5C-D showed a main effect of food restriction improving performance for both Control and DIOWL groups (Figure 3.5E), and a main effect of body composition state (Figure 3.5F). There were no differences between the ad libitum groups, but the food restricted DIOWL mice performed better than the food restricted Control mice (Figure

3.5E). Each group performed better in a food restricted state than they did *ad libitum* (Figure 3.5F). Female mice showed the same relationships, except that the main effect of body composition state did not reach the significance threshold of $p < 0.05$ (Figure B.4). Together these data indicate that the increased operant feeding in DIOWL animals does not arise from a chronic heightened drive to feed, that it is only manifest under acute food restriction.

Transient hyperleptinemia suppressed weight gain in calorie restricted animals returned to ad libitum conditions and imparted temporary leptin resistance.

Over the course of 12 weeks, a cohort of male wild type mice was assayed in the Binge procedure (Figure 3.2B) and then implanted with osmotic minipumps delivering either leptin (45µg/day) or PBS, and their performance was assessed during pump operation and after depletion (Figure 3.6A). Implantation of the leptin minipumps led to resistance to additional acute leptin treatment, which was reversed after minipump depletion (Figure 3.6B & Figure B.5A-F), despite having persistent elevated plasma leptin after pump depletion (Figure B.5H). Mice that received the leptin minipumps weighed significantly less than the mice that were implanted with the PBS minipumps, during the pump operation. After minipump depletion the weight of the leptin pump group rebounded to the level of the PBS group (Figure 3.6C), and this was evident immediately after minipump depletion (Figure B.5G). Implantation of the leptin minipumps did not lead to weight loss as expected, but a failure to gain weight normally following a switch from food restriction to *ad libitum* conditions (Figure 3.6D).

Hyperleptinemia did not impact Binge performance or feeding. However, the reversal of hyperleptinemia led to increased earning, but not eating of pellets.

In the Binge task there were no differences in food consumed between PBS or leptin minipump groups at any of the experimental stages (Figure 3.6E). While there were no differences in the amount of food eaten, the leptin minipump mice earned more food than the PBS group after the pumps were depleted, but not during pump operation (Figure 3.6F).

Discussion

The prevalence of obesity in modern society is escalating at an alarming rate. Contributing to this rise, people who have lost weight show tendencies to relapse to obesity or weight gain, which has been documented for over 60 years [187-191]. The rationale for the studies presented here was to identify potential behavioral differences associated with changes in body weight; specifically to test our hypothesis that weight loss imparts a long-term impact on an animal's behavior, which may contribute to relapse to weight gain. Furthermore, we sought to test the notion that *Pomc* expression or MCR signaling could provide viable therapeutic avenues to curb behavioral changes associated with weight loss. The studies presented here utilize two models of obesity, PD mice and DIO mice. The first represents a monogenic form of obesity that is rare in the human population and the latter a more ethologically relevant model which better captures the pandemic at hand. PD mice become obese on normal mouse chow, primarily through eating larger meals and hypolocomotion. DIO mice become obese eating a HFHS diet. Weight loss was induced in PD mice through calorie restriction, and in DIO mice by a switch to normal chow plus additional calorie restriction when necessary.

The FR1 performances provided some surprises and some results that were anticipated.

The behavior of the obese groups, both the obese PD and DIO mice, were unexpected. Experience in our lab indicated that the obese PD animals have trouble acquiring operant lever pressing behavior. Indeed, they did display deficits in learning the behavior (data not shown), but once the behavior was acquired they performed better than Control animals. Given the prevalence of DIO in our modern society we expected that mice in this state would outperform Control animals, indicating dysfunctional behavior that would exacerbate obesity. However, they behaved worse than Control mice, showing a lack of motivation to earn and eat the reward pellets, despite acute hunger. This may be due to the difference in the diet used to make them obese and the pellets utilized in the operant chambers. Even when acutely food restricted these mice received an equivalent caloric supplement of the HFHS chow outside of the operant chambers and the compositional and hedonic contrast with the reward pellets may devalue the pellets for these mice, leading to earning and eating less of them.

The weight-loss animals displayed the same relative increase in performance that we expected and consistent with reports of relapse to obesity. However, we did not expect the PDWL animals perform as well as they did, we expected improved performance, but not that they would reach a performance ceiling in the assay. Finally, we expected that the Restored mice would perform the same as Control animals. Previous work has shown that *Pomc*-restoration in PDWL mice can normalize their body-weight trajectory [54, 57], but those studies followed animals that were housed with ad libitum access to normal chow, and didn't assess any motivated behaviors. Collectively between the performance of the PD and DIO groups, we gained valuable insight that both weight-loss and *Pomc*-deficiency each increase the motivation to earn and eat in this assay, and in the case of PDWL animals that they have an additive action. The performance of the Restore group is particularly intriguing because prior to *Pomc*-

restoration these animals ate the most at the quickest pace, and then after tamoxifen treatment they returned to the same level as the PDO and DIOWL groups. Since *Pomc* expression has been enabled, this indicates that their enhanced performance compared to Control animals can be attributed to the history of weight-loss, and also tells us that there are persistent physiological changes associated with weight loss that impact motivated feeding, despite the fact that these animals now maintain a normal growth trajectory when allowed to free-feed. The findings with the PR3 assay further allude to this phenomenon, and also turned out differently than we expected. We hypothesized that the DIOWL animals would perform better than the Control animals under mild food restriction and *ad libitum* conditions. However, we only observed a difference when the animals were challenged with mild food restriction. Again this indicates that weight-loss imparts persistent changes, but that acute hunger is needed to allow them to manifest.

The FR1 task as is stands creates a black and white picture of mouse operant feeding behavior. Can the animal keep up with the paradigm or can it not? The window created by the program only frames this question into the ability to eat and earn subsequent pellets within 13 seconds or 43 seconds in a given trial, which leaves a large window of possibility, which combined with the fact that the PDWL animals hit its ceiling of measurement, necessitated a different assay. The Binge paradigm emerged in the hopes of being able to differentiate subtle differences in operant feeding behavior. This program did address the temporal fidelity, however it also led to the animals wasting a lot of the food they earned, whereas in the FR1 task the animals did not leave hardly any food waste. This messy feeding required collecting the leftovers and weighing them for each session, which turned out to be a critical measure.

The Binge data from the PD mice undergoing the progressive weight loss really wasn't surprising. The fact that the potentiation of performance is correlated with degree of weight-loss fits in well with early work from Stellar and Hill where they measured water consumption following varying periods of water deprivation and found a similar stepwise relationship [205] to what we observed with food consumption. The primary difference being that our animals were not completely deprived of the primary stimulus, and in fact received the same daily food supplement as the Control animals during behavioral assessment.

The Binge data from the mice that were implanted with the leptin-delivering osmotic minipumps is perhaps the most surprising of all the studies included here. We expected that there would be obvious behavioral deficits during the pump operation, yet there were none. The only measure where we found a difference between the PBS pump and Leptin pump groups was in the amount of food that they earned in the task after the minipumps were depleted, and after the mice had re-gained leptin sensitivity. It was not a subtle difference, they earned ~50% more pellets than the PBS pump group, but did not eat them. The same earning without eating behavior is evident in the male PD mice assayed in the Binge task. In the first week of behavioral assessment they only eat ~50% of the food that they earn, and throughout weight loss their earning doesn't change much, only that they eat more of what they earn with each subsequent weight loss step. This behavior was not seen in the female PD animals, who earned more and ate most of the food that they earned throughout weight loss. This fact may provide an important point in isolating the specificity of weight-loss effects from Pomc-deficiency in operant feeding. Both DIO and PDO animals are hyperleptinemic and resistant to acute leptin administration [57, 206], although it is important to note that just because the mice do not respond to additional leptin, does not mean that they do not retain leptin action [207]. After weight loss both groups experience a reversal of

hyperleptinemia and concurrent enhancement of operant feeding from their previous state. Clearly this can only account for half of the equation because the Leptin pump animals did not eat the food they earned, so something else associated with weight loss must fuel the drive to eat.

We did encounter a strange result from our ELISA measurements of plasma leptin levels, where the leptin pump group displayed extreme variability in this measure, and also registered even greater leptin levels after the minipump depletion (Figure B.5H). While strange, this effect has been documented and discussed in greater detail elsewhere [208], and because of this we place greater emphasis on the acute leptin treatment effects (Figure 3.5B and Figure B.5A-F) in assessing the efficacy of the minipumps in achieving hyperleptinemia-induced leptin resistance.

Perhaps the most encouraging result comes from the experiment with the interleaved appetitive and aversive trials under the influence of NDP-MSH. First, the NDP-MSH was able to potently suppress the augmented drive to eat in the PDWL animals, which exhibit near maximal performance in the FR1 task. PD animals have been shown to be hypersensitive to synthetic melanocortins [118], but those studies were not conducted in PDWL mice. Second, Control animals displayed deficits in appetitive behavior as well, with minimal impact on their aversive performance, indicating that in a normal animal pharmacologically targeting the central melanocortin system may be viable avenue to suppress feeding without blanket deficits in all motivated behaviors, as was also demonstrated with regards to conditioned taste aversion [209].

Most of the data presented in this chapter may likely reflect acute manifestations of a phenomenon that has been observed for more than 100 years, compensatory growth. Rats at a variety of ages were prevented from normal growth, for varying periods, through food restriction and low-protein diets, then displayed rapid normalization of growth and body weight when switched to an excess of resources [201]. This phenomenon of compensatory growth has been

demonstrated across several mammalian and avian species [195-200]. Yet, the rate of this growth can be attenuated when the return to excess food is coupled with moderate exercise [210]. Furthermore, rats that experience even one week of food restriction exhibit greater calorie efficiency when returned to pair-feeding with control animals [211]. The increase in calorie efficiency was attributed to a decrease in the metabolic need for body maintenance, and the allowance for subsequent ingested calories to be used for the restoration of body composition, where the degree of conserved energy was proportional to an extent to the prior caloric deficit [212].

We observed several examples where the phenomenon of compensatory growth may explain our findings. As part of Appendix B we provide data from a separate cohort of PDWL mice that were weight matched to Control animals (these animals were not used in any of the behavioral studies presented). They displayed incredible metabolic efficiency, and were able to maintain the same body weights of Control animals with a fraction of the food (Figure B.1B), then when they are returned to ad libitum food access they display astonishing overnight weight gain, which continued for the one week that we followed their growth (Figure B.1C-D). We also observed a milder form of compensatory growth in our DIO animals. After the behavioral studies had concluded and the animals were housed with *ad libitum* access to food for about one month, and the last thing that we did was measure their snout-to-anus length. This revealed pretty striking differences between groups, where the DIO animals were over 1 cm longer than the Control animals, and the DIOWL animals were also longer than the Controls in both male and female animals (Figure B.6H-I). The PD animals were closer in body length than the DIO groups, but the PDO animals were the longest, followed by the Restore group, then by the PDWL and Control mice (Figure B.1A). Similar relationships were found in the body weights

and in the lean mass NMR measures from the DIO groups, conducted a few days prior to the body length measures. Comparison of the body weights showed that the DIOWL animals were now heavier than the Control animals (Figure B.6B-C), and that they had greater lean mass (Figure B.6F-G), with no difference in fat mass (Figure B.6D-E). Then in our leptin minipump experiment, where we observed that the mice that received the leptin failed to gain weight post surgically (Figure 3.6D) like the PBS pump group and maintained lower weights throughout pump operation, yet after pump depletion they displayed a growth rebound and reached the same weights as the PBS pump group (Figure 3.6C).

Underlying a lot of the weight loss utilized in these studies, and the animals' nutritional state during the behavioral assays is calorie restriction. It would be foolish not to acknowledge the role that it may play in bringing forth many of the findings presented here. Food restriction leads to many changes in gene expression and functional interactions, and has been demonstrated to increase behavioral sensitivity to drugs of abuse and is associated with binge eating [213]. Chronic food restriction or fasting increases Arc *Agrp* and *Npy* mRNA expression, while reducing the expression of *Pomc* and *Cartpt* [214-220], effects that are intensified by access to a running wheel [221], and mitigated by treatment with leptin [222, 223]. This effect is evident in the amount of messenger present, as well as a change in the number of labeled cells [224]. Food deprivation also reduced the mRNA expression of the other hypothalamic pro-opio peptides, proDynorphin and proEnkephalin [225]. Leptin treatment alone in *ob/ob* mice increased Pomc expression [215, 226], while decreasing *Agrp* expression [227]. Hypothalamic *Pomc*, *Npy*, and *Lepr* display daily dynamics in their expression, which disappear with food restriction [228]. Calorie restriction also increases mRNA levels of *Th* and *Slc6a3* (dopamine transporter) in the VTA of male rats [229], and increases *D2dr* expression; whereas in obese rats *D2dr* expression

is attenuated [230]. Food restriction enhances pharmacological activation of dopamine D1Rs and D2Rs, without impacting D3R function [231, 232], and the presentation of food after food deprivation causes DA release in the NAc, which can be blocked by leptin administration [233]. Chronic food restriction also impacts the reinforcing properties of drugs, where it accentuates low dose amphetamine induced conditioned place preference (CPP), decreases CPP at higher doses, increases high dose amphetamine induced locomotion and blunts amphetamine induced dopamine release [234]. Additionally, acute food deprivation increases oral and intravenous drug intake in rats [235]. In the NAc of food restricted rats, D1R stimulation leads to increased NMDA NR1 subunit phosphorylation and consequent increases in NMDA receptor-dependent CaMK II and ERK1/2 signaling, and increased NMDA receptor/ERK1/2-dependent phosphorylation of the nuclear transcription factor, CREB. The upregulated cellular responses to D1R agonist challenge may underlie the augmentation of drug reward and appetitive instrumental learning during periods of food restriction [236, 237]. Short periods of food deprivation can also induce major changes in the metabolic function of adipocytes that can persist even after return to ad libitum conditions and normalization of body composition. Interestingly the rate of lipolysis is greatest at the initiation of food deprivation, than after prolonged periods [238]. Repeated weight loss and regain results in increased food efficiency, meaning that a history of weight loss makes it harder to lose weight and easier to gain weight in the future [239, 240], and can also lead to glucose intolerance [241].

Similarly to how food restriction tips the hypothalamic balance between *Pomc* and *Agrp*, most rodent models of obesity have a default imbalance between these genes. PD, *ob/ob*, *db/db*, and DIO animals, all have a relative AgRP-heavy imbalance in steady-state *AgRP* and *Pomc* mRNA expression levels [206, 214, 215, 217, 242], and not surprisingly in at least in *db/db* mice

this imbalance is intensified by fasting [214]. In all of these models of obesity, they eat fewer, but larger meals with longer inter-meal intervals (IMIs), in both nocturnal and diurnal periods [122, 243-245]. Furthermore, acute central leptin potently reduces meal frequency without impacting meal size in the rat [246], while intra-ARC infusion of leptin in a mouse suppresses food intake for up to 38 hours, through a reduction in meal size and meal number, and can be blocked by ICV or intra-NTS administration of SHU9119 [247].

The adipocyte hormone leptin regulates the function of both POMC- and AgRP-neurons, and is essential for normal energy homeostasis [248-250] and establishing the body weight set-point [57]. Mice that lack leptin or leptin receptors (*ob/ob* and *db/db*, respectively) become massively obese and diabetic [214, 215, 217]. *Ob/ob* mice also have reduced *Pomc* expression, and reduced circulating testosterone and elevated corticosterone, all of which are normalized after leptin treatment [226].

Melanocortin- and leptin-signaling converge throughout the hypothalamus and in the following mesolimbic nuclei: VTA, NAc, amygdala, and LH [192-194]. The VTA is the central hub of mesolimbic DA neurons, the NAc and Amy are two of the most prominent targets of DA input which are necessary for appetitive- and aversive-related behaviors [251], and the LH directly modulates activity in the VTA and is reciprocally connected with the NAc [252, 253]. In an assay designed to measure the rewarding value of sweetened solutions versus DA neuron stimulation, mice preferred sucrose to non-caloric sucralose, and optogenetic DA neuron stimulation over sucralose, but not sucrose. However, the animals preferred the combination of sucralose paired with DA neuron stimulation over sucrose, and this effect was attenuated by leptin administration. Furthermore, leptin administration suppressed sucrose-induced DA neuron activation, showing roles for leptin and DA in establishing the rewarding value of nutritive

substances [254]. Knockdown of AgRP or neonatal ablation of AgRP neurons leads to enhancement of dopaminergic signaling and dopamine-associated behaviors [255]. Pharmacology studies have uncovered roles for MCR agonists to decrease ethanol consumption and antagonists to increase intake; a behavior regarded to involve mesolimbic neural circuitry. These effects can be driven by local application to the VTA or NAc [91, 92, 256]. Furthermore, it was shown that MCR agonism enhances the ability of MOR antagonism to blunt binge-like ethanol consumption [257]. Counterintuitively, PD mice display severe deficits in ethanol consumption and preferences compared to wildtype mice [258]. Additionally, MC4R expression in striatal D1R-expressing medium spiny neurons is necessary for stress-induced anhedonia [259] and locomotor sensitization to cocaine [131, 260]. Furthermore, after long-term L-DOPA treatment, rats displayed elevated body weight months after the cessation of exposure, indicating that the refraction from drug exposure contributed to initiating mechanisms of compensatory weight gain, and again placing DA into the light as a potent contributor in the maintenance of body composition [261]. Consistently, obesity-prone rats have less extracellular and stimulated DA release [262], and bilateral hypothalamic infusion of dopamine in male Zucker rats drastically reduces food intake by reducing meal size, albeit increasing meal frequency [263]. In female rats, haloperidol (D2R inverse agonist) treatment increased *Pomc* expression, while bromocriptine (D2R agonist) decreased it [264].

Overall, the data in this chapter indicate that body weight does impact motivated consummatory behavior. Specifically weight loss after obesity potentiates binge-like feeding, when an animal is experiencing hunger. This phenomenon could contribute to the high rates of relapse to weight gain and the growing rate of obesity. Furthermore, we demonstrated that *Pomc* expression and pharmacologically targeting MCRs can be effective as therapeutic avenues to

help curb the weight loss induced increase in the drive to earn food, but that there are other physiological changes associated with weight loss that need to be investigated.

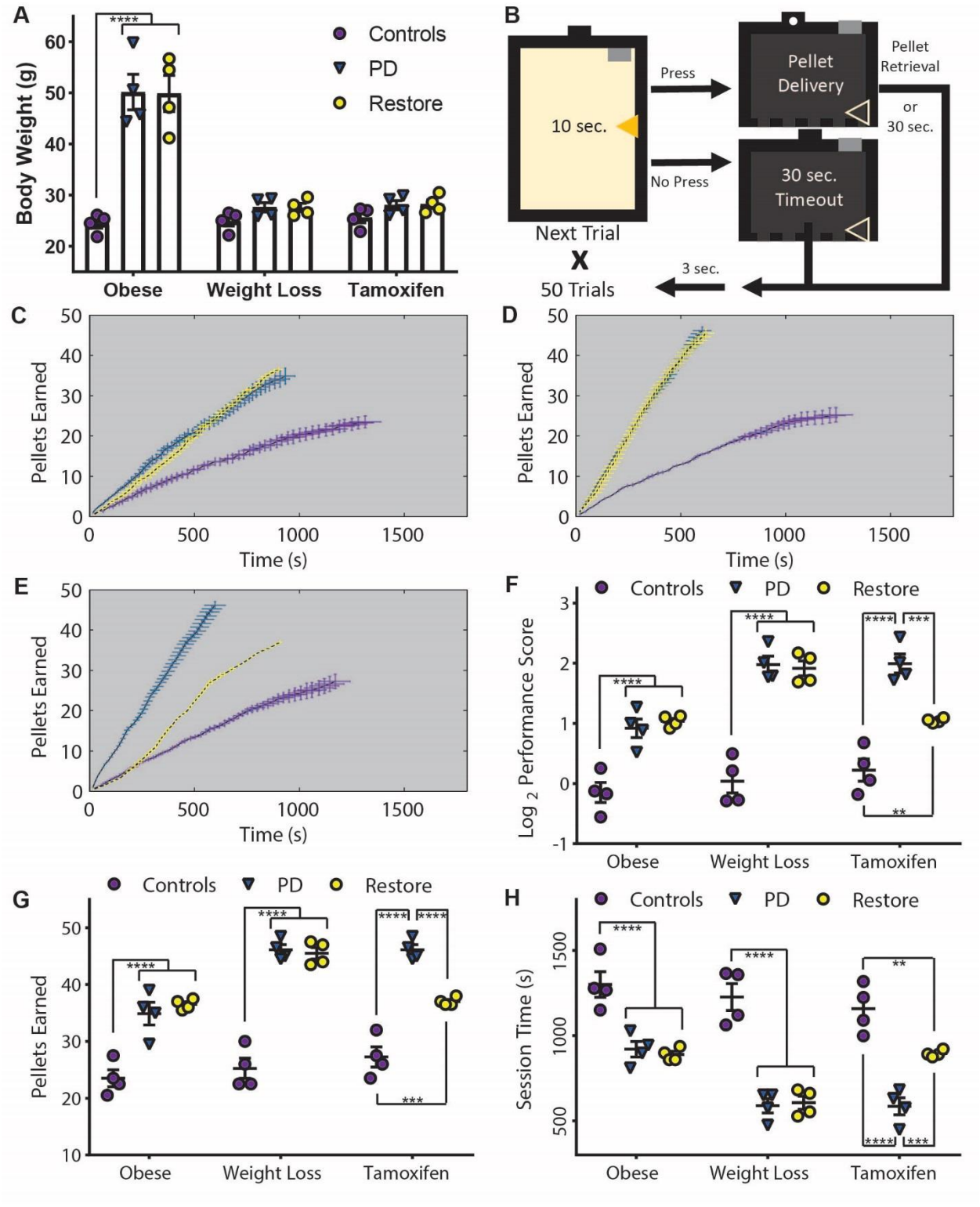
A
Body Weight (g)
Controls
PD
Restore
Obese
Weight Loss
Tamoxifen
B
10 sec.
Press
No Press
Pellet Delivery
30 sec. Timeout
Pellet Retrieval
or 30 sec.
Next Trial
X
50 Trials
3 sec.
C
D
Pellets Earned
Time (s)
E
F
Log 2 Performance Score
G
H
Session Time (s)

Fig 3.1: Comparison of FR1 operant performance between male Control, PD, and Restore mice, through obesity, weight loss, and tamoxifen treatment. **A,** Body weights during the three behavioral testing periods, while the PD mice were obese, after calorie-restriction-induced weight loss, and after tamoxifen treatment. **B,** Schematic of the FR1 task, representing the operant chamber depicting the illumination of the houselight and extension of the lever during a single trial and the possible outcomes, along with turning off the houselight and lever retraction. **C,** Group averages (±SEM) of pellets earned and session time at each of the 50 trials during the Obese stage. **D,** Group averages (±SEM) of pellets earned and session time at each of the 50 trials during the Weight Loss stage. **E,** Group averages (±SEM) of pellets earned and session time at each of the 50 trials during the Tamoxifen stage. **F,** Log_2 transformed performance score of each mouse's average session. Weight-loss enhanced the performance of both PD and Restore groups, and tamoxifen treatment partially reversed the behavior of the Restore group, to the same level as when they were obese **G,** Pellets earned in the average FR1 session for each mouse. The same relationships reported in Panel F were found, where the more pellets earned, the greater the performance. **H,** Time to completion in the average FR1 session for each mouse. Again the same relationships were found, where shorter session time indicates greater performance. Control mice are represented by purple, PD by blue, and Restore mice by yellow. *'s indicate a significant difference between bracketed groups. The number of characters indicate the p-value (1: < 0.05, 2: < 0.01, 3: < 0.001, and 4: < 0.0001).

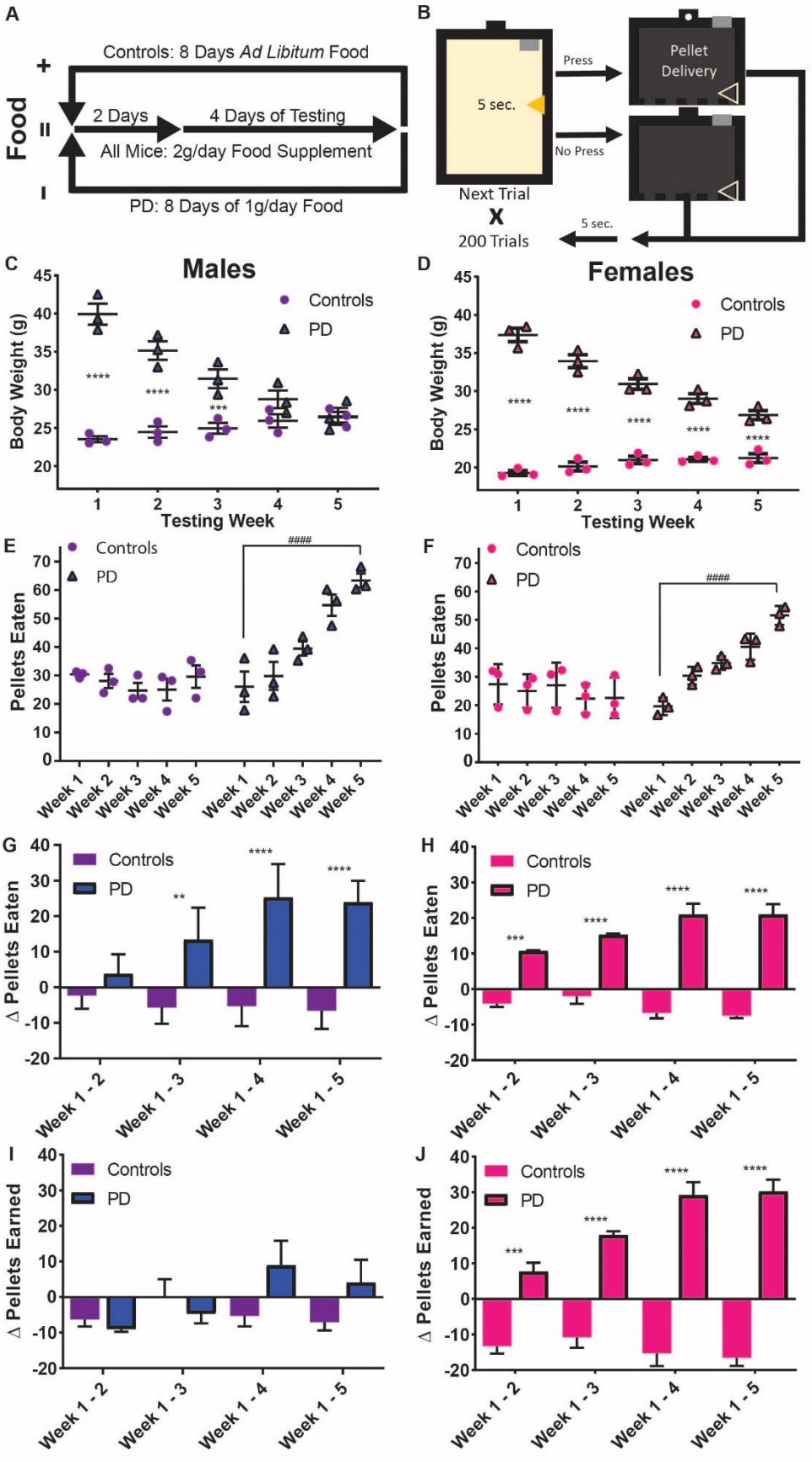
A
Controls: 8 Days *Ad Libitum* Food
Food
2 Days
4 Days of Testing
All Mice: 2g/day Food Supplement
PD: 8 Days of 1g/day Food
B
5 sec.
Press
No Press
Pellet Delivery
Next Trial
X
200 Trials
5 sec.
C
Males
Controls
PD
Body Weight (g)
Testing Week
D
Females
Controls
PD
Body Weight (g)
Testing Week
E
Controls
PD
Pellets Eaten
Week 1
Week 2
Week 3
Week 4
Week 5
F
Controls
PD
Pellets Eaten
G
Controls
PD
Δ Pellets Eaten
Week 1 - 2
Week 1 - 3
Week 1 - 4
Week 1 - 5
H
Controls
PD
Δ Pellets Eaten
I
Controls
PD
Δ Pellets Earned
J
Controls
PD
Δ Pellets Earned

Fig 3.2: Assessment of progressive weight loss on operant feeding in PD and Control mice. **A,** Experiment overview laying out the bi-weekly order and schedule of diet and behavioral testing periods. **B,** Body weight during the 5 behavioral testing periods over the course of the 10 week experiment. The behavioral and body weight data is averaged over the last two days of each period. **C,** Schematic of the Binge feeding task, representing the operant chamber depicting the illumination of the houselight and extension of the lever during 1 of the 200 session trials and the possible outcomes, along with turning off the houselight and lever retraction. **D,** Comparison of the amount of the food eaten during the Binge paradigm, calculated as the number of pellets earned minus the amount of food leftover, between the Control and PD animals. PD mice ate more food during the task with each subsequent testing epoch, whereas Control animals did not change their consumption. **E,** Pair-wise assessments between the change in session consumption for each group compared to how much they ate in the first testing epoch. PD mice ate significantly more than Control animals starting the in the 3rd testing epoch. Control mice are represented by the filled blue circles and bars, while the PD mice by the blue outlined upward triangles and bars. *'s indicate a significant difference between adjacent underlying groups, #'s indicate a significant main effect of an interaction between Time and Group assessed by Two-way RM ANOVA. The number of characters indicate the p-value (1: < 0.05, 2: < 0.01, 3: < 0.001, and 4: < 0.0001).

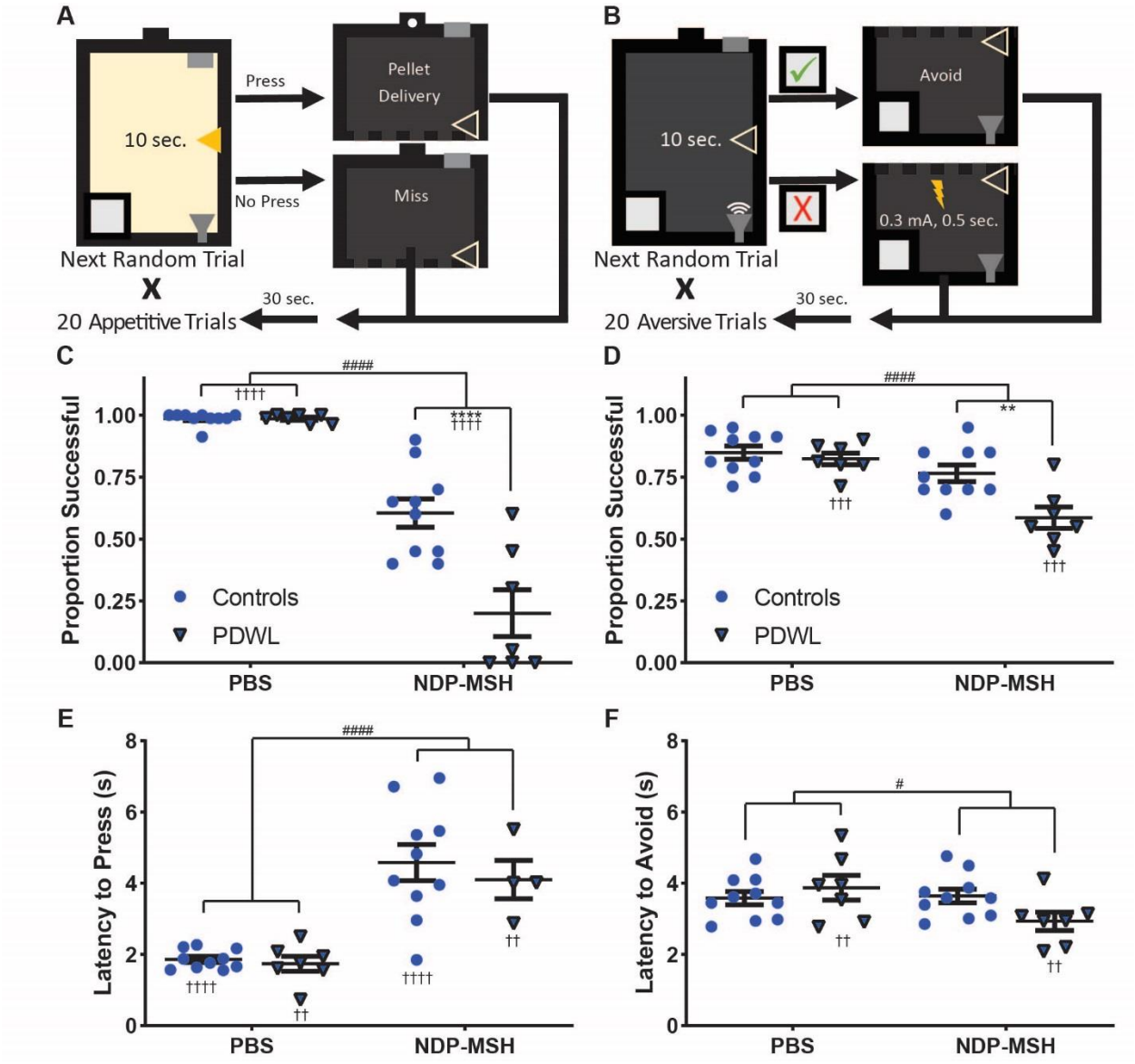
A
10 sec.
Press
No Press
Pellet Delivery
Miss
Next Random Trial
X
20 Appetitive Trials
30 sec.
B
10 sec.
Avoid
0.3 mA, 0.5 sec.
Next Random Trial
X
20 Aversive Trials
30 sec.
C
Proportion Successful
1.00
0.75
0.50
0.25
0.00
Controls
PDWL
PBS
NDP-MSH
D
Proportion Successful
Controls
PDWL
PBS
NDP-MSH
E
Latency to Press (s)
8
6
4
2
0
PBS
NDP-MSH
F
Latency to Avoid (s)
PBS
NDP-MSH

Fig 3.3: The impact of pharmacological activation of MC3/4Rs on interleaved appetitive consummatory behavior and aversive avoidance in male PDWL and Control mice. **A,** Schematic of the operant chambers during one of the appetitive trials, depicting the illumination of the houselight and extension of the lever during a single trial of the 20 randomly presented trials and the possible outcomes, along with turning off the houselight and lever retraction. **B,** Schematic of the operant chambers during one of the aversive trials, depicting the auditory tone during 1 of 20 randomly presented trials, and the possible outcomes of an imminent footshock or avoidance of the shock. **C,** Successful completion of the appetitive trials with PBS and NDP-MSH treatment. NDP-MSH substantially decreased performance in both Control and PDWL animals. However, PDWL mice were more severely impacted than Control animals. **D,** Successful completion of aversive trials with PBS and NDP-MSH. There was a main effect of NDP-MSH reducing performance. However, the Control animals did not significantly differ between treatments, only the PDWL group. **E,** Latency to lever press in appetitive trials. NDP-MSH treatment increased the latency to press in successful trials for both groups (there are fewer data points for the NDP-MSH treatment for the PDWL group, because there were animals that failed to perform any lever presses under treatment). **F,** Latency to avoid foot shock in aversive trials. Like the success in these trials, there was a main effect of NDP-MSH treatment, but only the PDWL showed a change. However, they were quicker to avoid, so while less successful overall, when they performed the task they did it faster. Control mice are represented by the blue filled circles, while the PDWL mice by the blue outlined downward triangles. *'s indicate a significant difference between adjacent underlying groups, †'s indicate a significant difference from the same group's performance in the other treatment condition, #'s indicate a significant main effect assessed by Two-way RM ANOVA. The number of characters indicate the p-value (1: < 0.05, 2: < 0.01, 3: < 0.001, and 4: < 0.0001).

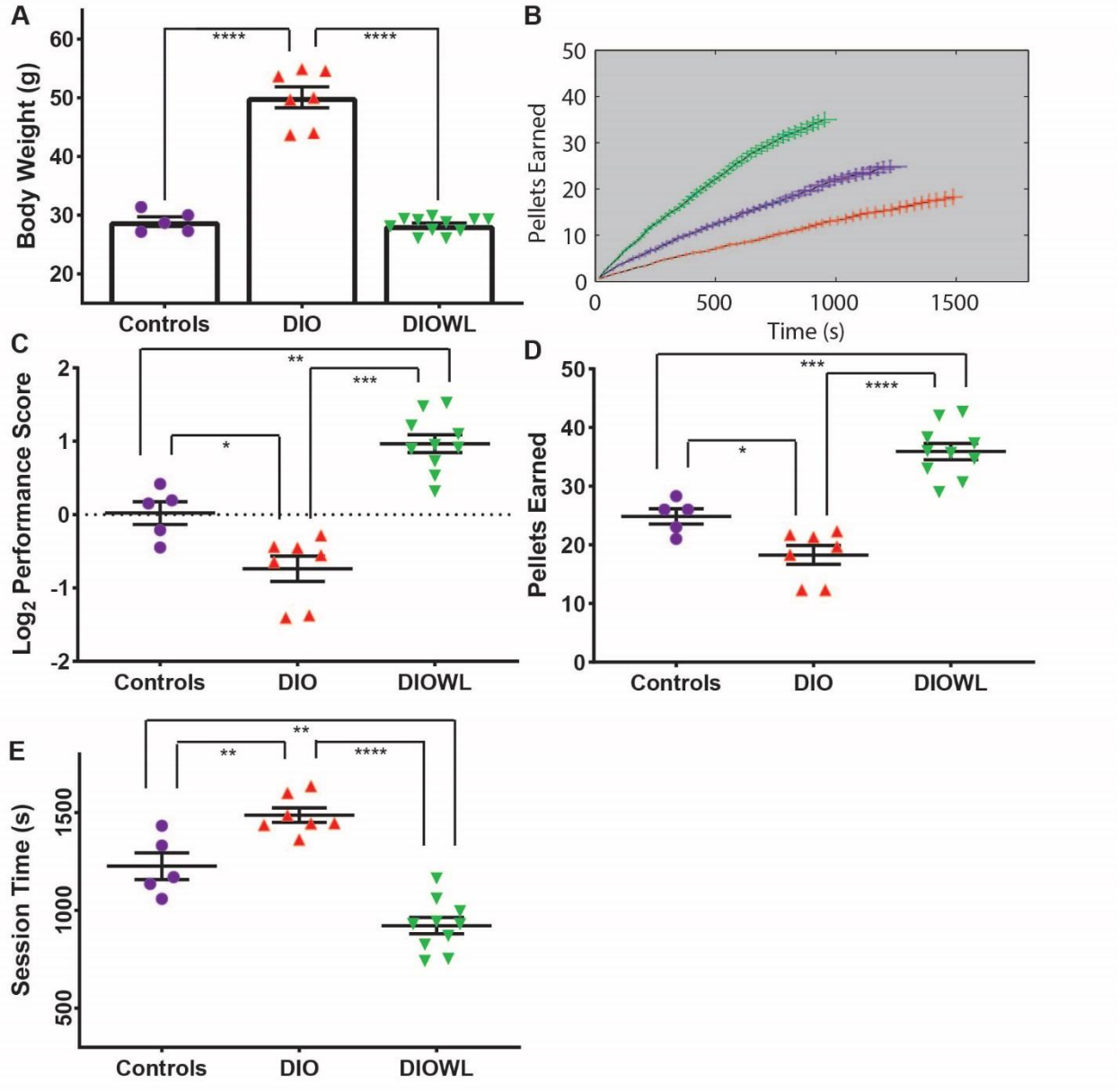
A
Body Weight (g)
60
50
40
30
20
****
****
Controls
DIO
DIOWL
B
Pellets Earned
50
40
30
20
10
0
0
500
1000
1500
Time (s)
C
Log2 Performance Score
2
1
0
-1
-2
**
***
*
Controls
DIO
DIOWL
D
Pellets Earned
50
40
30
20
10
0
***
****
*
Controls
DIO
DIOWL
E
Session Time (s)
1500
1000
500
**
**
****
Controls
DIO
DIOWL

Fig 3.4: Comparison of FR1 operant performance between male DIO, DIOWL, and Control mice. **A,** Schematic of the FR1 task, representing the operant chamber depicting the illumination of the houselight and extension of the lever during a single trial and the possible outcomes, along with turning off the houselight and lever retraction **B,** Group averages (±SEM) of pellets earned and session time at each of the 50 trials. **C,** Log_2 transformed performance score of each mouse's average session. Weight-loss groups (DIOWL and PDWL) mice performed better than their respective obese groups (DIO and PDO), and PD groups outperformed their respective DIO groups. The Restore mice exhibited partial normalization of FR1 behavior, similar to DIOWL and PDO mice. **D,** Pellets earned in the average FR1 session for each mouse. The same relationships reported in Panel C were found, where the more pellets earned the greater the performance. **E,** Time to completion in the average FR1 session for each mouse. Again the same relationships were found, where shorter session time indicates greater performance. Control mice are represented by purple, DIO by red, DIOWL by green, PDO by orange, PDWL by blue, and Restore mice by yellow. Individual Control and Restore data points are shown with circles, obese animals by upward triangles, and weight-loss animals by downward triangles. Animals from DIO cohorts are shown with filled shapes, and mice from PD cohorts are outlined in black. *'s indicate a significant difference between bracketed groups, †'s indicate a significant difference from every other group. The exception is that there were no measured differences between DIOWL, PDO, and Restore groups for any measure. The number of characters indicate the p-value (1: < 0.05, 2: < 0.01, 3: < 0.001, and 4: < 0.0001).

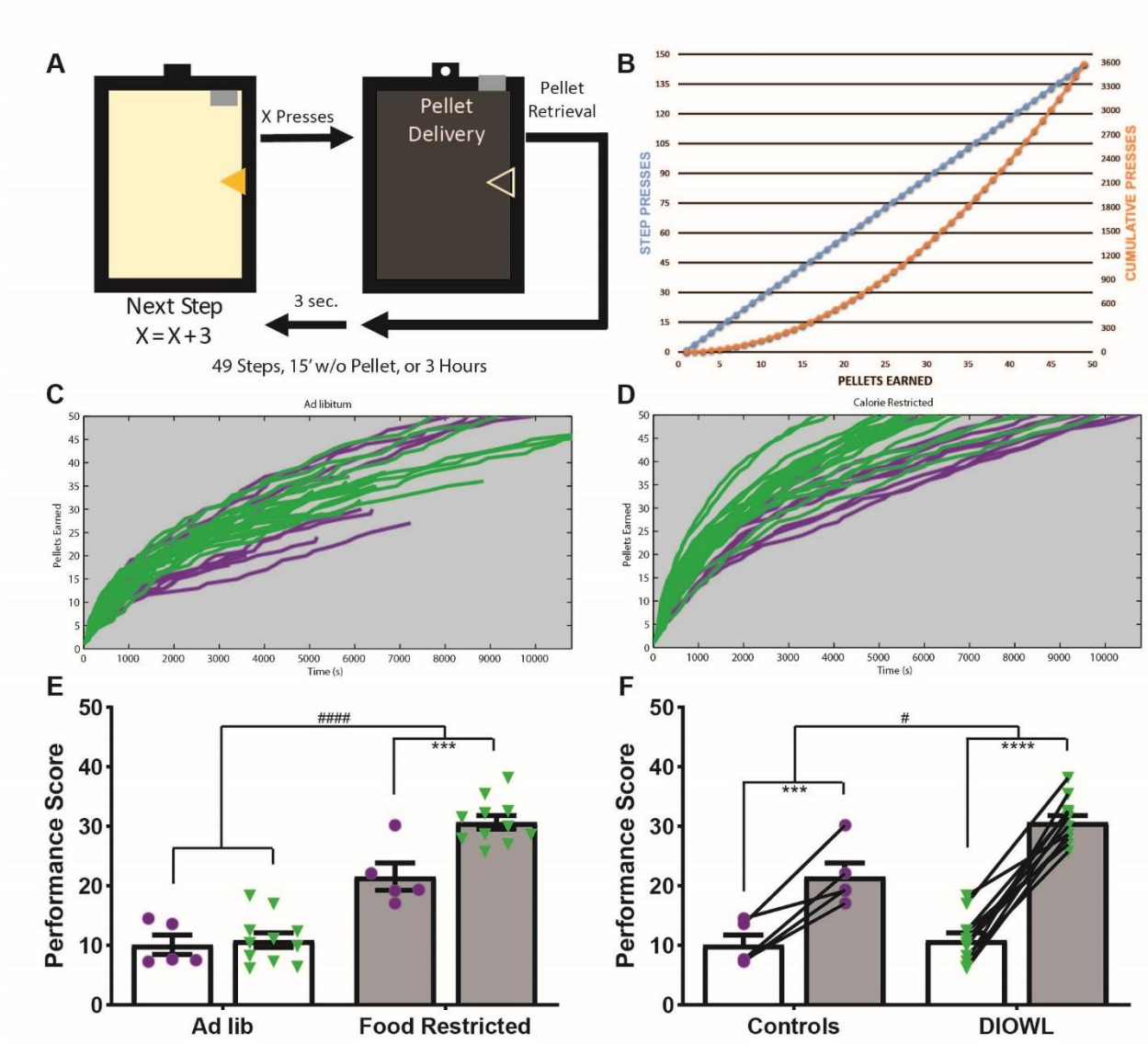
A
X Presses
Pellet Delivery
Pellet Retrieval
Next Step X=X+3
3 sec.
49 Steps, 15' w/o Pellet, or 3 Hours
B
STEP PRESSES
CUMULATIVE PRESSES
PELLETS EARNED
C
Ad libitum
Pellets Earned
Time (s)
D
Calorie Restricted
Pellets Earned
Time (s)
E
Performance Score
####
***
Ad lib
Food Restricted
F
Performance Score
#
***
****
Controls
DIOWL

Fig 3.5: Comparison of Progressive Ratio performance between male Control and DIOWL mice in an *ad libitum* and food restricted state. **A,** Schematic of the Progressive Ratio task, representing the operant chamber with the houselight illuminated and lever extended during a single progressive ratio step, followed by the pellet delivery, lever retraction, and houselight deillumination. **B,** The relationship between the number of presses required at each step of the paradigm with regards to the cumulative session presses to complete the task. **C,** Single session traces from individual mice housed with *ad libitum* access to food, showing the number of pellets achieved versus session time, comprised of the two sessions with the best performance for each animal. **D,** Single session traces from individual mice under mild, acute food restriction, comprised of the two sessions with the best performance for each animal. **E,** Comparison of group and condition differences in Progressive Ratio performance. Food restricted mice performed better than ad libitum mice, and food restricted DIOWL animals outperformed food restricted Control mice. **F,** Comparison of food restriction-induced potentiation of progressive ratio performance. Control mice are represented by purple lines or circles and DIOWL animals by green lines or downward triangles. *Ad libitum* conditions are represented by white bars and food restriction conditions by grey bars. *'s indicate a significant difference between bracketed groups, #'s indicate a significant main effect assessed by Two-way RM ANOVA. The number of characters indicate the p-value (1: < 0.05, 2: < 0.01, 3: < 0.001, and 4: < 0.0001).

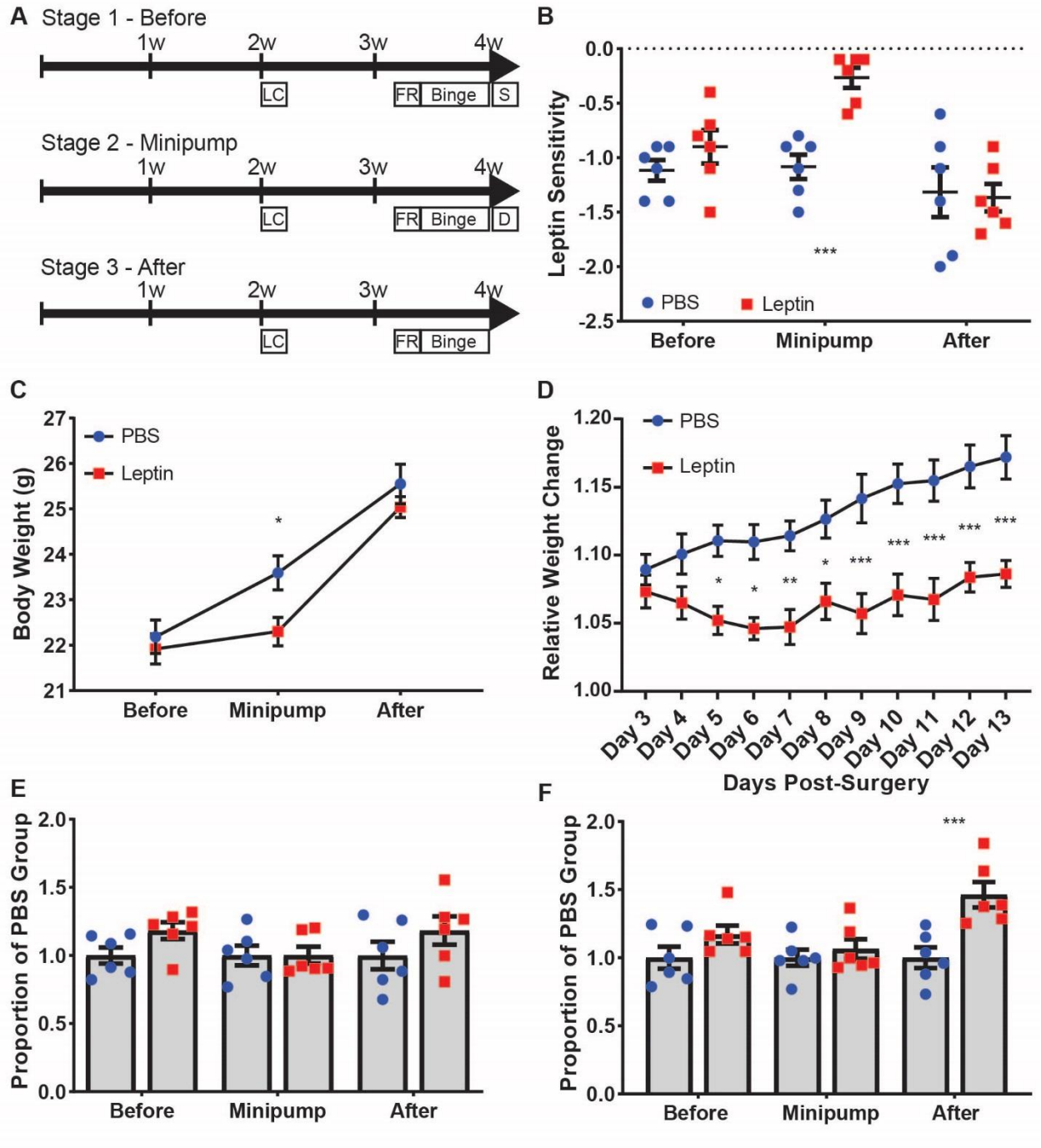
A
Stage 1 - Before
1w
2w
3w
4w
LC
FR
Binge
S
Stage 2 - Minipump
D
Stage 3 - After
B
Leptin Sensitivity
PBS
Leptin
Before
Minipump
After
C
Body Weight (g)
D
Relative Weight Change
Day 3
Day 4
Day 5
Day 6
Day 7
Day 8
Day 9
Day 10
Day 11
Day 12
Day 13
Days Post-Surgery
E
Proportion of PBS Group
F

Fig 3.6: Efficacy and effect of leptin minipump implantation, and the reversal of hyperleptinemia increases binge earning, but not eating. **A,** Schematic of the experiment structure and timeline. LC is the acute leptin challenge to assess leptin sensitivity, FR is the period of food restriction prior to behavior, Binge is the behavioral testing period, S is the surgical implantation of the osmotic minipumps, and D represents when the minipumps were depleted according to the manufacturers specifications. **B,** Leptin sensitivity measured as the difference in body weight change to 24 hour leptin treatment vs 24 hour PBS treatment. The only group that did not show a marked difference in body weight during acute leptin treatment were the mice that received the leptin minipumps, during pump operation. **C,** Body weights during behavioral periods. Mice that received leptin minipumps weighed less than the PBS minipump cohort, only during pump operation. The PBS minipump cohort was heavier at each behavioral point, whereas the leptin minipump group was only heavier after the pumps were depleted. **D,** Post-surgical weight change. The leptin minipump mice failed to gain weight after a return from mild food restriction to *ad libitum* food access. **E,** Food eaten during the Binge paradigm, normalized to the PBS minipump group. No significant differences were measured. **F,** Food earned during the Binge paradigm, normalized to the PBS minipump group. The leptin minipump group earned significantly more pellets after minipump operation, but did not eat the pellets earned. PBS minipump cohort mice are represented by the blue filled circles, while the mice that received the leptin minipumps by the red filled squares. *'s indicate a significant difference between adjacent groups assessed by Two-way RM ANOVA. The number of characters indicate the p-value (1: < 0.05, 2: < 0.01, and 3: < 0.001).

Table 3.1: Descriptive statistics table for Chapter III

Figure	Sample size	Mean ± SEM	Measure
3.1a	Obese:		Body Weight
	Controls: n = 4	24.48 ± 0.92	
	PD: n = 4	50.15 ± 3.48	
	Restore: n = 4	49.90 ± 3.54	
	Weight Loss:		
	Controls: n = 4	24.93 ± 0.96	
	PD: n = 4	27.63 ± 0.91	
	Restore: n = 4	27.58 ± 0.80	
	Tamoxifen:		
	Controls: n = 4	25.63 ± 1.01	
	PD: n = 4	28.05 ± 0.90	
	Restore: n = 4	28.25 ± 0.85	
3.1f	Obese:		Log2 Performance Score
	Controls: n = 4	-0.15 ± 0.17	
	PD: n = 4	0.92 ± 0.16	
	Restore: n = 4	1.04 ± 0.05	
	Weight Loss:		
	Controls: n = 4	0.04 ± 0.19	
	PD: n = 4	1.98 ± 0.14	
	Restore: n = 4	1.92 ± 0.12	
	Tamoxifen:		
	Controls: n = 4	0.22 ± 0.19	
	PD: n = 4	2.00 ± 0.16	
	Restore: n = 4	1.05 ± 0.02	
3.1g	Obese:		Pellets Earned
	Controls: n = 4	23.50 ± 1.47	
	PD: n = 4	34.88 ± 1.98	
	Restore: n = 4	36.50 ± 0.46	
	Weight Loss:		
	Controls: n = 4	25.25 ± 1.79	
	PD: n = 4	46.13 ± 0.90	
	Restore: n = 4	45.50 ± 1.02	
	Tamoxifen:		
	Controls: n = 4	27.25 ± 1.79	
	PD: n = 4	46.13 ± 0.90	
	Restore: n = 4	37.00 ± 0.35	
3.1h	Obese:		Session Time (s)
	Controls: n = 4	1300.9 ± 74.8	
	PD: n = 4	920.1 ± 45.3	
	Restore: n = 4	889.2 ± 18.5	
	Weight Loss:		
	Controls: n = 4	1226.7 ± 79.0	
	PD: n = 4	589.1 ± 41.8	
	Restore: n = 4	606.4 ± 38.4	
	Tamoxifen:		
	Controls: n = 4	1158.3 ± 70.7	

	PD: n = 4 Restore: n = 4	585.0 ± 50.0 895.1 ±9.6	
Figure	Sample size	Mean ± SEM	Measure
3.2c	Control: n = 3 PD: n = 3	Data order: Control, PD Week 1: 23.52 ± 0.40, 39.92 ± 1.38 Week 2: 24.45 ± 0.75, 35.15 ± 1.21 Week 3: 24.95 ± 0.71, 31.45 ± 1.23 Week 4: 25.92 ± 0.88, 28.77 ± 1.16 Week 5: 26.40 ± 0.70, 26.52 ± 1.11	Grams
3.2d	Control: n = 3 PD: n = 3	Data order: Control, PD Week 1: 19.27 ± 0.32, 37.37 ± 0.87 Week 2: 20.12 ± 0.55, 33.93 ± 0.84 Week 3: 20.97 ± 0.48, 30.93 ± 0.68 Week 4: 21.05 ± 0.25, 29.02 ± 0.64 Week 5: 21.22 ± 0.59, 26.85 ± 0.61	Grams
3.2e	Control: n = 3 PD: n = 3	Data order: Control, PD Week 1: 0.61 ± 0.01, 0.52 ± 0.11 Week 2: 0.56 ± 0.05, 0.60 ± 0.10 Week 3: 0.49 ± 0.05, 0.79 ± 0.05 Week 4: 0.50 ± 0.08, 1.10 ± 0.08 Week 5: 0.59 ± 0.08, 1.27 ± 0.05	Grams (Each Pellet = 20mg)
3.2f	Control: n = 3 PD: n = 3	Data order: Control, PD Week 1: 0.55 ± 0.08, 0.39 ± 0.04 Week 2: 0.50 ± 0.07, 0.61 ± 0.04 Week 3: 0.54 ± 0.09, 0.70 ± 0.03 Week 4: 0.45 ± 0.06, 0.81 ± 0.05 Week 5: 0.45 ± 0.08, 1.03 ± 0.04	Grams (Each Pellet = 20mg)
3.2g	Control: n = 3 PD: n = 3	Data order: Control, PD Week 1-2: -0.05 ± 0.04, 0.08 ± 0.06 Week 1-3: -0.11 ± 0.05, 0.27 ± 0.10 Week 1-4: -0.11 ± 0.06, 0.51 ± 0.11 Week 1-5: -0.13 ± 0.06, 0.48 ± 0.07	Grams (Each Pellet = 20mg)
3.2h	Control: n = 3 PD: n = 3	Data order: Control, PD Week 1-2: -0.08 ± 0.02, 0.22 ± 0.01 Week 1-3: -0.04 ± 0.04, 0.31 ± 0.01 Week 1-4: -0.13 ± 0.03, 0.42 ± 0.06 Week 1-5: -0.15 ± 0.01, 0.42 ± 0.06	Grams (Each Pellet = 20mg)
3.2i	Control: n = 3 PD: n = 3	Data order: Control, PD Week 1-2: -0.13 ± 0.04, -0.18 ± 0.02 Week 1-3: 0.00 ± 0.1, -0.10 ± 0.06 Week 1-4: -0.11 ± 0.06, 0.18 ± 0.14 Week 1-5: -0.14 ± 0.05, 0.08 ± 0.13	Grams (Each Pellet = 20mg)
3.2j	Control: n = 3 PD: n = 3	Data order: Control, PD Week 1-2: -0.27 ± 0.04, 0.15 ± 0.05 Week 1-3: -0.22 ± 0.06, 0.36 ± 0.02 Week 1-4: -0.31 ± 0.07, 0.58 ± 0.07 Week 1-5: -0.33 ± 0.05, 0.61 ± 0.07	Grams (Each Pellet = 20mg)
Figure	Sample size	Mean ± SEM	Measure
3.3c	Controls: n = 10	PBS: 0.97 ± 0.01 NDP-MSH: 0.61 ± 0.06	Proportion Successful

	PDWL: n = 7	PBS: 0.97 ± 0.01 NDP-MSH: 0.20 ± 0.10	
3.3d	Controls: n = 10 PDWL: n = 7	PBS: 0.85 ± 0.03 NDP-MSH: 0.77 ± 0.03 PBS: 0.82 ± 0.02 NDP-MSH: 0.59 ± 0.04	Proportion Successful
3.3e	Controls: n = 10 PDWL: n = 7	PBS: 1.86 ± 0.09 NDP-MSH: 4.58 ± 0.51 PBS: 1.74 ± 0.21 NDP-MSH: 4.10 ± 0.54	Latency to Press (s)
3.3f	Controls: n = 10 PDWL: n = 7	PBS: 3.58 ± 0.19 NDP-MSH: 3.64 ± 0.20 PBS: 3.88 ± 0.35 NDP-MSH: 2.93 ± 0.25	Latency to Avoid (s)
Figure	Sample size	Mean ± SEM	Measure
3.4a	Controls: n = 5 DIO: n = 7 DIOWL: n = 10	28.92 ± 0.80 50.09 ± 1.79 28.28 ± 0.40	Grams
3.4c	Controls: n = 5 DIO: n = 7 DIOWL: n = 10	0.02 ± 0.16 -0.74 ± 0.17 0.123.36E-3	Log2 Performance Score
3.4d	Controls: n = 5 DIO: n = 7 DIOWL: n = 10	24.87 ± 1.29 18.3 ± 1.62 35.93 ± 1.40	Pellets Earned
3.4e	Controls: n = 5 DIO: n = 7 DIOWL: n = 10	1226 ± 68 1487 ± 37 922 ± 42	Session Time (s)
Figure	Sample size	Mean ± SEM	Measure
3.5e-f	Controls: n = 5 DIOWL: n = 11	Ad libitum: 10.12 ± 1.62 Food Restricted: 21.57 ± 2.30 Ad libitum: 10.87 ± 1.21 Food Restricted: 30.70 ± 1.13	Performance Score
Figure	Sample size	Mean ± SEM	Measure
3.6b	PBS: n = 6 Leptin: n = 6	Data order: PBS, Leptin Before: -1.12 ± 0.10, -0.90 ± 0.15 Minipump: -1.08 ± 0.11, -0.27 ± 0.09 After: -1.32 ± 0.23, -1.37 ± 0.13	Grams
3.6c	PBS: n = 6 Leptin: n = 6	Data order: PBS, Leptin Before: 22.18 ± 0.37, 21.92 ± 0.32 Minipump: 23.59 ± 0.37, 22.3 ± 0.31 After: 25.55 ± 0.44,25.04 ± 0.23	Grams
3.6d	PBS: n = 6 Leptin: n = 6	Data order: PBS, Leptin Day 3: 1.09 ± 0.01, 1.07 ± 0.01 Day 4: 1.10 ± 0.02, 1.07 ± 0.01 Day 5: 1.11 ± 0.01, 1.05 ± 0.01 Day 6: 1.11 ± 0.01, 1.05 ± 0.01 Day 7: 1.12 ± 0.01, 1.05 ± 0.01 Day 8: 1.13 ± 0.01, 1.07 ± 0.01 Day 9: 1.14 ± 0.02, 1.06 ± 0.02 Day 10: 1.15 ± 0.02, 1.07 ± 0.02 Day 11: 1.16 ± 0.02, 1.07 ± 0.02 Day 12: 1.17 ± 0.02, 1.08 ± 0.01 Day 13: 1.17 ± 0.02, 1.09 ± 0.01	Proportion of Pre-surgery Body Weight

3.6e	PBS: n = 6 Leptin: n = 6	Data order: PBS, Leptin Before: 1.00 ± 0.06, 1.18 ± 0.06 Minipump: 1.00 ± 0.07, 1.00 ± 0.06 After: 1.00 ± 0.10, 1.18 ± 0.10	Proportion of PBS Group
3.6f	PBS: n = 6 Leptin: n = 6	Data order: PBS, Leptin Before: 1.00 ± 0.08, 1.17 ± 0.07 Minipump: 1.00 ± 0.06, 1.06 ± 0.07 After: 1.00 ± 0.08, 1.46 ± 0.09	Proportion of PBS Group

Table 3.2: Statistical tests table for Chapter III

Figure	Type of test	Statistical data	P Value		Sig.
3.1a	Two-way RM ANOVA	Interaction: F(4,18) = 31.89	6.01E-08		####
		Treatment: F(2,18) = 114.7	5.71E-11		####
		Group: F(2,9) = 16.22	1.04E-03		##
		Tukey's multiple comparisons test		q	
		Obese:			
		Controls vs. PD	5.57E-10	13.96	****
		Controls vs. Restore	6.86E-10	13.82	****
		PD vs. Restore	9.95E-01	0.14	ns
		Weight Loss:			
		Controls vs. PD	5.60E-01	1.47	ns
		Controls vs. Restore	5.72E-01	1.44	ns
		PD vs. Restore	1.00E+00	0.03	ns
		Tamoxifen			
		Controls vs. PD	0.625002	1.32	ns
		Controls vs. Restore	0.577564	1.43	ns
		PD vs. Restore	9.97E-01	0.11	ns
		Controls:			
		Obese vs. Weight Loss	9.70E-01	0.33	ns
		Obese vs. Tamoxifen	8.22E-01	0.85	ns
		Weight Loss vs. Tamoxifen	9.29E-01	0.52	ns
		PD:			
		Obese vs. Weight Loss	2.04E-09	16.63	****
		Obese vs. Tamoxifen	2.77E-09	16.31	****
		Weight Loss vs. Tamoxifen	9.73E-01	0.31	ns
		Restore:			
		Obese vs. Weight Loss	2.36E-09	16.48	****
		Obese vs. Tamoxifen	3.84E-09	15.98	****
		Weight Loss vs. Tamoxifen	9.34E-01	0.50	ns
3.1f	Two-way RM ANOVA	Interaction: F(4,18) = 14.72	1.67E-05		####
		Treatment: F(2,18) = 42.06	1.64E-07		####
		Group: F(2,9) = 50.47	1.29E-05		####
		Tukey's multiple comparisons test		q	
		Obese:			
		Controls vs. PD	4.18E-05	7.47	****
		Controls vs. Restore	8.96E-06	8.29	****
		PD vs. Restore	8.32E-01	0.82	ns
		Weight Loss:			
		Controls vs. PD	9.94E-10	13.58	****
		Controls vs. Restore	2.05E-09	13.12	****
		PD vs. Restore	9.43E-01	0.46	ns
		Tamoxifen			
		Controls vs. PD	6.66E-09	12.39	****
		Controls vs. Restore	0.00103	5.76	**
		PD vs. Restore	2.04E-04	6.63	***
		Controls:			
		Obese vs. Weight Loss	3.82E-01	1.92	ns
		Obese vs. Tamoxifen	3.63E-02	3.84	*
		Weight Loss vs. Tamoxifen	3.86E-01	1.91	ns
		PD:			
		Obese vs. Weight Loss	1.09E-06	10.97	****

		Obese vs. Tamoxifen	9.09E-07	11.12	****
		Weight Loss vs. Tamoxifen	9.94E-01	0.14	ns
		Restore:			
		Obese vs. Weight Loss	1.39E-05	9.07	****
		Obese vs. Tamoxifen	9.97E-01	0.10	ns
		Weight Loss vs. Tamoxifen	1.60E-05	8.98	****
3.1g	Two-way RM ANOVA	Interaction: F(4,18) = 12.53	4.79E-05		####
		Treatment: F(2,18) = 37.16	4.07E-07		####
		Group: F(2,9) = 87.88	1.24E-06		####
		Tukey's multiple comparisons test		q	
		Obese:			
		Controls vs. PD	4.33E-06	8.68	****
		Controls vs. Restore	4.54E-07	9.92	****
		PD vs. Restore	6.59E-01	1.24	ns
		Weight Loss:			
		Controls vs. PD	3.11E-11	15.93	****
		Controls vs. Restore	6.13E-11	15.45	****
		PD vs. Restore	9.39E-01	0.48	ns
		Tamoxifen			
		Controls vs. PD	2.86E-10	14.40	****
		Controls vs. Restore	4.4E-05	7.44	****
		PD vs. Restore	1.08E-04	6.96	***
		Controls:			
		Obese vs. Weight Loss	4.94E-01	1.64	ns
		Obese vs. Tamoxifen	5.80E-02	3.50	ns
		Weight Loss vs. Tamoxifen	4.02E-01	1.87	ns
		PD:			
		Obese vs. Weight Loss	1.99E-06	10.51	****
		Obese vs. Tamoxifen	1.99E-06	10.51	****
		Weight Loss vs. Tamoxifen	>0.999	0.00	ns
		Restore:			
		Obese vs. Weight Loss	3.60E-05	8.41	****
		Obese vs. Tamoxifen	9.42E-01	0.47	ns
		Weight Loss vs. Tamoxifen	7.11E-05	7.94	****
3.1h	Two-way RM ANOVA	Interaction: F(4,18) = 12.29	5.41E-05		####
		Treatment: F(2,18) = 36.18	4.94E-07		####
		Group: F(2,9) = 39.34	3.56E-05		####
		Tukey's multiple comparisons test		q	
		Obese:			
		Controls vs. PD	6.68E-05	7.22	****
		Controls vs. Restore	2.22E-05	7.80	****
		PD vs. Restore	9.10E-01	0.59	ns
		Weight Loss:			
		Controls vs. PD	1.09E-08	12.09	****
		Controls vs. Restore	1.88E-08	11.76	****
		PD vs. Restore	9.71E-01	0.33	ns
		Tamoxifen			
		Controls vs. PD	8.57E-08	10.87	****
		Controls vs. Restore	0.004211	4.99	**
		PD vs. Restore	8.28E-04	5.88	***
		Controls:			
		Obese vs. Weight Loss	2.91E-01	2.20	ns
		Obese vs. Tamoxifen	2.06E-02	4.22	*

		Weight Loss vs. Tamoxifen	3.46E-01	2.03	ns
		PD:			
		Obese vs. Weight Loss	5.10E-06	9.80	****
		Obese vs. Tamoxifen	4.33E-06	9.92	****
		Weight Loss vs. Tamoxifen	9.96E-01	0.12	ns
		Restore:			
		Obese vs. Weight Loss	3.77E-05	8.38	****
		Obese vs. Tamoxifen	9.92E-01	0.18	ns
		Weight Loss vs. Tamoxifen	2.93E-05	8.55	****
Figure	Type of test	Statistical data	P Value		Sig.
3.2c	Two-way RM ANOVA	Interaction: F(4,16) = 589.4	< 1e-15		####
		Time: F(4,16) = 246.9	3.70E-14		####
		Group: F(1,4) = 27.68	6.25E-03		##
		Sidak's multiple comparisons test		t	
		Controls vs. PD			
		Week 1	1.18E-09	11.63	****
		Week 2	1.31E-06	7.59	****
		Week 3	8.47E-04	4.61	***
		Week 4	2.54E-01	2.02	ns
		Week 5	1.00E+00	0.08	ns
3.2d	Two-way RM ANOVA	Interaction: F(4,16) = 153.7	1.5E-12		####
		Time: F(4,16) = 70.72	5.78E-10		####
		Group: F(1,4) = 198.4	1.48E-04		###
		Sidak's multiple comparisons test		t	
		Controls vs. PD			
		Week 1	2.20E-14	20.94	****
		Week 2	3.72E-12	15.98	****
		Week 3	1.38E-09	11.53	****
		Week 4	6.14E-08	9.22	****
		Week 5	1.19E-05	6.52	****
3.2e	Two-way RM ANOVA	Interaction: F(4,16) = 20.92	3.4E-06		####
		Time: F(4,16) = 18.48	7.62E-06		####
		Group: F(1,4) = 16.52	1.53E-02		#
		Sidak's multiple comparisons test		t	
		Controls vs. PD			
		Week 1	9.20E-01	0.87	ns
		Week 2	9.98E-01	0.36	ns
		Week 3	3.69E-02	2.98	*
		Week 4	3.73E-05	5.99	****
		Week 5	6.17E-06	6.83	****
3.2f	Two-way RM ANOVA	Interaction: F(4,16) = 40.16	3.75E-08		####
		Time: F(4,16) = 21.10	3.21E-06		####
		Group: F(1,4) = 7.35	5.34E-02		ns
		Sidak's multiple comparisons test		t	
		Controls vs. PD			
		Week 1	4.48E-01	1.78	ns
		Week 2	> 0.99	1.24	ns
		Week 3	4.35E-01	1.80	ns
		Week 4	2.24E-03	4.19	**
		Week 5	8.68E-06	6.66	****
3.2g	Two-way RM ANOVA	Interaction: F(3,12) = 7.32	4.75E-03		##
		Time: F(3,12) = 3.96	3.56E-02		#
		Group: F(1,4) = 35.37	4.01E-03		##

		Sidak's multiple comparisons test		t	
		Controls vs. PD			
		Week 1-2	7.01E-01	1.17	ns
		Week 1-3	8.49E-03	3.66	**
		Week 1-4	9.24E-05	5.88	****
		Week 1-5	9.58E-05	5.86	****
3.2h	Two-way RM ANOVA	Interaction: F(3,12) = 8.97	2.16E-03		##
		Time: F(3,12) = 2.20	1.40E-01		ns
		Group: F(1,4) = 194.2	1.54E-04		###
		Sidak's multiple comparisons test		t	
		Controls vs. PD			
		Week 1-2	1.21E-04	5.74	***
		Week 1-3	2.09E-05	6.69	****
		Week 1-4	4.12E-08	10.72	****
		Week 1-5	2.66E-08	11.06	****
3.2i	Two-way RM ANOVA	Interaction: F(3,12) = 5.26	1.51E-02		#
		Time: F(3,12) = 3.54	5.82E-02		ns
		Group: F(1,4) = 3.37	3.82E-01		ns
3.2j	Two-way RM ANOVA	Interaction: F(3,12) = 32.38	4.93E-06		####
		Time: F(3,12) = 17.54	1.10E-04		###
		Group: F(1,4) = 105.0	5.12E-04		###
		Sidak's multiple comparisons test		t	
		Controls vs. PD			
		Week 1-2	2.64E-04	5.34	***
		Week 1-3	6.70E-06	7.34	****
		Week 1-4	1.90E-08	11.32	****
		Week 1-5	9.11E-09	11.92	****
Figure	Type of test	Statistical data	P Value		Sig.
3.3c	Two-way RM ANOVA	Interaction: F(1,15) = 15.33	1.38E-03		##
		Group: F(1,15) = 14.68	1.63E-03		##
		Treatment: F(1,15) = 127.6	9.81E-09		####
		Sidak's multiple comparisons test		t	
		Controls vs. PDWL			
		PBS	1.00E+00	0.01	ns
		NDP-MSH	1.21E-05	5.48	****
		PBS vs. NDP-MSH			
		Controls	7.65E-05	5.75	****
		DIOWL	1.11E-07	9.92	****
3.3d	Two-way RM ANOVA	Interaction: F(1,15) = 6.46	2.26E-02		#
		Group: F(1,15) = 8.47	1.08E-02		#
		Treatment: F(1,15) = 28.21	8.72E-05		####
		Sidak's multiple comparisons test		t	
		Controls vs. PDWL			
		PBS	8.29E-01	0.55	ns
		NDP-MSH	1.11E-03	3.86	**
		PBS vs. NDP-MSH			
		Controls	9.29E-02	2.16	ns
		DIOWL	2.51E-04	5.12	***
3.3e	Mixed Effects Model (REML)	Interaction: F(1,27) = 0.20	1.38E-03		ns
		Group: F(1,27) = 0.56	1.63E-03		ns
		Treatment: F(1,27) = 40.29	9.81E-09		####
		Sidak's multiple comparisons test		t	
		Controls vs. PDWL			

		PBS	9.66E-01	0.24	ns
		NDP-MSH	6.90E-01	0.78	ns
		PBS vs. NDP-MSH			
		Controls	6.30E-06	5.85	****
		DIOWL	2.37E-03	3.62	**
3.3f	Two-way RM ANOVA	Interaction: F(1,15) = 10.39	5.68E-03		##
		Group: F(1,15) = 0.47	5.04E-01		ns
		Treatment: F(1,15) = 8.04	1.25E-02		#
		Sidak's multiple comparisons test		t	
		Controls vs. PDWL			
		PBS	6.37E-01	0.86	ns
		NDP-MSH	9.04E-02	2.08	ns
		PBS vs. NDP-MSH			
		Controls	9.45E-01	0.30	ns
		DIOWL	2.56E-03	3.95	**
Figure	Type of test	Statistical data	P Value		Sig.
3.4a	One-way ANOVA	F(2,19) = 137.4	2.07E-12		####
		Tukey's multiple comparisons test		q	
		Controls vs. DIO	1.76E-10	17.77	****
		Controls vs. DIOWL	9.11E-01	0.58	ns
		DIO vs. DIOWL	3.24E-12	22.17	****
3.4c	One-way ANOVA	F(2,19) = 37.61	2.48E-07		####
		Tukey's multiple comparisons test		q	
		Controls vs. DIO	1.19E-02	4.56	*
		Controls vs. DIOWL	1.11E-03	6.06	**
		DIO vs. DIOWL	1.67E-07	12.15	****
3.4d	One-way ANOVA	F(2,19) = 39.87	1.59E-07		####
		Tukey's multiple comparisons test		q	
		Controls vs. DIO	3.30E-02	3.88	*
		Controls vs. DIOWL	2.61E-04	6.98	***
		DIO vs. DIOWL	1.28E-07	12.36	****
3.4e	One-way ANOVA	F(2,19) = 41.42	1.18E-07		####
		Tukey's multiple comparisons test		q	
		Controls vs. DIO	6.30E-03	4.97	**
		Controls vs. DIOWL	9.08E-04	6.19	***
		DIO vs. DIOWL	7.67E-08	12.78	****
Figure	Type of test	Statistical data	P Value		Sig.
3.5e-f	Two-way RM ANOVA	Interaction: F(1,14) = 10.18	6.54E-03		##
		Group: F(1,14) = 8.00	1.34E-02		#
		Treatment: F(1,14) = 142.3	1.01E-08		####
		Sidak's multiple comparisons test		t	
3.5e		Controls vs. DIOWL			
		Ad libitum	9.28E-01	0.35	ns
		Food Restricted	5.22E-04	4.18	***
3.5f		Ad libitum vs. Food Restricted			
		Controls	2.37E-04	5.27	***
		DIOWL	3.98E-09	13.52	****
Figure	Type of test	Statistical data	P Value		Sig.
3.6b	Two-way RM ANOVA	Interaction: F(2,20) = 3.65	4.45E-02		#
		Stage: F(2,20) = 8.24	2.46E-03		##
		Group: F(1,10) = 25.86	4.74E-04		###
		Sidak's multiple comparisons test		t	
		PBS vs. Leptin			

		Before	6.39E-01	1.08	ns
		Minipump	9.27E-04	4.08	***
		After	9.93E-01	0.25	ns
		PBS			
		Before vs. Minipump	9.99E-01	0.14	ns
		Before vs. After	7.83E-01	0.86	ns
		Minipump vs. After	6.95E-01	1.00	ns
		Leptin			
		Before vs. Minipump	3.85E-02	2.73	*
		Before vs. After	1.65E-01	2.01	ns
		Minipump vs. After	4.00E-04	4.74	***
3.6c	Two-way RM ANOVA	Interaction: F(2,20) = 3.66	4.43E-02		#
		Stage: F(2,20) = 143.1	1.41E-12		####
		Group: F(1,10) = 2.51	1.44E-01		ns
		Sidak's multiple comparisons test		t	
		PBS vs. Leptin			
		Before	9.32E-01	0.54	ns
		Minipump	3.96E-02	2.63	*
		After	6.70E-01	1.04	ns
		PBS			
		Before vs. Minipump	1.44E-02	4.82	*
		Before vs. After	9.67E-04	8.75	***
		Minipump vs. After	8.00E-04	9.11	***
		Leptin			
		Before vs. Minipump	3.35E-01	1.83	ns
		Before vs. After	6.68E-04	9.46	***
		Minipump vs. After	1.02E-04	13.96	***
3.6d	Two-way RM ANOVA	Interaction: F(10,100) = 6.611	8.57E-08		####
		Time: F(10,100) = 18.02	< 1e-15		####
		Group: F(1,10) = 15.14	3.01E-03		##
		Sidak's multiple comparisons test		t	
		PBS vs. Leptin			
		Day 3	9.96E-01	0.85	ns
		Day 4	4.95E-01	1.90	ns
		Day 5	2.67E-02	3.10	*
		Day 6	1.11E-02	3.378	*
		Day 7	6.19E-03	3.55	**
		Day 8	1.95E-02	3.20	*
		Day 9	1.99E-04	4.48	***
		Day 10	3.62E-04	4.331	***
		Day 11	1.10E-04	4.63	***
		Day 12	3.85E-04	4.32	***
		Day 13	1.58E-04	4.54	***
3.6e	Two-way RM ANOVA	Interaction: F(2,20) = 1.29	4.43E-02		ns
		Stage: F(2,20) = 1.29	1.41E-12		ns
		Group: F(1,10) = 2.16	1.44E-01		ns
		Sidak's multiple comparisons test		t	
		PBS vs. Leptin			
		Before	3.05E-01	1.63	ns
		Minipump	1.00E+00	0.02	ns
		After	3.02E-01	1.63	ns
3.6f	Two-way RM ANOVA	Interaction: F(2,20) = 10.89	6.33E-04		###
		Stage: F(2,20) = 10.89	6.33E-04		###
		Group: F(1,10) = 6.23	3.16E-02		#

		Sidak's multiple comparisons test PBS vs. Leptin		t	
		Before	3.16E-01	1.61	ns
		Minipump	9.09E-01	0.60	ns
		After	4.25E-04	4.36	***

CHAPTER IV

Summary, Conclusions & Future Directions

POMC neurons have been a research focus for a few decades, and their importance in maintaining normal metabolic homeostasis and body composition is solidified. Work over the last several years has cast light on their heterogeneous nature, yet still too often they are type-cast as a simple counterweight to AgRP neurons, and their opioid nature has been vastly overshadowed by their melanocortin action. Using Cre-recombinase reversible neuron-specific *Pomc*-deficient animals I have demonstrated that the neurotransmitter identity of POMC neurons is not as black and white as previously described and that Pomc expression impacts operant feeding uniquely from and additively with weight loss.

In Chapter II, I showed that histological overlap between POMC-peptide immunoreactivity and a tdTomato reporter lineage trace for *Vglut2* neurons resulted in an even split in tdTomato^{+} and tdTomato^{-} POMC immunoreactive neurons, indicating that all POMC neurons cannot have expressed *Vglut2*. Then I assessed the impact of restoring *Pomc* expression specifically to glutamatergic neurons, using a Cre recombinase reversible *Pomc*-deficient mouse and a Vglut2-ires-Cre mice. This resulted in a nearly complete normalization of the POMC system, including the presence of *Gad67*$^{+}$ *Pomc* neurons, contradicting the lineage trace data and indicating that all of these *Pomc* neurons must have expressed *Vglut2* at point. Together these findings uncovered a previously unknown phenomenon, wherein *Pomc* neurons can exhibit

plasticity in their neurotransmitter identity, that in the *Pomc*-deficient mice by opening one avenue of *Pomc* expression resulted in near normalization of the entire system. This work finished with triple-label in situ hybridization (ISH) for *Pomc*, *Vglut2,* and *Gad67*. Overlap between all of the labels revealed a sizeable population of *Pomc* neurons that express both *Vglut2* and *Gad67,* and that there is a distinct rostral-caudal pattern in the localization of *Pomc* neurons that express one or both of the markers, where the *Vglut2* and *Gad67 Pomc* neurons were most prevalent in the rostral Arc, and the *Vglut2/Gad67 Pomc* neurons were most abundant in the caudal Arc.

In Chapter III, I demonstrated that Pomc-deficiency, obesity, weight loss, Pomc-restoration after weight loss, and agonism of melanocortin receptors (MCRs) all impact operant feeding. Using two mouse models of obesity, Pomc-deficient mice and diet-induced obese (DIO) mice, I found that weight loss and Pomc-deficiency each uniquely impart an increased drive to earn and eat food, and that they act additively in Pomc-deficient mice who have lost weight. Additionally, restoring *Pomc* expression in those mice only partially normalized their performance, indicating that the history of weight loss imparted an impact independent of Pomc-deficiency. I then showed that a history of weight loss intensified future mild hunger in DIO mice assayed in a progressive ratio task, without a lasting impact on basal drive. Next, I established that the increase in operant feeding performance in the *Pomc*-deficient mice is correlated with how much weight they have lost. Then, I showed that the reversal of hyperleptinemia potentiates the drive to earn food, but not eat it, after leptin sensitivity has been restored. Lastly, I demonstrated that pharmacological agonism of MCRs suppresses food intake, overcoming *Pomc*-deficiency and weight loss, with minimal impact on other motivated behavior.

Through our own subjective experiences, it seems intuitive to view hunger and feeding as driving forces, but from an ethological perspective, it is inhibition of the melanocortin circuitry that drives these behaviors, while activation prevents them and shifts animal behavior toward other maintenance actions including yawning, stretching, grooming, sleeping and sexual behavior. Pharmacological flooding of the brain with either MC4R or MOR agonists almost certainly does not represent the natural signaling events that occur on a minute-to-minute or day-to-day basis. Perhaps it is only through the interplay of the fast neurotransmission- and peptidergic-signals conveyed by POMC neurons that an animal is able to normally transition through their behavioral repertoire?

A fact that is not emphasized enough is that small and frequent homeostatic adjustments in the dynamics of neural communication can lead to large functional outcomes throughout the life of an animal. Humans do not become obese nor lose weight overnight. It is only through compounded actions having an additive influence that these outcomes are reached. These facts make it difficult to disentangle the signaling dynamics of meal structure on a short-term scale or to discover small differences in neural circuit function that mark the inflection points between hunger and satiation. It is easy to attribute major functional significance to any component of a system when we observe overt phenotypes that emerge after hijacking a circuit by chemo- or optogenetics or by creating monogenetic null alleles. Until we are able to observe and predict subtle changes in the network dynamics underlying metabolic homeostasis as a whole, we will most likely continue to misassign the functional weight of individual components in the network.

Faced with the rampant rise in the frequency of obesity, societally we label it as a disease and/or a pandemic. Yes, it is problematic and leads to many of other comorbidities that inflict widespread health and financial burdens. However, evolutionarily it is a good thing. Animals that

are able to build energy stores in times of excess are better able to withstand periods of scarcity. Our bodies are doing exactly what they have been slowly molded to do over the last 300 million years. The constant excess that we experience now is the new historical scenario.

After reviewing the literature that comprises Chapter I a few voids jumped out. First, when it comes to POMC-based activity dynamics, we have largely swung interpretations of data from one extreme to the other with no idea of the normal balance or hierarchy of signaling. Which natural stimuli or circumstances lead to release of α-MSH and/or β-end, with or without release of fast synaptic transmitters and other peptides and at what specific locations in the brain? Is POMC-neuron activation sufficient or is the concurrent engagement of other signaling pathways needed to regulate feeding behavior? For example, a recent study suggested that cannabinoid input coupled with POMC neuron activation may mediate the actions of β-end release, without concomitant α-MSH secretion, because administration of a cannabinoid 1 receptor agonist induced feeding that was potentiated by concurrent pharmacogenetic stimulation of POMC neurons [265]. The authors attributed the potentiation of feeding to selectively induced β-end release from POMC neurons. However, without repeating these experiments in β-end KO mice it is impossible to rule out the possibility of other mechanisms leading to the observed behavioral changes.

Furthermore, as a field it appears that the pharmacological interrogation of mesolimbic and hypothalamic nuclei with MOR and MCR agents stopped in its tracks. There was good coverage of these areas concerning MOR pharmacology, but is really lacking with melanocortins, and especially combining MOR with MCR pharmacology. This may just be a reflection of the times and at a point when mouse genetic models really started taking off. Pharmacological studies using local application to multiple neural nuclei are labor and time

intensive, and with the constant generation of new mouse models, fell out of favor or at least their presence diminished.

The findings presented in Chapter II raise more questions than answers. The biggest of all is: would we have observed analogous results if we had used a Gad67-Cre mouse instead of the Vglut2-Cre mouse? The basis for this question also presents another question: what proportion of the *Gad67*$^{+}$ *Pomc* neurons that arose from Vglut2-Cre driven Pomc restoration are actually dual-phenotype *Gad67/Vglut2*$^{+}$ *Pomc* neurons like those found with triple-label ISH? The only way to answer these questions would be to repeat the restoration experiment using both a Vglut2-Cre and a Gad67-Cre mouse and then to conduct the triple-label ISH the same as before. The outcome of that experiment would be interesting, but still would not provide much more functional insight than we were already able to provide. We were attempting to define the role of glutamatergic POMC neurons, which seemed a simple enough goal. Given that we found *Pomc* neurons can exhibit flexibility in this phenotype, an additional component is needed to not only restore Pomc expression in a Vglut2-Cre specific manner, but to also confine *Pomc* expression to these cells whilst removing Gad67. Meaning that we would need a triple transgenic animal that is: Vglut2$^{Cre/+}$; Pomc$^{FN\Delta2/FN\Delta2}$; Gad67$^{lox/lox}$. Then to isolate the function of GABAergic POMC neurons we need the complementary mouse: Gad67$^{Cre/+}$; Pomc$^{FN\Delta2/FN\Delta2}$; Vglut2$^{lox/lox}$. This situation also highlights the need for a floxed nPE1/nPE2 allele mouse, to remove neuronal *Pomc* expression in a Cre-dependent manner, which could be subbed for the Pomc$^{FN\Delta2/FN\Delta2}$ mouse in the proposed crosses, and between those combinations we could address both the sufficiency and necessity of each neurotransmitter type in POMC neurons. The informative potential of all these mice is predicated on the assumptions that Vglut2 and Gad67 are necessary for glutamatergic and GABAergic signaling, respectively; that there are no proteins that could

compensate in their absence and allow GABA or glutamate function, even if impaired. Since we observed the emergence of *Gad67*$^{+}$ *Pomc* neurons through the Vglut2 avenue in the otherwise neural *Pomc*-deficient animals, the question remains of are there natural internal or external conditions that drive this activity in normal animals, and if so what are they? This is a difficult question to address. My inclination is to think that this would only be manifest in response to environmental changes and the accompanying physiological changes. I discussed that steady state *Pomc* mRNA levels are highly subject to the nutritional state of an animal, and that in cases of food deprivation or restriction that *Pomc* expression decreases. For animals in the wild, these changes in nutritional state are usually accompanied by seasonal changes. Even changing the photoperiod length without a change in food availability is sufficient to initiate a lot of changes to the hypothalamic landscape. In hamsters, switching from long days to short days leads to substantial weight loss, increased α-MSH and CPE immunoreactivity in the Arc [266], changed the methylation state of the *Dio3* promoter region [267], and changed tanycytic structure along the ventral 3rd ventricle [268], in a manner consistent with increasing the permeability of the blood-hypothalamic-brain barrier seen in fasting [269, 270]. Furthermore, in rats the switch between photoperiods was demonstrated to initiate switching of the neurotransmitter identity between hypothalamic dopamine and somatostatin neurons [176]. Perhaps it is through seasonal-like changes and challenges that we would be able to capture the potential for adaptability within POMC neurons and cell types throughout the brain? As long as we house animals in constant conditions, usually 12hr light-dark cycles at constant temperature and ad libitum food access we'll never know. In fact, it makes more sense to at least characterize the hypothalamic landscape in at least two states, representing both ends of the spectrum that an animal in the wild would experience: 1) long days with ad lib access to food to represent summer, and 2) short days

with limited resource availability to represent winter. Between those extremes we would be able to better assess the dynamic range of the systems that we study, and may actually simplify our functional interpretations, instead of always assessing the animals in what is a transition state consistent with the onset of fall.

Additionally, how widespread is the presence of dual glutamatergic and GABAergic neurons throughout the brain? This question seems a lot easier to address, at least using dual reporter expression. A mouse that could be used already exists and is available through Jackson Labs (B6.Cg-*Gt(ROSA)26Sor*$^{tm1.3(CAG\text{-}tdTomato,\text{-}EGFP)Pjen}$/J), this mouse, the RC::FLTG mouse, has an frt-flanked stop cassette and a loxP-flanked tdTomato-stop cassette preventing eGFP expression. Exposure to Flp-recombinase excises the frt-flanked stop cassette leading to tdTomato expression, and subsequent exposure to Cre-recombinase leads to eGFP expression. So all Flp-only cells turn red and cells that contain both Flp and Cre turn green. These animals could be used in two separate crosses: 1) Vglut2-Flp; Gad67-Cre; RC::FLTG and 2) Vglut2-Cre; Gad67-Flp; RC::FLTG. Together these crosses would detect how potentially widespread dual glutamatergic and GABAergic neurons are throughout the brain, allow tracing of where they project, and highlight whether there is directionality in their emergence (i.e. Vglut2 to Gad67 or Gad67 to Vglut2). This would have to be combined with ISH for both markers as well to gauge whether the eGFP^{+} cells still express both genes or whether they transitioned from one to the other.

Lastly from Chapter II it remains to be determined whether the dual *Vglut2/Gad67 Pomc* neurons actually release both GABA and glutamate, and if so are they released simultaneously, or do different activation conditions lead to release of one versus the other? This is an extremely difficult question to tackle. It would definitely be easier to determine whether in general dual

Vglut2/Gad67 neurons release both, rather than trying to refine the specificity down to POMC neurons. The RC::FLTG crosses mentioned before could be used in conjunction with a viral approach, which would express channelrhodopsin under a similar two-key construct as the RC::FLTG. The intended target of the virus would have to be determined after histological feedback, and it would be beneficial to sample from several areas. Physiological preparations of neural tissue containing the intended cells could be used to measure excitatory and inhibitory postsynaptic properties following different optogenetic stimulation properties.

Chapter III definitely raises a lot of questions for future studies to address, so I'll go through the ones that I thought of while compiling the data. Regarding the data presented in Figure 3.2, the observations from the Restore group are the most intriguing. First, the fact that their behavior was not normalized to the level of the Control group is telling. We know from prior experiments that the animal model is effective at restoring *Pomc* expression to sufficient levels to normalize body composition and growth trajectory [54, 57], and we predicted that other behavioral measures would also be normalized. Their performance by the end of the sessions turned out to be similar to that of the PDO and DIOWL animals, but looking at the within session dynamic of their behavior (Figure 3.2B) tells a different story. It almost appears that there are three distinct phases to their behavior: the initial phase (first 10% of the session) where their performance more closely matches that of the DIO animals, the middle phase (next 50% of the session) where their performance mirrors that of the PDWL mice, and the final phase (last 40% of the session) where they progress like the PDO and DIOWL mice. This doesn't appear to be a one off effect driven by one animal, because the margins of error at each point for this group are tighter than some of the other groups despite having the fewest animals contributing to the measures. The stark differences between groups in this assay alone point toward a plethora of

investigative lines, whether that be differences in gene expression on a region-by-region or cell-to-cell level, or differences in signaling properties in cellular excitability, nuclear network dynamics, or brain wide communication.

Given the effect we found after depletion of the leptin minipumps in increasing the earning of food without eating it, it would be useful to look at the phenomenon of weight loss and its impact on operant feeding in the leptin KO ob/ob mice. These mice become massively obese, but their adipose tissue does not produce leptin. I'm not totally sure what I would expect from their performance. They are deficient in steady state *Pomc* mRNA, so that would indicate that they should perform better than control mice. However, after weight loss the question would come down to, is leptin necessary for earning food? I'm inclined to say no, and that we would most likely observe a similar potentiation of performance like in the PDWL animals, maybe not to the same extent because they do have some POMC. As mentioned earlier several groups have reported elevated *Agrp* expression following food restriction, and that AgRP neurons exhibit increased in vivo neuronal activity following food deprivation and that degree of the increase is correlated with the degree of the mounting caloric deficit. Could changes in *Agrp* expression or AgRP neuron activity be responsible for all of the weight loss effects that we observed, and the driver of compensatory weight gain in general? To address this, our Cre-reversible PD mice could be used in conjunction with the *Agrp*$^{DTR/+}$ mice (they selectively express the diphtheria toxin receptor on AgRP neurons) used by Luquet et al. [10]. The resultant mice would become massively obese, and would then undergo calorie-restriction-induced weight loss to return their weight to the level of control animals. Three treatment conditions would be needed: 1) animals that receive tamoxifen only, 2) animals that receive diphtheria toxin only, and 3) animals that receive both tamoxifen and diphtheria toxin. The first group should show the same effect that we

observed in our Restore group in the FR1 experiment and show a partial normalization of performance. If AgRP neurons are responsible for the impact of weight loss increasing performance in the task, we should also observe a partial normalization of performance in the second group. Then is *Pomc* restoration and AgRP neuron ablation each partially normalize performance, then the third group should show a complete normalization of performance to the level of the control animals. The concern with this approach and using AgRP neuron ablation is that without intervention those animals will starve themselves. However, Denis et al. [42] found that increasing the palatability of the food or stimulating dopamine neurons can circumvent starvation, and the pellets that were utilized in the operant procedures presented here are more palatable than the regular mouse chow. This also leads to the question of whether the reinforcers themselves contributed to the effects observed, and whether I would have found the same interactions using the grain-based pellets that are more comparable to normal chow.

Lastly regarding Chapter III, in Figure 3.3 I present data from DIOWL and Control mice undergoing a progressive ratio task in both an *ad libitum* and a mildly food restricted state, and found that the DIOWL animals showed a greater increase in performance under food restriction than the Control animals. I interpreted this effect as a history of weight loss intensifying the acute hunger. It would be interesting to see whether that potentiation is specific to weight loss or whether *Pomc*-deficiency would also impart the same acute effect. To address this, a cohort of PDO mice and controls would be assayed in the same fashion. If the effect was specific to a history of weight loss, I would expect that both the PDO and the controls would show the same increase in performance. However, given that I found the PDO perform better in the FR1 task performed under mild food restriction, I expect that the results of this would mirror those observed in the DIOWL mice.

Finally, regarding neuroscience in general. As a graduate student one of the things that bothered me the most was the lack of a clear unifying goal in neuroscience, or even on as a field in energy homeostasis. In 2017 a review was published in Neuron [271] titled, "Toward a Wiring Diagram Understanding of Appetite Control." At first I thought that this was an excellent step and proposal, but the more that I thought about it, the more that I disagreed with the goal as a whole. With the computing power available to us today, to settle for an understanding on this level would be a failure, which would do a disservice to us all. It represents an antiquated way of thinking about neuroscience and physiology. The brain is an infinitely complicated and simple structure. Infinitely complicated in the number of permutations and calculations that it is able to perform, and simple in that it is comprised of a finite number of cells that represent tangible components in a functional structure. Problems arise as soon as we paint it into a static state. The brain is a process, a culmination of each and every previous state that it has experienced, whose initial organization is dictated through genetic and environmental mechanisms that are of themselves subject to the experiences of an organisms parents. It is constantly undergoing growth, development, refinement, and decay; all of which are subject to extrinsic and intrinsic forces. Through these principles no two organisms are the same. As a field, as neuroscientists, our goal should be producing a four-dimensional representation of total neural function. Toward this goal we can identify the biological data and computational data needed to make this a reality, and in doing so solve the problems that we are all trying to solve independently.

References:

1. Krude, H., Biebermann, H., Luck, W., Horn, R., Brabant, G., and Gruters, A. 1998. Severe early-onset obesity, adrenal insufficiency and red hair pigmentation caused by POMC mutations in humans. *Nat Genet*. **19**(2): p. 155-7.

2. Challis, B.G. 2002. A missense mutation disrupting a dibasic prohormone processing site in pro-opiomelanocortin (POMC) increases susceptibility to early-onset obesity through a novel molecular mechanism. *Human Molecular Genetics*. **11**(17): p. 1997-2004.

3. Biebermann, H., Castaneda, T.R., van Landeghem, F., von Deimling, A., Escher, F., Brabant, G., Hebebrand, J., Hinney, A., Tschop, M.H., Gruters, A., and Krude, H. 2006. A role for beta-melanocyte-stimulating hormone in human body-weight regulation. *Cell Metab*. **3**(2): p. 141-6.

4. Lee, Y.S., Challis, B.G., Thompson, D.A., Yeo, G.S., Keogh, J.M., Madonna, M.E., Wraight, V., Sims, M., Vatin, V., Meyre, D., Shield, J., Burren, C., Ibrahim, Z., Cheetham, T., Swift, P., Blackwood, A., Hung, C.C., Wareham, N.J., Froguel, P., Millhauser, G.L., O'Rahilly, S., and Farooqi, I.S. 2006. A POMC variant implicates beta-melanocyte-stimulating hormone in the control of human energy balance. *Cell Metab*. **3**(2): p. 135-40.

5. Vaisse, C., Clement, K., Guy-Grand, B., and Froguel, P. 1998. A frameshift mutation in human MC4R is associated with a dominant form of obesity. *Nat Genet*. **20**(2): p. 113-4.

6. Yeo, G.S., Farooqi, I.S., Aminian, S., Halsall, D.J., Stanhope, R.G., and O'Rahilly, S. 1998. A frameshift mutation in MC4R associated with dominantly inherited human obesity. *Nat Genet*. **20**(2): p. 111-2.

7. Lee, Y.S., Poh, L.K., Kek, B.L., and Loke, K.Y. 2008. Novel melanocortin 4 receptor gene mutations in severely obese children. *Clin Endocrinol (Oxf)*. **68**(4): p. 529-35.

8. Mencarelli, M., Walker, G.E., Maestrini, S., Alberti, L., Verti, B., Brunani, A., Petroni, M.L., Tagliaferri, M., Liuzzi, A., and Di Blasio, A.M. 2008. Sporadic mutations in melanocortin receptor 3 in morbid obese individuals. *Eur J Hum Genet*. **16**(5): p. 581-6.

9. Zhan, C., Zhou, J., Feng, Q., Zhang, J.E., Lin, S., Bao, J., Wu, P., and Luo, M. 2013. Acute and long-term suppression of feeding behavior by POMC neurons in the brainstem and hypothalamus, respectively. *J Neurosci*. **33**(8): p. 3624-32.

10. Luquet, S., Perez, F.A., Hnasko, T.S., and Palmiter, R.D. 2005. NPY/AgRP neurons are essential for feeding in adult mice but can be ablated in neonates. *Science*. **310**(5748): p. 683-5.

11. Wu, Q., Howell, M.P., Cowley, M.A., and Palmiter, R.D. 2008. Starvation after AgRP neuron ablation is independent of melanocortin signaling. *Proc Natl Acad Sci U S A*. **105**(7): p. 2687-2692.

12. Ollmann, M.M., Wilson, B.D., Yang, Y.-K., Kerns, J.A., Chen, Y., Gantz, I., and Barsh, G.S. 1997. Antagonism of Central Melanocortin Receptors in Vitro and in Vivo by Agouti-Related Protein. *Science*. **278**(5335): p. 135-138.

13. de Souza, F.S., Santangelo, A.M., Bumaschny, V., Avale, M.E., Smart, J.L., Low, M.J., and Rubinstein, M. 2005. Identification of neuronal enhancers of the proopiomelanocortin gene by transgenic mouse analysis and phylogenetic footprinting. *Mol Cell Biol*. **25**(8): p. 3076-86.

14. de Souza, F.S., Nasif, S., Lopez-Leal, R., Levi, D.H., Low, M.J., and Rubinsten, M. 2011. The estrogen receptor alpha colocalizes with proopiomelanocortin in hypothalamic neurons and binds to a conserved motif present in the neuron-specific enhancer nPE2. *Eur J Pharmacol*. **660**(1): p. 181-7.

15. Franchini, L.F., Lopez-Leal, R., Nasif, S., Beati, P., Gelman, D.M., Low, M.J., de Souza, F.J., and Rubinstein, M. 2011. Convergent evolution of two mammalian neuronal enhancers by sequential exaptation of unrelated retroposons. *Proc Natl Acad Sci U S A*. **108**(37): p. 15270-5.

16. Lam, D.D., de Souza, F.S., Nasif, S., Yamashita, M., Lopez-Leal, R., Otero-Corchon, V., Meece, K., Sampath, H., Mercer, A.J., Wardlaw, S.L., Rubinstein, M., and Low, M.J. 2015. Partially redundant enhancers cooperatively maintain Mammalian pomc expression above a critical functional threshold. *PLoS Genet*. **11**(2): p. e1004935.

17. de Souza, F.S., Bumaschny, V.F., Low, M.J., and Rubinstein, M. 2005. Subfunctionalization of expression and peptide domains following the ancient duplication of the proopiomelanocortin gene in teleost fishes. *Mol Biol Evol*. **22**(12): p. 2417-27.

18. Mountjoy, K.G. 2010. Functions for pro-opiomelanocortin-derived peptides in obesity and diabetes. *Biochem J*. **428**(3): p. 305-24.

19. Wardlaw, S.L. 2011. Hypothalamic proopiomelanocortin processing and the regulation of energy balance. *Eur J Pharmacol*. **660**(1): p. 213-9.

20. Eberle, A.N., *Proopiomelanocortin and the Melanocortin Peptides*, in *The Melanocortin Receptors*, R.D. Cone, Editor. 2000, Humana Press Inc. p. 3-67.

21. Wallingford, N., Perroud, B., Gao, Q., Coppola, A., Gyengesi, E., Liu, Z.W., Gao, X.B., Diament, A., Haus, K.A., Shariat-Madar, Z., Mahdi, F., Wardlaw, S.L., Schmaier, A.H., Warden, C.H., and Diano, S. 2009. Prolylcarboxypeptidase regulates food intake by inactivating alpha-MSH in rodents. *J Clin Invest*. **119**(8): p. 2291-303.

22. Rubinstein, M. and Low, M.J. 2017. Molecular and functional genetics of the proopiomelanocortin gene, food intake regulation and obesity. *FEBS Lett*. **591**(17): p. 2593-2606.

23. Betley, J.N., Cao, Z.F., Ritola, K.D., and Sternson, S.M. 2013. Parallel, redundant circuit organization for homeostatic control of feeding behavior. *Cell*. **155**(6): p. 1337-50.

24. King, C.M. and Hentges, S.T. 2011. Relative number and distribution of murine hypothalamic proopiomelanocortin neurons innervating distinct target sites. *PLoS One*. **6**(10): p. e25864.

25. Veening, J.G., Gerrits, P.O., and Barendregt, H.P. 2012. Volume transmission of beta-endorphin via the cerebrospinal fluid; a review. *Fluids Barriers CNS*. **9**(1): p. 16.

26. Veening, J.G. and Barendregt, H.P. 2015. The effects of beta-endorphin: state change modification. *Fluids Barriers CNS*. **12**: p. 3.

27. Chai, B., Li, J.Y., Zhang, W., Wu, X., Zhang, C., and Mulholland, M.W. 2010. Melanocortin-4 receptor activation promotes insulin-stimulated mTOR signaling. *Peptides*. **31**(10): p. 1888-93.

28. Rodrigues, A.R., Almeida, H., and Gouveia, A.M. 2015. Intracellular signaling mechanisms of the melanocortin receptors: current state of the art. *Cell Mol Life Sci*. **72**(7): p. 1331-45.

29. Ghamari-Langroudi, M., Digby, G.J., Sebag, J.A., Millhauser, G.L., Palomino, R., Matthews, R., Gillyard, T., Panaro, B.L., Tough, I.R., Cox, H.M., Denton, J.S., and Cone, R.D. 2015. G-protein-independent coupling of MC4R to Kir7.1 in hypothalamic neurons. *Nature*. **520**(7545): p. 94-8.

30. Asai, M., Ramachandrappa, S., Joachim, M., Shen, Y., Zhang, R., Nuthalapati, N., Ramanathan, V., Strochlic, D.E., Ferket, P., Linhart, K., Ho, C., Novoselova, T.V., Garg, S., Ridderstrale, M., Marcus, C., Hirschhorn, J.N., Keogh, J.M., O'Rahilly, S., Chan, L.F., Clark, A.J., Farooqi, I.S., and Majzoub, J.A. 2013. Loss of function of the melanocortin 2 receptor accessory protein 2 is associated with mammalian obesity. *Science*. **341**(6143): p. 275-8.

31. Mandelblat-Cerf, Y., Ramesh, R.N., Burgess, C.R., Patella, P., Yang, Z., Lowell, B.B., and Andermann, M.L. 2015. Arcuate hypothalamic AgRP and putative POMC neurons show opposite changes in spiking across multiple timescales. *Elife*. **4**.

32. Betley, J.N., Xu, S., Cao, Z.F.H., Gong, R., Magnus, C.J., Yu, Y., and Sternson, S.M. 2015. Neurons for hunger and thirst transmit a negative-valence teaching signal. *Nature*. **521**(7551): p. 180-185.

33. Chen, Y., Lin, Y.C., Kuo, T.W., and Knight, Z.A. 2015. Sensory detection of food rapidly modulates arcuate feeding circuits. *Cell*. **160**(5): p. 829-841.

34. van den Top, M., Lee, K., Whyment, A.D., Blanks, A.M., and Spanswick, D. 2004. Orexigen-sensitive NPY/AgRP pacemaker neurons in the hypothalamic arcuate nucleus. *Nat Neurosci*. **7**(5): p. 493-4.

35. Krashes, M.J., Koda, S., Ye, C., Rogan, S.C., Adams, A.C., Cusher, D.S., Maratos-Flier, E., Roth, B.L., and Lowell, B.B. 2011. Rapid, reversible activation of AgRP neurons drives feeding behavior in mice. *J Clin Invest*. **121**(4): p. 1424-8.

36. Aponte, Y., Atasoy, D., and Sternson, S.M. 2011. AGRP neurons are sufficient to orchestrate feeding behavior rapidly and without training. *Nat Neurosci*. **14**(3): p. 351-5.

37. Wei, Q., Krolewski, D.M., Moore, S., Kumar, V., Li, F., Martin, B., Tomer, R., Murphy, G.G., Deisseroth, K., Watson, S.J., Jr., and Akil, H. 2018. Uneven balance of power between hypothalamic peptidergic neurons in the control of feeding. *Proc Natl Acad Sci U S A*. **115**(40): p. E9489-E9498.

38. Dietrich, M.O., Zimmer, M.R., Bober, J., and Horvath, T.L. 2015. Hypothalamic Agrp neurons drive stereotypic behaviors beyond feeding. *Cell*. **160**(6): p. 1222-32.

39. Cansell, C., Denis, R.G., Joly-Amado, A., Castel, J., and Luquet, S. 2012. Arcuate AgRP neurons and the regulation of energy balance. *Front Endocrinol (Lausanne)*. **3**: p. 169.

40. Tong, Q., Ye, C.P., Jones, J.E., Elmquist, J.K., and Lowell, B.B. 2008. Synaptic release of GABA by AgRP neurons is required for normal regulation of energy balance. *Nat Neurosci*. **11**(9): p. 998-1000.

41. Wu, Q., Boyle, M.P., and Palmiter, R.D. 2009. Loss of GABAergic signaling by AgRP neurons to the parabrachial nucleus leads to starvation. *Cell*. **137**(7): p. 1225-34.

42. Denis, R.G., Joly-Amado, A., Webber, E., Langlet, F., Schaeffer, M., Padilla, S.L., Cansell, C., Dehouck, B., Castel, J., Delbes, A.S., Martinez, S., Lacombe, A., Rouch, C., Kassis, N., Fehrentz, J.A., Martinez, J., Verdie, P., Hnasko, T.S., Palmiter, R.D., Krashes, M.J., Guler, A.D., Magnan, C., and Luquet, S. 2015. Palatability Can Drive Feeding Independent of AgRP Neurons. *Cell Metab*. **22**(4): p. 646-57.

43. Padilla, S.L., Carmody, J.S., and Zeltser, L.M. 2010. Pomc-expressing progenitors give rise to antagonistic neuronal populations in hypothalamic feeding circuits. *Nat Med*. **16**(4): p. 403-5.

44. Hentges, S.T., Nishiyama, M., Overstreet, L.S., Stenzel-Poore, M., Williams, J.T., and Low, M.J. 2004. GABA release from proopiomelanocortin neurons. *J Neurosci*. **24**(7): p. 1578-83.

45. Hentges, S.T., Otero-Corchon, V., Pennock, R.L., King, C.M., and Low, M.J. 2009. Proopiomelanocortin expression in both GABA and glutamate neurons. *J Neurosci*. **29**(43): p. 13684-90.

46. Dicken, M.S., Tooker, R.E., and Hentges, S.T. 2012. Regulation of GABA and glutamate release from proopiomelanocortin neuron terminals in intact hypothalamic networks. *J Neurosci*. **32**(12): p. 4042-8.

47. Vong, L., Ye, C., Yang, Z., Choi, B., Chua, S., Jr., and Lowell, B.B. 2011. Leptin action on GABAergic neurons prevents obesity and reduces inhibitory tone to POMC neurons. *Neuron*. **71**(1): p. 142-54.

48. Jarvie, B.C. and Hentges, S.T. 2012. Expression of GABAergic and glutamatergic phenotypic markers in hypothalamic proopiomelanocortin neurons. *J Comp Neurol*. **520**(17): p. 3863-76.

49. Wittmann, G., Hrabovszky, E., and Lechan, R.M. 2013. Distinct glutamatergic and GABAergic subsets of hypothalamic pro-opiomelanocortin neurons revealed by in situ hybridization in male rats and mice. *J Comp Neurol*. **521**(14): p. 3287-302.

50. Padilla, S.L., Reef, D., and Zeltser, L.M. 2012. Defining POMC neurons using transgenic reagents: impact of transient Pomc expression in diverse immature neuronal populations. *Endocrinology*. **153**(3): p. 1219-31.

51. Sanz, E., Quintana, A., Deem, J.D., Steiner, R.A., Palmiter, R.D., and McKnight, G.S. 2015. Fertility-regulating Kiss1 neurons arise from hypothalamic POMC-expressing progenitors. *J Neurosci*. **35**(14): p. 5549-56.

52. Dennison, C.S., King, C.M., Dicken, M.S., and Hentges, S.T. 2016. Age-dependent changes in amino acid phenotype and the role of glutamate release from hypothalamic proopiomelanocortin neurons. *J Comp Neurol*. **524**(6): p. 1222-35.

53. Jones, G.L., Wittmann, G., Yokosawa, E.B., Yu, H., Mercer, A.J., Lechan, R.M., and Low, M.J. 2019. Selective restoration of Pomc expression in glutamatergic POMC neurons: Evidence for a dynamic hypothalamic neurotransmitter network. *eneuro*.

54. Bumaschny, V.F., Yamashita, M., Casas-Cordero, R., Otero-Corchon, V., de Souza, F.S., Rubinstein, M., and Low, M.J. 2012. Obesity-programmed mice are rescued by early genetic intervention. *J Clin Invest*. **122**(11): p. 4203-12.

55. Lam, D.D., Attard, C.A., Mercer, A.J., Myers, M.G., Jr., Rubinstein, M., and Low, M.J. 2015. Conditional expression of Pomc in the Lepr-positive subpopulation of POMC neurons is sufficient for normal energy homeostasis and metabolism. *Endocrinology*. **156**(4): p. 1292-302.

56. Burke, L.K., Doslikova, B., D'Agostino, G., Greenwald-Yarnell, M., Georgescu, T., Chianese, R., Martinez de Morentin, P.B., Ogunnowo-Bada, E., Cansell, C., Valencia-Torres, L., Garfield, A.S., Apergis-Schoute, J., Lam, D.D., Speakman, J.R., Rubinstein, M., Low, M.J., Rochford, J.J., Myers, M.G., Evans, M.L., and Heisler, L.K. 2016. Sex difference in physical activity, energy expenditure and obesity driven by a subpopulation of hypothalamic POMC neurons. *Mol Metab*. **5**(3): p. 245-252.

57. Chhabra, K.H., Adams, J.M., Jones, G.L., Yamashita, M., Schlapschy, M., Skerra, A., Rubinstein, M., and Low, M.J. 2016. Reprogramming the body weight set point by a reciprocal interaction of hypothalamic leptin sensitivity and Pomc gene expression reverts extreme obesity. *Mol Metab*. **5**(10): p. 869-881.

58. Ben-Ari, Y. 2002. Excitatory actions of gaba during development: the nature of the nurture. *Nat Rev Neurosci*. **3**(9): p. 728-39.

59. Herbison, A.E. and Moenter, S.M. 2011. Depolarising and hyperpolarising actions of GABA(A) receptor activation on gonadotrophin-releasing hormone neurones: towards an emerging consensus. *J Neuroendocrinol*. **23**(7): p. 557-69.

60. Haam, J., Popescu, I.R., Morton, L.A., Halmos, K.C., Teruyama, R., Ueta, Y., and Tasker, J.G. 2012. GABA is excitatory in adult vasopressinergic neuroendocrine cells. *J Neurosci*. **32**(2): p. 572-82.

61. Savontaus, E., Breen, T.L., Kim, A., Yang, L.M., Chua, S.C., Jr., and Wardlaw, S.L. 2004. Metabolic effects of transgenic melanocyte-stimulating hormone overexpression in lean and obese mice. *Endocrinology*. **145**(8): p. 3881-91.

62. Tsujii, S. and Bray, G.A. 1989. Acetylation alters the feeding response to MSH and beta-endorphin. *Brain Res Bull*. **23**(3): p. 165-9.

63. Ludwig, D.S., Mountjoy, K.G., Tatro, J.B., Gillette, J.A., Frederich, R.C., Flier, J.S., and Maratos-Flier, E. 1998. Melanin-concentrating hormone: a functional melanocortin antagonist in the hypothalamus. *Am J Physiol*. **274**(4 Pt 1): p. E627-33.

64. Poggioli, R., Vergoni, A.V., and Bertolini, A. 1986. ACTH-(1-24) and alpha-MSH antagonize feeding behavior stimulated by kappa opiate agonists. *Peptides*. **7**(5): p. 843-8.

65. McMinn, J.E., Wilkinson, C.W., Havel, P.J., Woods, S.C., and Schwartz, M.W. 2000. Effect of intracerebroventricular alpha-MSH on food intake, adiposity, c-Fos induction, and neuropeptide expression. *Am J Physiol Regul Integr Comp Physiol*. **279**(2): p. R695-703.

66. Vergoni, A.V., Bertolini, A., Mutulis, F., Wikberg, J.E., and Schioth, H.B. 1998. Differential influence of a selective melanocortin MC4 receptor antagonist (HS014) on melanocortin-induced behavioral effects in rats. *Eur J Pharmacol*. **362**(2-3): p. 95-101.

67. Fan, W., Boston, B.A., Kesterson, R.A., Hruby, V.J., and Cone, R.D. 1997. Role of melanocortinergic neurons in feeding and the *agouti* obesity syndrome. *Nature*. **385**: p. 165-168.

68. Cowley, M.A., Pronchuk, N., Fan, W., Dinulescu, D.M., Colmers, W.F., and Cone, R.D. 1999. Integration of NPY, AGRP, and melanocortin signals in the hypothalamic paraventricular nucleus: evidence of a cellular basis for the adipostat. *Neuron*. **24**(1): p. 155-63.

69. Rossi, M., Kim, M.S., Morgan, D.G., Small, C.J., Edwards, C.M., Sunter, D., Abusnana, S., Goldstone, A.P., Russell, S.H., Stanley, S.A., Smith, D.M., Yagaloff, K., Ghatei, M.A., and Bloom, S.R. 1998. A C-terminal fragment of Agouti-related protein increases feeding and antagonizes the effect of alpha-melanocyte stimulating hormone in vivo. *Endocrinology*. **139**(10): p. 4428-31.

70. Murphy, B., Nunes, C.N., Ronan, J.J., Harper, C.M., Beall, M.J., Hanaway, M., Fairhurst, A.M., Van der Ploeg, L.H., MacIntyre, D.E., and Mellin, T.N. 1998. Melanocortin mediated inhibition of feeding behavior in rats. *Neuropeptides*. **32**(6): p. 491-7.

71. Murphy, B., Nunes, C.N., Ronan, J.J., Hanaway, M., Fairhurst, A.M., and Mellin, T.N. 2000. Centrally administered MTII affects feeding, drinking, temperature, and activity in the Sprague-Dawley rat. *J Appl Physiol* **89**(1): p. 273-82.

72. Azzara, A.V., Sokolnicki, J.P., and Schwartz, G.J. 2002. Central melanocortin receptor agonist reduces spontaneous and scheduled meal size but does not augment duodenal preload-induced feeding inhibition. *Physiology & Behavior*. **77**: p. 411-416.

73. Zheng, H., Patterson, L.M., Phifer, C.B., and Berthoud, H.R. 2005. Brain stem melanocortinergic modulation of meal size and identification of hypothalamic POMC projections. *Am J Physiol Regul Integr Comp Physiol*. **289**(1): p. R247-58.

74. Sutton, G.M., Duos, B., Patterson, L.M., and Berthoud, H.R. 2005. Melanocortinergic modulation of cholecystokinin-induced suppression of feeding through extracellular signal-regulated kinase signaling in rat solitary nucleus. *Endocrinology*. **146**(9): p. 3739-47.

75. Dutia, R., Meece, K., Dighe, S., Kim, A.J., and Wardlaw, S.L. 2012. beta-Endorphin antagonizes the effects of alpha-MSH on food intake and body weight. *Endocrinology*. **153**(9): p. 4246-55.

76. Benoit, S.C., Clegg, D.J., Barrera, J.G., Seeley, R.J., and Woods, S.C. 2003. Learned meal initiation attenuates the anorexic effects of the melanocortin agonist MTII. *Diabetes*. **52**(11): p. 2684-8.

77. Clegg, D.J., Benoit, S.C., Air, E.L., Jackman, A., Tso, P., D'Alessio, D., Woods, S.C., and Seeley, R.J. 2003. Increased dietary fat attenuates the anorexic effects of intracerebroventricular injections of MTII. *Endocrinology*. **144**(7): p. 2941-6.

78. Thiele, T.E., van Dijk, G., Yagaloff, K.A., Fisher, S.L., Schwartz, M., Burn, P., and Seeley, R.J. 1998. Central infusion of melanocortin agonist MTII in rats: assessment of c-Fos expression and taste aversion. *Am J Physiol*. **274**(1 Pt 2): p. R248-54.

79. Brown, K.S., Gentry, R.M., and Rowland, N.E. 1998. Central injection in rats of a-melanocyte-stimulating hormone analog: effects on food intake and brain Fos. *Regulatory Peptides*. **78**: p. 89-94.

80. Hagan, M.M., Benoit, S.C., Rushing, P.A., Pritchard, L.M., Woods, S.C., and Seeley, R.J. 2001. Immediate and Prolonged Patterns of Agouti-Related Peptide-(83–132)-Induced c-Fos Activation in Hypothalamic and Extrahypothalamic Sites. *Endocrinology*. **142**(3): p. 1050-1056.

81. Zheng, H., Corkern, M.M., Crousillac, S.M., Patterson, L.M., Phifer, C.B., and Berthoud, H.R. 2002. Neurochemical phenotype of hypothalamic neurons showing Fos expression 23 h after intracranial AgRP. *Am J Physiol Regul Integr Comp Physiol*. **282**(6): p. R1773-81.

82. Giraudo, S.Q., Billington, C.J., and Levine, A.S. 1998. Feeding effects of hypothalamic injection of melanocortin 4 receptor ligands. *Brain Res*. **809**(2): p. 302-6.

83. Kim, M.S., Rossi, M., Abusnana, S., Sunter, D., Morgan, D.G.A., Small, C.J., Edwards, C.M.B., Heath, M.M., Stanley, S.A., Seal, S.J., Bhatti, J.R., Smith, D.M., Ghatei, M.A., and Bloom, S.R. 2000. Hypothalamic Localization of the Feeding Effect of Agouti-Related Peptide and a-Melanocyte–Stimulating Hormone. *Diabetes*. **49**: p. 177-182.

84. Argiolas, A., Melis, M.R., Murgia, S., and Schioth, H.B. 2000. ACTH- and alpha-MSH-induced grooming, stretching, yawning and penile erection in male rats: site of action in the brain and role of melanocortin receptors. *Brain Res Bull*. **51**(5): p. 425-31.

85. Lindblom, J., Opmane, B., Mutulis, F., Mutule, I., Petrovska, R., Klusa, V., Bergstrom, L., and Wikberg, J.E.S. 2001. The MC4 receptor mediates a-MSH induced release of nucleus accumbens dopamine. *NeuroReport*. **12**(10): p. 2155-2158.

86. Torre, E. and Celis, M.E. 1988. Cholinergic mediation in the ventral tegmental area of alpha-melanotropin induced excessive grooming: changes of the dopamine activity in the nucleus accumbens and caudate putamen. *Life Sci*. **42**(17): p. 1651-7.

87. Torre, E. and Celis, M.E. 1986. Alpha-MSH injected into the substantia nigra or intraventricularly alters behavior and the striatal dopaminergic activity. *Neurochem Int*. **9**(1): p. 85-89.

88. Versteeg, D.H.G., Florijn, W.J., Holtmaat, A.J.G.D., Gispen, W.H., and De Wildt, D.J. 1993. Synchronism of pressor response and grooming behavior in freely moving, conscious rats following intracerebroventicular administration of ACTH/MSH-like peptides. *Brain Res*. **631**: p. 265-269.

89. Haynes, W.G., Morgan, D.A., Djalali, A., Sivitz, W.I., and Mark, A.L. 1999. Interactions Between the Melanocortin System and Leptin in Control of Sympathetic Nerve Traffic. *Hypertension*. **33**: p. 542-547.

90. Cabeza de Vaca, S., Kim, G.Y., and Carr, K.D. 2002. The melanocortin receptor agonist MTII augments the rewarding effect of amphetamine in ad-libitum-fed and food-restricted rats. *Psychopharmacology (Berl)*. **161**(1): p. 77-85.

91. Navarro, M., Cubero, I., Chen, A.S., Chen, H.Y., Knapp, D.J., Breese, G.R., Marsh, D.J., and Thiele, T.E. 2005. Effects of melanocortin receptor activation and blockade on ethanol intake: a possible role for the melanocortin-4 receptor. *Alcohol Clin Exp Res*. **29**(6): p. 949-57.

92. Lerma-Cabrera, J.M., Carvajal, F., de la Torre, L., de la Fuente, L., Navarro, M., Thiele, T.E., and Cubero, I. 2012. Control of food intake by MC4-R signaling in the lateral hypothalamus, nucleus accumbens shell and ventral tegmental area: interactions with ethanol. *Behav Brain Res*. **234**(1): p. 51-60.

93. Silva, R.M., Hadjimarkou, M.M., Rossi, G.C., Pasternak, G.W., and Bodnar, R.J. 2001. beta-Endorphin-Induced Feeding: Pharmacological Characterization Using Selective Opioid Antagonists and Antisense Probes in Rats. *THE JOURNAL OF PHARMACOLOGY AND EXPERIMENTAL THERAPEUTICS*. **297**(2): p. 590-596.

94. Grossman, H.C., Hadjimarkou, M.M., Silva, R.M., Giraudo, S.Q., and Bodnar, R.J. 2003. Interrelationships between μ opioid and melanocortin receptors in mediating food intake in rats. *Brain Research*. **991**(1-2): p. 240-244.

95. Sanger, D.J. and McCarthy, P.S. 1980. Differential effects of morphine on food and water intake in food deprived and freely-feeding rats. *Psychopharmacology*. **72**(1): p. 103-6.

96. Bakshi, V.P. and Kelley, A.E. 1993. Striatal regulation of morphine-induced hyperphagia: an anatomical mapping study. *Psychopharmacology (Berl)*. **111**(2): p. 207-14.

97. Bakshi, V.P. and Kelley, A.E. 1993. Feeding induced by opioid stimulation of the ventral striatum: role of opiate receptor subtypes. *J Pharmacol Exp Ther*. **265**(3): p. 1253-60.

98. Mucha, R.F. and Iversen, S.D. 1986. Increased Food Intake after Opioid Microinjections into Nucleus Accumbens and Ventral Tegmental Area of Rat. *Brain Res*. **397**: p. 214-224.

99. Giraudo, S.Q., Billington, C.J., and Levine, A.S. 1998. Effects of the opioid antagonist naltrexone on feeding induced by DAMGO in the central nucleus of the amygdala and in the paraventricular nucleus in the rat. *Brain Res*. **782**(1-2): p. 18-23.

100. Ragnauth, A., Moroz, M., and Bodnar, R.J. 2000. Multiple opioid receptors mediate feeding elicited by mu and delta opioid receptor subtype agonists in the nucleus accumbens shell in rats. *Brain Res*. **876**(1-2): p. 76-87.

101. Lamonte, N., Echo, J.A., Ackerman, T.F., Christian, G., and Bodnar, R.J. 2002. Analysis of opioid receptor subtype antagonist effects upon mu opioid agonist-induced feeding elicited from the ventral tegmental area of rats. *Brain Res*. **929**: p. 96-100.

102. Znamensky, V., Echo, J.A., Lamonte, N., Christian, G., Ragnauth, A., and Bodnar, R.J. 2001. gamma-Aminobutyric acid receptor subtype antagonists differentially alter opioid-induced feeding in the shell region of the nucleus accumbens in rats. *Brain Res*. **906**(1-2): p. 84-91.

103. Ikeda, H., Ardianto, C., Yonemochi, N., Yang, L., Ohashi, T., Ikegami, M., Nagase, H., and Kamei, J. 2015. Inhibition of opioid systems in the hypothalamus as well as the mesolimbic area suppresses feeding behavior of mice. *Neuroscience*. **311**: p. 9-21.

104. Will, M.J., Franzblau, E.B., and Kelley, A.E. 2003. Nucleus accumbens mu-opioids regulate intake of a high-fat diet via activation of a distributed brain network. *J Neurosci*. **23**(7): p. 2882-8.

105. MacDonald, A.F., Billington, C.J., and Levine, A.S. 2003. Effects of the opioid antagonist naltrexone on feeding induced by DAMGO in the ventral tegmental area and in the nucleus accumbens shell region in the rat. *Am J Physiol Regul Integr Comp Physiol*. **285**(5): p. R999-R1004.

106. MacDonald, A.F., Billington, C.J., and Levine, A.S. 2004. Alterations in food intake by opioid and dopamine signaling pathways between the ventral tegmental area and the shell of the nucleus accumbens. *Brain Res*. **1018**(1): p. 78-85.

107. Zheng, H., Townsend, R.L., Shin, A.C., Patterson, L.M., Phifer, C.B., and Berthoud, H.R. 2010. High-fat intake induced by mu-opioid activation of the nucleus accumbens is inhibited by Y1R-blockade and MC3/4R- stimulation. *Brain Res*. **1350**: p. 131-8.

108. Kawahara, Y., Kaneko, F., Yamada, M., Kishikawa, Y., Kawahara, H., and Nishi, A. 2013. Food reward-sensitive interaction of ghrelin and opioid receptor pathways in mesolimbic dopamine system. *Neuropharmacology*. **67**: p. 395-402.

109. Kim, E.M., Quinn, J.G., Levine, A.S., and O'Hare, E. 2004. A bi-directional mu-opioid-opioid connection between the nucleus of the accumbens shell and the central nucleus of the amygdala in the rat. *Brain Res*. **1029**(1): p. 135-9.

110. DiFeliceantonio, A.G. and Berridge, K.C. 2012. Which cue to 'want'? Opioid stimulation of central amygdala makes goal-trackers show stronger goal-tracking, just as sign-trackers show stronger sign-tracking. *Behav Brain Res*. **230**(2): p. 399-408.

111. Clegg, D.J., Air, E.L., Woods, S.C., and Seeley, R.J. 2002. Eating Elicited by Orexin-A, But Not MelaninConcentrating Hormone, Is Opioid Mediated. *Endocrinology*. **143**(8): p. 2995-3000.

112. Hagan, M.M., Rushing, P.A., Benoit, S.C., Woods, S.C., and Seeley, R.J. 2001. Opioid receptor involvement in the effect of AgRP(83–132) on food intake and food selection. *Am J Physiol Regulatory Integrative Comp Physiol*. **280**: p. R814–R821.

113. Markowitz, C.E., Berkowitz, K.M., Jaffe, S.B., and Wardlaw, S.L. 1992. Effect of opioid receptor antagonism on proopiomelanocortin peptide levels and gene expression in the hypothalamus. *Mol Cell Neurosci*. **3**(3): p. 184-90.

114. Garcia de Yebenes, E. and Pelletier, G. 1993. Opioid Regulation of Proopiomelanocortin (POMC) Gene Expression in the Rat Brain as Studied by in situ Hybridization. *Neuropeptides*. **25**: p. 91-94.

115. Anghel, A., Jamieson, C.A., Ren, X., Young, J., Porche, R., Ozigbo, E., Ghods, D.E., Lee, M.L., Liu, Y., Lutfy, K., and Friedman, T.C. 2010. Gene expression profiling following short-term and long-term morphine exposure in mice uncovers genes involved in food intake. *Neuroscience*. **167**(2): p. 554-66.

116. Yaswen, L., Diehl, N., Brennan, M.B., and Hochgeschwender, U. 1999. Obesity in the mouse model of pro-opiomelanocortin deficiency responds to peripheral melanocortin. *Nature Medicine*. **5**(9): p. 1066-1070.

117. Challis, B.G., Coll, A.P., Yeo, G.S.H., Pinnock, S.B., Dickson, S.L., Thresher, R.R., Dixon, J., Zahn, D., Rochford, J.J., White, A., Oliver, R.L., Millington, G.W., Aparicio, S.A., Colledge, W.H., Russ, A.P., Carlton, M.B., and O'Rahilly, S. 2004. Mice lacking pro-opiomelanocortin are sensitive to high-fat feeding but respond normally to the acute anorectic effects of peptide-YY3–36. *Proc Natl Acad Sci U S A*. **101**(13): p. 4695-4700.

118. Tolle, V. and Low, M.J. 2008. In vivo evidence for inverse agonism of Agouti-related peptide in the central nervous system of proopiomelanocortin-deficient mice. *Diabetes*. **57**(1): p. 86-94.

119. Martin, N.M., Small, C.J., Sajedi, A., Liao, X.H., Weiss, R.E., Gardiner, J.V., Ghatei, M.A., and Bloom, S.R. 2004. Abnormalities of the hypothalamo-pituitary-thyroid axis in the pro-opiomelanocortin deficient mouse. *Regul Pept*. **122**(3): p. 169-72.

120. Corander, M.P., Rimmington, D., Challis, B.G., O'Rahilly, S., and Coll, A.P. 2011. Loss of agouti-related peptide does not significantly impact the phenotype of murine POMC deficiency. *Endocrinology*. **152**(5): p. 1819-28.

121. Smart, J.L., Tolle, V., and Low, M.J. 2006. Glucocorticoids exacerbate obesity and insulin resistance in neuron-specific proopiomelanocortin-deficient mice. *J Clin Invest*. **116**(2): p. 495-505.

122. Richard, C.D., Tolle, V., and Low, M.J. 2011. Meal pattern analysis in neural-specific proopiomelanocortin-deficient mice. *Eur J Pharmacol*. **660**(1): p. 131-8.

123. Chhabra, K.H., Morgan, D.A., Tooke, B.P., Adams, J.M., Rahmouni, K., and Low, M.J. 2017. Reduced renal sympathetic nerve activity contributes to elevated glycosuria and

improved glucose tolerance in hypothalamus-specific Pomc knockout mice. *Mol Metab*. **6**(10): p. 1274-1285.

124. Tooke, B.P., Yu, H., Adams, J.M., Jones, G.L., Sutton-Kennedy, T., Mundada, L., Qi, N.R., Low, M.J., and Chhabra, K.H. 2018. Hypothalamic POMC or MC4R deficiency impairs counterregulatory responses to hypoglycemia in mice. *Mol Metab*.

125. Huszar, D., Lynch, C.A., Fairchild-Huntress, V., Fang, Q., Berkemeier, L.R., Gu, W., Kesterson, R.A., Boston, B.A., Cone, R.D., Smith, F.J., Campfield, L.A., Burn, P., and Lee, F. 1997. Targeted Disruption of the Melanocortin-4 Receptor Results in Obesity in Mice. *Cell*. **88**: p. 131-141.

126. Ste. Marie, L., Miura, G.I., Marsh, D.J., Yagaloff, K., and Palmiter, R.D. 2000. A metabolic defect promotes obesity in mice lacking melanocortin-4 receptors. *Proc Natl Acad Sci U S A*. **97**(22): p. 12339-12344.

127. Balthasar, N., Dalgaard, L.T., Lee, C.E., Yu, J., Funahashi, H., Williams, T., Ferreira, M., Tang, V., McGovern, R.A., Kenny, C.D., Christiansen, L.M., Edelstein, E., Choi, B., Boss, O., Aschkenasi, C., Zhang, C.Y., Mountjoy, K., Kishi, T., Elmquist, J.K., and Lowell, B.B. 2005. Divergence of melanocortin pathways in the control of food intake and energy expenditure. *Cell*. **123**(3): p. 493-505.

128. Rossi, J., Balthasar, N., Olson, D., Scott, M., Berglund, E., Lee, C.E., Choi, M.J., Lauzon, D., Lowell, B.B., and Elmquist, J.K. 2011. Melanocortin-4 receptors expressed by cholinergic neurons regulate energy balance and glucose homeostasis. *Cell Metab*. **13**(2): p. 195-204.

129. Vella, K.R., Ramadoss, P., Lam, F.S., Harris, J.C., Ye, F.D., Same, P.D., O'Neill, N.F., Maratos-Flier, E., and Hollenberg, A.N. 2011. NPY and MC4R signaling regulate thyroid hormone levels during fasting through both central and peripheral pathways. *Cell Metab*. **14**(6): p. 780-90.

130. Srisai, D., Gillum, M.P., Panaro, B.L., Zhang, X.M., Kotchabhakdi, N., Shulman, G.I., Ellacott, K.L., and Cone, R.D. 2011. Characterization of the hyperphagic response to dietary fat in the MC4R knockout mouse. *Endocrinology*. **152**(3): p. 890-902.

131. Cui, H. and Lutter, M. 2013. The expression of MC4Rs in D1R neurons regulates food intake and locomotor sensitization to cocaine. *Genes Brain Behav*. **12**(6): p. 658-65.

132. Morgan, D.A., McDaniel, L.N., Yin, T., Khan, M., Jiang, J., Acevedo, M.R., Walsh, S.A., Ponto, L.L., Norris, A.W., Lutter, M., Rahmouni, K., and Cui, H. 2015. Regulation of glucose tolerance and sympathetic activity by MC4R signaling in the lateral hypothalamus. *Diabetes*. **64**(6): p. 1976-87.

133. Klawonn, A.M., Fritz, M., Nilsson, A., Bonaventura, J., Shionoya, K., Mirrasekhian, E., Karlsson, U., Jaarola, M., Granseth, B., Blomqvist, A., Michaelides, M., and Engblom, D. 2018. Motivational valence is determined by striatal melanocortin 4 receptors. *J Clin Invest*. **128**(7): p. 3160-3170.

134. Butler, A.A., Kesterson, R.A., Khong, K., Cullen, M.J., Pelleymounter, M.A., Dekoning, J., Baetscher, M., and Cone, R.D. 2000. A Unique Metabolic Syndrome Causes Obesity in the Melanocortin-3 Receptor-Deficient Mouse. *Endocrinology*. **141**: p. 3518-3521.

135. Chen, A.S., Marsh, D.J., Trumbauer, M.E., Frazier, E.G., Guan, X., Yu, H., Rosenblum, C.I., Vongs, A., Feng, Y., Cao, L., Metzger, J.M., Strack, A.M., Camacho, R.E., Mellin, T.E., Nunes, C.N., Min, W., Fisher, J., Gopal-Truter, S., MacIntyre, D.E., Chen, H.Y., and Van der Ploeg, L.H.T. 2000. Inactivation of the mouse melanocortin-3 receptor results in increased fat mass and reduced lean body mass. *Nature Genetics*. **26**: p. 97-102.

136. Rowland, N.E., Schaub, J.W., Robertson, K.L., Andreasen, A., and Haskell-Luevano, C. 2010. Effect of MTII on food intake and brain c-Fos in melanocortin-3, melanocortin-4, and double MC3 and MC4 receptor knockout mice. *Peptides*. **31**(12): p. 2314-7.

137. Ellacott, K.L., Murphy, J.G., Marks, D.L., and Cone, R.D. 2007. Obesity-induced inflammation in white adipose tissue is attenuated by loss of melanocortin-3 receptor signaling. *Endocrinology*. **148**(12): p. 6186-94.

138. Renquist, B.J., Murphy, J.G., Larson, E.A., Olsen, D., Klein, R.F., Ellacott, K.L., and Cone, R.D. 2012. Melanocortin-3 receptor regulates the normal fasting response. *Proc Natl Acad Sci U S A.* **109**(23): p. E1489-98.

139. Lippert, R.N., Ellacott, K.L., and Cone, R.D. 2014. Gender-specific roles for the melanocortin-3 receptor in the regulation of the mesolimbic dopamine system in mice. *Endocrinology*. **155**(5): p. 1718-27.

140. Ghamari-Langroudi, M., Cakir, I., Lippert, R.N., Sweeney, P., Litt, M.J., Ellacott, K.L.J., and Cone, R.D. 2018. Regulation of energy rheostasis by the melanocortin-3 receptor. *Sci Adv*. **4**(8): p. eaat0866.

141. Rubinstein, M., Japon, M.A., and Low, M.J. 1993. Introduction of a point mutation into the mouse genome by homologous recombination in embryonic stem cells using a replacement type vector with a selectable marker. *Nucleic Acids Research*. **21**(11): p. 2613-2617.

142. Rubinstein, M., Mogil, J.S., Japon, M.A., Chan, E.C., Allen, R.G., and Low, M.J. 1996. Absence of opioid stress-induced analgesia in mice lacking B-endorphin by site-directed mutagenesis. *Proc Natl Acad Sci U S A.* **93**: p. 3995-4000.

143. Appleyard, S.M., Hayward, M., Young, J.I., Butler, A.A., Cone, R.D., Rubinstein, M., and Low, M.J. 2003. A role for the endogenous opioid beta-endorphin in energy homeostasis. *Endocrinology*. **144**(5): p. 1753-60.

144. Low, M.J., Hayward, M.D., Appleyard, S.M., and Rubinstein, M. 2003. State-Dependent Modulation of Feeding Behavior by Proopiomelanocortin-Derived β-Endorphin. *Ann N Y Acad Sci*. **994**: p. 192-201.

145. Barfield, E.T., Moser, V.A., Hand, A., and Grisel, J.E. 2013. beta-endorphin modulates the effect of stress on novelty-suppressed feeding. *Front Behav Neurosci*. **7**: p. 19.

146. Matthes, H.W., Maldonado, R., Simonin, F., Valverde, O., Slowe, S., Kitchen, I., Befort, K., Dierich, A., Le Meur, M., Dolle, P., Tzavara, E., Hanoune, J., Roques, B.P., and Kieffer, B.L. 1996. Loss of morphine-induced analgesia, reward effect and withdrawal symptoms in mice lacking the mu-opioid-receptor gene. *Nature*. **383**(6603): p. 819-23.

147. Sora, I., Takahashi, N., Funada, M., Ujike, H., Revay, R.S., Donovan, D.M., Miner, L.L., and Uhl, G.R. 1997. Opiate receptor knockout mice define mu receptor roles in endogenous nociceptive responses and morphine-induced analgesia. *Proc Natl Acad Sci U S A*. **94**(4): p. 1544-9.

148. Schuller, A.G., King, M.A., Zhang, J., Bolan, E., Pan, Y.X., Morgan, D.J., Chang, A., Czick, M.E., Unterwald, E.M., Pasternak, G.W., and Pintar, J.E. 1999. Retention of heroin and morphine-6 beta-glucuronide analgesia in a new line of mice lacking exon 1 of MOR-1. *Nat Neurosci*. **2**(2): p. 151-6.

149. Loh, H.H., Liu, H.C., Cavalli, A., Yang, W., Chen, Y.F., and Wei, L.N. 1998. mu Opioid receptor knockout in mice: effects on ligand-induced analgesia and morphine lethality. *Brain Res Mol Brain Res*. **54**(2): p. 321-6.

150. Han, W., Hata, H., Imbe, H., Liu, Q.R., Takamatsu, Y., Koizumi, M., Murphy, N.P., Senba, E., Uhl, G.R., Sora, I., and Ikeda, K. 2006. Increased body weight in mice lacking mu-opioid receptors. *Neuroreport*. **17**(9): p. 941-4.

151. Zuberi, A.R., Townsend, L., Patterson, L., Zheng, H., and Berthoud, H.R. 2008. Increased adiposity on normal diet, but decreased susceptibility to diet-induced obesity in mu-opioid receptor-deficient mice. *Eur J Pharmacol*. **585**(1): p. 14-23.

152. Tabarin, A., Chaves, Y.D., Carmona, M.C., Catargi, B., Zorrilla, E.P., Roberts, A.J., Coscina, D.V., Rousset, S., Redonnet, A., Parker, G.C., Inoue, K., Ricquier, D., Pe´nicaud, L., Kieffer, B.L., and Koob, G.F. 2005. Resistance to Diet-Induced Obesity in mu-Opioid Receptor–Deficient Mice. *Diabetes*. **54**: p. 3510-3516.

153. Roberts, A.J., McDonald, J.S., Heyser, C.J., Kieffer, B.L., Matthes, H.W.D., Koob, G.F., and Gold, L.H. 2000. mu-Opioid Receptor Knockout Mice Do Not Self-Administer Alcohol. *THE JOURNAL OF PHARMACOLOGY AND EXPERIMENTAL THERAPEUTICS*. **293**(3): p. 1002-1008.

154. Hall, F.S., Sora, I., and Uhl, G.R. 2001. Ethanol consumption and reward are decreased in μ-opiate receptor knockout mice. *Psychopharmacology*. **154**: p. 43-49.

155. Papaleo, F., Kieffer, B.L., Tabarin, A., and Contarino, A. 2007. Decreased motivation to eat in μ-opioid receptor-deficient mice. *European Journal of Neuroscience*. **25**(11): p. 3398-3405.

156. Ostlund, S.B., Kosheleff, A., Maidment, N.T., and Murphy, N.P. 2013. Decreased consumption of sweet fluids in mu opioid receptor knockout mice: a microstructural analysis of licking behavior. *Psychopharmacology (Berl)*. **229**(1): p. 105-13.

157. Hall, F.S., Goeb, M., Li, X.F., Sora, I., and Uhl, G.R. 2004. mu-Opioid receptor knockout mice display reduced cocaine conditioned place preference but enhanced sensitization of cocaine-induced locomotion. *Brain Res Mol Brain Res*. **121**(1-2): p. 123-30.

158. Kas, M.J., van den Bos, R., Baars, A.M., Lubbers, M., Lesscher, H.M., Hillebrand, J.J., Schuller, A.G., Pintar, J.E., and Spruijt, B.M. 2004. Mu-opioid receptor knockout mice show diminished food-anticipatory activity. *Eur J Neurosci*. **20**(6): p. 1624-32.

159. Jang, C., Lee, S., Yoo, J., Yan, J., Song, D., Loh, H.H., and Ho, I.K. 2003. Impaired water maze learning performance in mu-opioid receptor knockout mice. *Molecular Brain Research*. **117**: p. 68-72.

160. Tian, M., Broxmeyer, H.E., Fan, Y., Lai, Z., Zhang, S., Aronica, S., Cooper, S., Bigsby, R.M., Steinmetz, R., Engle, S.J., Mestek, A., Pollock, J.D., Lehman, M.N., Jansen, H.T., Ying, M., Stambrook, P.J., Tischfield, J.A., and Yu, L. 1997. Altered Hematopoiesis, Behavior, and Sexual Function in μ Opioid Receptor–deficient Mice. *The Journal of Experimental Medicine*. **185**(8): p. 1517-1522.

161. Foo, K.S., Hellysaz, A., and Broberger, C. 2014. Expression and colocalization patterns of calbindin-D28k, calretinin and parvalbumin in the rat hypothalamic arcuate nucleus. *J Chem Neuroanat*. **61-62**: p. 20-32.

162. Chhabra, K.H., Adams, J.M., Fagel, B., Lam, D.D., Qi, N., Rubinstein, M., and Low, M.J. 2016. Hypothalamic POMC Deficiency Improves Glucose Tolerance Despite Insulin Resistance by Increasing Glycosuria. *Diabetes*. **65**: p. 660-672.

163. Kao, Y.H., Lassova, L., Bar-Yehuda, T., Edwards, R.H., Sterling, P., and Vardi, N. 2004. Evidence that certain retinal bipolar cells use both glutamate and GABA. *J Comp Neurol*. **478**(3): p. 207-18.

164. Zander, J.F., Munster-Wandowski, A., Brunk, I., Pahner, I., Gomez-Lira, G., Heinemann, U., Gutierrez, R., Laube, G., and Ahnert-Hilger, G. 2010. Synaptic and vesicular coexistence of VGLUT and VGAT in selected excitatory and inhibitory synapses. *J Neurosci*. **30**(22): p. 7634-45.

165. Gutierrez, R. 2002. Activity-dependent expression of simultaneous glutamatergic and GABAergic neurotransmission from the mossy fibers in vitro. *J Neurophysiol*. **87**(5): p. 2562-70.

166. Gutiérrez, R. 2003. The GABAergic phenotype of the "glutamatergic" granule cells of the dentate gyrus. *Progress in Neurobiology*. **71**(5): p. 337-358.

167. Gutiérrez, R.R.-P., H.; Maqueda, J.; Vivar, C.; Ramírez, M.; Morales, M. A.; Lamas, M. 2003. Plasticity of the GABAergic Phenotype of the "Glutamatergic" Granule Cells of the Rat Dentate Gyrus. *The Journal of Neuroscience*. **23**(13): p. 5594-5598.

168. Walker, M.C., Ruiz, A., and Kullmann, D.M. 2001. Monosynaptic GABAergic signaling from dentate to CA3 with a pharmacological and physiological profile typical of mossy fiber synapses. *Neuron*. **29**(3): p. 703-15.

169. Gomez-Lira, G., Lamas, M., Romo-Parra, H., and Gutierrez, R. 2005. Programmed and induced phenotype of the hippocampal granule cells. *J Neurosci*. **25**(30): p. 6939-46.

170. Ottem, E.N., Godwin, J.G., Krishnan, S., and Petersen, S.L. 2004. Dual-phenotype GABA/glutamate neurons in adult preoptic area: sexual dimorphism and function. *J Neurosci*. **24**(37): p. 8097-105.

171. Gillespie, D.C., Kim, G., and Kandler, K. 2005. Inhibitory synapses in the developing auditory system are glutamatergic. *Nat Neurosci*. **8**(3): p. 332-8.

172. Root, D.H., Mejias-Aponte, C.A., Zhang, S., Wang, H.L., Hoffman, A.F., Lupica, C.R., and Morales, M. 2014. Single rodent mesohabenular axons release glutamate and GABA. *Nat Neurosci*. **17**(11): p. 1543-51.

173. El Mestikawy, S., Wallen-Mackenzie, A., Fortin, G.M., Descarries, L., and Trudeau, L.E. 2011. From glutamate co-release to vesicular synergy: vesicular glutamate transporters. *Nat Rev Neurosci*. **12**(4): p. 204-16.

174. Spitzer, N.C. 2015. Neurotransmitter Switching? No Surprise. *Neuron*. **86**(5): p. 1131-44.

175. Spitzer, N.C. 2017. Neurotransmitter Switching in the Developing and Adult Brain. *Annu Rev Neurosci*. **40**: p. 1-19.

176. Dulcis, D., Jamshidi, P., Leutgeb, S., and Spitzer, N.C. 2013. Neurotransmitter switching in the adult brain regulates behavior. *Science*. **340**(6131): p. 449-53.

177. Meng, D., Li, H.Q., Deisseroth, K., Leutgeb, S., and Spitzer, N.C. 2018. Neuronal activity regulates neurotransmitter switching in the adult brain following light-induced stress. *Proc Natl Acad Sci U S A*. **115**(20): p. 5064-5071.

178. Stincic, T.L., Grachev, P., Bosch, M.A., Ronnekleiv, O.K., and Kelly, M.J. 2018. Estradiol Drives the Anorexigenic Activity of Proopiomelanocortin Neurons in Female Mice. *eNeuro*. **5**(4).

179. Mercer, A.J.L., S. I.; de Souza, F. S. J.; Rubinstein, M.; Low, M. J. *Redefining the synaptic projection patterns of the hypothalamic proopiomelanocortin circuit*. in *The Obesity Society Annual Meeting*. 2014. Boston, MA.

180. Song, A.J. and Palmiter, R.D. 2018. Detecting and Avoiding Problems When Using the Cre-lox System. *Trends Genet*. **34**(5): p. 333-340.

181. Lam, B.Y.H., Cimino, I., Polex-Wolf, J., Nicole Kohnke, S., Rimmington, D., Iyemere, V., Heeley, N., Cossetti, C., Schulte, R., Saraiva, L.R., Logan, D.W., Blouet, C., O'Rahilly, S., Coll, A.P., and Yeo, G.S.H. 2017. Heterogeneity of hypothalamic pro-opiomelanocortin-expressing neurons revealed by single-cell RNA sequencing. *Mol Metab*. **6**(5): p. 383-392.

182. Boulland, J.L., Qureshi, T., Seal, R.P., Rafiki, A., Gundersen, V., Bergersen, L.H., Fremeau, R.T., Jr., Edwards, R.H., Storm-Mathisen, J., and Chaudhry, F.A. 2004. Expression of the vesicular glutamate transporters during development indicates the widespread corelease of multiple neurotransmitters. *J Comp Neurol*. **480**(3): p. 264-80.

183. Williams, K.W., Margatho, L.O., Lee, C.E., Choi, M., Lee, S., Scott, M.M., Elias, C.F., and Elmquist, J.K. 2010. Segregation of acute leptin and insulin effects in distinct populations of arcuate proopiomelanocortin neurons. *J Neurosci*. **30**(7): p. 2472-9.

184. NIDDK, N.-. *Overweight & Obesity Statistics*. 2019 4/14/19]; Available from: https://www.niddk.nih.gov/health-information/health-statistics/overweight-obesity.

185. WHO. *Overweight and Obesity*. 2019 4/14/19]; Available from: https://www.who.int/gho/ncd/risk_factors/overweight/en/.

186. CDC. *Adult Obesity Facts*. 2019 4/14/19]; Available from: https://www.cdc.gov/obesity/data/adult.html.

187. Stunkard, A. 1959. The Results of Treatment for Obesity. *A.M.A. Archives of Internal Medicine*. **103**(1).

188. MacCuish, A.C., Munro, J.F., and Duncan, L.J. 1968. Follow-up study of refractory obesity treated by fasting. *Br Med J*. **1**(5584): p. 91-2.

189. Sohar, E. and Sneh, E. 1973. Follow-up of obese patients: 14 years after a successful reducing diet. *Am J Clin Nutr*. **26**(8): p. 845-8.

190. Johnson, D. and Drenick, E.J. 1977. Therapeutic fasting in morbid obesity. *Arch Intern Med*. **137**(10): p. 1381-2.

191. Ochner, C.N., Barrios, D.M., Lee, C.D., and Pi-Sunyer, F.X. 2013. Biological mechanisms that promote weight regain following weight loss in obese humans. *Physiol Behav*. **120**: p. 106-13.

192. Mercer, A.J., Hentges, S.T., Meshul, C.K., and Low, M.J. 2013. Unraveling the central proopiomelanocortin neural circuits. *Front Neurosci*. **7**: p. 19.

193. Myers, M.G., Cowley, M.A., and Munzberg, H. 2008. Mechanisms of leptin action and leptin resistance. *Annu Rev Physiol*. **70**: p. 537-56.

194. Sternson, S.M., Nicholas Betley, J., and Cao, Z.F. 2013. Neural circuits and motivational processes for hunger. *Curr Opin Neurobiol*. **23**(3): p. 353-60.

195. Wilson, P.N. and Osbourn, D.F. 1960. Compensatory growth after undernutrition in mammals and birds. *Biol Rev Camb Philos Soc*. **35**: p. 324-63.

196. Quimby, F.H. 1948. Food and water economy of the young rat during chronic starvation and recovery. *J Nutr*. **36**(1): p. 177-86.

197. Da Costa, E. and Clayton, R. 1950. Studies of dietary restriction and rehabilitation. I. Weight Changes and Food Consumption in Rats. *J Nutr*. **41**(4): p. 537-549.

198. Levitsky, D.A., Faust, I., and Glassman, M. 1976. The ingestion of food and the recovery of body weight following fasting in the naive rat. *Physiol Behav*. **17**(4): p. 575-80.

199. Harris, R.B. and Martin, R.J. 1984. Recovery of body weight from below "set point" in mature female rats. *J Nutr*. **114**(6): p. 1143-50.

200. Bjorntorp, P. and Yang, M.U. 1982. Refeeding after fasting in the rat: effects on body composition and food efficiency. *Am J Clin Nutr*. **36**(3): p. 444-9.

201. Osborne, T.B.M., L. B. 1915. The resumption of growth after long continued failure to grow. *The Journal of Biological Chemistry*. **23**: p. 439-454.

202. Cannon, W.B. 1929. Organization for Physiological Homeostasis. *Physiological Reviews*. **9**(3): p. 399-431.

203. Stellar, E. 1954. The physiology of motivation. *Psychological Review*. **61**(1): p. 5-22.

204. Ishimoto, T., Lanaspa, M.A., Rivard, C.J., Roncal-Jimenez, C.A., Orlicky, D.J., Cicerchi, C., McMahan, R.H., Abdelmalek, M.F., Rosen, H.R., Jackman, M.R., MacLean, P.S., Diggle, C.P., Asipu, A., Inaba, S., Kosugi, T., Sato, W., Maruyama, S., Sanchez-Lozada, L.G., Sautin, Y.Y., Hill, J.O., Bonthron, D.T., and Johnson, R.J. 2013. High-fat and high-sucrose (western) diet induces steatohepatitis that is dependent on fructokinase. *Hepatology*. **58**(5): p. 1632-43.

205. Stellar, E. and Hill, J.H. 1952. The rat's rate of drinking as a function of water deprivation. *Journal of Comparative and Physiological Psychology*. **45**(1): p. 96-102.

206. Enriori, P.J., Evans, A.E., Sinnayah, P., Jobst, E.E., Tonelli-Lemos, L., Billes, S.K., Glavas, M.M., Grayson, B.E., Perello, M., Nillni, E.A., Grove, K.L., and Cowley, M.A. 2007. Diet-induced obesity causes severe but reversible leptin resistance in arcuate melanocortin neurons. *Cell Metab*. **5**(3): p. 181-94.

207. Ottaway, N., Mahbod, P., Rivero, B., Norman, L.A., Gertler, A., D'Alessio, D.A., and Perez-Tilve, D. 2015. Diet-induced obese mice retain endogenous leptin action. *Cell Metab*. **21**(6): p. 877-82.

208. Ravussin, Y., LeDuc, C.A., Watanabe, K., Mueller, B.R., Skowronski, A., Rosenbaum, M., and Leibel, R.L. 2014. Effects of chronic leptin infusion on subsequent body weight

and composition in mice: Can body weight set point be reset? *Mol Metab*. **3**(4): p. 432-40.

209. Wirth, M.M., Olszewski, P.K., Yu, C., levine, A.S., and Giraudo, S.Q. 2001. Paraventricular hypothalamic a-melanocyte-stimulating hormone and MTII reduce feeding without causing aversive effects. *Peptides*. **22**: p. 129-134.

210. Presta, E., Yang, M.U., Segal, K.R., and Bjorntorp, P. 1984. Energy depot replenishment in rats during refeeding after fasting: effect of exercise. *Am J Clin Nutr*. **40**(5): p. 1011-6.

211. Ozelci, A., Romsos, D.R., and Leveille, G.A. 1978. Influence of initial food restriction on subsequent body weight gain and body fat accumulation in rats. *J Nutr*. **108**(11): p. 1724-32.

212. Hill, J.O., Fried, S.K., and DiGirolamo, M. 1984. Effects of fasting and restricted refeeding on utilization of ingested energy in rats. *Am J Physiol*. **247**(2 Pt 2): p. R318-27.

213. Carr, K.D. 2007. Chronic food restriction: enhancing effects on drug reward and striatal cell signaling. *Physiol Behav*. **91**(5): p. 459-72.

214. Mizuno, T.M.K., S.P.; Bergen, H.T.; Roberts, J.L.; Priest, C.A.; Mobb, C.V. 1998. Hypothalamic Pro-Opiomelanocortin mRNA Is Reduced By Fasting in ob/ob and db/db Mice, but Is Stimulated by Leptin. *Diabetes*. **47**: p. 294-297.

215. Schwartz, M.W., Seeley, R.J., Woods, S.C., Weigle, D.S., Campfield, L.A., Burn, P., and Baskin, D.G. 1997. Leptin increases hypothalamic pro-opiomelanocortin mRNA expression in the rostral arcuate nucleus. *Diabetes*. **46**(12): p. 2119-23.

216. Savontaus, E., Conwell, I.M., and Wardlaw, S.L. 2002. Effects of adrenalectomy on AGRP, POMC, NPY and CART gene expression in the basal hypothalamus of fed and fasted rats. *Brain Res*. **958**(1): p. 130-8.

217. Schwartz, M.W., Baskin, D.G., Bukowski, T.R., Kuijper, J.L., Foster, D., Lasser, G., Prunkard, D.E., Porte, D., Jr., Woods, S.C., Seeley, R.J., and Weigle, D.S. 1996. Specificity of leptin action on elevated blood glucose levels and hypothalamic neuropeptide Y gene expression in ob/ob mice. *Diabetes*. **45**(4): p. 531-5.

218. Hahn, T.M., Breininger, J.F., Baskin, D.G., and Schwartz, M.W. 1998. Coexpression of Agrp and NPY in fasting-activated hypothalamic neurons. *Nat Neurosci*. **1**(4): p. 271-2.

219. Baskin, D.G., Breininger, J.F., and Schwartz, M.W. 1999. Leptin receptor mRNA identifies a subpopulation of neuropeptide Y neurons activated by fasting in rat hypothalamus. *Diabetes*. **48**(4): p. 828-33.

220. Bi, S., Robinson, B.M., and Moran, T.H. 2003. Acute food deprivation and chronic food restriction differentially affect hypothalamic NPY mRNA expression. *Am J Physiol Regul Integr Comp Physiol*. **285**(5): p. R1030-6.

221. de Rijke, C.E., Hillebrand, J.J., Verhagen, L.A., Roeling, T.A., and Adan, R.A. 2005. Hypothalamic neuropeptide expression following chronic food restriction in sedentary and wheel-running rats. *J Mol Endocrinol*. **35**(2): p. 381-90.

222. Korner, J., Savontaus, E., Chua, S.C., Jr., Leibel, R.L., and Wardlaw, S.L. 2001. Leptin regulation of Agrp and Npy mRNA in the rat hypothalamus. *J Neuroendocrinol*. **13**(11): p. 959-66.

223. Mercer, A.J., Stuart, R.C., Attard, C.A., Otero-Corchon, V., Nillni, E.A., and Low, M.J. 2014. Temporal changes in nutritional state affect hypothalamic POMC peptide levels independently of leptin in adult male mice. *Am J Physiol Endocrinol Metab*. **306**(8): p. E904-15.

224. Brady, L.S., Smith, M.A., Gold, P.W., and Herkenham, M. 1990. Altered expression of hypothalamic neuropeptide mRNAs in food-restricted and food-deprived rats. *Neuroendocrinology*. **52**(5): p. 441-7.

225. Kim, E.M., Welch, C.C., Grace, M.K., Billington, C.J., and Levine, A.S. 1996. Chronic food restriction and acute food deprivation decrease mRNA levels of opioid peptides in arcuate nucleus. *Am J Physiol*. **270**(5 Pt 2): p. R1019-24.

226. Thornton, J.E., Cheung, C.C., Clifton, D.K., and Steiner, R.A. 1997. Regulation of hypothalamic proopiomelanocortin mRNA by leptin in ob/ob mice. *Endocrinology*. **138**(11): p. 5063-6.

227. Arvaniti, K., Huang, Q., and Richard, D. 2001. Effects of leptin and corticosterone on the expression of corticotropin-releasing hormone, agouti-related protein, and proopiomelanocortin in the brain of ob/ob mouse. *Neuroendocrinology*. **73**(4): p. 227-36.

228. Xu, B., Kalra, P.S., Farmerie, W.G., and Kalra, S.P. 1999. Daily changes in hypothalamic gene expression of neuropeptide Y, galanin, proopiomelanocortin, and adipocyte leptin gene expression and secretion: effects of food restriction. *Endocrinology*. **140**(6): p. 2868-75.

229. Lindblom, J., Johansson, A., Holmgren, A., Grandin, E., Nedergard, C., Fredriksson, R., and Schioth, H.B. 2006. Increased mRNA levels of tyrosine hydroxylase and dopamine transporter in the VTA of male rats after chronic food restriction. *Eur J Neurosci*. **23**(1): p. 180-6.

230. Thanos, P.K., Michaelides, M., Piyis, Y.K., Wang, G.J., and Volkow, N.D. 2008. Food restriction markedly increases dopamine D2 receptor (D2R) in a rat model of obesity as assessed with in-vivo muPET imaging ([11C] raclopride) and in-vitro ([3H] spiperone) autoradiography. *Synapse*. **62**(1): p. 50-61.

231. Carr, K.D., Tsimberg, Y., Berman, Y., and Yamamoto, N. 2003. Evidence of increased dopamine receptor signaling in food-restricted rats. *Neuroscience*. **119**(4): p. 1157-67.

232. Collins, G.T., Calinski, D.M., Newman, A.H., Grundt, P., and Woods, J.H. 2008. Food restriction alters N'-propyl-4,5,6,7-tetrahydrobenzothiazole-2,6-diamine dihydrochloride (pramipexole)-induced yawning, hypothermia, and locomotor activity in rats: evidence for sensitization of dopamine D2 receptor-mediated effects. *J Pharmacol Exp Ther*. **325**(2): p. 691-7.

233. Krügel, U., Schraft, T., Kittner, H., Kiess, W., and Illes, P. 2003. Basal and feeding-evoked dopamine release in the rat nucleus accumbens is depressed by leptin. *European Journal of Pharmacology*. **482**(1-3): p. 185-187.

234. Stuber, G.D., Evans, S.B., Higgins, M.S., Pu, Y., and Figlewicz, D.P. 2002. Food restriction modulates amphetamine-conditioned place preference and nucleus accumbens dopamine release in the rat. *Synapse*. **46**(2): p. 83-90.

235. Carroll, M.E., France, C.P., and Meisch, R.A. 1979. Food deprivation increases oral and intravenous drug intake in rats. *Science*. **205**(4403): p. 319-21.

236. Haberny, S.L. and Carr, K.D. 2005. Food restriction increases NMDA receptor-mediated calcium-calmodulin kinase II and NMDA receptor/extracellular signal-regulated kinase 1/2-mediated cyclic amp response element-binding protein phosphorylation in nucleus accumbens upon D-1 dopamine receptor stimulation in rats. *Neuroscience*. **132**(4): p. 1035-43.

237. Haberny, S.L., Berman, Y., Meller, E., and Carr, K.D. 2004. Chronic food restriction increases D-1 dopamine receptor agonist-induced phosphorylation of extracellular signal-regulated kinase 1/2 and cyclic AMP response element-binding protein in caudate-putamen and nucleus accumbens. *Neuroscience*. **125**(1): p. 289-98.

238. Owens, J.L., Thompson, D., Shah, N., and DiGirolamo, M. 1979. Effects of fasting and refeeding in the rat on adipocyte metabolic functions and response to insulin. *J Nutr*. **109**(9): p. 1584-91.

239. Brownell, K.D., Greenwood, M.R., Stellar, E., and Shrager, E.E. 1986. The effects of repeated cycles of weight loss and regain in rats. *Physiol Behav*. **38**(4): p. 459-64.

240. Gray, D.S., Fisler, J.S., and Bray, G.A. 1988. Effects of repeated weight loss and regain on body composition in obese rats. *Am J Clin Nutr*. **47**(3): p. 393-9.

241. Simonds, S.E., Pryor, J.T., and Cowley, M.A. 2018. Repeated weight cycling in obese mice causes increased appetite and glucose intolerance. *Physiol Behav*. **194**: p. 184-190.

242. Huang, X.F., Han, M., South, T., and Storlien, L. 2003. Altered levels of POMC, AgRP and MC4-R mRNA expression in the hypothalamus and other parts of the limbic system of mice prone or resistant to chronic high-energy diet-induced obesity. *Brain Res*. **992**(1): p. 9-19.

243. Farley, C., Cook, J.A., Spar, B.D., Austin, T.M., and Kowalski, T.J. 2003. Meal pattern analysis of diet-induced obesity in susceptible and resistant rats. *Obes Res*. **11**(7): p. 845-51.

244. Strohmayer, A.J. and Smith, G.P. 1987. The meal pattern of genetically obese (ob/ob) mice. *Appetite*. **8**(2): p. 111-23.

245. Ho, A. and Chin, A. 1988. Circadian feeding and drinking patterns of genetically obese mice fed solid chow diet. *Physiol Behav*. **43**(5): p. 651-6.

246. Zorrilla, E.P., Inoue, K., Valdez, G.R., Tabarin, A., and Koob, G.F. 2005. Leptin and post-prandial satiety: acute central leptin more potently reduces meal frequency than meal size in the rat. *Psychopharmacology (Berl)*. **177**(3): p. 324-35.

247. Zheng, H., Patterson, L.M., Rhodes, C.J., Louis, G.W., Skibicka, K.P., Grill, H.J., Myers, M.G., Jr., and Berthoud, H.R. 2010. A potential role for hypothalamomedullary POMC projections in leptin-induced suppression of food intake. *Am J Physiol Regul Integr Comp Physiol*. **298**(3): p. R720-8.

248. Varela, L. and Horvath, T.L. 2012. Leptin and insulin pathways in POMC and AgRP neurons that modulate energy balance and glucose homeostasis. *EMBO Rep*. **13**(12): p. 1079-86.

249. Cowley, M.A.S., J. L.; Rubinstein, M.; Cerdan, M. G.; Diano, S.; Horvath, T. L.; Cone, R. D.; Low, M. J. 2001. Leptin activates anorexigenic POMC neurons through a neural network in the arcuate nucleus. *Nature*. **411**: p. 480-484.

250. Cowley, M.A., Cone, R., Enriori, P., Louiselle, I., Williams, S.M., and Evans, A.E. 2003. Electrophysiological actions of peripheral hormones on melanocortin neurons. *Ann N Y Acad Sci*. **994**: p. 175-86.

251. Russo, S.J. and Nestler, E.J. 2013. The brain reward circuitry in mood disorders. *Nat Rev Neurosci*. **14**(9): p. 609-25.

252. Barbano, M.F., Wang, H.L., Morales, M., and Wise, R.A. 2016. Feeding and Reward Are Differentially Induced by Activating GABAergic Lateral Hypothalamic Projections to VTA. *J Neurosci*. **36**(10): p. 2975-85.

253. Fulton, S. 2010. Appetite and reward. *Front Neuroendocrinol*. **31**(1): p. 85-103.

254. Domingos, A.I., Vaynshteyn, J., Voss, H.U., Ren, X., Gradinaru, V., Zang, F., Deisseroth, K., de Araujo, I.E., and Friedman, J. 2011. Leptin regulates the reward value of nutrient. *Nat Neurosci*. **14**(12): p. 1562-8.

255. Dietrich, M.O., Bober, J., Ferreira, J.G., Tellez, L.A., Mineur, Y.S., Souza, D.O., Gao, X.B., Picciotto, M.R., Araujo, I., Liu, Z.W., and Horvath, T.L. 2012. AgRP neurons regulate development of dopamine neuronal plasticity and nonfood-associated behaviors. *Nat Neurosci*. **15**(8): p. 1108-10.

256. Roseberry, A.G., Stuhrman, K., and Dunigan, A.I. 2015. Regulation of the mesocorticolimbic and mesostriatal dopamine systems by alpha-melanocyte stimulating hormone and agouti-related protein. *Neurosci Biobehav Rev*. **56**: p. 15-25.

257. Navarro, M., Carvajal, F., Lerma-Cabrera, J.M., Cubero, I., Picker, M.J., and Thiele, T.E. 2015. Evidence that Melanocortin Receptor Agonist Melanotan-II Synergistically Augments the Ability of Naltrexone to Blunt Binge-Like Ethanol Intake in Male C57BL/6J Mice. *Alcohol Clin Exp Res*. **39**(8): p. 1425-33.

258. Zhou, Y., Rubinstein, M., Low, M.J., and Kreek, M.J. 2017. Hypothalamic-specific proopiomelanocortin deficiency reduces alcohol drinking in male and female mice. *Genes Brain Behav*. **16**(4): p. 449-461.

259. Lim, B.K., Huang, K.W., Grueter, B.A., Rothwell, P.E., and Malenka, R.C. 2012. Anhedonia requires MC4R-mediated synaptic adaptations in nucleus accumbens. *Nature*. **487**(7406): p. 183-9.

260. Caruso, V., Lagerstrom, M.C., Olszewski, P.K., Fredriksson, R., and Schioth, H.B. 2014. Synaptic changes induced by melanocortin signalling. *Nat Rev Neurosci*. **15**(2): p. 98-110.

261. Reinholz, J., Skopp, O., Breitenstein, C., Bohr, I., Winterhoff, H., and Knecht, S. 2008. Compensatory weight gain due to dopaminergic hypofunction: new evidence and own incidental observations. *Nutr Metab (Lond)*. **5**: p. 35.

262. Geiger, B.M., Behr, G.G., Frank, L.E., Caldera-Siu, A.D., Beinfeld, M.C., Kokkotou, E.G., and Pothos, E.N. 2008. Evidence for defective mesolimbic dopamine exocytosis in obesity-prone rats. *FASEB J*. **22**(8): p. 2740-6.

263. Yang, Z. 1997. Bilateral Hypothalamic Dopamine Infusion in Male Zucker Rat Suppresses Feeding Due to Reduced Meal Size. *Pharmacology Biochemistry and Behavior*. **58**(3): p. 631-635.

264. Tong, Y. and Pelletier, G. 1992. Role of dopamine in the regulation of proopiomelanocortin (POMC) mRNA levels in the arcuate nucleus and pituitary gland of the female rat as studied by in situ hybridization. *Molecular Brain Research*. **15**(1-2): p. 27-32.

265. Koch, M., Varela, L., Kim, J.G., Kim, J.D., Hernandez-Nuno, F., Simonds, S.E., Castorena, C.M., Vianna, C.R., Elmquist, J.K., Morozov, Y.M., Rakic, P., Bechmann, I., Cowley, M.A., Szigeti-Buck, K., Dietrich, M.O., Gao, X.B., Diano, S., and Horvath, T.L. 2015. Hypothalamic POMC neurons promote cannabinoid-induced feeding. *Nature*. **519**(7541): p. 45-50.

266. Helwig, M., Herwig, A., Heldmaier, G., Barrett, P., Mercer, J.G., and Klingenspor, M. 2013. Photoperiod-dependent regulation of carboxypeptidase E affects the selective processing of neuropeptides in the seasonal Siberian hamster (Phodopus sungorus). *J Neuroendocrinol*. **25**(2): p. 190-7.

267. Stevenson, T.J. and Prendergast, B.J. 2013. Reversible DNA methylation regulates seasonal photoperiodic time measurement. *Proc Natl Acad Sci U S A*. **110**(41): p. 16651-6.

268. Bolborea, M., Laran-Chich, M.P., Rasri, K., Hildebrandt, H., Govitrapong, P., Simonneaux, V., Pevet, P., Steinlechner, S., and Klosen, P. 2011. Melatonin controls photoperiodic changes in tanycyte vimentin and neural cell adhesion molecule expression in the Djungarian hamster (Phodopus sungorus). *Endocrinology*. **152**(10): p. 3871-83.

269. Langlet, F., Levin, B.E., Luquet, S., Mazzone, M., Messina, A., Dunn-Meynell, A.A., Balland, E., Lacombe, A., Mazur, D., Carmeliet, P., Bouret, S.G., Prevot, V., and Dehouck, B. 2013. Tanycytic VEGF-A boosts blood-hypothalamus barrier plasticity and access of metabolic signals to the arcuate nucleus in response to fasting. *Cell Metab*. **17**(4): p. 607-17.

270. Langlet, F., Mullier, A., Bouret, S.G., Prevot, V., and Dehouck, B. 2013. Tanycyte-like cells form a blood-cerebrospinal fluid barrier in the circumventricular organs of the mouse brain. *J Comp Neurol*. **521**(15): p. 3389-405.

271. Andermann, M.L. and Lowell, B.B. 2017. Toward a Wiring Diagram Understanding of Appetite Control. *Neuron*. **95**(4): p. 757-778.

272. Campbell, J.N., Macosko, E.Z., Fenselau, H., Pers, T.H., Lyubetskaya, A., Tenen, D., Goldman, M., Verstegen, A.M., Resch, J.M., McCarroll, S.A., Rosen, E.D., Lowell, B.B., and Tsai, L.T. 2017. A molecular census of arcuate hypothalamus and median eminence cell types. *Nat Neurosci*. **20**(3): p. 484-496.

273. Chen, R., Wu, X., Jiang, L., and Zhang, Y. 2017. Single-Cell RNA-Seq Reveals Hypothalamic Cell Diversity. *Cell Rep*. **18**(13): p. 3227-3241.

274. Romanov, R.A., Zeisel, A., Bakker, J., Girach, F., Hellysaz, A., Tomer, R., Alpar, A., Mulder, J., Clotman, F., Keimpema, E., Hsueh, B., Crow, A.K., Martens, H., Schwindling, C., Calvigioni, D., Bains, J.S., Mate, Z., Szabo, G., Yanagawa, Y., Zhang, M.D., Rendeiro, A., Farlik, M., Uhlen, M., Wulff, P., Bock, C., Broberger, C., Deisseroth, K., Hokfelt, T., Linnarsson, S., Horvath, T.L., and Harkany, T. 2017. Molecular interrogation of hypothalamic organization reveals distinct dopamine neuronal subtypes. *Nat Neurosci*. **20**(2): p. 176-188.

275. Butler, A., Hoffman, P., Smibert, P., Papalexi, E., and Satija, R. 2018. Integrating single-cell transcriptomic data across different conditions, technologies, and species. *Nat Biotechnol*. **36**(5): p. 411-420.

276. Macosko, E.Z., Basu, A., Satija, R., Nemesh, J., Shekhar, K., Goldman, M., Tirosh, I., Bialas, A.R., Kamitaki, N., Martersteck, E.M., Trombetta, J.J., Weitz, D.A., Sanes, J.R., Shalek, A.K., Regev, A., and McCarroll, S.A. 2015. Highly Parallel Genome-wide Expression Profiling of Individual Cells Using Nanoliter Droplets. *Cell*. **161**(5): p. 1202-1214.

APPENDIX A

Supplement to Chapter II

The raw counts of single-cell RNA-sequencing was collected from 4 studies: Campbell et al. 2017 [272](GSE90806), Chen et al. 2017 [273](GSE897544), Lam et al. 2017 [181](GSE92707), and Romanov et al. 2017 [274](GSE74672). Cells with at least one raw count of Pomc gene were screened out and normalized using build in method in Seurat v2.0 software [275, 276]. Cells with different conditions, such as high fat diet, and food deprivation, were removed. Since Lam et al. 2017 used flow cytometry to sort out fluorescently labeled $Pomc^{+}$ cells, all of the sequencing data was included. Log transformed expression values were linearized, highlighting a distinct expression threshold. Only genes with linearized expression greater than 0.85 were included in the analysis, genes with expression less than or equal to 0.85 were treated as zero. Between all of the data sets 1358 neurons were identified to express Pomc.

Genes of interest were determined by combining the gene lists from the following Qiagen RT2 ProfilerTM Mouse PCR Arrays: Amino Acid Metabolism I and II, Androgen Receptor Signaling Targets, Dopamine & Serotonin Pathway, Estrogen Receptor Signaling, GABA & Glutamate, Glucocorticoid Signaling, GPCR Signaling Pathway FinderTM, Neurogenesis, Neuronal Ion Channels, Neurotransmitter Receptors, Neurotrophins and Receptors, Nuclear Receptors & Coregulators, Obesity, Signal Transduction Pathway FinderTM, Stem Cell, and Transcription Factors. After combining all of the gene lists, there were 700 genes that were

expressed in all of the data sets, and the analysis was limited to those. Each cell was assessed for the presence of each gene and the data is represented in Table A.1, as the percent of Pomc-Only (% PO; blue), percent or Gad67+ Pomc cells (% G67; red), percent of Vglut2+ Pomc cells (% VG2; grey), or the percent of Pomc neurons with both Gad67 and Vglut2 (% Dual; purple), that express each gene, and the relative expression level of each gene.

Table A.1: Selected gene ontology analysis of available *Pomc* neuron single-cell RNA-sequencing data

Gene	Protein	PO %	G67 %	VG2 %	Dual %	PO Exp.	G67 Exp.	VG2 Exp.	Dual Exp.
Pomc	Proopiomelanocortin	100.0	100.0	100.0	100.0	42.97	26.00	40.49	44.56
Gad1	Glutamate decarboxylase 1	0.0	100.0	0.0	100.0	0.00	7.40	0.00	6.49
Slc17a6	Vesicular glutamate transporter 2	0.0	0.0	100.0	100.0	0.00	0.00	11.74	9.93
Aasdhppt	L-aminoadipate-semialdehyde dehydrogenase-phosphopantetheinyl transferase	19.14	32.51	37.31	44.44	3.33	3.33	4.95	5.79
Abat	4-Aminobutyrate aminotransferase	47.37	70.69	72.48	75.85	4.53	5.42	8.22	8.22
Abcc4	ATP-binding cassette sub-family C member 4	5.98	4.93	11.01	17.39	6.81	7.45	17.59	21.83
Abcg2	ATP-binding cassette super-family G member 2	11.48	9.36	18.35	30.92	14.07	7.28	29.85	30.20
Abhd2	Abhydrolase domain-containing protein 2	8.61	6.16	9.48	18.84	6.12	6.13	15.58	19.19
Acadm	acyl-Coenzyme A dehydrogenase, C-4 to C-12 straight chain	33.73	36.95	37.61	37.20	3.45	3.11	5.74	7.44
Acads	Acyl-CoA dehydrogenase, C-2 to C-3 short chain	7.18	11.08	17.13	31.40	7.34	5.18	28.54	27.96
Acadsb	short/branched chain specific acyl-CoA dehydrogenase	33.49	46.80	56.27	65.22	4.91	4.04	10.79	12.48
Acat1	Acetyl-CoA acetyltransferase, mitochondrial	50.96	71.92	69.42	70.05	4.53	5.43	6.86	5.26
Acat2	Acetyl-CoA acetyltransferase, cytosolic	19.86	31.28	35.47	36.23	4.58	4.63	4.69	4.07
Ache	Acetylcholinesterase	24.64	58.37	59.63	71.50	4.75	4.31	5.68	5.52
Acsl3	Long-chain-fatty-acid—CoA ligase 3	52.39	56.16	70.64	78.26	7.72	6.73	18.79	24.63
Acsl4	Long-chain-fatty-acid—CoA ligase 4	16.27	33.50	44.65	48.79	4.29	3.68	6.41	8.41
Acsl5	Long-chain-fatty-acid—CoA ligase 5	17.70	30.79	33.03	45.89	7.99	5.07	25.94	30.58
Acy1	Aminoacylase-1	7.42	7.88	9.17	11.59	3.98	3.27	5.30	6.05
Adamts1	A disintegrin and metalloproteinase with thrombospondin motifs 1	20.10	17.98	20.18	40.58	8.37	7.74	24.70	23.07
Adar	Double-stranded RNA-specific adenosine deaminase	26.32	45.81	51.68	64.73	6.13	5.04	16.38	19.19
Adarb1	Double-stranded RNA-specific editase 1	11.24	23.15	27.52	29.47	2.80	3.78	5.76	3.81
Adcy1	Adenylyl cyclase type 1	2.87	4.93	18.35	25.60	10.26	6.82	15.70	20.70
Adcy2	Adenylyl cyclase type 2	8.85	19.46	21.10	28.02	4.71	3.55	8.33	11.99
Adcy3	Adenylyl cyclase type 3	9.57	24.88	33.03	50.72	6.63	4.19	9.20	11.10
Adcy5	Adenylyl cyclase type 5	6.46	19.95	26.30	33.82	4.59	4.13	10.99	13.38
Adcy7	Adenylyl cyclase type 7	1.91	3.94	17.13	27.05	22.02	13.47	24.01	27.03
Adcyap1	Pituitary adenylate cyclase-activating polypeptide	1.67	4.19	23.24	18.36	10.59	3.61	12.70	13.35
Adcyap1r1	Pituitary adenylate cyclase-activating polypeptide type I receptor	21.77	48.52	48.32	56.52	4.47	4.40	5.22	6.00
Adh5	Alcohol dehydrogenase class-3	45.45	54.93	49.85	57.49	3.84	4.21	6.92	6.92

Adi1	1,2-dihydroxy-3-keto-5-methylthiopentene dioxygenase	21.77	29.31	28.75	37.68	4.30	3.46	7.27	7.84
Adipor1	Adiponectin receptor 1	33.49	34.24	39.14	37.68	4.34	2.91	4.73	3.52
Adipor2	Adiponectin receptor 2	29.19	33.50	36.39	49.76	5.20	3.64	5.09	5.17
Adora1	adenosine A_1 receptor	11.24	6.65	24.77	30.92	10.22	14.12	33.34	42.99
Adra1a	alpha-1A adrenergic receptor	2.39	5.67	16.51	24.15	12.91	9.69	19.62	21.59
Adra2a	alpha-2A adrenergic receptor	7.42	6.65	22.02	32.85	7.86	8.23	18.89	20.43
Adrb1	beta-1 adrenergic receptor	5.74	5.17	12.84	17.87	5.58	4.20	7.65	12.70
Adrbk1	Beta adrenergic receptor kinase	12.20	22.66	36.09	43.00	5.81	3.53	13.20	13.88
Adrbk2	Beta-adrenergic receptor kinase 2	16.03	29.06	35.17	51.69	8.83	5.30	21.64	23.21
Adsl	Adenylosuccinate lyase	12.44	26.85	26.91	39.13	3.95	3.97	5.09	7.72
Adss	Adenylosuccinate synthetase isozyme 2	27.51	42.12	50.15	58.94	3.61	4.25	10.09	12.34
Aff1	AF4/FMR2 family member 1	7.18	4.19	15.60	25.60	5.78	8.84	25.92	23.53
Agrp	Agouti-related protein	8.85	30.79	10.70	25.12	18.30	30.64	9.63	15.52
Agtr1a	Angiotensin II receptor type 1	2.15	3.69	4.89	12.08	11.52	4.74	14.99	11.42
Agtrap	Type-1 angiotensin II receptor-associated protein	17.46	10.59	12.23	15.94	3.41	4.12	5.77	6.25
Ahcy	Adenosylhomocysteinase	7.18	17.73	28.13	38.16	6.77	5.59	19.23	22.95
Ahr	aryl hydrocarbon receptor	3.11	4.19	15.90	26.57	25.99	20.67	42.20	46.28
Ak2	Adenylate kinase 2	19.14	34.98	39.76	51.69	4.12	3.40	8.72	9.93
Akap1	A kinase anchor protein 1, mitochondrial	9.57	15.27	23.55	34.78	7.32	6.29	13.32	16.02
Akt1	RAC-alpha serine/threonine-protein kinase	12.92	21.43	31.80	43.96	6.79	5.27	14.21	16.76
Akt2	RAC-beta serine/threonine-protein kinase	12.92	13.05	22.32	36.23	6.84	6.41	21.53	22.65
Akt3	RAC-gamma serine/threonine-protein kinase	10.77	18.23	22.32	24.15	3.15	3.08	3.07	2.35
Alas1	Delta-aminolevulinate synthase 1	23.44	31.53	32.72	43.96	5.60	4.24	14.75	17.50
Aldh18a1	Delta-1-pyrroline-5-carboxylate synthetase (P5CS)	5.74	11.82	22.94	37.20	17.76	8.55	31.86	33.88
Aldh2	Aldehyde dehydrogenase, mitochondrial	34.45	37.93	40.67	47.34	7.37	4.65	14.86	18.41
Aldh4a1	Delta-1-pyrroline-5-carboxylate dehydrogenase, mitochondrial	12.44	15.76	20.18	24.64	2.60	5.55	13.39	15.46
Aldh5a1	Succinate-semialdehyde dehydrogenase, mitochondrial	14.59	19.70	24.16	32.37	4.25	3.92	5.91	4.88
Aldh6a1	Methylmalonate-semialdehyde dehydrogenase [acylating], mitochondrial	15.07	17.24	16.21	22.71	3.10	3.41	6.09	4.41
Aldh9a1	4-trimethylaminobutyraldehyde dehydrogenase	30.62	43.60	40.67	43.96	3.55	3.54	5.61	5.17
Alk	Anaplastic lymphoma kinase	2.15	4.19	18.04	28.50	18.16	11.82	24.31	27.40
Ampd3	AMP deaminase 3	6.94	10.10	10.40	18.84	4.23	3.87	3.33	4.36
Anxa4	Annexin A4	9.81	2.96	12.84	19.81	4.46	6.17	12.00	15.59
Apbb1	Amyloid beta A4 precursor protein-binding family B member 1	48.80	74.14	76.45	83.57	4.98	5.35	8.51	8.15
Apc	Adenomatous polyposis coli	44.02	52.71	60.55	74.88	5.39	5.71	14.83	17.11
Apip	APAF1-interacting protein	17.94	28.33	33.64	48.31	5.79	3.42	16.02	17.24
Apoe	Apolipoprotein E	44.98	39.90	36.70	42.51	42.51	7.80	9.89	9.68
App	Amyloid precursor protein	93.78	98.77	89.91	83.09	20.51	22.66	35.69	25.83
Appbp2	Amyloid protein-binding protein 2	33.49	54.19	48.01	54.59	3.61	4.37	5.06	4.05
Ar	androgen receptor	16.75	20.20	23.24	31.88	3.71	3.39	4.67	4.58
Arg2	Arginase, type II	2.87	5.42	14.98	21.74	10.57	4.38	8.46	9.53
Arid5b	AT-rich interactive domain-containing protein 5B	24.40	38.18	33.94	47.83	4.84	4.29	6.14	7.06

Arnt	aryl hydrocarbon receptor nuclear translocator	6.22	9.11	18.35	31.40	7.34	7.43	21.92	23.61
Arrb2	Beta-arrestin-2	15.55	32.27	35.17	44.93	4.00	3.25	7.64	8.64
Artn	Artemin	0.48	2.71	3.36	8.21	1.16	1.43	7.75	8.42
Ascl1	Achaete-scute homolog 1	3.83	2.46	11.62	22.71	14.34	12.05	25.27	25.63
Ash1l	histone-lysine N-methyltransferase	41.63	59.61	61.77	74.40	5.25	5.45	11.93	14.28
Asl	argininosuccinate lyase	5.26	11.08	16.82	20.77	4.00	3.47	9.10	12.31
Asns	Asparagine synthetase	27.03	53.45	62.69	73.91	5.38	4.28	13.51	15.45
Asph	Aspartyl/asparaginyl beta-hydroxylase	32.06	52.71	62.39	71.01	5.35	4.06	9.74	11.37
Ass1	Argininosuccinate synthetase	29.19	58.37	51.99	66.67	4.21	3.72	7.52	9.30
Atf1	Cyclic AMP-dependent transcription factor ATF-1	9.57	11.58	20.80	32.37	7.31	6.52	20.03	22.77
Atf2	Activating transcription factor 2	32.06	56.16	50.76	49.76	4.24	4.47	5.44	3.91
Atf3	Cyclic AMP-dependent transcription factor ATF-3	19.62	12.32	19.88	33.82	19.82	17.17	41.39	42.07
Atf4	Activating transcription factor 4 (tax-responsive enhancer element B67)	48.33	64.29	55.05	60.39	4.56	4.13	5.20	4.59
Atrn	Attractin	18.42	19.70	38.53	42.51	3.53	3.92	4.52	4.15
Auh	3-Methylglutaconyl-CoA hydratase	27.51	45.81	42.51	45.41	3.88	3.92	5.86	4.10
Avpr1a	Vasopressin receptor 1A	1.91	8.37	16.82	25.12	31.28	10.54	37.67	42.24
Axin1	Axin-1	8.37	12.81	15.29	21.74	3.69	3.43	7.34	6.79
Axin2	axis inhibition protein 2	12.92	13.79	22.63	35.27	13.05	11.03	52.63	54.79
Bax	bcl-2-like protein 4	24.40	34.73	37.61	41.06	3.21	3.40	5.49	5.93
Bbc3	Bcl-2-binding component 3	6.46	7.39	21.71	31.88	11.16	9.89	21.87	25.83
Bcar1	Breast cancer anti-estrogen resistance protein 1	20.10	22.17	28.44	36.23	4.45	3.62	9.01	9.35
Bcat1	Branched chain amino acid transaminase 1	21.05	44.58	55.66	62.80	6.34	5.31	13.60	17.15
Bcat2	Branched-chain amino acid aminotransferase	2.63	4.19	10.09	18.36	7.29	4.36	12.47	8.73
Bckdha	2-oxoisovalerate dehydrogenase subunit alpha, mitochondrial	18.66	28.57	34.25	40.58	7.33	5.30	23.83	30.59
Bcl2	B-cell lymphoma 2	15.55	14.78	23.85	39.61	4.12	4.26	11.81	12.99
Bcl2l1	Bcl-2-like 1	24.16	35.22	32.11	46.38	4.04	4.04	7.66	9.21
Bcl6	B-cell lymphoma 6 protein	8.61	8.62	16.21	26.57	8.24	8.31	21.19	24.90
Bdnf	Brain-derived neurotrophic factor	4.55	3.69	29.97	30.92	12.78	11.59	16.32	19.00
Best1	Bestrophin-1	4.55	10.84	17.43	28.02	15.24	9.05	33.95	36.69
Birc3	Baculoviral IAP repeat-containing protein3	3.11	2.96	15.29	24.15	34.70	36.19	65.06	72.55
Bmp1	Bone morphogenetic protein 1	10.53	9.36	19.27	24.64	5.56	4.56	13.75	10.52
Bmp3	Bone morphogenetic protein 3	4.07	5.42	9.48	21.26	4.27	5.56	10.81	12.73
Bmper	BMP binding endothelial regulator	1.91	7.64	17.74	22.71	12.22	7.30	20.30	23.16
Brd8	Bromodomain-containing protein 8	37.32	54.68	47.40	45.89	4.16	4.66	5.74	3.56
Brs3	bombesin receptor subtype 3	5.02	7.64	20.80	39.13	11.13	10.77	20.61	19.06
Btg2	NGF-inducible anti-proliferative protein PC3	31.82	34.98	37.92	47.34	10.91	8.29	17.94	20.66
Btrc	F-box/WD repeat-containing protein 1A	14.59	34.24	37.00	47.83	3.28	3.52	6.44	7.51
Cacna1a	P/Q voltage-dependent calcium channel	10.77	27.09	39.45	46.38	8.08	4.94	15.23	18.43
Cacna1b	voltage-dependent N-type calcium channel subunit alpha-1B	11.72	27.09	31.19	45.41	5.85	4.77	14.76	17.84

Cacna1c	Calcium channel, voltage-dependent, L type, alpha 1C subunit	4.55	7.64	18.35	30.43	6.58	8.25	13.47	15.10
Cacna1d	Calcium channel, voltage-dependent, L type, alpha 1D subunit	12.92	20.44	31.19	43.48	7.52	5.27	15.53	18.52
Cacna1g	Calcium channel, voltage-dependent, T type, alpha 1G subunit	3.11	9.85	23.85	29.47	6.64	6.85	8.93	8.91
Cacna1i	Calcium channel, voltage-dependent, T type, alpha 1I subunit	1.91	5.17	16.21	28.99	15.44	9.59	15.72	14.40
Cacnb1	Voltage-dependent L-type calcium channel subunit beta-1	6.70	15.76	17.13	19.32	3.69	2.58	4.64	3.65
Cacnb2	Voltage-dependent L-type calcium channel subunit beta-2	5.26	14.29	18.04	27.05	3.48	3.10	7.96	4.92
Cacnb3	Voltage-dependent L-type calcium channel subunit beta-3	9.33	25.86	26.30	23.67	5.39	3.27	5.63	4.15
Cacng2	Calcium channel, voltage-dependent, gamma subunit 2	16.75	47.04	50.76	48.79	4.10	3.73	4.31	2.54
Cacng4	Voltage-dependent calcium channel gamma-4 subunit	28.47	39.16	36.09	48.79	4.62	4.51	8.43	10.20
Cad	carbamoyl-phosphate synthetase 2, aspartate transcarbamylase, and dihydroorotase	5.50	5.17	17.74	28.99	10.31	9.29	23.56	23.90
Calcr	calcitonin receptor	4.78	20.20	22.63	31.88	12.95	5.50	25.21	28.32
Calcrl	Calcitonin receptor-like	4.78	2.71	11.62	20.77	7.49	2.90	8.21	6.54
Camkk2	Calcium/calmodulin-dependent protein kinase 2	9.81	15.27	33.03	42.51	5.24	5.44	11.69	13.37
Cartpt	Cocaine- and amphetamine-regulated transcript	40.19	53.69	59.33	83.57	35.91	36.99	32.42	36.75
Casp3	Caspase-3	8.61	12.07	11.31	14.98	4.21	3.42	5.68	7.59
Cat	Catalase	19.14	8.62	25.69	29.47	4.68	5.20	12.44	15.78
Cbln1	Cerebellin-1	2.63	1.97	25.99	26.57	14.67	10.04	11.79	13.48
Cckar	Cholecystokinin A receptor	3.35	6.40	21.41	28.50	5.74	5.39	10.66	13.98
Cckbr	cholecystokinin B receptor	5.50	3.45	18.04	27.05	8.12	15.18	26.35	26.80
Ccna2	Cyclin-A2	1.67	1.97	3.67	4.83	7.69	2.71	13.94	6.38
Ccnd1	Cyclin D1	21.53	19.95	18.35	19.32	6.63	4.85	5.56	6.82
Ccnd2	G1/S-specific cyclin-D2	26.32	17.49	26.30	33.82	5.66	5.95	10.59	11.79
Ccne1	G1/S-specific cyclin-E1	2.39	10.34	13.46	16.91	8.30	4.58	9.30	8.33
Ccne2	Cyclin E2	3.35	9.61	17.43	17.39	5.38	2.85	3.45	1.77
Cd44	CD44 antigen	17.70	7.88	19.27	31.40	3.02	2.78	6.96	7.34
Cdc42	Cell division control protein 42 homolog	82.78	95.57	93.27	98.07	9.71	11.65	19.42	20.96
Cdh2	neural cadherin	39.00	51.97	55.66	71.01	5.04	5.12	13.07	13.79
Cdk5	Cell division protein kinase 5	45.45	70.44	70.03	79.23	5.27	4.97	9.96	11.17
Cdk5r1	Cyclin-dependent kinase 5 activator 1	27.51	52.46	58.41	57.00	4.21	4.64	6.51	5.40
Cdk5rap2	CDK5 regulatory subunit-associated protein 2	9.81	8.62	3.67	9.66	2.39	2.85	6.10	6.81
Cdkn1a	cyclin-dependent kinase inhibitor 1	25.12	16.26	19.88	26.09	9.02	5.70	8.53	8.28
Cdkn1b	Cyclin-dependent kinase inhibitor 1B	38.52	43.35	41.59	58.45	4.70	4.27	11.14	14.18
Cdo1	Cysteine dioxygenase	13.16	24.14	33.33	37.68	4.45	4.86	7.48	9.94
Cebpb	CCAAT/enhancer-binding protein beta	12.68	13.05	22.02	28.99	5.03	2.83	11.47	15.78
Cebpg	CCAAT/enhancer-binding protein gamma	33.01	31.03	42.20	52.17	6.72	6.23	18.15	23.10

Cenpn	Centromere protein N	2.63	2.96	11.01	18.84	10.97	4.61	15.28	21.25
Cflar	CASP8 and FADD-like apoptosis regulator	17.70	10.59	17.43	27.05	4.52	4.46	7.43	9.39
Chrm1	muscarinic acetylcholine receptor M_1	1.20	2.96	4.89	7.25	5.84	3.39	4.92	10.42
Chrm2	muscarinic acetylcholine receptor M_2	4.31	8.62	22.94	34.30	11.37	7.87	21.15	23.86
Chrm5	muscarinic acetylcholine receptor M_5	2.63	4.93	16.82	26.57	10.50	10.61	19.69	19.89
Chrna4	Neuronal acetylcholine receptor subunit alpha-4	2.15	4.68	20.18	26.09	7.97	6.89	13.27	14.91
Cited2	Cbp/p300-interacting transactivator 2	24.40	31.28	35.78	48.31	4.30	5.33	11.84	12.59
Ckb	Brain-type creatine kinase	81.82	93.84	90.83	94.20	10.99	12.10	16.71	13.36
Clasrp	Splicing factor, arginine/serine-rich 16	15.55	31.28	37.31	40.10	6.61	5.21	15.66	21.12
Clcn2	Chloride channel protein 2	5.74	13.79	18.04	21.74	3.80	3.90	6.63	6.51
Clcn3	H^+/Cl^- exchange transporter 3	57.89	79.06	76.76	89.37	6.90	7.20	15.43	18.56
Clcn7	Chloride channel 7 alpha subunit	9.09	13.05	17.13	19.81	3.17	3.58	3.99	2.22
Cln3	Battenin	10.53	9.61	18.96	29.47	3.64	3.54	11.95	11.13
Cnr1	Cannabinoid receptor type 1	5.98	11.58	30.28	25.60	3.30	4.72	6.93	8.31
Cntfr	ciliary neurotrophic factor receptor	8.37	10.59	12.54	16.43	3.31	3.31	9.48	9.41
Col2a1	Collagen, type II, alpha 1	1.67	2.71	14.07	25.12	25.17	14.16	29.00	27.01
Col4a2	Collagen alpha-2(IV) chain	16.27	24.88	27.52	43.00	8.38	5.67	18.27	19.67
Comt	Catechol-*O*-methyltransferase	47.13	59.36	55.05	58.94	4.07	4.24	7.05	6.30
Cops2	COP9 signalosome complex subunit 2	45.69	68.47	59.02	57.00	4.56	4.85	5.94	4.84
Cpd	Carboxypeptidase D	26.79	23.65	40.98	46.38	5.47	4.98	14.49	20.38
Cpe	Carboxypeptidase E	83.01	94.58	86.85	88.41	10.64	11.23	15.16	12.35
Cpt2	Carnitine O-palmitoyltransferase 2, mitochondrial	9.57	12.81	11.93	9.66	3.35	2.37	3.69	5.12
Creb1	CAMP responsive element binding protein 1	20.57	26.11	29.05	27.05	3.36	3.33	5.39	3.79
Creb3	Cyclic AMP-responsive element-binding protein 3	38.28	63.79	64.53	80.19	5.12	4.61	13.26	15.46
Crebbp	CREB-binding protein	28.95	43.10	47.71	67.15	6.15	5.38	19.89	22.22
Crhr1	Corticotropin-releasing hormone receptor 1	1.67	2.96	2.75	4.35	6.74	2.63	4.60	4.21
Csf1	colony stimulating factor 1	16.27	20.69	19.57	28.99	3.69	3.75	8.08	9.62
Ctgf	connective tissue growth factor	5.02	2.96	13.46	18.84	8.71	3.25	5.11	4.30
Ctnna1	Catenin alpha-1	36.36	26.60	31.80	36.23	5.51	3.61	7.87	9.07
Ctnnb1	β-catenin	51.91	60.84	62.69	70.05	7.54	5.65	12.97	13.72
Ctsd	Cathepsin D	68.66	77.34	81.35	92.75	7.88	6.65	19.08	21.65
Cyb561	Cytochrome b561	26.56	42.12	48.01	64.25	4.90	4.52	15.48	18.92
Cyp2u1	cytochrome P450, family 2, subfamily U, polypeptide 1	3.35	6.65	8.87	9.66	6.01	4.03	6.96	8.28
Dbi	Acyl-CoA-binding protein	55.02	51.23	45.26	54.59	28.59	9.72	8.78	10.88
Dbt	Lipoamide acyltransferase component of branched-chain alpha-keto acid dehydrogenase complex, mitochondrial	12.92	18.72	13.76	21.26	3.54	3.00	4.31	4.46
Dcx	Neuronal migration protein doublecortin	4.78	13.30	19.57	32.37	7.59	4.27	9.09	9.79
Ddc	Aromatic-L-amino-acid decarboxylase	21.05	29.80	34.56	44.44	6.13	7.00	7.49	6.59
Ddx5	DEAD box protein 5	84.45	94.33	90.21	90.34	11.72	12.37	16.60	14.14
Dhcr24	24-Dehydrocholesterol reductase	23.21	29.06	44.34	49.28	8.00	6.28	12.22	15.75
Diras2	GTP-binding protein Di-Ras2	7.18	10.34	25.38	33.82	9.43	7.55	19.02	23.89

Dld	Dihydrolipoamide dehydrogenase	33.73	52.71	47.40	49.28	3.71	3.89	5.60	3.70
Dlg4	PSD-95	20.10	45.57	53.82	64.73	6.63	5.24	14.22	16.08
Dll1	Delta-like protein 1	2.63	3.69	4.89	6.76	4.01	7.08	10.64	6.43
Dll3	Delta-like 3	2.39	4.68	17.43	25.12	44.96	24.46	58.63	68.20
Dlst	Dihydrolipoyllysine-residue succinyltransferase component of 2-oxoglutarate dehydrogenase complex, mitochondrial	19.38	33.74	36.39	33.33	3.17	3.42	3.99	2.99
Dnmt1	DNA (cytosine-5)-methyltransferase 1	17.46	32.51	33.03	48.31	4.71	4.51	14.42	15.45
Dr1	Protein Dr1	13.40	18.97	27.22	30.92	4.54	3.71	8.19	9.20
Dtx1	Protein deltex-1	25.60	43.84	46.18	60.87	6.57	5.06	16.85	20.11
Dtx2	E3 ubiquitin-protein ligase	4.31	4.43	12.54	20.29	6.13	11.60	15.82	25.15
Dusp1	Dual specificity protein phosphatase 1	34.69	37.93	32.42	32.85	8.76	7.09	7.27	5.47
Dusp14	Dual specificity protein phosphatase 14	17.22	20.94	17.43	21.74	3.17	3.51	3.55	2.91
Dvl1	Segment polarity protein dishevelled homolog DVL-1	16.75	27.83	25.99	35.75	3.11	3.28	6.25	7.07
Dvl3	Segment polarity protein dishevelled homolog DVL-3	2.39	4.43	7.95	10.63	4.25	4.17	6.19	7.45
E2f6	Transcription factor E2F6	16.51	30.30	38.23	45.89	8.06	5.51	21.54	29.07
Eaf2	ELL-associated factor 2	0.48	1.72	7.65	8.21	23.95	3.09	11.01	14.47
Ebag9	Receptor-binding cancer antigen expressed on SiSo cells	20.57	36.95	33.64	39.13	4.37	3.84	6.43	6.71
Echs1	Enoyl Coenzyme A hydratase, short chain, 1, mitochondrial	36.36	48.77	39.76	43.00	3.67	3.47	4.14	2.94
Efna5	Ephrin A5	25.36	47.29	48.32	64.73	5.44	4.95	13.50	15.49
Efnb1	Ephrin-B1	13.88	24.63	27.52	36.71	3.67	3.49	8.36	8.44
Egr1	NGFI-A	48.33	52.71	49.85	56.04	12.99	11.82	12.58	10.67
Ehd3	Eps15 homology domain-containing protein 3	15.07	32.27	41.90	49.76	5.33	4.07	9.03	10.38
Ehhadh	Peroxisomal bifunctional enzyme	2.39	1.97	9.17	14.01	10.32	6.89	13.33	17.12
Elk1	ETS domain-containing protein Elk-1	8.85	13.05	23.55	30.92	4.67	4.20	13.60	15.93
Elk4	ETS domain-containing protein Elk-4	5.02	6.40	6.12	9.18	5.22	3.02	5.68	6.12
Ell2	RNA polymerase II elongation factor	10.05	12.56	22.32	28.99	6.65	5.82	15.96	21.86
Endod1	Endonuclease domain-containing 1 protein	26.56	39.16	43.43	48.31	4.65	4.26	6.73	7.13
Enoph1	Enolase-phosphatase E1	17.70	31.53	37.61	40.58	3.85	4.14	6.15	6.96
Ep300	Histone acetyltransferase p300	18.18	22.41	26.91	34.30	3.54	2.82	6.27	6.35
Ephb1	Ephrin type-B receptor 1	11.72	9.36	21.71	22.71	5.09	6.71	8.58	10.02
Errfi1	ERBB receptor feedback inhibitor 1	15.55	24.88	19.57	26.57	2.87	3.53	3.60	2.76
Esr1	Estrogen receptor alpha	12.92	19.21	29.66	40.10	6.50	5.36	12.58	13.73
Esrra	Estrogen-related receptor alpha	3.11	8.87	13.46	15.46	4.85	4.79	8.09	7.92
Esrrg	Estrogen-related receptor gamma	2.87	3.20	14.68	21.26	14.32	9.23	16.55	19.41
Ets2	Protein C-ets-2	22.01	34.24	41.59	47.83	4.88	4.13	6.82	7.23
Fah	Fumarylacetoacetase	10.05	14.53	14.37	12.56	3.04	3.07	4.51	4.89
Fam105a	Inactive ubiquitin thioesterase	5.50	12.56	23.24	33.82	10.77	6.66	23.63	26.73
Fgf1	acidic fibroblast growth factor	10.77	12.07	23.55	35.75	7.76	6.18	21.80	21.45
Fgf9	Glia-activating factor	9.57	11.08	29.66	38.16	7.37	5.39	10.06	10.75
Fgfr1	Fibroblast growth factor receptor 1	34.69	39.90	49.24	64.25	4.43	4.77	15.54	17.71
Fkbp5	FK506 binding protein 5	7.89	13.30	19.57	28.50	4.88	3.58	9.66	10.39
Flna	Filamin A, alpha	17.94	12.32	23.55	32.85	5.58	5.79	19.30	22.57
Fos	Proto-oncogene c-Fos	51.44	56.65	44.65	48.31	23.93	20.13	19.56	15.24

Fosl2	Fos-related antigen 2	10.05	10.10	18.65	28.50		6.64	6.64	18.59	19.06
Frs2	Fibroblast growth factor receptor substrate 2	6.94	9.11	22.94	31.88		14.77	10.40	34.79	42.34
Frs3	Fibroblast growth factor receptor substrate 3	5.02	14.29	24.46	23.67		5.86	3.11	8.33	9.31
Fth1	Ferritin heavy chain	98.33	99.01	94.50	96.14		27.21	27.71	27.76	20.97
Fus	RNA-binding protein FUS/TLS	67.70	83.74	79.51	87.92		6.09	6.85	9.44	9.42
Fzd5	Frizzled-5	13.40	12.32	18.04	32.37		5.75	6.73	24.58	22.48
G6pdx	Glucose-6-phosphate 1-dehydrogenase X	11.72	17.98	26.61	40.10		4.85	3.68	13.92	12.48
Gabbr1	Gamma-aminobutyric acid (GABA) B receptor, 1	56.94	82.02	86.24	94.20		6.72	6.37	13.68	14.60
Gabbr2	Gamma-aminobutyric acid (GABA) B receptor, 2	7.42	20.20	18.96	27.05		2.86	2.47	6.17	3.46
Gabra1	Gamma-aminobutyric acid receptor subunit alpha-1	15.79	40.15	45.87	45.41		6.90	6.00	8.51	4.97
Gabra2	Gamma-aminobutyric acid receptor subunit alpha-2	15.79	47.29	49.85	56.52		4.50	5.17	6.68	5.17
Gabra4	Gamma-aminobutyric acid receptor subunit alpha-4	5.02	14.78	26.61	26.09		5.09	5.28	7.39	7.67
Gabra5	Gamma-aminobutyric acid (GABA) A receptor, alpha 5	26.32	53.94	48.62	62.80		5.53	5.14	9.32	10.33
Gabrb1	Gamma-aminobutyric acid receptor subunit beta-1	23.92	57.14	59.63	69.57		5.55	4.68	9.43	9.65
Gabrb3	Gamma-aminobutyric acid receptor subunit beta-3	30.86	62.32	61.47	73.91		5.03	4.64	8.13	10.23
Gabre	Gamma-aminobutyric acid receptor subunit epsilon	7.89	27.09	12.54	18.36		2.70	2.97	6.22	4.28
Gabrg1	Gamma-aminobutyric acid receptor subunit gamma-1	23.44	44.58	43.12	45.89		4.89	4.90	5.43	4.31
Gabrg2	Gamma-aminobutyric acid receptor subunit gamma-2	28.95	62.56	72.78	73.91		5.91	6.58	9.88	7.61
Gabrg3	$GABA_A$ receptor-γ3	16.75	22.17	34.25	44.93		5.84	3.80	11.97	15.78
Gabrq	Gamma-aminobutyric acid receptor subunit theta	18.90	34.48	33.03	48.79		4.44	3.52	9.63	11.17
Gad2	Glutamate decarboxylase 2	39.47	79.06	44.65	64.25		7.74	14.27	8.87	8.61
Gadd45a	Growth arrest and DNA-damage-inducible protein GADD45 alpha	11.72	15.27	19.88	27.05		3.35	4.24	7.31	8.83
Gadd45b	Growth arrest and DNA-damage-inducible, beta	16.99	10.10	16.51	29.95		7.09	8.82	25.76	22.79
Gal	Galanin	9.81	26.60	16.21	28.99		11.12	23.63	14.00	11.92
Gamt	Guanidinoacetate N-methyltransferase	14.83	14.04	26.91	30.92		8.57	4.71	13.48	16.94
Gatm	Glycine amidinotransferase, mitochondrial	16.27	12.81	14.98	19.81		13.75	9.05	12.43	9.23
Gcat	Glycine C-acetyltransferase	5.26	9.11	17.43	22.71		4.42	6.36	13.05	15.07
Gcdh	Glutaryl-CoA dehydrogenase	11.72	19.21	23.55	32.85		4.30	3.41	13.60	11.44
Gclc	Glutamate—cysteine ligase catalytic subunit	21.77	30.79	39.76	46.38		4.11	3.47	7.96	9.87
Gclm	Glutamate-cysteine ligase regulatory subunit	41.63	49.26	44.65	54.59		4.22	3.69	8.20	8.09
Gdpd1	Lysophospholipase D	35.65	60.59	68.81	75.85		5.77	6.20	14.16	17.52
Gfpt1	Glucosamine—fructose-6-phosphate aminotransferase isomerizing 1	24.16	39.90	41.59	57.00		3.16	3.47	13.06	15.10
Gfra1	GDNF family receptor alpha-1	18.66	26.60	27.83	38.16		4.89	3.74	7.67	6.49
Gfra2	GDNF family receptor alpha-2	10.53	26.60	25.08	37.20		5.10	3.55	7.87	6.52
Ghr	Growth hormone receptor	10.29	31.28	26.30	40.10		6.80	3.42	17.38	20.57
Ghsr	ghrelin receptor	1.44	9.36	11.62	20.77		7.13	4.40	14.73	20.33

Gldc	Glycine decarboxylase	4.55	4.68	12.84	18.36	8.32	7.64	16.93	16.11
Glp1r	glucagon-like peptide-1 receptor	1.44	2.46	9.17	18.36	2.10	3.68	7.21	9.53
Gls	Glutaminase 2 (liver, mitochondrial)	28.95	58.13	59.33	69.08	4.43	5.14	10.19	10.77
Glud1	glutamate dehydrogenase 1	38.76	54.43	57.19	73.43	3.98	3.99	6.66	6.58
Glul	Glutamine synthetase	40.91	37.93	36.70	40.58	8.44	4.15	5.28	4.91
Gmfb	Glia maturation factor beta	33.01	51.23	56.88	70.05	4.70	4.33	7.59	8.09
Gnai1	Guanine nucleotide-binding protein G(i), alpha-1 subunit	46.41	75.12	74.92	85.99	6.30	6.57	9.83	11.74
Gnaq	Guanine nucleotide-binding protein G(q) subunit alpha	49.52	71.67	67.89	62.80	4.16	4.94	6.04	5.09
Gnas	GNAS complex locus	98.56	99.01	94.50	91.30	34.44	50.62	51.80	38.13
Got1	Aspartate aminotransferase, cytoplasmic	39.95	77.83	71.87	69.08	4.64	6.77	10.85	7.09
Got2	Aspartate aminotransferase, mitochondrial	21.05	46.06	53.52	65.22	5.97	4.83	13.72	16.85
Gphn	Gephyrin	26.08	45.57	49.85	62.80	4.92	4.35	7.75	8.27
Gpi1	Glucose-6-phosphate isomerase	54.07	79.06	71.56	77.78	5.29	6.70	9.58	7.83
Gpt	Alanine aminotransferase 1	3.83	2.96	13.46	22.22	9.12	8.68	14.62	17.64
Gria1	Glutamate receptor 1	40.19	72.41	71.25	83.09	5.65	6.45	9.58	8.70
Gria2	Glutamate ionotropic receptor AMPA type subunit 2	61.96	94.58	95.41	97.10	10.19	14.30	20.38	19.51
Gria3	Glutamate receptor 3	14.11	28.82	32.11	41.55	5.76	5.78	6.23	6.13
Gria4	Glutamate receptor 4	20.57	45.81	46.79	53.14	5.55	4.64	14.49	17.65
Grik1	Glutamate receptor, ionotropic, kainate 1	6.22	16.26	29.66	37.68	13.13	6.76	16.43	18.30
Grik2	Glutamate ionotropic receptor kainate type subunit 2	11.72	20.20	22.94	25.60	3.25	3.54	4.56	3.67
Grik4	glutamate receptor, ionotropic, kainate 4	7.42	12.81	9.48	13.04	2.51	2.98	4.47	6.60
Grik5	Glutamate receptor, ionotropic kainate 5	24.88	48.52	44.34	45.89	3.93	3.68	6.20	8.41
Grin1	Glutamate [NMDA] receptor subunit zeta-1	19.38	45.07	47.40	57.49	4.26	4.35	6.15	6.30
Grin2a	Glutamate [NMDA] receptor subunit epsilon-1	5.02	9.11	14.07	23.67	3.69	3.17	10.08	11.71
Grin2b	*N*-methyl D-aspartate receptor subtype 2B	17.22	39.90	42.20	58.94	5.56	3.65	7.70	10.21
Grk4	G protein-coupled receptor kinase 4	9.33	4.19	12.23	20.29	1.92	3.42	6.33	8.16
Grk6	G protein-coupled receptor kinase 6	11.96	17.98	29.97	37.20	5.31	3.25	10.37	13.22
Grm1	glutamate receptor, metabotropic 1	13.40	21.18	31.19	39.61	5.08	4.56	5.74	3.55
Grm2	Metabotropic glutamate receptor 2	1.20	1.72	17.74	28.50	23.42	16.49	20.69	25.52
Grm5	Metabotropic glutamate receptor 5	15.07	28.08	45.57	48.79	5.81	6.67	10.33	10.56
Grm7	Metabotropic glutamate receptor 7	5.98	18.23	34.56	39.61	8.94	5.42	14.59	19.24
Grm8	Metabotropic glutamate receptor 8	2.87	8.87	20.80	34.30	11.30	8.22	11.87	11.95
Grp	Gastrin-releasing peptide	2.39	7.14	14.37	22.71	25.82	8.52	26.78	27.39
Gsk3a	Glycogen synthase kinase-3 alpha	17.46	28.08	41.28	49.76	6.28	5.22	14.31	18.83
Gsk3b	Glycogen synthase kinase 3 beta	64.83	85.47	85.02	88.41	5.88	7.40	11.31	11.86
Gsr	Glutathione reductase	16.99	23.89	31.19	43.00	4.08	4.19	13.99	16.76
Gtf2b	Transcription factor II B	34.93	56.65	54.13	63.77	4.67	3.71	12.37	13.34
Gtf2f1	General transcription factor IIF subunit 1	43.54	58.62	58.72	64.25	4.13	4.71	6.23	5.45

Gucy1a3	Guanylate cyclase soluble subunit alpha-3	14.35	23.40	38.23	42.03		5.85	5.33	10.12	10.40
Hadh	Hydroxyacyl-Coenzyme A dehydrogenase	17.94	13.05	19.88	31.88		9.47	8.96	41.11	40.74
Hadhb	Trifunctional enzyme subunit beta, mitochondrial	25.84	34.48	39.45	57.49		5.67	4.95	16.88	18.26
Hcn1	Potassium/sodium hyperpolarization-activated cyclic nucleotide-gated channel 1	4.55	10.84	21.71	31.88		7.14	4.39	12.70	14.01
Hcn2	Potassium/sodium hyperpolarization-activated cyclic nucleotide-gated ion channel 2	3.59	8.87	15.29	25.60		9.56	5.24	21.50	18.71
Hcrtr1	Orexin receptor type 1	2.63	4.93	17.13	24.64		17.72	6.48	13.48	20.83
Hcrtr2	Orexin receptor type 2	4.07	6.65	23.24	26.09		8.02	7.60	9.79	17.64
Hdac1	Histone deacetylase 1	27.75	30.30	22.63	30.92		3.99	3.28	4.84	5.19
Hdac2	Histone deacetylase 2	42.58	66.75	60.86	71.50		6.48	5.76	17.82	22.05
Hdac3	Histone deacetylase 3	28.23	47.78	46.48	61.84		4.63	4.29	8.55	9.62
Hdac4	Histone deacetylase 4	9.33	12.07	22.32	34.78		5.77	5.43	20.54	22.22
Hdac5	Histone deacetylase 5	18.18	21.43	31.80	30.92		3.59	3.46	6.53	8.20
Hdac6	Histone deacetylase 6	11.00	18.23	34.25	43.00		6.17	4.39	11.62	13.30
Hdac7	Histone deacetylase 7	12.68	23.40	23.85	34.78		3.95	3.87	5.06	4.34
Herc3	Probable E3 ubiquitin-protein ligase	12.44	32.76	29.97	39.13		3.55	3.17	4.33	4.05
Herpud1	Homocysteine-responsive endoplasmic reticulum-resident ubiquitin-like domain member 1 protein	40.43	57.88	51.07	50.72		4.93	4.08	5.74	4.80
Hey1	Hairy/enhancer-of-split related with YRPW motif protein 1	13.16	11.33	20.80	27.05		5.09	4.32	11.29	10.65
Hibadh	3-hydroxyisobutyrate dehydrogenase	29.67	48.52	44.95	59.90		6.40	4.70	21.44	25.46
Hibch	3-hydroxyisobutyryl-CoA hydrolase, mitochondrial	13.64	22.66	28.75	37.68		5.01	4.02	10.07	10.48
Hif1a	Hypoxia-inducible factor 1-alpha	21.29	41.13	36.39	54.11		4.91	4.09	7.66	10.00
Hmgcl	3-hydroxy-3-methylglutaryl-CoA lyase	18.90	30.54	36.09	50.72		5.19	4.57	15.17	16.95
Hmox1	heme oxygenase (decycling) 1	4.55	3.94	13.76	24.64		16.44	20.23	48.81	47.55
Hnmt	Histamine N-methyltransferase	10.05	15.52	31.80	36.71		6.18	6.13	10.00	13.61
Homer1	Homer protein homolog 1	11.00	14.78	30.28	39.61		5.80	5.55	14.22	17.46
Homer2	Homer protein homolog 2	5.98	12.07	24.46	30.43		7.04	5.87	7.89	13.33
Hpgd	Hydroxyprostaglandin dehydrogenase 15-(NAD)	2.63	2.46	14.07	21.26		13.01	9.57	23.74	24.01
Hrh1	Histamine H_1 receptor	7.66	10.10	25.99	39.13		10.24	8.89	21.19	24.35
Hsd17b10	17-β-Hydroxysteroid dehydrogenase X	28.95	35.71	42.20	52.17		4.63	3.64	12.52	15.35
Hsf1	Heat shock factor 1 (HSF1)	12.20	20.20	25.99	36.23		10.41	7.40	35.70	40.88
Hsp90aa1	Heat shock protein HSP 90-alpha	92.11	98.52	91.44	85.51		19.37	28.59	38.65	27.77
Hspa9	Mitochondrial 70kDa heat shock protein (mtHsp70)	60.05	79.31	81.96	86.47		5.48	5.77	9.58	10.47
Hspb1	Heat shock protein 27	14.35	7.39	6.73	10.14		12.13	6.64	10.83	9.74
Htr1a	serotonin 1A receptor	2.39	6.65	16.51	25.12		24.02	11.87	35.42	40.40
Htr1f	serotonin 1F receptor	1.44	2.96	14.68	24.64		37.53	20.45	26.66	29.65
Htr2a	serotonin 2a receptor	0.72	0.74	1.22	4.35		2.93	10.32	13.52	14.89
Htr2c	serotonin 2c receptor	3.35	8.13	9.79	13.04		3.19	6.23	5.96	3.67
Htr4	serotonin 4 receptor	1.20	1.48	7.34	15.94		2.69	15.34	15.21	10.48
Htr5a	serotonin 5a receptor	1.91	3.69	12.23	25.60		13.12	9.65	19.42	18.68
Htr6	serotonin 6 receptor	2.15	2.22	14.37	25.12		23.98	28.65	28.24	32.42
Htr7	serotonin 7 receptor	1.20	7.39	17.13	18.84		9.55	4.41	12.06	14.15

Iars	Leucyl-tRNA synthetase, cytoplasmic	11.00	17.73	37.61	42.51	5.86	4.69	10.25	13.17
Ido1	Indoleamine-pyrrole 2,3-dioxygenase	1.67	3.45	4.28	8.21	5.41	4.98	7.34	9.05
Ifrd1	Interferon-related developmental regulator 1	27.75	21.67	26.61	28.99	5.48	4.58	5.03	4.71
Igf1r	insulin-like growth factor 1	22.25	14.53	33.03	35.27	8.05	5.56	16.70	23.74
Igfbp4	Insulin-like growth factor-binding protein 4	7.18	4.68	15.29	22.71	7.56	9.46	17.47	21.53
Igfbp5	Insulin-like growth factor-binding protein 5	27.51	20.94	35.47	46.86	11.91	7.34	9.21	9.84
Il1r1	Interleukin 1 receptor, type I	3.35	1.48	3.36	5.80	2.81	4.04	17.85	7.30
Il6st	Glycoprotein 130	18.66	25.37	24.77	34.30	4.23	2.73	6.87	7.30
Insr	insulin receptor	15.31	14.29	25.69	38.16	9.27	8.85	34.06	37.98
Irf1	Interferon regulatory factor 1	14.59	9.36	18.96	29.47	6.35	7.48	17.97	23.18
Irs2	Insulin receptor substrate 2	28.95	46.06	37.92	52.17	4.46	4.25	11.20	12.28
Isl1	Insulin gene enhancer protein	31.34	64.04	43.12	73.91	6.35	5.38	9.68	8.46
Itgb3bp	Centromere protein R	13.88	16.50	24.16	35.27	4.97	4.13	12.89	16.60
Itpr1	Inositol 1,4,5-trisphosphate receptor type 1	17.94	20.69	33.64	44.93	3.95	3.69	10.18	10.89
Ivd	Isovaleryl-CoA dehydrogenase, mitochondrial	20.57	28.82	37.31	49.76	5.06	3.93	12.03	12.44
Jag1	Jagged1	6.46	3.94	15.29	24.64	8.27	10.53	20.99	19.57
Jun	c-Jun	61.96	70.69	62.69	78.26	16.99	12.56	20.98	20.62
Junb	Transcription factor jun-B	40.43	43.60	40.67	52.66	12.68	7.76	19.71	23.11
Jund	Transcription factor JunD	58.85	74.63	70.03	76.33	7.80	6.64	11.50	12.39
Kat2a	Histone acetyltransferase KAT2A	11.48	24.63	23.85	26.09	3.79	3.11	4.71	4.26
Kat2b	P300/CBP-associated factor	10.77	7.88	11.31	14.49	3.55	3.51	6.77	15.35
Kat5	Histone acetyltransferase	17.22	32.27	38.23	51.21	4.39	3.35	8.75	10.11
Kcna1	Potassium voltage-gated channel subfamily A member 1	9.09	9.85	14.37	21.74	10.61	7.55	9.56	9.83
Kcna2	Potassium voltage-gated channel subfamily A member 2	10.05	17.24	33.64	43.48	5.23	4.90	9.27	11.57
Kcna5	Potassium voltage-gated channel, shaker-related subfamily, member 5	13.64	22.66	27.22	41.55	4.15	3.44	9.63	10.12
Kcna6	Potassium voltage-gated channel subfamily A member 6	7.66	16.26	29.66	24.15	5.27	4.40	8.64	10.70
Kcnab1	Voltage-gated potassium channel subunit beta-1	9.57	17.00	22.94	38.16	10.51	6.78	26.96	26.96
Kcnab2	Voltage-gated potassium channel subunit beta-2	3.35	11.82	12.84	21.74	2.66	3.25	7.36	5.40
Kcnab3	Voltage-gated potassium channel subunit beta-3	0.96	1.97	3.06	6.76	7.87	3.36	17.94	11.65
Kcnb1	Potassium voltage-gated channel, Shab-related subfamily, member 1	15.07	28.82	30.89	28.02	3.51	3.74	4.73	2.75
Kcnb2	Potassium voltage-gated channel subfamily B member 2	5.50	9.85	16.21	16.43	5.07	4.28	8.06	7.55
Kcnc1	Potassium voltage-gated channel subfamily C member 1	26.32	58.37	60.24	73.91	7.57	5.55	11.16	13.44
Kcnc2	Potassium voltage-gated channel subfamily C member 2	8.85	24.14	26.30	41.06	3.36	3.51	5.86	6.44
Kcnd2	Potassium voltage-gated channel subfamily D member 2	16.75	34.73	48.93	55.56	9.04	6.39	23.69	29.96
Kcnd3	Potassium voltage-gated channel subfamily D member 3	8.13	20.44	25.38	34.78	3.80	2.93	5.14	5.62
Kcnh1	Potassium voltage-gated channel subfamily H member 1	2.63	7.39	10.40	10.63	2.59	5.06	3.31	7.05

Kcnh2	Potassium voltage-gated channel subfamily H member 2	12.68	13.79	14.07	13.53	2.69	2.73	3.23	2.75
Kcnh6	Potassium voltage-gated channel subfamily H member 6	0.48	2.71	7.65	10.63	8.03	11.83	15.93	15.77
Kcnh7	Potassium voltage-gated channel subfamily H member 7	4.55	4.19	11.31	12.56	3.66	2.34	7.87	4.58
Kcnh8	Potassium voltage-gated channel subfamily H member 8	3.59	9.36	15.90	24.64	8.69	5.09	13.68	12.92
Kcnj12	ATP-sensitive inward rectifier potassium channel 12	4.07	5.42	22.32	28.99	17.31	13.79	27.82	35.16
Kcnj14	Potassium inwardly-rectifying channel, subfamily J, member 14	1.67	3.69	13.76	23.67	54.93	23.67	51.41	52.84
Kcnj3	Potassium inwardly-rectifying channel, subfamily J, member 3	12.44	20.20	27.22	42.51	4.10	2.87	7.44	7.95
Kcnj5	G protein-activated inward rectifier potassium channel 4	4.55	7.39	16.51	27.05	20.15	11.40	42.58	43.18
Kcnj6	G protein-activated inward rectifier potassium channel 2	3.11	7.64	9.79	10.14	7.55	3.11	9.45	10.13
Kcnj9	G protein-activated inward rectifier potassium channel 3	15.07	33.00	40.67	50.24	5.98	4.92	11.54	14.51
Kcnk1	Potassium channel subfamily K member 1	11.96	30.30	39.14	54.59	5.22	3.64	9.03	9.25
Kcnma1	Calcium-activated potassium channel subunit alpha-1	13.16	29.06	40.67	42.51	5.72	4.00	8.59	6.68
Kcnmb4	Calcium-activated potassium channel subunit beta-4	9.57	7.64	23.55	32.85	5.08	2.69	6.90	7.79
Kcnn2	Potassium intermediate/small conductance calcium-activated channel, subfamily N, member 2	4.78	4.93	5.81	7.73	3.97	3.78	9.39	9.75
Kcnn3	SK3 (KCa2.3)	8.61	9.61	22.63	36.71	6.69	8.14	19.55	18.50
Kcnq2	Potassium voltage-gated channel subfamily KQT member 2	7.42	29.56	35.78	47.34	5.22	4.07	6.36	6.56
Kcnq3	$K_V7.3$	6.46	10.84	25.99	35.75	14.82	10.48	28.62	34.88
Klf13	Kruppel-like factor 13	25.12	29.06	31.50	35.27	5.02	4.61	6.81	7.14
Klf9	Krueppel-like factor 9	39.95	39.90	42.51	47.83	5.13	5.91	8.81	9.81
L1cam	L1CAM	26.08	55.42	56.88	64.73	4.47	3.74	6.94	5.83
Lama1	Laminin subunit alpha-1	2.39	3.69	15.29	25.12	33.00	21.35	45.49	45.31
Lap3	Cytosol aminopeptidase	21.53	29.56	27.83	31.88	4.82	3.48	5.00	4.68
Lars	Leucyl-tRNA synthetase, cytoplasmic	23.92	30.54	27.83	33.33	3.87	3.06	5.16	4.50
Ldha	Lactate dehydrogenase A	67.46	84.73	82.26	84.06	6.43	6.86	9.56	7.80
Lepr	Leptin receptor	3.59	5.42	6.12	11.59	3.04	1.83	10.84	8.09
Lgals1	Galectin-1	7.66	3.20	9.48	15.46	10.62	10.15	18.06	21.25
Lifr	Leukemia inhibitory factor receptor	6.94	5.91	6.42	9.18	3.55	3.53	7.40	3.16
Lpl	Lipoprotein lipase	3.83	4.19	12.23	21.26	7.33	6.48	13.47	16.24
Lrig1	Leucine-rich repeats and immunoglobulin-like domains protein 1	9.57	3.45	4.59	9.66	2.82	2.66	9.67	6.98
Lrrfip2	Leucine-rich repeat flightless-interacting protein 2	27.99	45.57	37.61	46.86	4.39	3.66	4.35	6.13
Ltbp1	Latent-transforming growth factor beta-binding protein 1	2.87	2.22	7.95	12.08	8.06	8.60	14.96	15.83
Maf	Transcription factor Maf	9.33	6.90	17.13	25.12	7.36	7.62	26.65	28.74
Maged1	Melanoma-associated antigen D1	84.21	96.80	96.33	92.75	9.89	17.43	17.74	17.16
Maoa	Monoamine oxidase A	24.64	28.57	43.43	49.28	7.57	4.31	11.76	14.99
Maob	Monoamine oxidase B	19.38	20.94	26.30	33.33	4.50	4.92	6.73	6.03
Mapk1	Mitogen-activated protein kinase 1	38.52	63.05	71.25	80.19	5.40	5.54	13.36	15.35

Max	myc-associated factor X	27.51	43.84	41.90	52.17	4.49	4.04	10.19	10.28
Mc3r	Melanocortin receptor 3	4.55	15.52	22.94	30.43	11.94	4.37	12.89	16.74
Mccc2	Methylcrotonyl CoA carboxylase	15.31	24.38	31.19	46.86	4.04	3.29	11.78	12.56
Mcee	Methylmalonyl CoA epimerase	34.21	40.89	44.95	62.32	4.77	4.17	13.98	16.46
Mchr1	Melanin-concentrating hormone receptor 1	6.46	14.29	17.13	17.87	3.33	3.36	6.07	5.35
Mcl1	Induced myeloid leukemia cell differentiation protein	26.08	28.82	23.24	24.15	4.09	3.17	4.67	5.03
Mdk	neurite growth-promoting factor 2	18.90	8.62	13.46	21.26	4.10	5.01	17.60	18.52
Med1	Mediator of RNA polymerase II transcription subunit 1	17.94	24.88	26.91	28.50	3.17	3.66	7.64	6.03
Med12	Mediator of RNA polymerase II transcription, subunit 12 homolog	5.50	8.13	11.01	13.04	4.56	3.17	6.63	7.98
Med13	Mediator complex subunit 13	20.10	23.40	32.42	38.16	3.65	4.76	8.45	10.30
Med14	Mediator of RNA polymerase II transcription subunit 14	6.70	11.58	18.04	18.36	2.32	2.54	4.66	3.65
Med16	Mediator of RNA polymerase II transcription subunit 16	12.92	17.24	22.02	24.64	3.58	3.42	5.65	5.97
Med17	Mediator of RNA polymerase II transcription subunit 17	14.11	16.26	20.49	26.09	3.61	4.22	9.76	12.05
Med24	Mediator of RNA polymerase II transcription subunit 24	15.79	26.11	30.28	34.30	4.19	3.51	6.84	8.44
Med4	Mediator of RNA polymerase II transcription subunit 4	16.51	29.80	31.80	38.16	3.61	3.64	5.67	4.31
Mef2a	Myocyte-specific enhancer factor 2A	23.68	34.48	29.05	28.99	5.43	4.05	4.84	4.24
Mef2c	Myocyte-specific enhancer factor 2C	17.94	20.94	29.36	41.06	10.07	7.43	23.04	25.31
Mif	Macrophage migration inhibitory factor	63.88	87.19	87.46	92.75	7.63	10.02	16.05	14.86
Mt1	Metallothionein	50.00	40.39	48.93	49.28	27.73	10.55	11.92	10.39
Mt2	Metallothionein-2	38.52	22.17	21.10	26.57	15.23	5.96	5.41	5.69
Mt3	Metallothionein-3	50.72	66.26	63.91	72.46	8.40	7.10	15.22	16.95
Mta1	Metastasis-associated protein	16.51	17.49	27.83	30.92	3.00	3.50	10.01	13.33
Mtap	S-methyl-5'-thioadenosine phosphorylase	11.00	17.73	22.02	31.40	6.15	4.31	9.51	9.03
Mtr	Methionine synthase	2.15	2.71	4.28	7.73	8.93	5.28	12.79	10.86
Mut	Methylmalonyl-CoA mutase (MCM), mitochondrial	22.25	26.11	30.58	35.27	3.76	3.05	6.51	6.27
Myc	*Myc*	5.74	8.37	17.43	30.43	9.59	7.77	21.95	22.31
Nab2	NGFI-A-binding protein 2	3.83	7.14	15.90	24.64	7.50	10.60	23.47	26.97
Ncam1	Neural cell adhesion molecule	73.68	92.12	92.66	96.62	8.34	10.85	18.97	20.99
Ncapd3	Condensin-2 complex subunit D3	10.77	15.02	18.65	22.22	3.65	4.36	8.53	9.00
Ncoa1	nuclear receptor coactivator 1	17.46	27.83	39.14	51.21	6.06	5.41	11.01	12.85
Ncoa2	nuclear receptor coactivator 2	10.05	17.73	29.36	43.00	4.93	4.18	17.53	17.22
Ncoa3	nuclear receptor coactivator 3	9.81	10.59	18.35	31.40	4.61	4.48	14.18	13.43
Ncoa4	Nuclear receptor coactivator 4	7.89	11.82	25.08	37.20	5.87	6.44	12.19	12.16
Ncoa6	Nuclear receptor coactivator 6	10.05	18.47	25.69	25.12	4.14	4.92	9.81	14.18
Ncor1	nuclear receptor co-repressor 1	49.04	64.53	62.08	62.32	4.54	4.84	7.80	6.45
Ncor2	nuclear receptor co-repressor 2	17.46	22.91	29.97	40.10	5.52	3.85	16.69	21.48
Ndn	Necdin	67.22	83.00	77.68	77.29	17.87	27.94	26.95	23.70
Ndrg1	Protein NDRG1	27.99	27.83	24.16	29.47	7.44	4.29	5.48	4.42
Neurod1	Neurogenic differentiation 1	2.87	1.97	12.23	10.63	10.87	11.12	8.98	12.87
Nf1	Neurofibromatosis type I	15.31	19.95	23.85	29.47	3.03	2.87	4.67	4.45
Nfat5	Nuclear factor of activated T-cells 5	15.55	20.69	26.61	40.58	3.81	3.47	8.04	8.03
Nfatc2	Nuclear factor of activated T-cells, cytoplasmic 2	4.78	9.11	21.41	30.92	18.70	11.81	37.43	43.59

Nfatc3	Nuclear factor of activated T-cells, cytoplasmic 3	5.50	6.65	11.31	20.29	3.13	4.06	11.86	14.04
Nfkb1	Nuclear factor NF-kappa-B p105 subunit	11.96	11.82	15.90	24.64	4.34	4.64	16.21	16.46
Nfkbia	nuclear factor of kappa light polypeptide gene enhancer in B-cells inhibitor, alpha	41.15	40.15	29.36	34.78	12.07	5.12	5.93	4.47
Nfyb	Nuclear transcription factor Y subunit beta	22.97	37.68	37.31	34.78	3.74	3.17	4.03	3.37
Ngfrap1	Protein BEX3	83.01	97.78	94.19	93.24	13.19	21.67	24.05	20.77
Nit2	Omega-amidase	13.40	23.89	34.86	43.96	5.41	4.90	14.47	16.67
Nmb	Neuromedin-B	15.79	15.02	13.76	23.67	2.65	2.74	8.12	11.54
Nog	Noggin	4.07	8.13	22.63	27.05	15.40	7.62	23.24	33.87
Nono	Non-POU domain-containing octamer-binding protein	22.97	38.18	34.25	44.93	3.83	3.14	5.08	4.38
Notch2	Neurogenic locus notch homolog protein 2	8.85	3.45	4.59	6.76	2.32	1.62	13.93	6.80
Nov	CCN3 (nephroblastoma overexpressed)	3.35	3.45	14.98	24.15	11.54	14.77	23.44	23.12
Npffr2	Neuropeptide FF receptor 2	0.96	1.48	8.26	15.94	14.05	16.76	17.57	14.14
Npy	Neuropeptide Y	22.49	45.07	18.96	30.92	22.27	55.50	8.48	21.78
Npy1r	Neuropeptide Y receptor type 1	18.18	22.91	35.78	50.72	5.23	4.76	6.05	5.94
Npy2r	Neuropeptide Y receptor type 2	24.16	47.29	33.64	54.59	4.15	3.77	10.06	12.26
Npy5r	Neuropeptide Y receptor type 5	9.33	16.26	28.44	47.34	8.40	3.73	14.46	14.71
Nqo1	NAD(P)H dehydrogenase [quinone] 1	6.46	4.19	15.29	22.22	6.91	10.07	21.17	24.75
Nr0b1	dosage-sensitive sex reversal, adrenal hypoplasia critical region, on chromosome X, gene 1 (DAX1)	1.44	4.43	11.31	11.11	13.08	6.07	19.40	20.18
Nr1d1	Rev-ErbA alpha	22.73	24.63	25.99	35.27	6.19	5.83	20.24	25.89
Nr1d2	Rev-ErbA beta	23.68	33.50	33.94	44.93	3.78	3.79	7.93	9.03
Nr1h2	Liver X receptor beta	12.44	13.05	17.74	23.19	3.98	5.13	10.91	12.27
Nr2c1	testicular receptor 2	5.50	5.91	16.82	24.64	4.65	5.84	14.10	14.32
Nr2c2	Testicular receptor 4	23.68	40.15	44.34	48.31	4.33	4.33	10.21	12.67
Nr2f1	COUP Transcription Factor 1	11.24	9.11	17.43	22.71	3.30	4.62	4.14	6.27
Nr2f2	COUP transcription factor 2	18.42	15.02	26.91	30.92	5.55	7.68	11.14	12.17
Nr2f6	V-erbA-related protein 2	8.37	10.84	15.90	19.81	3.45	3.25	5.65	5.53
Nr3c1	glucocorticoid receptor	51.67	66.50	53.21	62.32	5.58	4.70	5.97	5.12
Nr3c2	mineralocorticoid receptor	5.02	6.16	13.76	24.64	9.85	8.14	32.56	30.94
Nr4a1	nerve growth factor IB	24.64	17.24	23.85	36.23	6.93	6.87	18.65	20.48
Nr4a3	neuron-derived orphan receptor 1	6.22	4.93	6.42	14.49	4.92	3.37	5.29	7.21
Nr5a2	liver receptor homolog-1	3.83	18.23	7.03	16.91	3.13	3.53	7.96	5.19
Nr6a1	germ cell nuclear factor	2.15	4.19	13.76	26.09	19.27	11.63	19.63	18.99
Nrcam	Neuronal cell adhesion molecule	40.91	56.90	65.44	76.33	3.90	3.88	5.76	5.71
Nrg1	Neuregulin 1	2.63	5.91	16.82	22.71	8.31	8.04	16.77	16.33
Nrg4	Neuregulin 4	0.48	0.74	1.22	2.42	10.16	1.11	19.21	12.17
Nrip1	Nuclear receptor-interacting protein 1	9.81	10.84	11.31	15.94	3.78	4.20	4.56	4.38
Nrp1	Neuropilin-1	18.18	35.71	33.94	52.66	8.98	4.65	17.47	18.98
Nrp2	Neuropilin 2	20.57	23.65	29.05	41.55	3.96	5.27	13.09	14.57
Nsf	*N*-ethylmaleimide-sensitive factor	47.85	80.05	77.98	77.29	5.14	7.70	10.54	8.95
Ntrk2	Tropomyosin receptor kinase B	55.26	71.43	66.67	71.50	8.03	5.09	8.09	7.09
Nts	Neurotensin	3.35	10.59	16.82	24.64	19.60	15.84	24.38	28.55
Ntsr1	Neurotensin receptor type 1	3.11	5.17	20.49	30.43	19.49	13.39	18.47	26.20
Ntsr2	Neurotensin receptor type 2	7.18	3.69	13.46	24.64	6.88	12.76	19.39	20.26
Numb	Protein numb homolog	7.42	8.13	14.07	20.77	4.44	3.07	11.19	12.90
Oat	Ornithine aminotransferase	27.51	39.66	53.52	54.59	6.07	5.37	15.70	23.22

Odc1	Ornithine decarboxylase	16.99	15.27	18.96	29.47	3.86	4.73	6.79	8.32
Ogdh	Alpha-ketoglutarate dehydrogenase	33.97	53.20	50.15	49.76	3.88	3.74	6.06	7.12
Ogdhl	2-oxoglutarate dehydrogenase-like, mitochondrial	4.31	10.34	16.51	25.60	7.00	4.33	13.19	13.42
Oprk1	Kappa-type opioid receptor	4.31	10.84	17.13	14.98	3.43	5.32	8.05	7.44
Oprm1	μ-opioid receptors	2.63	3.20	14.07	24.15	36.90	31.68	62.97	63.19
Oxtr	oxytocin receptor	4.07	5.17	19.57	27.05	10.14	8.63	20.63	24.61
P4ha1	Prolyl 4-hydroxylase subunit alpha-1	32.78	41.87	30.58	41.06	3.45	3.27	4.32	3.71
Pafah1b1	Platelet-activating factor acetylhydrolase IB subunit alpha	74.64	90.89	83.18	89.86	6.90	9.25	10.73	8.01
Pak1ip1	p21-activated protein kinase-interacting protein 1	46.17	68.72	68.20	79.71	6.57	5.96	18.27	24.24
Pard3	Partitioning defective 3 homolog	23.21	33.74	21.71	31.88	4.12	3.46	5.32	6.21
Pard6a	Partitioning defective 6 homolog alpha	17.70	29.31	36.70	48.79	5.07	4.44	10.57	11.73
Pcca	propionyl-CoA carboxylase subunit alpha	12.20	22.91	31.19	39.13	5.55	3.71	10.15	10.64
Pcna	Proliferating cell nuclear antigen	27.03	29.56	31.50	39.61	4.68	4.51	6.69	7.78
Pdcd7	Programmed cell death protein 7	20.57	35.71	37.00	41.55	4.05	3.75	5.52	5.47
Pde10a	cAMP and cAMP-inhibited cGMP 3',5'-cyclic phosphodiesterase 10A	11.72	22.17	33.64	43.48	8.98	5.97	21.16	27.75
Pde4a	cAMP-specific 3',5'-cyclic phosphodiesterase 4A	8.37	18.72	32.42	37.68	16.91	10.20	34.99	51.57
Pde4b	cAMP-specific 3',5'-cyclic phosphodiesterase 4B	22.49	24.14	48.62	49.76	7.44	6.63	12.56	19.24
Pde4d	cAMP-specific 3',5'-cyclic phosphodiesterase 4D	8.61	20.69	23.24	28.50	5.14	4.56	6.36	5.24
Pdhb	Pyruvate dehydrogenase (lipoamide) beta	35.41	62.56	64.53	72.46	4.64	5.12	8.82	8.42
Pdp1	pyruvate dehyrogenase phosphatase catalytic subunit 1	12.68	25.62	30.58	30.92	3.25	3.97	5.04	5.85
Pdpk1	3-phosphoinositide-dependent protein kinase-1	24.64	42.12	50.76	59.42	4.31	4.25	6.38	7.54
Pdyn	Prodynorphin	13.64	18.47	28.44	34.30	4.16	3.63	5.65	4.58
Pelp1	Proline-, glutamic acid- and leucine-rich protein 1	21.29	30.79	36.09	52.66	5.57	4.38	16.43	19.05
Per1	period circadian protein homolog 1	19.38	18.23	27.22	25.60	4.47	3.70	10.02	8.35
Per2	period circadian regulator 2	4.31	4.43	8.56	7.73	2.25	2.81	9.93	9.97
Pgr	progesterone receptor	6.94	23.65	33.33	45.41	11.90	5.66	14.87	18.20
Phb2	Prohibitin-2	36.60	51.97	47.40	63.77	6.49	5.48	21.16	25.37
Pias1	E3 SUMO-protein ligase	17.46	29.31	29.97	45.41	3.35	4.11	8.95	9.21
Pik3ca	phosphatidylinositol-4,5-bisphosphate 3-kinase, catalytic subunit alpha	25.36	39.41	48.32	55.07	5.42	4.65	12.31	15.83
Pik3r1	Phosphatidylinositol 3-kinase regulatory subunit alpha	31.10	35.47	41.59	55.56	4.44	4.29	7.97	7.36
Pik3r3	Phosphatidylinositol 3-kinase regulatory subunit gamma	18.90	27.09	28.75	43.00	5.11	4.17	8.28	7.55
Pla2g6	85 kDa calcium-independent phospholipase A2	8.13	14.78	22.02	30.43	5.61	3.50	9.91	13.46
Plcb1	1-Phosphatidylinositol-4,5-bisphosphate phosphodiesterase beta-1	20.10	22.66	34.25	38.65	6.04	6.15	7.67	9.54
Pld1	Phospholipase D1	3.83	2.96	5.81	8.21	2.88	2.73	2.62	5.03
Plod3	Procollagen-lysine,2-oxoglutarate 5-dioxygenase 3	18.18	22.91	27.22	41.55	4.76	4.49	13.95	15.11

Pmepa1	Transmembrane prostate androgen-induced protein	13.40	14.04	30.28	37.20	7.55	5.56	16.16	19.97
Pou2f1	POU domain, class 2, transcription factor 1	9.57	12.07	24.46	34.30	9.49	9.70	30.33	34.60
Pou2f2	POU domain, class 2, transcription factor 2	11.72	28.08	21.10	29.47	4.29	3.61	4.79	5.47
Ppargc1a	Peroxisome proliferator-activated receptor gamma coactivator 1-alpha	7.66	10.84	16.51	20.77	2.14	4.34	7.78	4.92
Ppargc1b	Peroxisome proliferator-activated receptor gamma coactivator 1-beta	7.18	13.79	24.77	29.47	6.07	4.63	11.88	14.47
Ppat	Amidophosphoribosyltransferase	14.59	23.15	26.30	39.13	5.87	4.94	12.80	13.30
Prdx6	Peroxiredoxin-6	49.76	52.71	55.66	65.70	9.86	5.04	8.78	8.90
Prkaca	catalytic subunit α of protein kinase A	42.34	67.98	70.03	78.26	4.80	5.41	9.15	9.01
Prkca	Protein kinase C alpha	11.96	23.65	27.22	42.03	8.07	6.25	24.73	27.62
Prlhr	prolactin-releasing peptide receptor	0.48	1.72	3.98	4.83	1.07	2.75	14.62	13.50
Prodh	Proline dehydrogenase, mitochondrial	8.37	4.43	8.87	16.91	4.62	2.73	7.04	7.10
Prokr2	Prokineticin receptor 2	2.39	8.13	11.93	14.49	2.41	2.90	7.15	6.52
Psat1	Phosphoserine aminotransferase	21.05	12.32	18.35	23.67	3.92	4.25	8.29	6.79
Psmc3	26S protease regulatory subunit 6A	59.09	75.62	67.89	67.63	5.45	5.04	6.97	5.27
Psmc5	26S protease regulatory subunit 8	66.75	86.45	73.39	74.88	6.36	7.34	9.39	7.88
Psph	Phosphoserine phosphatase	19.38	11.82	15.29	15.94	2.76	3.28	4.21	3.16
Ptch1	Protein patched homolog 1	7.66	6.65	15.60	24.15	6.72	6.30	18.74	24.97
Ptger2	Prostaglandin E_2 receptor 2	1.44	6.40	6.12	13.04	3.45	2.83	10.06	7.64
Ptn	Pleiotrophin	70.10	62.32	59.02	62.32	22.16	8.06	10.09	7.94
Ptpn1	Tyrosine-protein phosphatase non-receptor type 1	19.86	34.24	27.83	30.43	3.99	3.47	4.11	3.71
Pycr1	Pyrroline-5-carboxylate reductase 1, mitochondrial	0.48	0.49	7.03	5.31	1.36	15.54	10.65	12.57
Pycrl	Pyrroline-5-carboxylate reductase	19.86	29.06	31.50	35.75	4.09	2.94	5.72	6.12
Rab4a	Ras-related protein Rab-4A	23.68	36.95	40.98	46.86	3.57	3.60	4.63	3.24
Rac1	Ras-related C3 botulinum toxin substrate 1	60.05	70.20	69.42	71.01	5.29	4.93	7.11	6.20
Rala	Ras-related protein Ral-A	42.58	56.90	58.10	65.70	4.87	4.08	6.63	5.36
Ramp3	Receptor activity modifying protein 3	4.55	6.40	18.65	27.54	17.22	13.32	28.44	31.86
Rara	Retinoic acid receptor alpha	9.81	6.90	13.46	25.60	4.77	8.02	17.52	20.49
Rarb	Retinoic acid receptor beta	2.15	6.40	10.70	17.87	4.70	4.53	7.92	8.34
Rarg	Retinoic acid receptor gamma	5.98	6.90	15.29	26.57	13.73	11.68	45.62	43.34
Rasa3	Ras GTPase-activating protein 3	9.09	7.88	18.96	26.57	4.16	6.54	16.74	17.02
Rb1	retinoblastoma protein	11.96	8.87	19.27	26.09	5.05	5.57	12.83	19.15
Rbpj	Recombining binding protein suppressor of hairless	10.29	13.30	19.57	23.19	4.09	3.06	7.41	8.58
Rel	proto-oncogene c-Rel	2.39	2.22	10.09	14.98	6.57	8.06	14.82	13.39
Rela	Transcription factor p65	14.59	7.88	17.74	27.05	4.10	5.40	10.80	12.91
Rgs2	Regulator of G-protein signaling 2	38.76	69.21	57.19	65.22	6.32	9.11	9.28	9.70
Rhob	Ras homolog gene family, member B	46.17	50.00	42.81	38.65	5.70	3.94	4.81	4.36
Rhou	RhoU	14.35	8.62	17.43	28.50	5.85	4.43	12.06	14.30
Robo1	Roundabout homolog 1	3.11	6.65	13.76	23.19	8.42	7.18	10.03	14.35
Rora	RAR-related orphan receptor alpha	16.03	22.17	28.75	31.40	4.76	4.30	12.30	16.22
Rtn4	Neurite outgrowth inhibitor	75.12	90.89	82.87	82.61	7.28	8.15	11.00	8.32

Rxra	Retinoid X receptor alpha	11.00	8.13	13.46	23.67	2.75	3.81	11.66	12.98
Rxrb	Retinoid X receptor beta	9.57	17.00	20.49	23.19	4.51	3.55	7.94	7.51
Rxrg	Retinoic acid receptor gamma	13.40	20.94	30.28	43.48	3.96	4.66	6.31	6.75
Ryr3	Ryanodine receptor 3	4.07	8.87	15.90	25.12	7.49	5.06	7.96	7.84
S100a6	S100 calcium-binding protein A6	26.79	11.08	10.70	14.49	8.89	4.08	5.99	7.00
S100b	S100 calcium-binding protein B	20.57	9.11	17.13	29.95	11.35	8.19	9.78	12.30
Safb	Scaffold attachment factor B	50.24	71.92	67.89	76.81	4.61	5.24	6.87	6.65
Sat1	Diamine acetyltransferase 1	34.21	33.00	38.23	45.89	5.84	4.28	8.48	9.70
Scn1a	Sodium channel protein type 1 subunit alpha	11.00	26.85	29.66	32.85	4.36	4.25	6.01	4.13
Scn1b	Sodium channel subunit beta-1	10.53	25.12	37.61	44.93	4.23	3.81	8.23	9.65
Scn2a1	sodium voltage-gated channel alpha subunit 2	33.01	68.23	67.28	66.18	5.42	6.34	9.87	7.85
Scn2b	Sodium channel subunit beta-2	20.33	44.09	57.49	70.05	4.04	4.69	10.32	9.95
Scn3a	Sodium channel, voltage-gated, type III, alpha subunit	21.53	62.07	58.41	60.39	5.72	4.99	7.00	5.96
Scn8a	Sodium channel, voltage gated, type VIII, alpha subunit	10.53	21.67	38.23	45.89	8.03	6.14	17.23	21.77
Sec22c	Vesicle-trafficking protein SEC22c	11.00	21.18	18.04	23.67	3.41	2.82	2.88	5.80
Sesn1	Sestrin 1	18.66	25.86	34.86	33.33	4.33	3.48	7.11	7.57
Sgk1	Serine/threonine-protein kinase Sgk1	18.66	22.66	19.88	24.15	6.36	4.10	6.46	6.91
Shank2	SH3 and multiple ankyrin repeat domains protein 2	4.55	10.34	7.65	10.14	2.67	3.36	14.64	10.21
Shh	Sonic hedgehog	1.20	4.93	7.34	6.76	5.41	3.36	6.65	9.35
Shmt2	Serine hydroxymethyltransferase, mitochondrial	8.13	12.07	14.07	28.02	3.68	3.92	16.94	17.20
Sigmar1	sigma-1 receptor	13.40	25.12	24.77	32.85	3.56	4.08	5.01	6.43
Slc12a5	Potassium-chloride transporter member 5	24.40	59.11	57.80	62.80	5.15	4.98	7.54	7.00
Slc18a1	Vesicular monoamine transporter 1	1.20	2.22	10.09	17.87	11.04	6.08	19.02	21.05
Slc18a2	vesicular monoamine transporter 2	10.29	16.26	14.68	31.88	4.61	5.46	6.99	6.47
Slc19a2	Thiamine transporter 1	6.22	13.05	18.35	33.33	5.24	4.78	8.52	7.60
Slc1a1	excitatory amino-acid transporter 3	15.31	27.34	25.08	31.88	4.85	3.42	4.70	3.14
Slc1a2	Excitatory amino acid transporter 2	21.53	17.73	28.75	37.20	7.52	4.55	9.49	8.90
Slc1a3	Solute carrier family 1 (glial high-affinity glutamate transporter), member 3	23.21	7.39	8.56	15.46	8.67	3.58	9.20	8.39
Slc1a6	Excitatory amino-acid transporter 4	9.33	13.05	24.16	31.88	9.62	9.81	30.07	36.46
Slc22a5	Solute carrier family 22 member 5	6.70	6.16	8.56	6.76	3.58	3.86	4.39	3.58
Slc26a2	Sulfate transporter	5.98	9.11	12.23	19.81	3.90	4.75	15.60	16.36
Slc27a4	Long-chain fatty acid transport protein 4	14.11	27.09	28.75	35.75	3.63	3.46	4.86	7.75
Slc2a1	Glucose transporter 1	31.34	18.47	28.44	31.40	13.18	6.77	8.24	7.62
Slc32a1	Vesicular inhibitory amino acid transporter (VGAT)	12.92	60.10	18.96	38.65	8.12	8.73	18.75	16.55
Slc38a1	Sodium-coupled neutral amino acid transporter 1	46.89	66.01	71.56	82.13	5.38	5.64	12.52	15.49
Slc6a1	Sodium- and chloride-dependent GABA transporter 1	20.10	29.06	33.64	44.93	4.51	5.28	8.86	10.52
Slc6a11	Sodium- and chloride-dependent GABA transporter 3	13.16	9.61	13.15	17.39	3.93	4.01	5.93	5.16

Slc7a11	Cystine/glutamate transporter	7.18	5.42	21.10	29.47	10.05	12.90	28.85	33.20
Slit2	Slit homolog 2 protein	13.40	11.08	25.99	29.47	3.59	5.73	8.01	11.54
Smad1	Mothers against decapentaplegic homolog 1	22.01	30.54	25.69	23.67	3.57	3.65	4.75	3.99
Smad4	Mothers against decapentaplegic homolog 4	16.03	14.78	22.02	26.57	3.57	4.40	10.16	7.91
Smad5	Mothers against decapentaplegic homolog 5	19.86	23.40	30.28	41.55	4.78	5.09	16.62	20.72
Smad9	Mothers against decapentaplegic homolog 9	1.91	7.39	8.87	12.56	8.67	3.67	9.94	11.13
Sms	Spermine synthase	17.22	43.10	55.35	63.29	5.64	5.08	11.47	14.40
Snca	Alpha-synuclein	15.31	39.41	44.95	50.24	6.41	6.45	10.47	7.74
Sncaip	Synphilin-1	4.78	4.68	16.82	26.09	11.71	16.93	33.79	36.19
Snta1	Alpha-1-syntrophin	11.24	19.70	25.99	36.71	8.24	5.38	22.97	28.25
Socs1	Suppressor of cytokine signaling 1	3.59	8.37	7.95	10.14	2.80	4.15	11.46	10.51
Socs3	Suppressor of cytokine signaling 3	18.18	12.56	8.26	14.49	4.48	4.27	6.76	6.80
Sod1	Superoxide dismutase [Cu-Zn]	83.25	94.09	81.04	83.09	9.09	11.46	14.45	10.61
Sorbs1	Sorbin and SH3 domain-containing protein 1	19.86	22.66	29.66	35.27	4.55	4.65	6.72	7.15
Sord	Sorbitol dehydrogenase	6.94	15.02	12.23	14.98	2.48	3.06	3.53	5.41
Sort1	Sortilin	16.03	17.24	26.61	32.85	2.91	3.32	4.88	4.51
Sox1	Transcription factor SOX-1	10.53	7.14	13.15	21.26	2.41	3.81	8.97	9.10
Sox2	SRY (sex determining region Y)-box 2	32.30	21.18	34.25	50.24	5.73	4.30	14.27	13.42
Sox3	Transcription factor SOX-3	4.55	7.88	8.87	17.87	2.81	2.81	3.12	4.67
Sp1	Transcription factor Sp1	13.40	11.33	21.41	33.82	3.92	5.01	11.52	11.38
Sp3	Sp3 transcription factor	20.10	26.35	26.61	37.68	4.27	4.38	7.28	8.82
Spdef	SAM pointed domain-containing Ets transcription factor	2.63	4.43	6.12	6.76	5.52	4.79	5.32	9.71
Spsb1	SPRY domain-containing SOCS box protein 1	9.09	4.68	8.87	11.59	3.31	3.14	3.50	3.96
Sqstm1	Sequestosome-1	81.58	95.07	93.88	96.14	8.10	10.41	16.85	18.11
Srf	Serum response factor	19.38	13.79	19.27	22.22	3.37	3.68	4.78	4.28
Srm	Spermidine synthase	19.14	36.70	35.17	38.16	3.91	3.77	6.67	6.29
Srr	Serine racemase	10.77	15.52	19.88	23.67	2.84	2.95	4.67	3.88
Sst	Somatostatin	13.16	22.17	28.44	43.00	25.94	31.33	41.08	40.43
Sstr1	Somatostatin receptor type 1	16.27	22.41	35.47	47.83	6.75	6.99	15.06	18.37
Sstr2	Somatostatin receptor type 2	5.02	7.14	19.57	25.12	8.79	6.26	22.22	30.95
Stat1	Signal transducer and activator of transcription 1	16.99	15.76	20.80	30.43	4.13	3.57	13.56	11.36
Stat2	Signal transducer and activator of transcription 2	10.29	11.58	19.88	28.99	3.59	3.20	12.15	16.88
Stat3	Signal transducer and activator of transcription 3	32.54	45.57	44.04	51.69	3.29	2.87	4.75	3.24
Stat5a	Signal transducer and activator of transcription 5A	2.39	3.45	4.59	9.66	2.53	3.11	9.43	6.44
Stat5b	Signal transducer and activator of transcription 5B	11.48	17.98	21.71	22.22	2.97	2.88	4.00	2.95
Stat6	Signal transducer and activator of transcription 6	5.74	3.45	13.46	22.71	8.80	7.54	25.73	23.18
Stk39	STE20/SPS1-related proline-alanine-rich protein kinase	27.51	38.92	33.94	35.27	3.60	3.28	5.45	3.89
Syn2	Synapsin II	41.87	77.83	73.09	70.53	6.20	7.61	9.15	7.45
Tbl1xr1	F-box-like/WD repeat-containing protein	16.51	16.01	23.55	35.27	5.35	6.95	20.76	25.49
Tbp	TATA-binding protein	7.89	16.75	24.46	39.61	4.87	4.28	12.52	12.68
Tcf7l2	Transcription factor 7-like 2	17.70	17.24	32.72	40.10	6.25	8.09	22.30	22.52

Tfg	Protein TFG	35.41	51.23	46.79	59.42	4.65	3.83	7.03	6.76
Tgfa	Transforming growth factor alpha	6.46	3.20	14.37	21.74	4.99	10.85	18.29	19.09
Tgfb1i1	Transforming growth factor beta-1-induced transcript 1 protein	6.46	4.43	6.42	6.76	2.64	3.13	6.93	7.72
Tgs1	Trimethylguanosine synthase	23.44	40.39	45.26	55.07	3.58	3.83	7.40	7.12
Th	Tyrosine hydroxylase	3.83	14.53	9.79	7.25	22.33	12.31	16.75	4.33
Thbs1	Thrombospondin 1	3.35	3.20	10.40	14.98	7.34	5.49	18.64	12.93
Thra	Thyroid hormone receptor alpha	58.13	72.91	70.95	80.19	6.69	6.23	13.96	16.53
Thrb	Thyroid hormone receptor beta	6.70	11.33	15.29	14.01	2.99	4.33	4.70	4.50
Tiparp	TCDD-inducible poly [ADP-ribose] polymerase	32.30	31.53	22.63	30.92	5.25	4.52	7.35	8.14
Tnr	Tenascin-R	11.00	17.49	15.29	28.02	3.00	3.03	4.82	4.37
Tpd52	Tumor protein D52	36.12	41.63	43.73	50.72	5.06	3.79	6.95	5.44
Trh	Thyrotropin Releasing Hormone	3.35	7.39	14.68	19.81	17.28	9.01	20.99	14.43
Trip4	Activating signal cointegrator 1	24.40	37.44	42.20	52.17	4.95	4.53	14.36	18.70
Tro	Trophinin	42.34	83.50	78.90	85.02	6.26	7.71	10.19	9.17
Trp53	Tumor protein p53	16.03	26.35	29.97	39.13	4.05	3.27	8.16	9.50
Trpc1	Transient receptor potential channel 1	4.78	8.62	15.60	23.67	8.24	3.69	8.17	9.90
Trpc3	Short transient receptor potential channel 3	0.72	1.72	12.84	14.98	4.71	12.95	12.47	17.03
Trpc6	Transient receptor potential cation channel, subfamily C, member 6	2.39	13.79	14.37	30.43	15.45	5.47	23.45	19.65
Trpm2	Transient receptor potential cation channel, subfamily M, member 2	3.35	7.39	17.13	28.50	7.43	7.30	16.36	20.40
Trpv2	Transient receptor potential cation channel subfamily V member 2	9.81	22.66	27.22	37.68	3.22	2.96	4.54	2.74
Tsc22d1	TSC22 domain family protein 1	73.21	88.18	84.71	91.30	11.19	8.72	10.95	11.49
Tsc22d3	TSC22 domain family protein 3	35.89	37.68	43.43	51.69	8.15	5.91	14.86	19.25
Tspo	Translocator protein	24.40	10.59	7.03	9.66	4.54	2.69	10.16	8.10
Tubb3	Class III β-tubulin	44.50	83.99	77.68	71.98	6.62	7.81	11.56	9.81
Txn1	Thioredoxin	70.57	87.44	74.31	73.91	6.75	7.21	9.17	7.12
Txnrd1	Thioredoxin reductase 1, cytoplasmic	39.95	62.56	51.68	58.94	4.26	4.51	5.38	5.44
Usp2	Ubiquitin carboxyl-terminal hydrolase 2	22.73	14.29	13.15	20.77	3.78	4.69	7.46	6.90
Usp54	Inactive ubiquitin carboxyl-terminal hydrolase 54	12.92	8.87	15.90	21.26	4.92	3.37	15.29	14.94
Vapa	VAMP-Associated Protein A	61.48	81.28	78.90	83.09	5.77	6.18	9.37	9.23
Vars2	Valyl-tRNA synthetase 2, mitochondria	5.02	11.08	12.84	19.81	4.47	3.35	5.37	6.36
Vegfa	Vascular endothelial growth factor A	9.81	13.05	21.71	22.22	3.64	3.45	6.80	8.42
Vldlr	very-low-density-lipoprotein receptor	21.77	31.53	40.37	51.69	7.01	5.91	19.32	23.65
Wars	Tryptophan--tRNA ligase, cytoplasmic	23.44	36.70	37.00	40.58	3.56	3.32	4.63	4.06
Wbscr22	Uncharacterized methyltransferase WBSCR22	24.88	36.70	27.83	33.33	3.25	3.42	3.75	3.02
Wipi1	WD repeat domain phosphoinositide-interacting protein 1	16.99	18.23	25.99	37.20	8.13	6.68	30.01	34.66
Wnt2b	Protein Wnt-2b	0.72	1.48	3.06	4.35	5.64	3.59	6.39	5.51
Wnt4	Wnt-4	8.13	9.11	13.46	11.11	2.74	2.97	4.84	4.06
Wnt5a	Protein Wnt-5a	8.13	9.85	12.84	18.84	3.28	2.31	2.78	2.93
Xbp1	X-box binding protein 1	40.43	65.76	61.77	74.40	4.34	4.78	6.95	6.59

Ywhaz	14-3-3 protein zeta/delta	77.27	95.57	80.73	80.19		8.02	11.89	17.13	12.37
Yy1	Yin Yang 1	28.95	40.64	37.92	41.06		3.98	4.12	6.55	5.69
Zbtb10	Zinc finger and BTB domain-containing protein 10	6.70	8.87	16.82	19.81		5.34	2.29	3.92	6.03
Zbtb16	Zinc finger and BTB domain-containing protein 16	9.09	9.61	22.63	28.99		7.89	8.05	21.57	26.34
Zfp189	Zinc finger protein 189	4.55	6.16	14.98	21.26		3.66	2.76	6.91	5.95
Zfp281	Zinc finger protein 281	19.62	32.51	42.20	50.72		3.99	3.38	3.68	3.55
Zfp36	Tristetraprolin	21.53	9.85	8.26	8.21		9.33	6.41	8.72	6.77
Zfp91	Zinc finger protein 91 homolog	36.12	46.31	37.61	42.51		4.64	3.89	5.11	5.65
Zhx3	Zinc fingers and homeoboxes protein 3	9.33	10.59	18.65	27.54		6.05	3.69	17.10	17.46

APPENDIX B

Supplement to Chapter III

The content contained in this appendix provides information that supports or was generated through the studies contained in Chapter III. The majority of the data is from the female groups that were run simultaneously with the male groups that comprised the data in Chapter III. The placement of the data as supplementary was to maintain consistency throughout the studies presented, and in all cases we observed similar phenomena in both sexes, with only minor differences in intensity or timing. Unfortunately, I did not perform all of those experiments in both sexes of mice. In the case of the PD groups in the FR1 task, I was unable to accrue a female cohort, the number of female animals with the genotypes needed just were not born in the same litters as the male mice that comprised the data presented. In the case of the minipump experiment, female mice were not included due to the intensive nature of the longevity of the experimental timeline and the animal handling times needed between behavior, acute leptin challenges, and surgeries. Furthermore, Figure B.1B-D contains data from independent PD animals and their controls that were utilized for other experiments whose data is not presented.

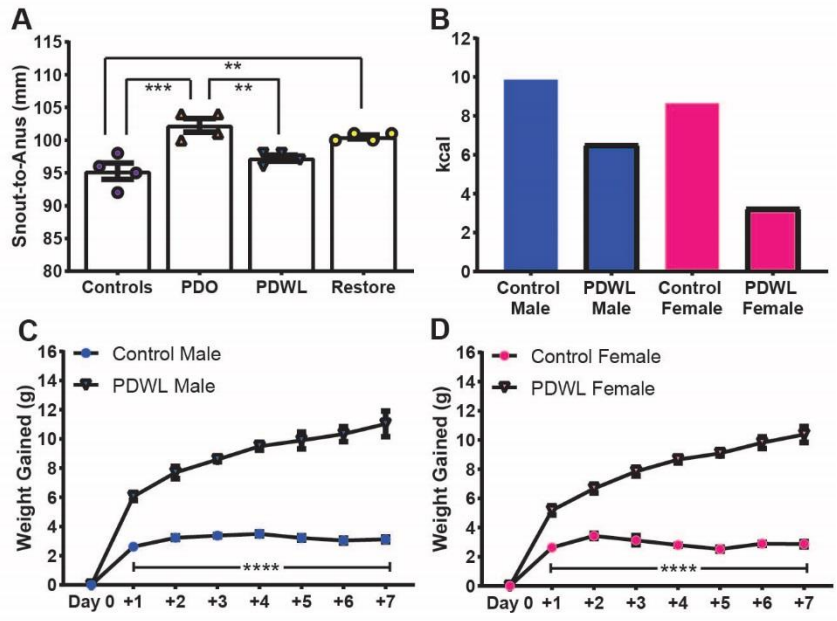
A
Snout-to-Anus (mm)
115
110
105
100
95
90
85
80
***
**
**
Controls
PDO
PDWL
Restore
B
kcal
12
10
8
6
4
2
0
Control Male
PDWL Male
Control Female
PDWL Female
C
Control Male
PDWL Male
Weight Gained (g)
16
14
12
10
8
6
4
2
0
****
Day 0
+1
+2
+3
+4
+5
+6
+7
D
Control Female
PDWL Female
Weight Gained (g)
16
14
12
10
8
6
4
2
0
****
Day 0
+1
+2
+3
+4
+5
+6
+7

Figure B.1: Supplement to Figure 3.1. Information regarding PD and PDWL mice. **A,** Body length of the PD groups assayed in the FR1 task, and a separate cohort of age matched PDO mice that were not used for behavior, after one month of ad lib food access (except the PDWL group, which had to be maintained on calorie restriction) following behavioral testing. **B,** Caloric supplement needed to maintain body weight of Control groups at 90% of their ad libitum weight, and PDWL groups weight matched to the Controls. **C,** Compensatory growth of male PDWL and Control animals maintained on calorie restriction then returned to ad libitum conditions. **D,** Compensatory growth of female PDWL and Control animals maintained on calorie restriction then returned to ad libitum conditions. Panel A: Control mice are represented by purple circles, PDO mice by orange upward triangles, PDWL mice by blue downward triangles, and Restore mice by yellow circles. Panels B-H: Control mice are represented by filled circles, and PD animals by outlined triangles. Male data is colored blue and female data pink. *'s indicate a significant difference between bracketed groups or at the notated points. The number of characters indicate the p-value (1: < 0.05, 2: < 0.01, 3: < 0.001, and 4: < 0.0001).

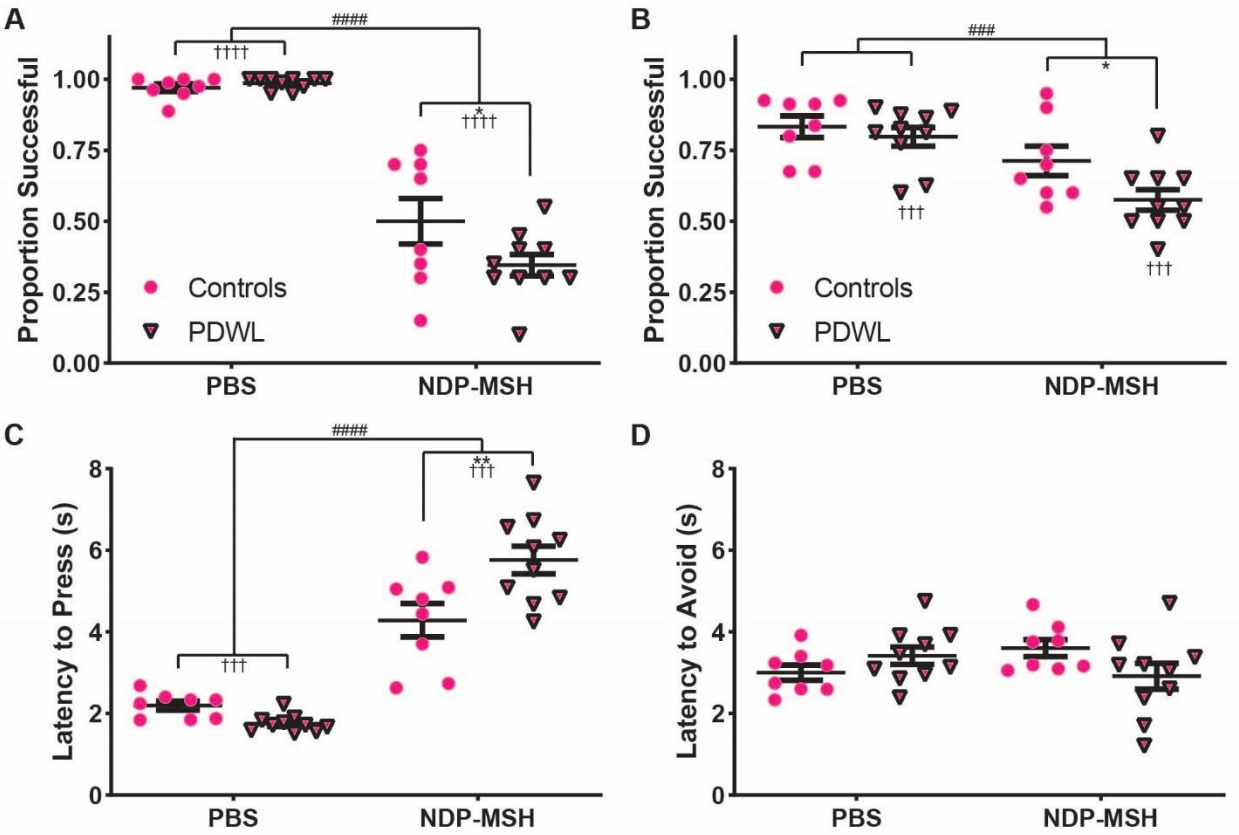
A
Proportion Successful
1.00
0.75
0.50
0.25
0.00
Controls
PDWL
PBS
NDP-MSH
####
††††
*
††††
B
Proportion Successful
1.00
0.75
0.50
0.25
0.00
Controls
PDWL
PBS
NDP-MSH
###
*
†††
†††
C
Latency to Press (s)
8
6
4
2
0
PBS
NDP-MSH
####
**
†††
†††
D
Latency to Avoid (s)
8
6
4
2
0
PBS
NDP-MSH

Figure B.2: Supplement to Figure 3.3. The impact of pharmacological activation of MC3/4Rs on interleaved appetitive consummatory behavior and aversive avoidance in female Control and PDWL mice. **A,** Successful completion of the appetitive trials with PBS and NDP-MSH treatment. NDP-MSH substantially decreased performance in both Control and PDWL animals. However, PDWL mice were more severely impacted than Control animals. **B,** Successful completion of aversive trials with PBS and NDP-MSH. There was a main effect of NDP-MSH reducing performance. However, the Control animals did not significantly differ between treatments, only the PDWL group. **C,** Latency to lever press in appetitive trials. NDP-MSH treatment increased the latency to press in successful trials for both groups. **D,** Latency to avoid foot shock in aversive trials. Like the success in these trials, there was a main effect of NDP-MSH treatment, but only the PDWL showed a change. However, they were quicker to avoid, so while less successful overall, when they performed the task they did it faster. Control mice are represented by the blue filled circles, while the PDWL mice by the blue outlined downward triangles. *'s indicate a significant difference between adjacent underlying groups, †'s indicate a significant difference from the same group's performance in the other treatment condition, #'s indicate a significant main effect assessed by Two-way RM ANOVA. The number of characters indicate the p-value (1: < 0.05, 2: < 0.01, 3: < 0.001, and 4: < 0.0001).

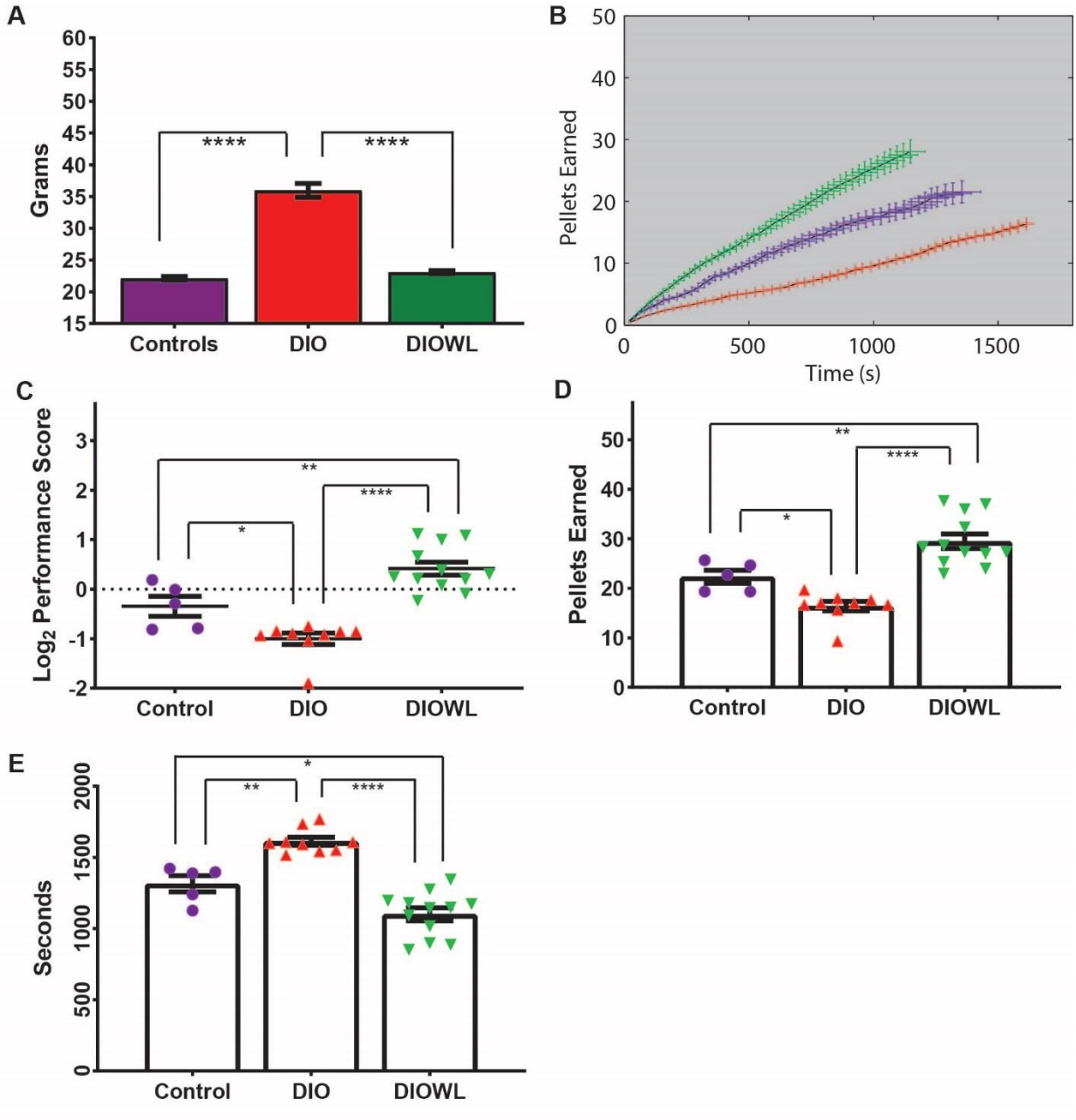
A
Grams
60
55
50
45
40
35
30
25
20
15
****
****
Controls
DIO
DIOWL
B
Pellets Earned
50
40
30
20
10
0
0
500
1000
1500
Time (s)
C
Log2 Performance Score
3
2
1
0
-1
-2
**
*
****
Control
DIO
DIOWL
D
Pellets Earned
50
40
30
20
10
0
**
*
****
Control
DIO
DIOWL
E
Seconds
2000
1500
1000
500
0
*
**
****
Control
DIO
DIOWL

Figure B.3: Supplement to Figure 3.4. Comparison of FR1 operant performance between female Control, DIO, and DIOWL groups. **A,** Body weight during behavioral testing of the female DIO groups. **B,** Group averages (±SEM) of pellets earned and session time at each of the 50 trials. **C,** Log_2 transformed performance score of each mouse's average session. DIOWL mice performed better than Control animals, which performed better than DIO mice. **D,** Pellets earned in the average FR1 session for each mouse, where the more pellets earned the greater the performance. The same relationships reported in Panel B were found. **E,** Time to completion in the average FR1 session for each mouse, where shorter session time indicates greater performance. Again the same relationships were found. Control mice are represented by purple, DIO by red, and DIOWL by green. Individual Control data points are shown with circles, obese animals by upward triangles, and weight-loss animals by downward triangles. *'s indicate a significant difference between bracketed groups. The number of characters indicate the p-value (1: < 0.05, 2: < 0.01, 3: < 0.001, and 4: < 0.0001).

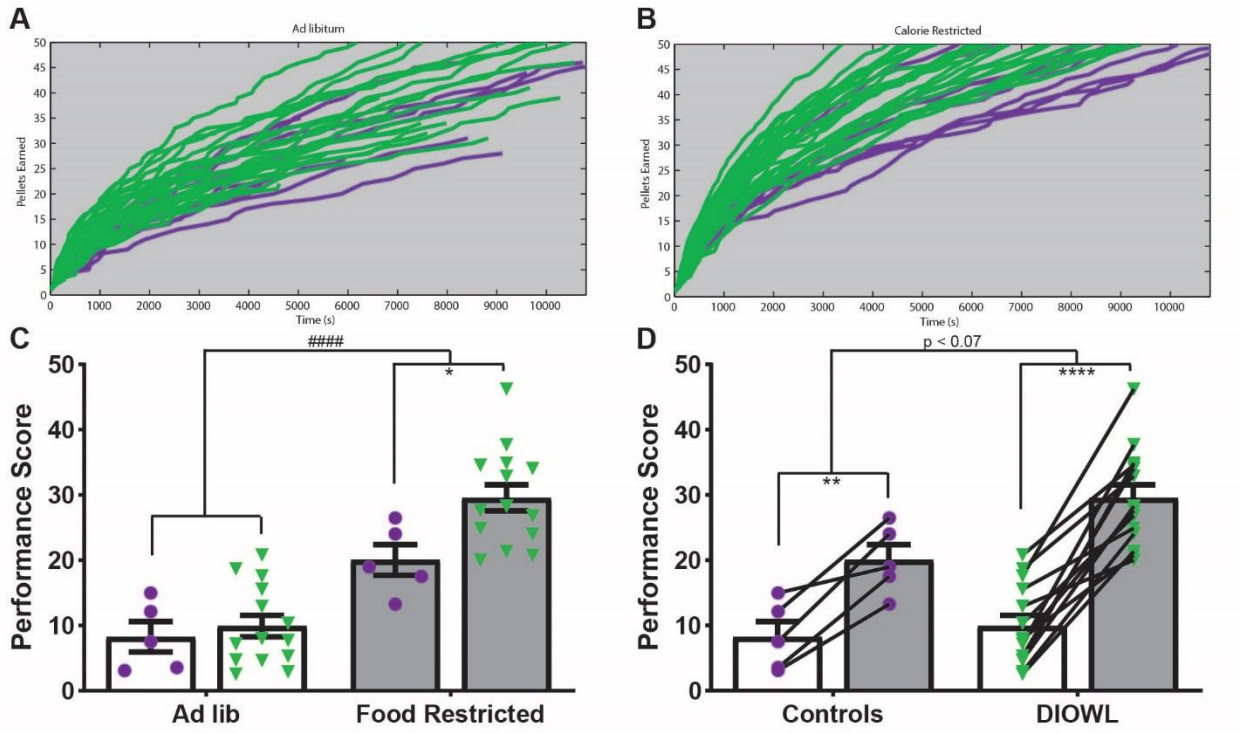
A
Ad libitum
Pellets Earned
Time (s)
B
Calorie Restricted
Pellets Earned
Time (s)
C
####
*
Performance Score
Ad lib
Food Restricted
D
p < 0.07
**
****
Performance Score
Controls
DIOWL

Fig B.4: Supplement to Figure 3.5. Comparison of Progressive Ratio performance between female Control and DIOWL mice in an *ad libitum* and food restricted state. **A,** Single session traces from individual mice housed with *ad libitum* access to food, showing the number of pellets achieved versus session time, comprised of the two sessions with the best performance for each animal. **B,** Single session traces from individual mice under mild, acute food restriction, comprised of the two sessions with the best performance for each animal. **C,** Comparison of group and condition differences in Progressive Ratio performance. Food restricted mice performed better than ad libitum mice, and food restricted DIOWL animals outperformed food restricted Control mice. **D,** Comparison of food restriction-induced potentiation of progressive ratio performance. Control mice are represented by purple lines or circles and DIOWL animals by green lines or downward triangles. *Ad libitum* conditions are represented by white bars and food restriction conditions by grey bars. *'s indicate a significant difference between bracketed groups, #'s indicate a significant main effect assessed by Two-way RM ANOVA. The number of characters indicate the p-value (1: < 0.05, 2: < 0.01, 3: < 0.001, and 4: < 0.0001).

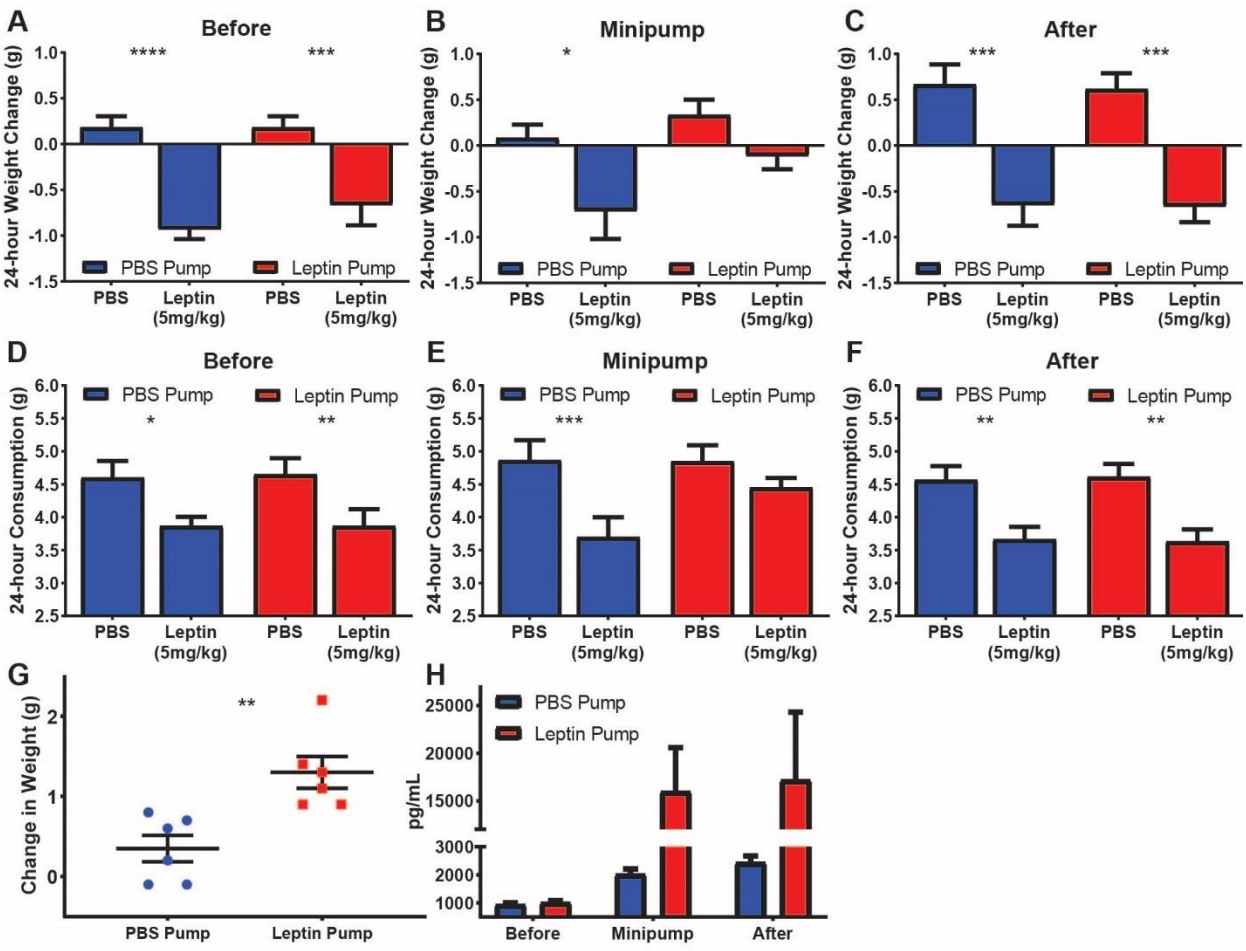
A
Before
24-hour Weight Change (g)
PBS Pump
Leptin Pump
PBS
Leptin (5mg/kg)
B
Minipump
C
After
D
Before
24-hour Consumption (g)
E
Minipump
F
After
G
Change in Weight (g)
PBS Pump
Leptin Pump
H
pg/mL
Before
Minipump
After

Fig B.5: Supplement to Figure 3.6. Validation of minipump operation. **A,** 24 hour body weight changes to acute injections of PBS and leptin prior to minipump implantation. Both groups of mice lost significantly more weight during leptin treatment **B,** 24 hour body weight changes to acute injections of PBS and leptin after minipump implantation. Only the PBS Pump group lost a significant amount of weight during leptin treatment **C,** 24 hour body weight changes to acute injections of PBS and leptin after minipump depletion. Both groups of mice lost significantly more weight during leptin treatment. **D,** 24 hour food intake during acute injections of PBS and leptin prior to minipump implantation. Both groups of mice ate significantly less during leptin treatment **E,** 24 hour food intake during acute injections of PBS and leptin after minipump implantation. Only the PBS Pump group ate significantly less during leptin treatment **F,** 24 hour food intake during acute injections of PBS and leptin after minipump depletion. Both groups of mice ate significantly less during leptin treatment. **G,** 48 hour body weight change after the manufacturer specified minipump depletion date. Leptin Pump mice gained more weight than the PBS Pump group over this span. **H,** Circulating leptin levels measured by ELISA. PBS Pump mice are represented by filled blue circles and bars, while the Leptin Pump mice by the red squares and bars. *'s indicate a significant difference between adjacent groups assessed by Two-way RM ANOVA. The number of characters indicate the p-value (1: < 0.05, 2: < 0.01, 3: < 0.001, and 4: < 0.0001).

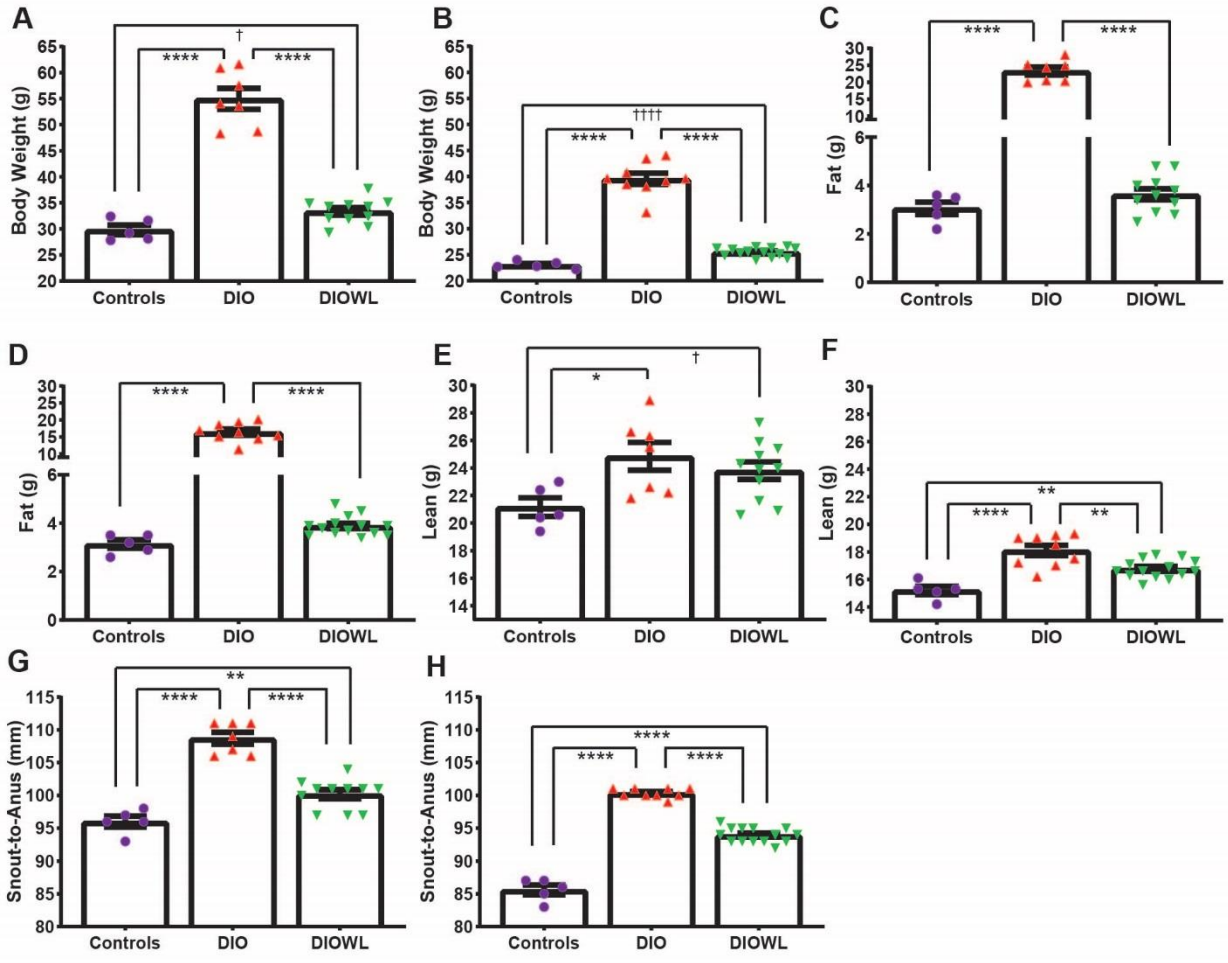
A
Body Weight (g)
Controls
DIO
DIOWL
B
Body Weight (g)
C
Fat (g)
D
Fat (g)
E
Lean (g)
F
Lean (g)
G
Snout-to-Anus (mm)
H
Snout-to-Anus (mm)

Figure B.6. Supplementary information regarding DIO and DIOWL mice. **A,** Body weight of male DIO groups, after one month of ad lib food access following behavioral testing. **B,** Body weight of female DIO groups, after one month of ad lib food access following behavioral testing. **C,** NMR-measured fat mass of male DIO groups, after one month of ad lib food access following behavioral testing. **D,** NMR-measured fat mass of female DIO groups, after one month of ad lib food access following behavioral testing. **E,** NMR-measured lean mass of male DIO groups, after one month of ad lib food access following behavioral testing. **F,** NMR-measured lean mass of female DIO groups, after one month of ad lib food access following behavioral testing. **G,** Body length of male DIO groups, after one month of ad lib food access following behavioral testing. **H,** Body length of female DIO groups, after one month of ad lib food access following behavioral testing. Control mice are represented by purple bars or circles, DIO animals by red bars or upward triangles, and DIOWL animals by green bars or downward triangles. *'s indicate a significant difference between bracketed groups measured with one-way ANOVA post-hoc Tukey's multiple comparisons test. †'s indicate a significant difference between bracketed groups measured with a two-tailed t-test. The number of characters indicate the p-value (1: < 0.05, 2: < 0.01, 3: < 0.001, and 4: < 0.0001).

Table B.1: Descriptive statistics table for Appendix B

Figure	Sample size	Mean ± SEM	Measure
B.1a	Controls: n = 4 PDO: n = 4 PDWL: n = 4 Restore: n = 4	95.3 ± 1.25 102.3 ± 1.03 97.3 ± 0.48 100.5 ± 0.29	Millimeters
B.1b	Control Males PDWL Males Control Females PDWL Females	9.87 6.56 8.65 3.28	kcal/mouse
B.1c Males	Control: n = 3 PDWL: n = 3	Data order: Control, PD Day 1: 2.62 ± 0.07, 6.07 ± 0.27 Day 2: 3.24 ± 0.11, 7.70 ± 0.42 Day 3: 3.38 ± 0.09, 8.60 ± 0.15 Day 4: 3.50 ± 0.14, 9.50 ± 0.27 Day 5: 3.22 ± 0.15, 9.90 ± 0.57 Day 6: 3.04 ± 0.17, 10.33 ± 0.52 Day 7: 3.12 ± 0.17, 11.03 ± 0.87	Grams
B.1d Females	Control: n = 3 PDWL: n = 3	Data order: Control, PD Day 1: 2.63 ± 0.18, 5.18 ± 0.32 Day 2: 3.43 ± 0.18, 6.68 ± 0.30 Day 3: 3.13 ± 0.32, 7.84 ± 0.29 Day 4: 2.80 ± 0.06, 8.66 ± 0.23 Day 5: 2.53 ± 0.13, 9.08 ± 0.17 Day 6: 2.90 ± 0.10, 9.82 ± 0.40	Grams
Figure	Sample size	Mean ± SEM	Measure
B.2a	Controls: n = 8 PDWL: n = 10	PBS: 0.97 ± 0.01 NDP-MSH: 0.50 ± 0.08 PBS: 0.99 ± 0.01 NDP-MSH: 0.35 ± 0.04	Proportion Successful
B.2b	Controls: n = 8 PDWL: n = 10	PBS: 0.83 ± 0.04 NDP-MSH: 0.71 ± 0.05 PBS: 0.80 ± 0.03 NDP-MSH: 0.58 ± 0.04	Proportion Successful
B.2c	Controls: n = 8 PDWL: n = 10	PBS: 2.20 ± 0.11 NDP-MSH: 4.29 ± 0.41 PBS: 1.75 ± 0.07 NDP-MSH: 5.76 ± 0.34	Latency to Press (s)
B.2d	Controls: n = 8 PDWL: n = 10	PBS: 3.00 ± 0.19 NDP-MSH: 3.61 ± 0.21 PBS: 3.42 ± 0.21 NDP-MSH: 2.91 ± 0.32	Latency to Avoid (s)
Figure	Sample size	Mean ± SEM	Measure
B.3a	Controls: n = 5 DIO: n = 9 DIOWL: n = 12	22.12 ± 0.28 35.98 ± 1.08 23.09 ± 0.24	Grams
B.3c	Controls: n = 5 DIO: n = 9	-0.34 ± 0.20 -1.00 ± 0.11	Log2 Performance Score

	DIOWL: n = 12	0.42 ± 0.13	
B.3d	Controls: n = 5 DIO: n = 9 DIOWL: n = 12	22.33 ± 1.32 16.41 ± 0.96 29.50 ± 1.46	Pellets Earned
B.3e	Controls: n = 5 DIO: n = 9 DIOWL: n = 12	1316 ± 57 1614 ± 28 1102 ± 45	Session Time (s)
Figure	Sample size	Mean ± SEM	Measure
B.4c-d	Controls: n = 5 DIOWL: n = 14	Ad libitum: 8.26 ± 2.34 Food Restricted: 20.05 ± 2.35 Ad libitum: 9.93 ± 1.64 Food Restricted: 29.57 ± 2.00	Performance Score
Figure	Sample size	Mean ± SEM	Measure
B.5a	PBS Pump: n = 6 Leptin Pump: n = 6	PBS: 0.183 ± 0.122 Leptin (5mg/kg): -0.933 ± 0.102 PBS: 0.183 ± 0.133 Leptin (5mg/kg): -0.667 ± 0.220	Grams
B.5b	PBS Pump: n = 6 Leptin Pump: n = 6	PBS: 0.083 ± 0.145 Leptin (5mg/kg): -0.717 ± 0.303 PBS: 0.333 ± 0.169 Leptin (5mg/kg): -0.117 ± 0.142	Grams
B.5c	PBS Pump: n = 6 Leptin Pump: n = 6	PBS: 0.667 ± 0.217 Leptin (5mg/kg): -0.650 ± 0.226 PBS: 0.617 ± 0.172 Leptin (5mg/kg): -0.667 ± 0.171	Grams
B.5d	PBS Pump: n = 6 Leptin Pump: n = 6	PBS: 4.6 ± 0.26 Leptin (5mg/kg): 3.9 ± 0.14 PBS: 4.7 ± 0.25 Leptin (5mg/kg): 3.9 ± 0.26	Grams
B.5e	PBS Pump: n = 6 Leptin Pump: n = 6	PBS: 4.9 ± 0.30 Leptin (5mg/kg): 3.7 ± 0.30 PBS: 4.9 ± 0.24 Leptin (5mg/kg): 4.5 ± 0.15	Grams
B.5f	PBS Pump: n = 6 Leptin Pump: n = 6	PBS: 4.6 ± 0.21 Leptin (5mg/kg): 3.7 ± 0.18 PBS: 4.6 ± 0.20 Leptin (5mg/kg): 3.6 ± 0.18	Grams
B.5g	PBS Pump: n = 6 Leptin Pump: n = 6	0.35 ± 0.17 PBS: 1.30 ± 0.20	Grams
B.5h	PBS: n = 6 Leptin: n = 6	Data order: PBS Pump, Leptin Pump Before: 941 ± 59, 1016 ± 67 Minipump: 2017 ± 197, 15984 ± 4598 After: 2436 ± 229, 17201 ± 7104	pg/mL
Figure	Sample size	Mean ± SEM	Measure
B.6a	Controls: n = 5 DIO: n = 7 DIOWL: n = 11	29.82 ± 0.93 54.96 ± 2.02 33.36 ± 0.72	Grams
B.6b	Controls: n = 5 DIO: n = 9 DIOWL: n = 12	23.02 ± 0.31 39.57 ± 1.06 25.49 ± 0.23	Grams
B.6c	Controls: n = 5 DIO: n = 7	3.06 ± 0.26 23.27 ± 1.17	Grams

	DIOWL: n = 11	3.64 ± 0.23	
B.6d	Controls: n = 5 DIO: n = 9 DIOWL: n = 12	3.14 ± 0.18 16.38 ± 0.91 3.89 ± 0.11	Grams
B.6e	Controls: n = 5 DIO: n = 7 DIOWL: n = 11	21.16 ± 0.67 24.84 ± 1.02 23.81 ± 0.64	Grams
B.6f	Controls: n = 5 DIO: n = 9 DIOWL: n = 12	15.20 ± 0.30 18.10 ± 0.38 16.76 ± 0.18	Grams
B.6g	Controls: n = 5 DIO: n = 7 DIOWL: n = 11	96.0 ± 0.84 108.7 ± 0.89 100.2 ± 0.69	Millimeters
B.6h	Controls: n = 5 DIO: n = 9 DIOWL: n = 12	85.6 ± 0.75 100.3 ± 0.24 93.9 ± 0.31	Millimeters

Table B.2: Statistical tests table for Appendix B

Figure	Type of test	Statistical data	P Value		Sig.
B.1a	One-way ANOVA	F(3,12) = 13.52	3.72E-04		###
		Tukey's multiple comparisons test		q	
		Controls vs. PDO	0.000442	8.168	***
		Controls vs. PDWL	0.389288	2.334	ns
		Controls vs. Restore	4.66E-03	6.13	**
		PDO vs. PDWL	6.65E-03	5.84	**
		PDO vs. Restore	4.98E-01	2.04	ns
		PDWL vs. Restore	8.16E-02	3.79	ns
B.1c	Two-way ANOVA	Interaction: F(6,36) = 41.85	9.00E-15		####
		Time: F(6,36) = 57.04	< 1e-15		####
		Group: F(1,6) = 318.0	2.00E-06		####
		Sidak's multiple comparisons test		t	
		Controls vs. PDWL			
		+1	5.35E-10	8.625	****
		+2	2.67E-13	11.16	****
		+3	2E-15	13.06	****
		+4	< 1e-15	15.01	****
		+5	< 1e-15	16.72	****
		+6	< 1e-15	18.25	****
		+7	< 1e-15	19.80	****
B.1d	Two-way ANOVA	Interaction: F(6,36) = 35.42	1.11E-13		####
		Time: F(6,36) = 31.39	5.28E-13		####
		Group: F(1,6) = 205.6	7.20E-06		####
		Sidak's multiple comparisons test		t	
		Controls vs. PDWL			
		+1	2.25E-05	5.366	****
		+2	1.72E-07	6.841	****
		+3	1.01E-11	9.917	****
		+4	1.10E-14	12.35	****
		+5	< 1e-15	13.79	****
		+6	< 1e-15	14.58	****
		+7	< 1e-15	15.83	****
Figure	Type of test	Statistical data	P Value		Sig.
B.2a	Two-way RM ANOVA	Interaction: F(1,16) = 5.05	3.91E-02		#
		Group: F(1,16) = 2.326	1.47E-01		ns
		Treatment: F(1,16) = 213.5	1.13E-10		####
		Sidak's multiple comparisons test		t	
		Controls vs. PDWL			
		PBS	9.56E-01	0.27	ns
		NDP-MSH	2.71E-02	2.61	*
		PBS vs. NDP-MSH			
		Controls	6.92E-07	8.29	****
		DIOWL	1.92E-09	12.64	****
B.2b	Two-way RM ANOVA	Interaction: F(1,16) = 2.098	1.67E-01		ns
		Group: F(1,16) = 3.963	6.39E-02		ns
		Treatment: F(1,16) = 23.61	1.74E-04		###
		Sidak's multiple comparisons test		t	
		Controls vs. PDWL			

		PBS	7.81E-01	0.63	ns
		NDP-MSH	3.87E-02	2.46	*
		PBS vs. NDP-MSH			
		Controls	7.09E-02	2.29	ns
		DIOWL	4.53E-04	4.73	***
B.2c	Two-way RM ANOVA	Interaction: F(1,16) = 13.31	2.16E-03		##
		Group: F(1,16) = 3.455	8.16E-02		ns
		Treatment: F(1,16) = 134.0	3.45E-09		####
		Sidak's multiple comparisons test		t	
		Controls vs. PDWL			
		PBS	4.39E-01	1.17	ns
		NDP-MSH	1.03E-03	3.86	**
		PBS vs. NDP-MSH			
		Controls	1.38E-04	5.32	***
		DIOWL	8.41E-09	11.42	****
B.2d	Two-way RM ANOVA	Interaction: F(1,16) = 8.576	9.84E-03		##
		Group: F(1,16) = 0.2231	6.43E-01		ns
		Treatment: F(1,16) = 0.0692	7.96E-01		ns
		Sidak's multiple comparisons test		t	
		Controls vs. PDWL			
		PBS	4.32E-01	1.18	ns
		NDP-MSH	1.10E-01	1.98	ns
		PBS vs. NDP-MSH			
		Controls	9.38E-02	2.14	ns
		DIOWL	1.22E-01	2.00	ns
Figure	Type of test	Statistical data	P Value		Sig.
B.3a	One-way ANOVA	F(2,23) = 77.36	3.49E-13		####
		Tukey's multiple comparisons test		q	
		Control vs. DIO	1.85E-09	12.15	****
		Control vs. DIOWL	8.29E-01	0.83	ns
		DIO vs. DIOWL	2.30E-12	15.94	****
B.3c	One-way ANOVA	F(2,23) = 29.80	4.12E-07		####
		Tukey's multiple comparisons test		q	
		Control vs. DIO	2.55E-02	3.98	*
		Control vs. DIOWL	6.47E-03	4.83	**
		DIO vs. DIOWL	2.49E-07	10.87	****
B.3d	One-way ANOVA	F(2,23) = 26.86	9.62E-07		####
		Tukey's multiple comparisons test		q	
		Control vs. DIO	4.01E-02	3.69	*
		Control vs. DIOWL	8.35E-03	4.67	**
		DIO vs. DIOWL	5.96E-07	10.31	****
B.3e	One-way ANOVA	F(2,23) = 39.39	3.73E-08		####
		Tukey's multiple comparisons test		q	
		Control vs. DIO	1.26E-03	5.78	**
		Control vs. DIOWL	1.45E-02	4.34	*
		DIO vs. DIOWL	2.03E-08	12.55	****
Figure	Type of test	Statistical data	P Value		Sig.
B.4c-d	Two-way RM ANOVA	Interaction: F(1,17) = 4.30	5.35E-02		ns
		Group: F(1,17) = 3.95	6.31E-02		ns
		Treatment: F(1,17) = 69.10	2.16E-07		####
		Sidak's multiple comparisons test		t	
B.4c		Controls vs. DIOWL			
		Ad libitum	8.59E-01	0.49	ns

B.4d		Food Restricted	1.64E-02	2.81	*
		Ad libitum vs. Food Restricted			
		Controls	4.10E-03	3.63	**
		DIOWL	2.58E-08	10.12	****
Figure	Type of test	Statistical data	P Value		Sig.
B.5a	Two-way RM ANOVA	Interaction: F(1,10) = 1.454	2.56E-01		ns
		Treatment: F(1,10) = 126.0	5.46E-07		####
		Group: F(1,10) = 0.318	5.85E-01		ns
		Sidak's multiple comparisons test		t	
		PBS vs. Leptin (5mg/kg)			
		PBS Pump	1.02E-05	8.79	****
		Leptin Pump	6.71E-05	7.08	****
B.5b	Two-way RM ANOVA	Interaction: F(1,10) = 0.911	3.62E-01		ns
		Treatment: F(1,10) = 11.62	6.68E-03		##
		Group: F(1,10) = 3.842	7.84E-02		ns
		Sidak's multiple comparisons test		t	
		PBS vs. Leptin (5mg/kg)			
		PBS Pump	2.30E-02	3.09	*
		Leptin Pump	2.14E-01	1.74	ns
B.5c	Two-way RM ANOVA	Interaction: F(1,10) = 0.012	9.14E-01		ns
		Treatment: F(1,10) = 75.20	5.77E-06		####
		Group: F(1,10) = 0.020	8.91E-01		ns
		Sidak's multiple comparisons test		t	
		PBS vs. Leptin (5mg/kg)			
		PBS Pump	2.00E-04	6.21	***
		Leptin Pump	2.46E-04	6.05	***
B.5d	Two-way RM ANOVA	Interaction: F(1,10) = 0.029	8.69E-01		ns
		Treatment: F(1,10) = 26.32	4.44E-04		###
		Group: F(1,10) = 0.007	9.33E-01		ns
		Sidak's multiple comparisons test		t	
		PBS vs. Leptin (5mg/kg)			
		PBS Pump	1.13E-02	3.51	*
		Leptin Pump	7.59E-03	3.75	**
B.5e	Two-way RM ANOVA	Interaction: F(1,10) = 7.129	2.35E-02		#
		Treatment: F(1,10) = 29.77	2.78E-04		###
		Group: F(1,10) = 1.232	2.93E-01		ns
		Sidak's multiple comparisons test		t	
		PBS vs. Leptin (5mg/kg)			
		PBS Pump	3.72E-04	5.75	***
		Leptin Pump	1.48E-01	1.97	ns
B.5f	Two-way RM ANOVA	Interaction: F(1,10) = 0.082	7.81E-01		ns
		Treatment: F(1,10) = 41.76	7.24E-05		####
		Group: F(1,10) = 0.001	9.72E-01		ns
		Sidak's multiple comparisons test		t	
		PBS vs. Leptin (5mg/kg)			
		PBS Pump	2.81E-03	4.37	**
		Leptin Pump	1.51E-03	4.77	**
B.5g	Upaired t test	t = 2.807, df = 10	1.86E-02		#
Figure	Type of test	Statistical data	P Value		Sig.
B.6a	One-way ANOVA	F(2,20) = 103.5	2.82E-11		####
		Tukey's multiple comparisons test		q	
		Control vs. DIO	2.87E-10	17.29	****
		Control vs. DIOWL	1.73E-01	2.65	ns

		DIO vs. DIOWL	1.42E-10	17.99	****
	t-test (Control-DIOWL)	t = 2.845, df = 14	1.30E-02		†
B.6b	One-way ANOVA	F(2,23) = 182.1	1E-15		####
		Tukey's multiple comparisons test		q	
		Control vs. DIO	1.15E-13	21.82	****
		Control vs. DIOWL	5.24E-02	3.49	ns
		DIO vs. DIOWL	4.10E-14	24.23	****
	t-test (Control-DIOWL)	t = 5.777, df = 15	2.23E-05		††††
B.6c	One-way ANOVA	F(2,20) = 298.6	1E-15		####
		Tukey's multiple comparisons test		q	
		Control vs. DIO	7.90E-14	27.27	****
		Control vs. DIOWL	8.23E-01	0.84	ns
		DIO vs. DIOWL	2.60E-14	32.09	****
B.6d	One-way ANOVA	F(2,23) = 198.0	< 1e-15		####
		Tukey's multiple comparisons test		q	
		Control vs. DIO	1.77E-13	21.28	****
		Control vs. DIOWL	6.41E-01	1.28	ns
		DIO vs. DIOWL	3.40E-14	26.21	****
B.6e	One-way ANOVA	F(2,20) = 4.227	2.94E-02		#
		Tukey's multiple comparisons test		q	
		Control vs. DIO	2.53E-02	4.04	*
		Control vs. DIOWL	9.03E-02	3.15	ns
		DIO vs. DIOWL	6.03E-01	1.37	ns
B.6f	One-way ANOVA	F(2,23) = 19.20	8.89E-06		####
		Tukey's multiple comparisons test		q	
		Control vs. DIO	6.14E-06	8.66	****
		Control vs. DIOWL	4.42E-03	5.00	**
		DIO vs. DIOWL	3.08E-03	5.21	**
B.6g	One-way ANOVA	F(2,20) = 53.66	9.15E-09		####
		Tukey's multiple comparisons test		q	
		Control vs. DIO	1.40E-08	13.80	****
		Control vs. DIOWL	6.33E-03	4.93	**
		DIO vs. DIOWL	3.89E-07	11.21	****
B.6h	One-way ANOVA	F(2,23) = 275.0	< 1e-15		####
		Tukey's multiple comparisons test		q	
		Control vs. DIO	3.30E-14	32.95	****
		Control vs. DIOWL	6.51E-13	19.94	****
		DIO vs. DIOWL	2.62E-12	18.70	****